Elaboration of cellularized hybrid macroporous materials by freeze-casting for soil bioremediation

Sarah Christoph

Université Pierre et Marie Curie

Ecole doctorale 397 - Physique et Chimie des Matériaux

Laboratoire de Chimie de la Matière Condensée de Paris

Thèse de doctorat de Chimie et Physico-Chimie des Matériaux

Elaboration par freeze-casting de matériaux poreux hybrides cellularisés pour la bioremédiation des sols

Elaboration of cellularized hybrid macroporous materials by freeze-casting for soil bioremediation

Présentée par Sarah Christoph

Présentée et soutenue publiquement le 27 Septembre 2017

Devant un jury composé de :

Dr Sylvie DERENNE	Directrice de Recherche CNRS (METIS - UPMC, Paris)	Présidente
Dr. Francisco DEL MONTE	Directeur de Recherche (GBM - ICMM-CSIC, Madrid)	Rapporteur
Dr. Vanessa PREVOT	Directrice de Recherche CNRS (ICCF - UBP, Clermont Ferrand)	Rapportrice
Dr. Bernard CATHALA	Directeur de Recherche (BIA - INRA, Nantes)	Examinateur
Dr. Sylvain DEVILLE	Directeur de Recherche CNRS (LSFC – CNRS/Saint-Gobain, Cavaillon)	Examinateur
Dr. Pierre BARRE	Chargé de Recherche CNRS (LG – ENS, Paris)	Invité
Dr. Thibaud CORADIN	Directeur de Recherche CNRS (LCMCP - UPMC, Paris)	Directeur de thèse
Dr. Francisco FERNANDES	Maître de Conférence UPMC (LCMCP - UPMC, Paris)	Encadrant de thèse

Remerciements

Je tiens en tout premier lieu à remercier Thibaud Coradin et Francisco Fernandes qui m'ont accueillie au LCMCP pour ce qui devait être un stage de Master de six mois et avec qui j'ai finalement eu la joie de partager trois années de thèse. Merci Thibaud pour ton enthousiasme, ta bonne humeur, tes bon conseils et ton œil neuf qui m'a souvent aidée à prendre un recul nécessaire. Merci Francisco de m'avoir fait confiance pour te lancer dans l'aventure de l'encadrement de thèse. Merci de m'avoir accompagnée à travers les problèmes techniques, le bricolage, les discussions théoriques et les résultats intriguant, à travers les manips réussies et (surtout) les manips ratées. Je n'aurais pas pu rêver un meilleur encadrement, merci du fond du cœur pour ta curiosité communicative, ton enthousiasme débordant, ta gentillesse et ta disponibilité sans faille.

Je souhaite également adresser tous mes remerciements aux membres de mon jury de thèse Francisco Del Monte et Vanessa Prevot, en qualité de rapporteurs ainsi que Pierre Barré, Bernard Cathala, Sylvie Derenne, et Sylvain Deville en tant qu'examinateurs. Je vous remercie pour le temps que vous avez accordé à la lecture de mon manuscrit. J'ai été ravie d'avoir la chance de pouvoir vous présenter mes travaux vous suis très reconnaissante pour vos commentaires et remarques ainsi que pour la discussion très enrichissante que nous avons pu partager lors de la soutenance.

Je tiens également à remercier la directrice du LCMCP Florence Babonneau de m'avoir acceptée au sein d'un laboratoire si propice à l'épanouissement tant scientifique que personnel, dans un environnement où excellence scientifique et convivialité semblent toujours aller de pair.

Merci à Christian Bonhomme et à l'ED 397, ainsi qu'au LABEX Matisse pour le financement de cette thèse, qui m'ont permis de me lancer dans le grand bain de la recherche dans des conditions plus que favorables.

Merci à Laurence Bonnet-Lericque pour son aide tout au long de la thèse et en particulier pour les aspects logistiques de la soutenance en elle-même. Un immense merci à Corinne Pozzo-Di Borgo et Hélène Gervais pour leur aide tout au long de ces trois ans. Merci pour votre sourire, votre efficacité et votre disponibilité face à toutes sortes d'appels à l'aide. Merci également à Diana Lesueur et Bernard Haye grâce à qui on ne manque de rien pour les manips.

Un grand merci également à toutes les personnes qui m'ont aidée pour caractériser mes échantillons et m'ont accordé leur temps et leur savoir-faire. Merci à Isabelle Génois pour m'avoir appris les secrets du MEB, de l'EDX et du BET (et merci pour tout le reste que ce soit lors des catastrophes de lyophilisateur ou pour les joies de l'inventaire et de l'étiquetage des produits chimiques). Merci Bernard Haye pour la préparation des échantillons de TEM et merci Patrick Le Griel et Gervaise Mosser pour l'observation. Merci à Guillaume Laurent pour la RMN (et la gestion du bidon d'azote liquide). Merci à Nora Abdoul-Aribi et Alexandre Bahezre pour l'ATG. Merci à Christophe Hélary et David Pinto pour m'avoir initiée à la microbiologie.

Je souhaite également à remercier les différentes personnes hors du LCMCP qui ont contribué à ces travaux. En premier lieu, un très grand merci à Pierre Barré du Laboratoire de Géologie de l'ENS. Merci pour ton aide, tes conseils et ta gentillesse, j'ai été ravie d'avoir l'occasion de travailler avec toi. Merci également à Catherine Garnier et Estelle Bonnin de l'INRA à Nantes, sans qui aucun des matériaux à base de pectine n'auraient pu être étudiés. Merci à Anne-Laure Rollet et Guillaume Meriguet du laboratoire Phenix pour leur expertise pour la caractérisation des échantillons en relaxométrie. Merci à Riccardo Sapienza et Soraya Caixeiro du King's College à Londres pour m'avoir montré que les mousses freeze-castées pouvaient être lumineuses. Merci à Martin Desimone et toute son équipe (en particulier Maria Foglia, Ines Echazu, Andrea Mebert) de l'Université de Buenos Aires pour m'avoir accueillie aussi chaleureusement.
Durant ces trois années de thèse j'ai également eu la joie de pouvoir travailler au Palais de la Découverte et je tenais à adresser un immense merci à toute l'équipe du département de Chimie, Sokunthéa Thlang, Frédérique Salpin, Véronique Polonovski, Ludovic Fournier et Claire Josse. Merci à tous de m'avoir fait confiance pour intégrer l'équipe, merci pour votre gentillesse et votre bonne humeur, merci de m'avoir transmis le goût de transmettre et merci de m'avoir offert la chance de vivre tous ces beaux moments de partage.
Enfin je ne peux pas terminer cette liste de remerciements sans évoquer les personnes avec qui j'ai partagé tant de choses au quotidien pendant ces trois années, autour d'un thé ou d'une coupe de champagne, dans les bureaux ou les labos, au détour d'un couloir ou à la cafétéria. Merci à tous les membres permanents de l'Equipe Matbio (Ahmed, Bernard, Carole, Cécile, Christophe, Corinne, Francisco, Gervaise, Léa, Sylvie et Thibaud) pour ces moments de d'échange et de convivialité. Merci en particulier au doctorants et post-doctorants de l'équipe Aurélien, Clément, David, Dounia, Estelle, François, Julien, Kankan, Kévin, Lise, Milena, Xiaolin et Yupeng avec qui ont toujours été de bonne compagnie que ce soit au labo ou en dehors. Merci à Alice, Marion et Aude pour leur sourire et leur bonne humeur à toute heure. Merci à Clément, Simon et Jérôme pour leurs visites dans notre bureau/salon de thé/coin des potins. Merci à Quentin, Igor et Guillaume qui étaient là de mon premier jour de master à mon dernier jour de thèse. Merci à Estelle, Olivier, Guillaume et David ou *l'autre* bureau 426. Merci enfin à tous ceux qui ont partagé leur bureau avec moi. Merci Olivier Da. d'avoir supporté le cliquetis des agitateurs magnétiques. Merci à Laurence, Olivier, Nora et Thierry de m'avoir accueillie dans votre bureau malgré mes faibles compétences secrétariales. Merci enfin à mes merveilleuses co-bureau du (vrai) bureau 426 Camille, Emmanuelle et Morgane. Merci pour le thé et le chocolat, les potins et les débats du vendredi soir, les fous rires et les larmes.
Pour conclure, je tiens à remercier ma famille et mes amis qui pendant plus de trois ans m'ont offert leur support, leur patience et leur attention dans tous les aspects de cette belle aventure.

A tous et à toutes, encore un immense merci.

Sarah

Table of Contents

General introduction

In the last few decades, the key importance of the human environmental footprint on the various ecosystems of the planet has slowly made its way into the collective consciousness. From this awareness, various initiatives have emerged for pollution monitoring, prevention and remediation, from individual actions to international consensus. Soil pollution is especially concerning due to the various pathways through which it can lead to bioaccumulation (leaching into ground water, accumulation in plants and microorganisms etc…) and ultimately impact all livings beings on Earth. In addition soils are particularly difficult to manage, compared for instance to waters: while *ex situ* approaches raise important logistical issues and can be highly disturbing for the local ecosystems, *in situ* treatments face the intrinsic complexity of solid yet highly dynamic media.

Bioremediation is Nature's response to pollution of a given ecosystem. It consists in the accumulation or degradation of contaminants by living organisms, including plants, but also animals (such as insects or earthworms) or diverse microorganisms (both eukaryotic, *i.e.* fungi or prokaryotic, *i.e.* bacteria). The natural response of a polluted ecosystem (bioattenuation) may however not always be efficient enough to provide total or quick enough restauration of the soil's original condition. In this case two main strategies have been devised to support the natural recovery of the considered environment[1,2]. Biostimulation requires the amendment of the soil with various nutrients to enhance the endogenous degradation activity. This approach is however limited by the composition of the local biological population. Alternatively, bioaugmentation consists in the introduction of exogenous organisms to provide the soil with the necessary remediation capabilities. This approach may be very efficient to degrade the targeted contaminants, but raises the question of the introduction of exogenous organisms which may responsible for severe unbalances in the original ecosystem. Regardless of the bioremediation approach, a limit to the use of living organisms is their sensitivity to their immediate environment. As a result the physico-chemical properties of the considered soil (for instance concentrations in contaminants or co-contaminants, pH, salinity, temperature etc…) may be deleterious to the viability of species relevant to bioremediation.

One way to limit the impact of the microorganisms' direct environment is to design immobilization matrices capable of hosting and protecting living cells. This approach has in particular been used for the design of bioactive materials for applications in environmental science[3]. Immobilization of organisms within an appropriate matrix can indeed provide valuable protection against detrimental physico-chemical conditions. In addition such entrapment can be a way to limit dispersion of exogenous organisms within a given ecosystem, thus preventing possible biological disequilibria. But the design of an ideal encapsulating matrix for organisms with bioremediation capabilities is a challenge on several levels.

The two main objectives of bioremediation approaches based on encapsulated cells are the efficiency of the depollution process and the confinement of the exogenous microorganisms within the matrix. These two apparently simple objectives are actually influenced by a wide range of interrelated parameters (see Figure 1). Some of these are dependent on the

characteristics of the polluted site (type of soil, temperature, physico-chemical properties of the soil but also nature of the contaminant) but part of them are related to the cellularized material itself. The device can be seen as the association of a functional unit (the encapsulated metabolically active microorganism) and of a structural part (the encapsulation matrix itself). The efficiency of the depollution process is primarily dependent on the metabolic activity of the entrapped microorganisms, but the structure of the matrix can also be crucial since it is likely to modify the diffusion rates of the substrates and therefore the depollution kinetics. Both functional and structural points of view must therefore be taken in account in the design of an efficient depollution device.

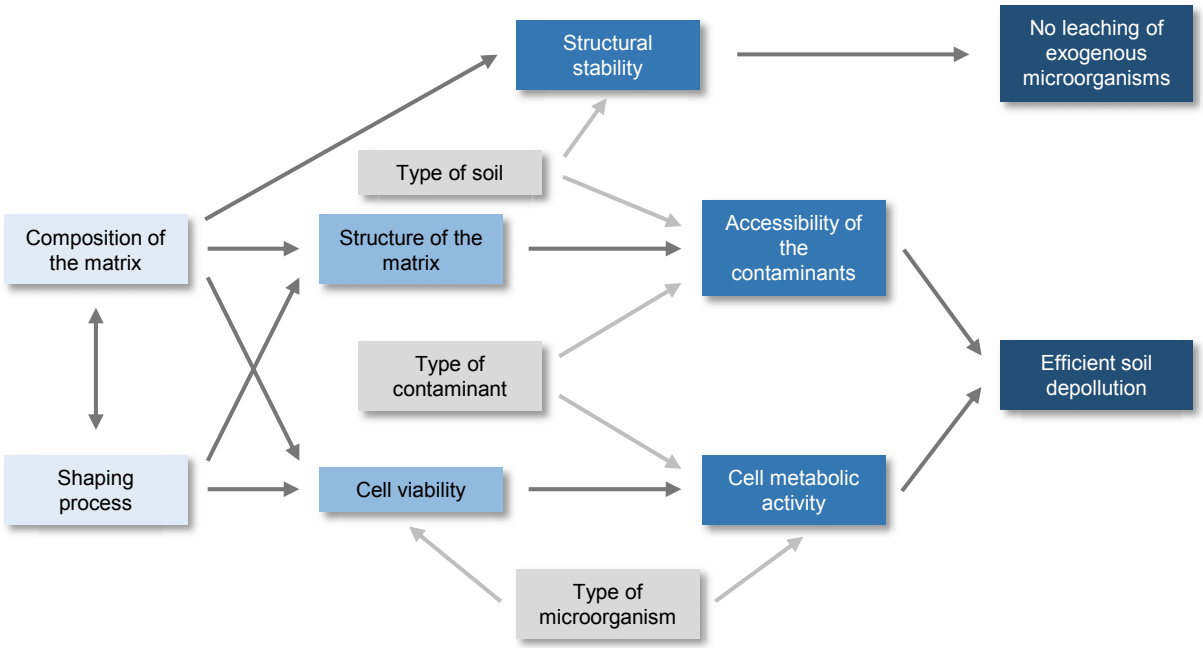

Figure 1: Bioremediations processes using encapsulated cells as biofunctional units are influenced by a wide variety of interdependent parameters.

Control of these aspects can be achieved through two inter-dependent routes. The composition of the encapsulation matrix must first be selected so as to be non-cytotoxic towards the encapsulated organisms, as well as, on a larger time and space scale, towards the whole considered ecosystem. The nature of the constituents of the matrix must also be chosen to ensure structural stability during the residency of the material in soil, as a way to prevent leaching of the entrapped exogenous organisms. These choices can however not be separated from material engineering aspects and, especially, the matrix shaping process that must also be compatible with encapsulation of living organisms.

Regarding the matrix composition, the literature has highlighted the interest of biopolymers as encapsulating matrices[4,5]. These polymers are usually found in organisms as part of the extracellular matrix or directly within the cell walls. As a result most of them are highly cytocompatible, which is a key feature when considering cell encapsulation. This cytocompatibility is however often accompanied by biodegradability, which may be a

valuable advantage for biomedical applications, but could be problematic regarding the stability of a matrix supposed to prevent cell leaching. One way to tune the mechanical properties of a matrix, while preserving part or all of its chemical functionalities is the use of hybrid or composites materials. As a result biopolymer-inorganic hybrid and more specifically biopolymer-silica hybrid and composites have been widely used for cell and microorganism encapsulation[6,7], and could be especially useful for bioremediation approaches[8].

From the structural point of view, matrices can adopt various shapes and structures. In the targeted application, elaboration of a porous material could provide valuable advantages regarding substrate diffusion. Ice-templating can be used for shaping a wide range of compounds (from ceramics to polymers) to yield lots of different pores morphology, including well controlled and tunable oriented pores. Such a porosity could be useful in facilitating substrate transport *via* capillary phenomena. In addition, the efficiency of freeze-casting for physical entrapment of living organisms and preservation of their metabolic activity has been demonstrated in several materials[9,10].

Based on a literature survey presented in Chapter I, we hypothesized in this PhD work that cellularized biopolymer-silica hybrid porous materials obtained by freeze-casting, a specific well-controlled and easily-tunable ice-templating technique, could prove very efficient in soil bioremediation processes (see Figure 2).

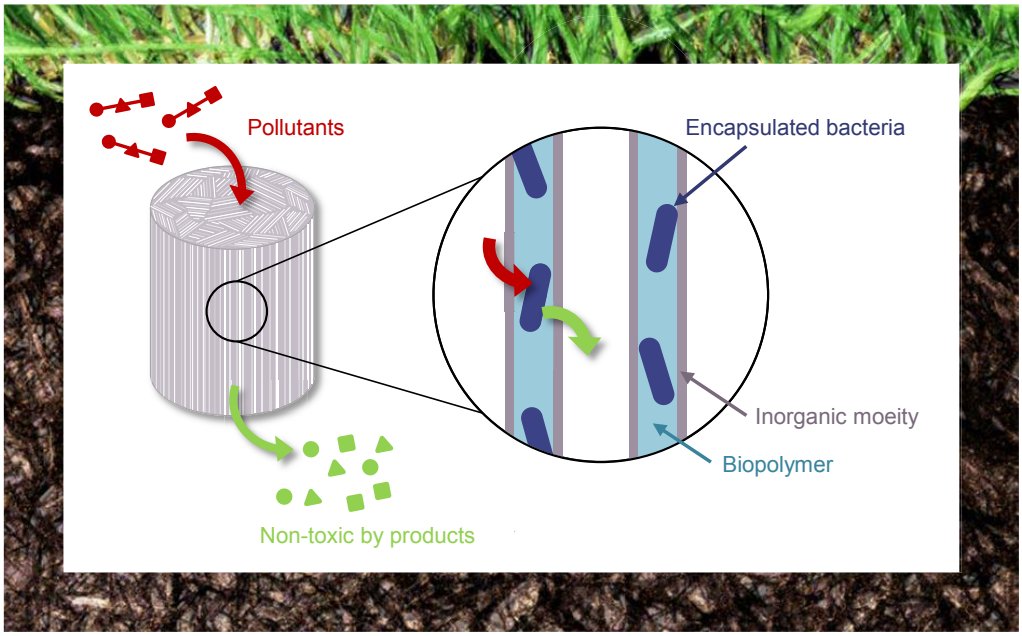

Figure 2: The goal of this work is to design a macroporous hybrid material for encapsulation of metabolically active bacteria. The biopolymer structure should provide biocompatibility while the silica layer should ensure structural stability of the material after prolonged stays in soil.

Our approach was based on the preparation of these materials in a two-step process:

1. encapsulation of the chosen microorganisms within a biopolymer porous structure through freeze-casting and subsequent lyophilization.

2. coating of the cellularized biopolymer scaffold with a silica layer using sol-gel chemistry.

Each of these steps had to be adapted to the nature of the compounds to ensure both control over the material morphology and compatibility with cell survival. The strategy we adopted to pinpoint parameters relevant for the control of structural and functional properties of the materials was to first develop the shaping strategy in absence of cells, but keeping in mind its implication for cell encapsulation (see Figure 3).

Freeze-casting of pectin foams was first investigated to identify the relevant parameters in the design of unidirectional porous foams (Chapter II). Sol-gel silica deposition using vapor phase precursor was then developed to yield a pectin-silica core-shell structure for the pore walls and gain control over the silica layer characteristics. The stability of such material was then evaluated in a reference soil (Chapter III).

Once the key parameters regarding the material's structure were identified, the process was applied to the encapsulation of model microorganisms to explore their influence on the material functionality. Adjustments of the process were implemented to ensure good cell compatibility while keeping control over the structural aspects (Chapter IV). Finally, optimization of the biopolymer nature, silicification process and cell type allowed for the successful evaluation of the depollution capabilities of the cellularized biopolymer-hybrid porous material in a real soil (Chapter V).

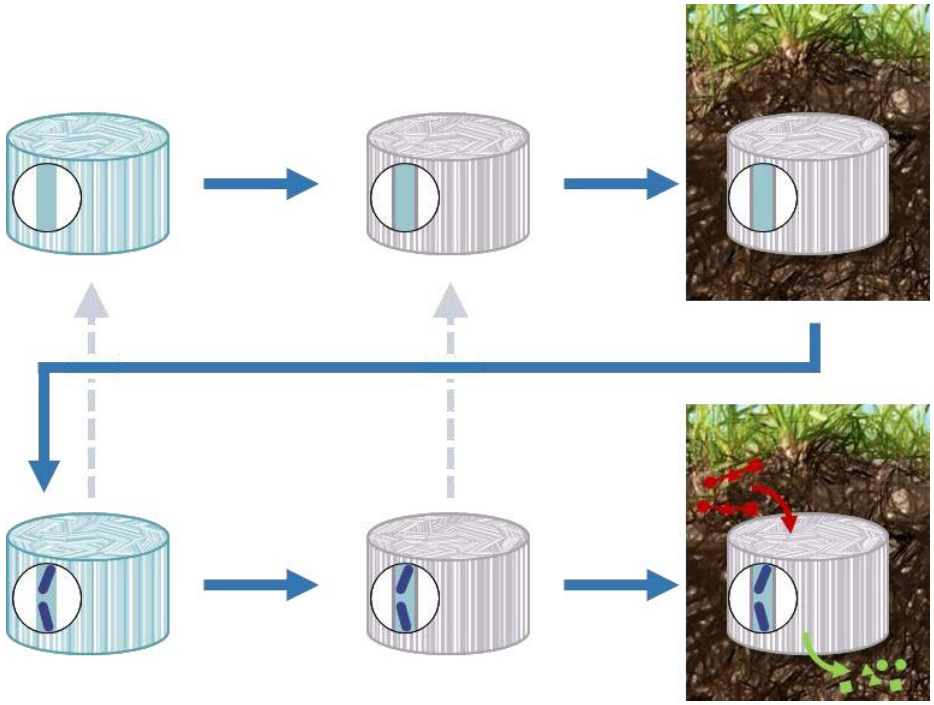

Figure 3: The shaping process was first developed on a material containing no cells to pinpoint relevant parameter to the structural aspects. The process was then applied and adjusted for encapsulation of living organisms. Efficiency of the cellularized hybrid porous material was then assessed in a soil contaminated with a model pollutant**.**

Chapter I : Context and state of the art

I.1 About soil pollution and depollution

I.1.a Soil contamination

Soil is a key component in the behavior and equilibrium of various ecosystems. It is at the root of chains and interactions between the various living organisms of these complex systems. Physical or chemical degradation of a given soil may have a wide range of negative consequences[11], directly on the local fauna and flora, but also indirectly on human health through different pathways including food and water consumption. As a result monitoring and protection of this precious resource is essential. In several cases however soils may be damaged by anthropic activities but also in some occurrences through natural phenomena. It is then essential to try to restore the considered ecosystem to its original state, concerning the physico-chemical composition of the soil but also regarding the endogenous microbial population. The notion of soil quality may be difficult to restrain to one set of physical or chemical characteristics, since soils are actually a set of interactions, fluxes and processes which may vary both in time (seasons) and space (depth). The soil condition may however be described by chemical (inorganic composition, nutrients, total organic content), physical (texture, erosion) and biological characteristics (microbial population).
The notion of pollution can be defined as the presence of an imbalance due to the prevalence of specific compounds. Rehabilitation of a polluted soil usually requires removal or degradation of the considered contaminant and return to the initial ecosystem equilibrium. This notion is however not as simple as it may initially appear, since a wide variety of phenomena may result in the displacement, immobilization or degradation of a target compound.
In addition, sources and types of pollutants are extremely diverse and polluted sites often simultaneously contain different types of pollutant. In addition, as was mentioned earlier, each soil is complex and unique ecosystem, which implies that any depollution process must be preceded by a careful analysis and characterization of the considered site.

I.1.a.i Common pollutants

Sources of contaminations are extremely diverse, but some classes of pollutants are especially widely used. They may be separated based on their chemical structure, their main sources and uses or even depending on their introduction pathways. The different categories however often overlap and one type of classification or the other may be more relevant to discuss certain families of pollutants.
The way certain pollutants may end up in a given soil is strongly dependent on their uses. Pollution of a given soil may be the result of single accidental events (oil spills for instance) or of repeated use of certain compounds in human activities as is the case regarding the use of pesticides[12]. Some contaminants may also have a non-anthropogenic origin such as wildfires[13]. The contamination vectors are also diverse, since pollutants may end-up in the

through a wide range of pathways, for instance by direct diffusion, through liquid infiltration or through the atmosphere (see Figure I.1).
Most contaminants can be traced to human industrial or commercial activities, among which agriculture and petrochemistry have often been pointed out as major actors. However non negligible contaminations can occur from ill disposal of common consumers goods and domestic materials (see Figure I.2 a). According to European Environment Agency (EEA) heavy metals as well as hydrocarbon derivatives (oil minerals and Polycyclic Aromatic Hydrocarbons (PAH)) are especially widely spread in the surveyed European soils(see Figure I.2 b).

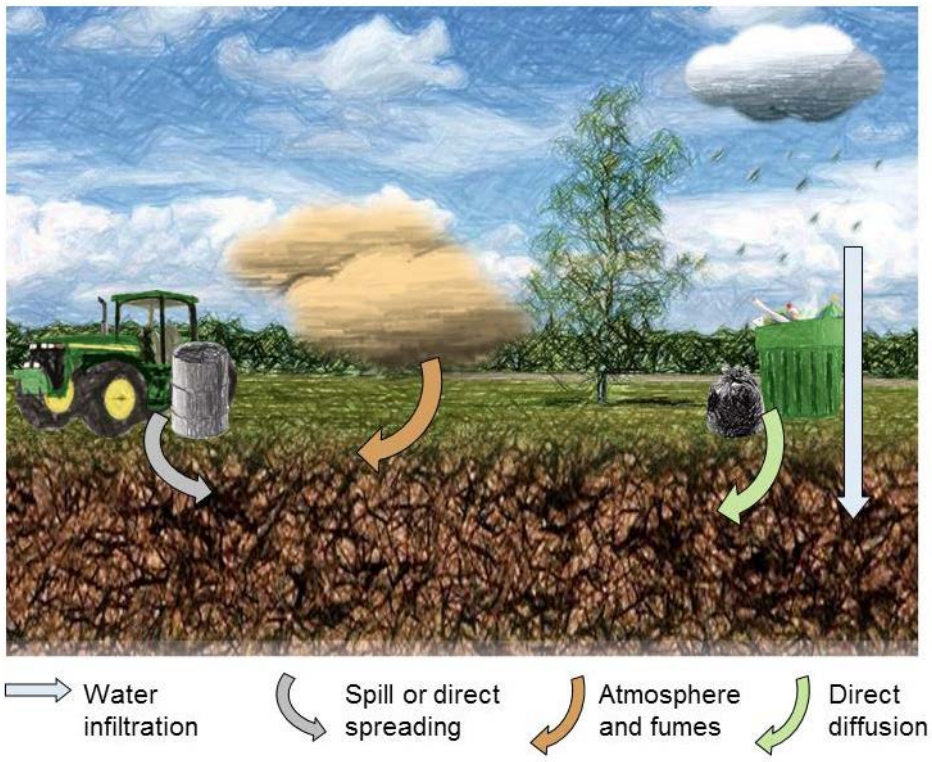

Figure I.1: Contaminants can reach soil through several different pathways. Pollution might for instance occur through isolated incidents or repeated exposures.

Several classes of pollutants have been pointed out as especially concerning. In particular pesticides and their fate in soils have attracted a considerable amount of attention[14–17] in the last few decades. This type of compounds are somewhat peculiar in the domain of pollutants since they are knowingly and repeatedly introduced in the environment, where they provide valuable advantages[18]. The ideal pesticide should "be toxic only to the target organism, be biodegradable and undesirable residues should not affect non- target surfaces"[16] but it is actually estimated that only a very small fraction of the used pesticides reach their intended targets[19,20].

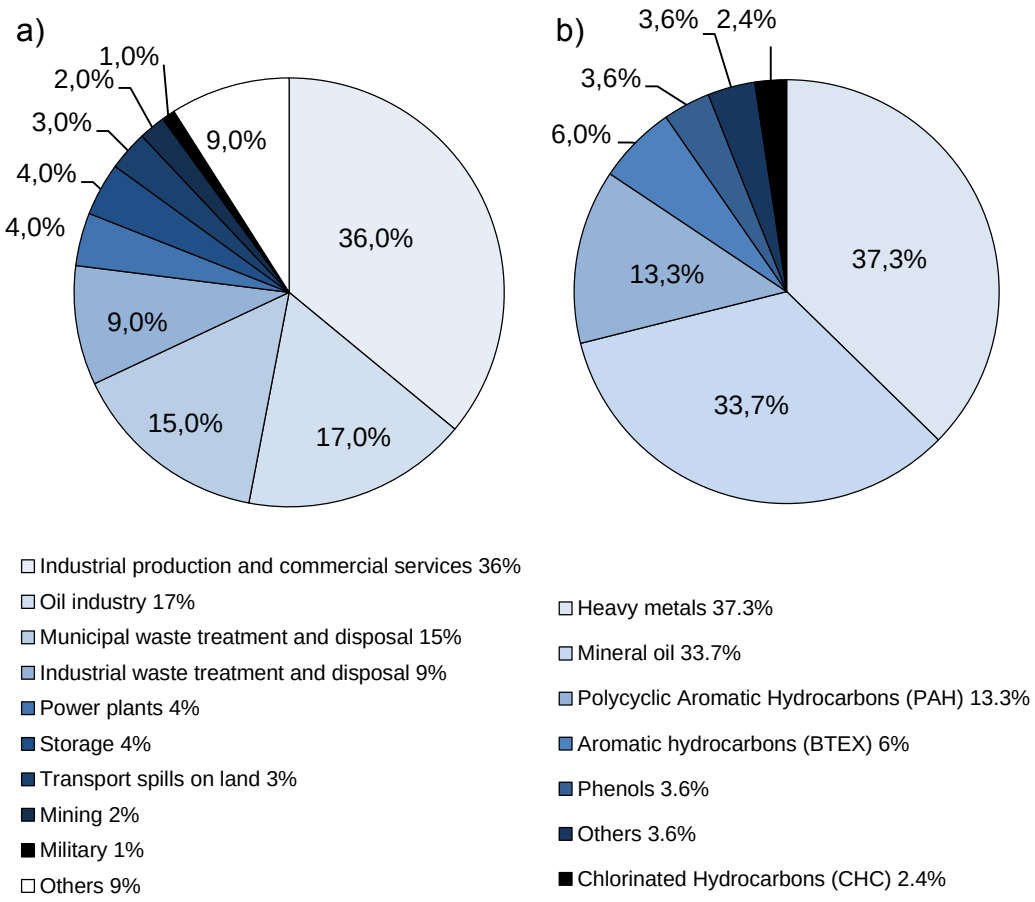

Figure I.2: Overview of economic activities causing soil pollution reveals predominant impact of industrial production and oil industry (a). Sources of contaminations have direct influence on the type of pollutants most commonly found in soil and groundwater (b). Data from European Environmental Agency published in 2009. Retrieved from http://www.eea.europa.eu in July 2017.

Even if pesticides are a major and well-advertised source of pollution, it is far from being the sole cause for soil contamination. Polycyclic Aromatic Hydrocarbons (PAH) have been of considerable concern for several decades[21] due to their ubiquity[22]. They are mainly the result of combustion processes ranging from natural fires[23] to domestic heating, urban traffic[24] and industrial incineration. Due to intensive use of coal in the 20th century industries, considerable amounts of PAH may be found in numerous soils[25]. Due to their chemical structure (two or more fused aromatic cycles (see Figure I.3 a) and their hydrophobicity[26] these compounds tend to be highly persistent[27].

Another family of hydrocarbon derivatives deemed of specific concern is the so called BTEX family, which regroups benzene, toluene, ethylbenzene and xylenes (see Figure I.3 b). These compounds are retrieved from fossil fuels and are widely used as solvents or additives in gasoline. As a result contamination sources include various industrial plants, gas stations but also large traffic axes. These compounds are especially concerning due to their very high toxicity. Diseases associated with BTEX exposure range from respiratory conditions to cardiovascular impediments, endocrine disruption or fertility disorders.

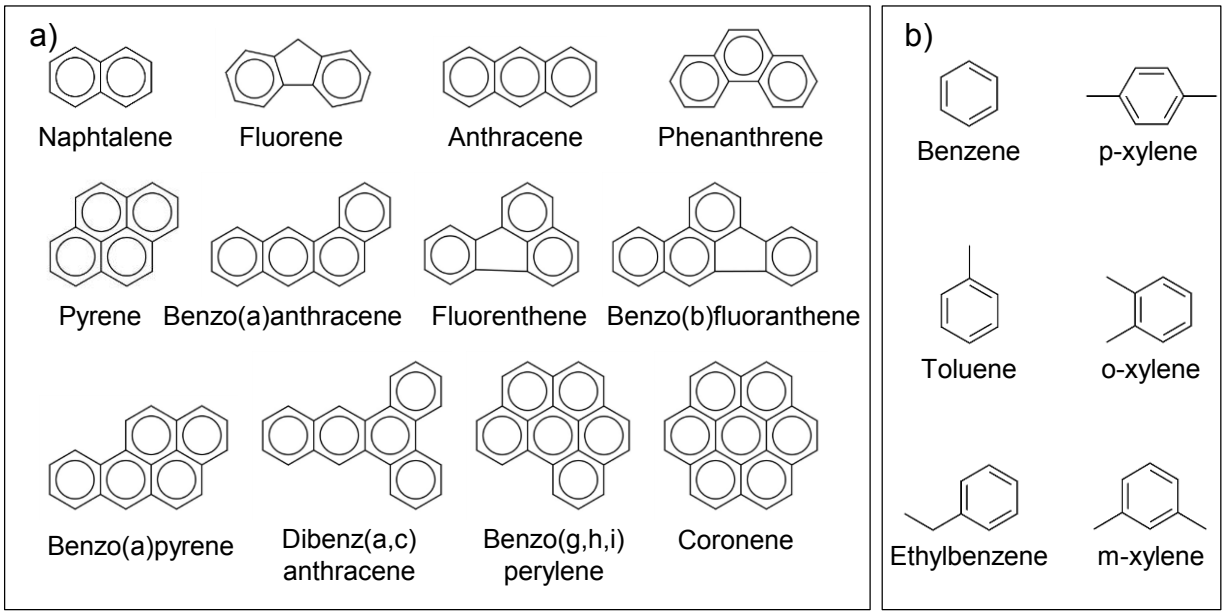

Figure I.3: (a) Common Polycyclic Aromatic Hydrocarbons. Adapted from Haritash *et al.*[28] (b) Chemical structure of BTEX (benzene, toluene, ethylbenzene, xylenes. Adapted from Bolden *et al.*[29].

Another class of common pollutants is dyes due the very large global demand and use. The main source of dye contamination is the textile industry. It is deemed that 10 to 25% dyes are lost during textile dyeing process, part of which may be directly released in the environment[30]. Most dyes are based on aromatic cycles substituted with various chemical functions, among which the azo group is particularly prominent[31]. As is the case for other organic contaminants, dye can chemically be broken down into various reaction products. Both dyes and by-products may represent risks for the contaminated ecosystems. Beside the visual pollution resulting from dye contamination, these chemical compounds have been reported to cause various conditions ranging from simple skin irritation or allergies to carcinogenic[32] and mutagenic effects[33].

If organic pollutants represent the majority of contaminants, inorganic compounds may also present a risk for environment and health. Metals are ubiquitous and present serious issues regarding the decontamination processes. Contrary to purely organic compounds, metals cannot be broken down into nontoxic compounds such as water or carbon dioxide. Remediation approaches for metals are therefore mainly based on redox modifications to minimize toxicity and mobility or on physical removal of the contaminants. Since these compounds cannot be degraded[34], they often bioaccumulate along the food chain[35,36] resulting in possible heavy metal poisoning which may induce wide range of conditions including kidney, pulmonary or cardiac damages, cognitive and neurological impairments as well a cancer[37].

Even if sources of contamination are diverse, the fate of the different contaminants share common features. Regardless of the type of pollutant, the issue of bioavailability has a major influence on possible environmental and health risk, as well as remediation possibilities.

I.1.a.ii Bioavailability is key

Once a contaminant reaches a given soil, it is susceptible to be subjected to diverse mobility pathways and to biotic or abiotic degradation (see Figure I.4)[38]. Pollutants in soil may be partially or totally soluble in water, which can result either in run off phenomena (chemicals are transported mainly at the surface of the soil) or in soil leaching (pollutants are transported in depth in the soil and often down to underground aquifers). Another possible way for the chemicals to be removed from the soil is though volatilization. In both cases, removal of the pollutants from the soil results in the contamination of another part of the ecosystem (water or atmosphere). Depending on the properties of the considered chemical, it may also be retained within the soil by adsorption phenomena (either or organic or inorganic compound of the soil). In addition, contaminants may be internalized and stored by different organisms (from bacteria to animals and plants), resulting in a possible bioaccumulation phenomenon. They may also be modified or degraded by living organisms or abiotic chemical reactions, sometimes resulting in complete decomposition of the contaminants into non-toxic compounds.

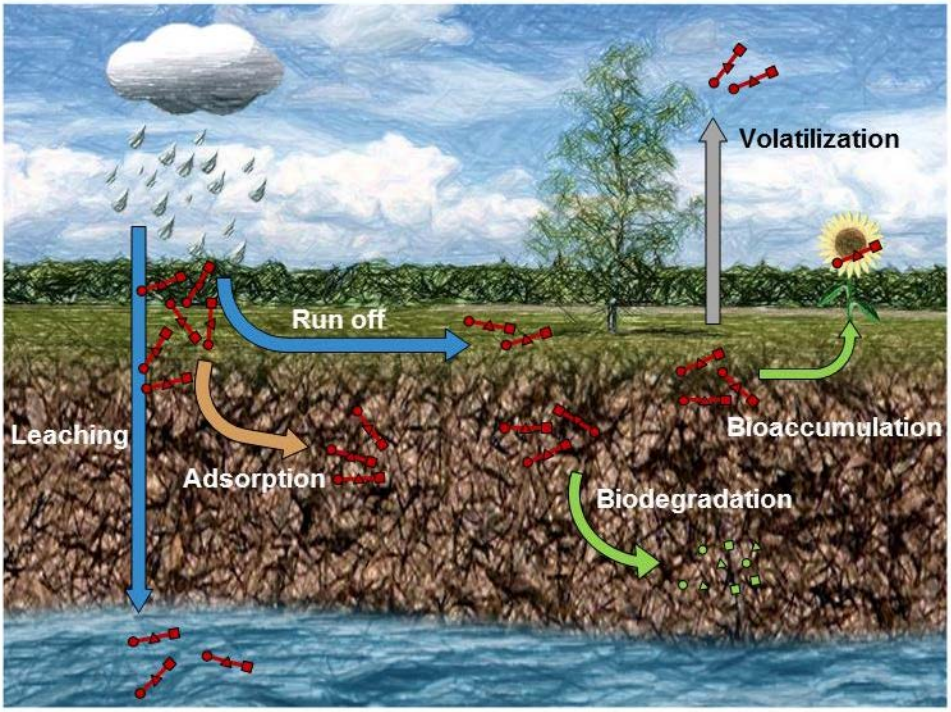

Figure I.4: Pollutants in soil may undergo a wide range of movements or transformations.

The fate of pollutants in the soil depends on the type of contaminant, especially on its chemical structure and properties, but the nature of soil itself is also of significant influence.
Soils are usually characterized by a wide range of parameters. Soils with different compositions in terms of texture, that is to say contents in sand (particles >50 µm), silt (2 µm < particles < 50 µm) and clay (particles < 2 µm) particles, may have very different behaviors regarding water permeability and adsorption properties. Physico-chemical properties of the

soil such as pH, redox potential, salinity, water and oxygen content, temperature or organic content[39,40] are likely to modify the bioavailability of the pollutants.
A distinction is often made between the environmental scientist's view which usually defines bioavailabity as the fraction of a given pollutant that can interact with living organisms (microorganisms, plants or animals)[41] (see Figure I.5) and the toxicologist's view which defines bioavailability as the amount of a given compound capable of entering the bloodstream[42]. In this work, the environmental scientist's definition was used as a reference.

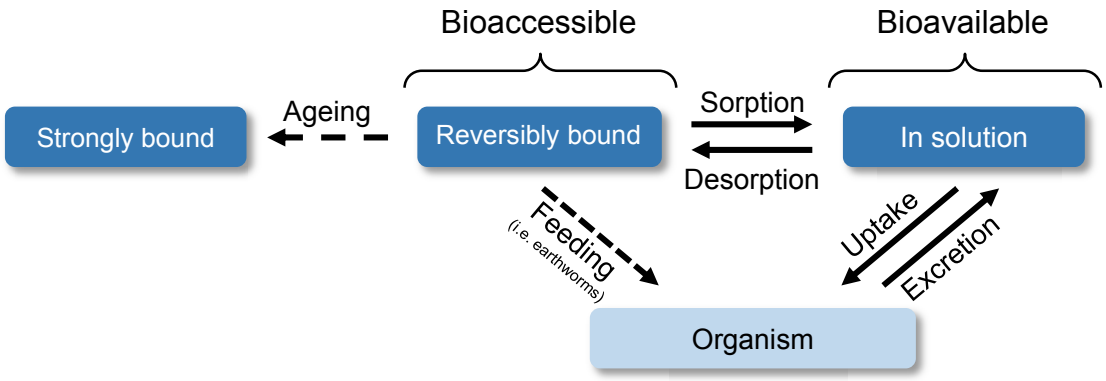

Figure I.5: The term bioavailability covers a wide range of processes including sorption and desorption and uptake by living organisms. Adapted from Sijm *et al.*[41]

Bioavailability of chemicals in soils is often evaluated based on the equilibrium between the adsorbed compounds and the surrounding water (Equilibrium Partition Theory (EPT)[43,44]). In this prospect, chemical properties of the considered pollutants are crucial, especially regarding hydrophobicity[22]. As a result, contaminants are often described based on their octanol-water partition coefficient (K_{OW})[45,46] in order to assess their tendency toward soil adsorption and more largely as an indicator of their bioavailability. Chemical compounds can however be bound to soil particle more or less tightly depending on the type of interactions involved (hydrophobic, ionic and electrostatic, van der Waals, hydrogen bond, ligand exchange etc…)[15].
In addition, soils are not a stationary ecosystems. As a result dynamics and mobility of contaminants as well as their bioavailability is variable in time. It is usually accepted that pollutants undergo ageing mechanisms after prolonged residency in soils due to slower, but stronger, adsorption mechanisms[47]. The bioavailable fraction may therefore diminish in function of time[48] (see Figure I.6).

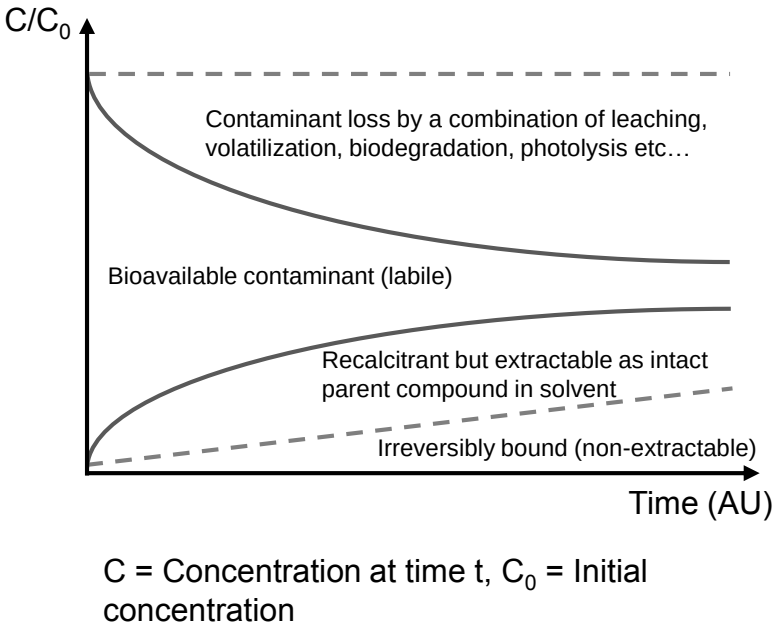

Figure I.6: After residency in soils, contaminants tend to become strongly bound to the soil thus limiting the bioavailable fraction. Adapted from Jones *et al*.[49]

Understanding the fate of contaminants and their bioavailability is essential to assess the environmental and health risks[50]. A highly toxic compound strongly bound in soil may never induce harmful effects. On the contrary, compounds with low intrinsic toxicity but highly bioavailable may accumulate in living organisms and become concentrated in specific organs resulting in deleterious effects for the concerned organism. One of the main difficulties in assessing the toxicity of specific compounds lies in the fact that the effects are entirely dependent on the dose. The notion of dose itself may be difficult to define, since a given compound may undergo different mechanisms of mobility, concentration or elimination within an organism. As a result the entry dose may not be the effective dose in sensitive target organs. In addition each organism has its own specificities and one compound may be highly toxic to one species and completely harmless or even beneficial to another. It has also been reported that toxicity of a combination of contaminants may induce synergistic toxicity, resulting in higher toxicity of the mixture compared to the sum of effects of each contaminant alone[51]. Finally the term toxicity has been defined as "the capacity of a chemical to cause injury"[42], which may in fact range from localized and reversible impacts to death of the considered organism. These factors concur to make the task of establishing regulations and standards regarding the threshold levels of hazardous chemical extremely complex. The diversity of pollutants implies a wide range of possible effects on the organisms, including toxicity, but in some cases the contaminant may also be used as part of the organisms' metabolism and therefore be biodegraded. As a result a high bioavailability, which might be detrimental from a toxicity point of view, may be seen as an advantage from the decontamination point of view[52].

I.1.b Bioremediation

As mentioned previously, soils may be contaminated by a wide range of chemical compounds. Once in the soil these compounds may be removed through various processes. They may simply migrate to other parts of the ecosystem (for instance leaching into groundwater or volatilize into the atmosphere) but can also be degraded through several mechanisms. These transformations may be abiotic (hydrolysis[53,54], photolysis[55]) or be part of biological processes (biodegradation). In some cases however these phenomena of natural attenuation may be inefficient or too slow. Active decontamination actions may therefore be needed to prevent toxic effects on the ecosystem and on human health.

I.1.b.i Soil depollution

The choice of the appropriate cleanup technology must be adapted both to the type of contaminant and to the characteristics of the polluted site. Other parameters such as cost effectiveness, volume of contaminated soil or time scales must also be taken in account when devising a soil remediation strategy. United States Environment Protection Agency provides a list of about twenty different approaches for remediation of soils and groundwater[56]. Main features of a few of these techniques are compiled in Table I.1. Each approach has its own specificities, advantages; drawbacks and range of applicability. Complete rehabilitation of a given soil may sometimes require the combined use of two or more different techniques.

There are several general approaches to manage risks in the case of a polluted soil. One of the main objectives is usually to prevent health hazards. Toxic compounds tend to enter organisms through transfer from another medium (air or water). One approach to limit risks therefore consists in trying to immobilize the compounds within the soil, or in other terms in limiting bioavailability of the pollutant. Techniques such as solidification or stabilization[57] and capping[58] are designed to limit the mobility of the pollutants. These approaches have however the drawback of leaving the pollutant within the soil, which may be problematic in the long run, since soils may undergo significant physical and chemical modifications. These approaches require therefore constant monitoring even after treatment.

Pollutants may also be physically removed from the polluted sites. The most straightforward approach is excavation, which is usually combined with other techniques such as thermal desorption[59], incineration or soil washing[60,61]. These methods are usually complex from a logistical point of view, especially in the case of large contaminated areas. They are however fast and efficient.

It is also possible to treat contaminated soil thanks to *in situ* methods. *In situ* thermal treatment[62] allows for extraction of the contaminant without excavation and in some case for direct degradation of the targeted chemicals. The recovered contaminants must then be stored or treated appropriately. Pollutants may also be degraded directly within the soil, for instance using *in situ* oxidation[63] or *in situ* reduction[64]. This however requires addition of oxidizing or reducing chemicals to the contaminated sites.

Table I.1: Comparison of the main cleanup techniques for soil remediation. Based on data from EPA[56].

Cleanup method	Description	Advantages	Limitations
Solidification and stabilization	Solidification is the formation of a solid block through addition of a binding agent (cement, asphalt, clay etc…) where compounds are immobilized. Stabilization is the chemical modification of contaminant to prevent leaching.	- Efficient for metals and radioactive contaminants - Quick and cost effective	- Contaminants are still in the soil - Not applicable for large areas
Capping	Installation of a cover (asphalt or concrete, vegetative layer, geomembrane, clay) over contaminated materials to prevent contact of the contaminated areas with human or animals.	- Quick and cost effective - Can be applied to large contaminated sites	- Contaminant is not removed from the site
Excavation	Physical removal of contaminated soil, sediments or sludge by digging. Excavated materials are usually treated with a complementary cleanup method. Cleaned soil may be used to refill the excavated site.	- Often quickest cleanup technique - Prevents propagation of the contamination	- Requires use of complementary technique - Requires precise mapping of contaminated area
Thermal desorption	Removal or volatile or semi volatile compound from soil by heating (between 100°C and 500°C). Vapors are collected to be further treated or recycled.	- Efficient for volatile or semi-volatile compounds - Possibility to condensate vapors for recycling	- Requires excavation - Not applicable for all types of soil (like soils with high clay or organic contents)
Soil washing	Separation of the contaminants from soil thanks to an appropriate washing liquid.	- Efficient for a wide range of pollutants (from fuel residues and organic compounds to metals - Efficient reduction of the contaminated volume	- Requires excavation - Wash solutions must be treated appropriately
Incineration	Burning of hazardous materials (soil, sludge but also liquids) at very high temperature (up to 1400°C). Pollutants are usually degraded but residual particles or acid gases may be formed. Residuals ashes can be treated or stored.	- Efficient on a wide range of pollutant - Low residuals amounts of polluted materials	- Requires excavation - Not efficient for metals - Requires a lot of fuel
In situ chemical reduction and oxidation	Use of reducing (ex zero valent iron) or oxidizing agents (ex permanganate, hydrogen peroxide, ozone) to change contaminants into less toxic or less mobile forms. Reactive agents may be directly injected in wells, or introduces as granules.	- *In situ* technique, no need for excavation - Can be used for deep contaminations	- Addition of chemicals to the polluted site - Diffusion of the reactive agents may be slow
In situ thermal treatment	Mobilization of pollutants in soil thanks to heat. Soil is heated and pollutants are directed towards wells for recovery and further treatment. Some types of pollutants may be directly degraded *in situ*.	- *In situ* technique - Can be used for deep contaminations	- Requires secondary treatment - Not very efficient on soil with high silt or clay contents

A wide range of physical and chemical remediation techniques exist to treat polluted soils. Most of them however require extensive logistic dispositions. Several of these techniques require complementary monitoring measures or treatments because the contaminants are not directly degraded. The *in situ* chemical cleanup techniques are efficient for the degradation of the pollutants but require the addition of chemical to the contaminated soil. One alternative to these physical and chemical techniques is to take advantage of the degradation capabilities displayed by a wide variety of living organisms.

I.1.b.ii Principles of bioremediation

Bioremediation can be defined as the use of biological entities for the degradation of contaminants. This apparently simple definition actually covers a wide range of processes since different living organisms (from bacteria and fungi to plants) may be involved in the remediation of various pollutants (hydrocarbons, metals, pesticides, dyes etc…) in a wide variety of environments (wastewaters, sediment, sludge, soil etc…). The term bioremediation also covers different approaches since the goal may simply be to remove the target contaminant from the considered ecosystem or to fully degrade the pollutant into nontoxic chemicals. Bioremediation approaches can be carried out with no or little involvement (*e.g.* natural *in situ* attenuation) or with fully engineered processes (*e.g. ex situ* bioaugmentation). This versatility may explain the increasing interest around bioremediation thematics in the last few decades[2,52,65,66], as illustrated by the growing number of publications related to soil bioremediation (see Figure I.7).

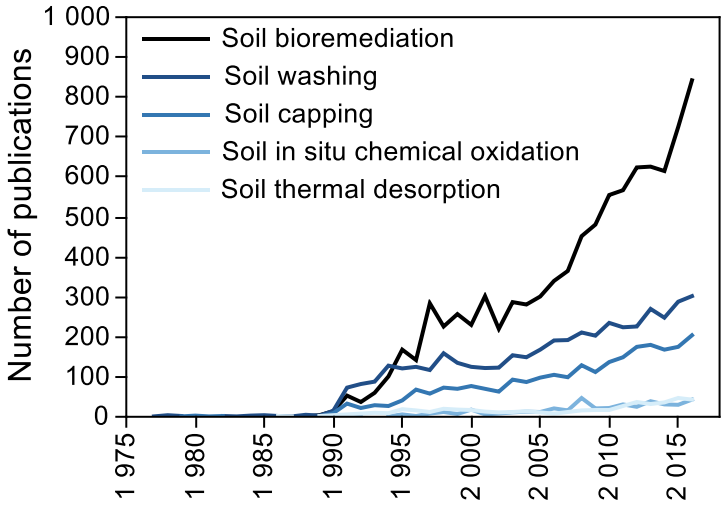

Figure I.7: Number of publications corresponding to various keywords. Results collected from Web of Science database (retrieved in July 2017).

The idea of bioremediation is actually much older since it is the basic principle behind the formation of compost[67,68]. Activated sludges have been used for wastewater treatment since the beginning of the 20th century[69,70]. Bioremediation in the modern acceptation of the term,

that is to say as a way to degrade pollutants, was introduced in the late 60s by George Robinson who used microorganisms to remediate oil spill along the Santa Barbara coast[1].

Bioremediation approaches have since been used for the depollution of a wide range of ecosystems (freshwater and marine environments, groundwater, sediment, sludge, soil) and with different types of contaminants. Different approaches, both *in situ* and *ex situ*[71,72] can be used. The choice of the appropriate strategy must take in account the characteristics of the contaminated site but also the type of pollutant itself. Many reviews have been devoted to the bioremediation of specific classes of pollutants such as metals[73,74], PAH[22,25,26,28,75,76], oil derivatives[77,78], pesticides[16,17] or dyes[79–81].

Another common way to classify bioremediation approaches is based on the type of organisms involved. This includes a wide variety of organisms from unicellular microorganisms to plants. Some definitions tend to limit the term bioremediation to the use of microorganisms and to consider phytoremediation, the use of plant, as a separate approach[2,82]. Plants are often favored for metal remediation[74,83,84] while microorganisms are often used for the degradation of organic chemicals. Phytoremediation strategies can actually be applied both for bioaccumulation of contaminants (including metals), as a way to immobilize or even extract contaminants[85], and as a way to fully mineralize organic pollutants into non-toxic compounds[86].

Animal biodegradation is very scarce compared to plant or microbial activity. Soil animals, especially earthworms, are however important as part as global remediation strategies, since they are *in situ* indicators of the ecosystem's health. Soil animal may also have a significant importance enhancing other bioremediation processes, especially microbial activity, by improvement of the soil fertility and aeration, as well as increase of pollutants bioavailability[87].

The generic term microorganism is used to refer to a wide range of potential vectors of bioremediation[88,89]. The three main types of microorganisms relevant to bioremediation are microalgae[90,91], fungi[79,91] (including yeast[92]) and bacteria[81,93]. Bacteria are actually the most represented type of microorganisms used in bioremediation approaches. This might be explained by their versatility and adaptability to a wide range of ecosystems[94,95]. As is the case for higher plants, microbial remediation may occur as bioaccumulation and subsequent limitation of leaching phenomena or as transformation of the considered pollutants (modification into as less toxic forms or full break-down of the compounds).

Regardless of the organism used, bioremediation mechanisms are often complex and not fully understood due to the large number of parameters involved. These parameters are actually very close to the ones used to describe soil quality. They include pH of the soil, presence of nutrients, presence of electron donors or acceptors, temperature, salinity. Presence of oxygen may also condition the efficiency of bioremediation processes since certain types of organisms require specifically aerobic or anaerobic conditions.

Models of degradation of one specific pollutant by one specific strain may be studied in laboratory, under closely controlled conditions, but *in situ* bioremediation is usually more

complex. In the case of *in situ* bioremediation processes it is common to find multiple contaminants or nutrients as well as different organisms. These different actors may interact and influence each other to create synergetic effects. Consortia of bacteria[96], bacteria and fungi[97], bacteria and algae[98] or microbes and animals[87] have for instance been identified in bioremediation processes[99].

Even if specific degradation mechanisms cannot be fully resolved, a few general processes involved in bioremediation have been identified. A distinction may be applied between processes that occur within the organisms and externally. In the latter case, mechanisms are often enzyme based, where the contaminants are used as substrates or co-substrates.

For processes occurring within the organisms, the first step is the internalization of the considered pollutant. This implies bioavailability of the pollutant. Organisms may excrete specific chemical to enhance bioavailability and facilitate internalization of the chemicals. Plant may for instance excrete chelator to make metals more available[100]. Similarly, bacteria have been reported to produce surfactants which may help in desorbing hydrophobic pollutants (for instance hydrocarbons) from soil particles[101]. Chemicals within the various organisms may have different fates. They may be toxic compounds and therefore be sequestrated or degraded as defensive mechanisms. In certain cases, chemical compounds which are considered as toxic compounds from human health perspective can actually be used as part of the metabolic activity of organisms (as primary substrate or in cometabolism) in bioremediation processes[102].

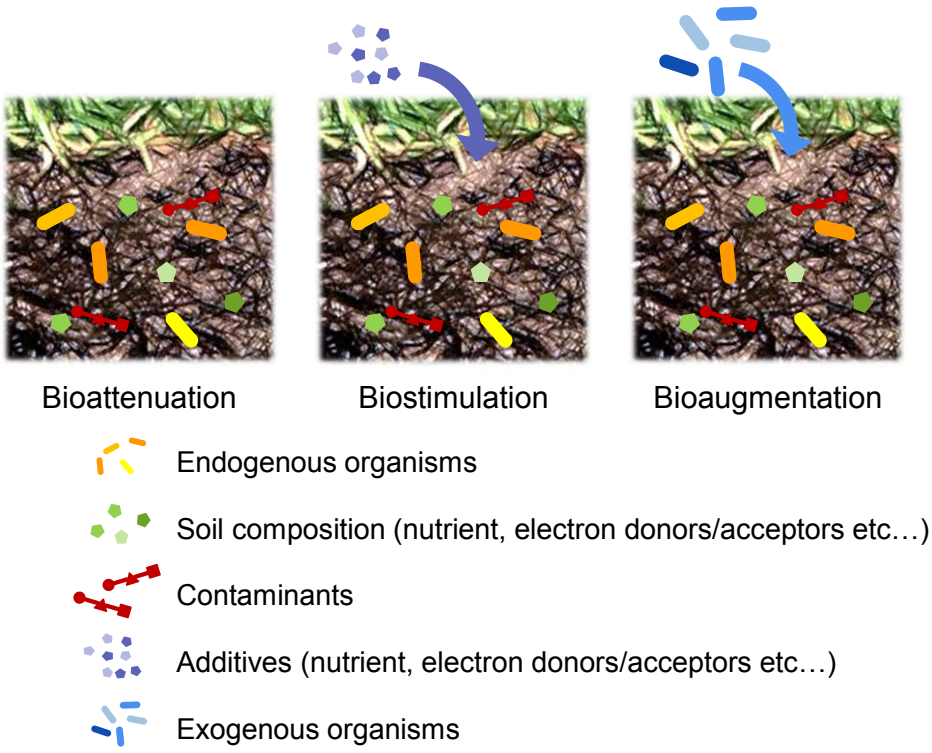

Figure I.8: Various approaches can be devised for bioremediation. Bioattenuation relies on natural degradation of the contaminants, while biostimulation consists in adding various chemical compounds to enhance degradation by endogenous microorganisms. Bioaugmentation relies the addition of microorganisms or microbial consortia in the polluted soil for remediation.

Understanding the mechanisms involved in bioremediation is essential to design organism-based soil depollution strategies. Three main approaches are generally distinguished regarding bioremediation, in particular microbial remediation: bioattenuation, biostimulation and bioaugmentation[1,52,66] (see Figure I.8).

One gram of soil is estimated to contain about 100 000 000 bacteria (up to 7000 species) and around 10 000 fungal colonies[16]. Such a rich biomass has a tremendous remediation potential and indeed one of the most common approach for soil remediation, bioattenuation, consists in exploiting the natural degradation capabilities of a given soil. In this case, the approach consists mainly in monitoring the evolution of the contaminant concentrations. This approach is often successful thanks to the adaptability of microorganisms which can use a wide variety of carbon sources but may also undergo selective evolution where most resistant strain prevail over strains which are not capable of degrading the considered contaminant. As a result efficient strains for the degradation of specific pollutants can often be isolated from the contaminated sites.

When the bioattenuation strategy is not efficient enough or too slow, various compound may be added to stimulate the natural metabolism of the endogenous microbial population. This general approach is called biostimulation and may consist in the addition of a wide range of compounds, including nutrients (carbon sources, nitrogen sources or electron donors and acceptors etc...)[103]. In some instances the initial pollutant may only be degraded as a cosubstrate. The soil may therefore need to be amended with a primary substrate to allow efficient remediation, which may itself be a contaminant such as toluene or phenol[104]. When considering aerobic degradation pathways, the oxygen content of the soil may be a limitation to the biodegradation efficiency. In this case, it is possible to inject oxygen in the soil. This specific type of biostimulation is called bioventing. As mentioned previously, bioavailability is essential for efficient biodegradation. Various chemical compounds may therefore be added to contaminated soils in order to enhance bioavailability, such as chelating agents for metals[105] or surfactants for hydrocarbons[61].

Even with favorable soil composition, some sites cannot be efficiently depolluted by the endogenous soil microbial population, either because the microorganisms are not intrinsically capable of metabolizing the specific contaminant or because the microbial population is too limited in number. Bioaugmentation approaches aim at introducing microorganisms within the soil to perform bioremediation. The organisms may be strains isolated from the site and cultivated to reach sufficient number or exogenous microorganisms selected for their known efficiency regarding the considered contaminant. These strains may for instance have been isolated from other sites contaminated by similar pollutants, or be genetically engineered strains[106,107]. In some cases microbial consortia may be design to take advantage of cooperative effects. For instance one organism may be chosen to enhance bioavailability of the targeted pollutant, another may metabolize the pollutant in question and another may produce nutrient to promote the metabolic activity or surfactants to enhance bioavailability. Introduction of microbial consortia may also be interesting in the case of co-contaminated

sites. Bioremediation is therefore a flexible and widely applicable strategy for depollution of contaminated soils. The approach has however some significant limitations.

I.1.b.iii Advantages and limitations of bioremediation approaches

As mentioned previously, one the main advantages of bioremediation is its versatility. The vast number of potentially degrading organisms and their uses in different consortia, as well as the possibility to add various nutrients and substrates makes bioremediation an option for the remediation of most contaminated sites. In addition, bioremediation approaches have been estimated to be competitive from the cost point of view, compared for instance to thermal or chemical treatments[2].

Most bioremediation strategies may be conducted both *in situ* and *ex situ*. *In situ* approaches are usually advantageous from the logistical and cost effectiveness perspective and may contribute to limit the environmental impact of the remediation process (no excavation, no destruction of fauna or flora). *Ex situ* approaches may however be favored when the soil must be amended with nutrients (biostimulation) or when parameters such as oxygen content or temperature must be controlled.

Table I.2: Biodegradability of different classes of chemical. Reproduced from Iwamoto *et al.*[2]

Chemical class	Examples	Biodegradability
Aromatic hydrocarbons	Benzene, tolune	Aerobic and anaerobic
Ketones and esters	Acetone, LEK	Aerobic and anaerobic
Petroleum hydrocarbons	Fuel oil	Aerobic
Chlorinated solvents	TCE, PCE	Aerobic (methanotrophs), anaerobic (reductive dechlorination)
Polyaromatic hydrocarbons	Anthracene, benzo(a)pyrene, creosote	Aerobic
Polychlorinated biphenyls	Arochlors	Some evidence, not readily degradable
Organic cyanides		Aerobic
Metals	Cadmium	Not degradable, experimental biosorption
Radioactive materials	Uranium, plutonium	Not biodegradable
Corrosives	Inorganic acids, caustics	Not biodegradable
Asbestos		Not biodegradable

The use of living organisms for depollution however presents some fundamental limitations. Bioremediation processes are often slow (from a few month to a few years) compared to physical methods for instance, and may therefore not be used when contamination must be

rapidly contained to prevent health risks. While a wide variety of contaminants can be degraded into nontoxic compounds, in some instances the metabolic pathways result in the formation of more toxic by-products[2,108]. Degradation mechanisms must therefore be studied in order to predict as accurately as possible the chemical intermediate likely to be produced during the degradation. Another possible limitation bioremediation is the fact that some types of chemical compounds cannot be degraded (see Table I.2). In the case of metal or radioactive compounds, this fact is inherent to the nature of the chemicals, and bioremediation suffers the same limitations as other remediation techniques. The compounds may be transformed into less toxic or less bioavailable forms and can be extracted from the contaminated sites (with phytoremediation for instance), but they cannot be fully degraded.

Another limitation of bioremediation processes is inherent to the use of living organisms. Contrary to chemical or physical processes, bioremediation phenomena are fragile equilibria. Some contaminants easily degraded when present in low concentration may be toxic to the microbial population at high levels. In other case, presence of co-contaminants may inhibit the metabolic activity of the considered metabolically active organisms. Living organisms may also be sensitive to other soil characteristics such as pH, temperature or salinity. One possible option to prevent such deleterious effects is to physically separate the microorganisms from the soil and high toxic compounds concentrations by encapsulating the cells within a compatible matrix[3,109].

I.2 About encapsulation

Immobilization of microorganisms in a matrix could provide valuable protection against deleterious effects of high contaminant concentrations or non-compatible physico-chemical characteristics of the soil. This leads to consider remediation approaches not as the use of biologically species but rather as the use of a full device which is the combination of a functional unit (the metabolically active organism) and of a structural part (the encapsulating matrix). The design of a cellularized material however cannot be considered solely from the material science point of view but rather with an approach integrating both material processing and biology. The main limitation is that structural requirements (for instance in term of mechanical properties or stability) may involve choice of materials or processes which are not compatible with living organisms.

When considering encapsulation in a matrix, several aspects must be addressed. The first aspect regards the composition of the matrix, which can be based on organic or inorganic compounds, but also be hybrid. The geometry and structure of the matrix must also be adapted to the targeted application. Whole cells (either eukaryotic or prokaryotic) have for instance been immobilized in different structures such as shells[110], films[111], beads[6], fibers[112] or gels[113] (see Figure I.9).

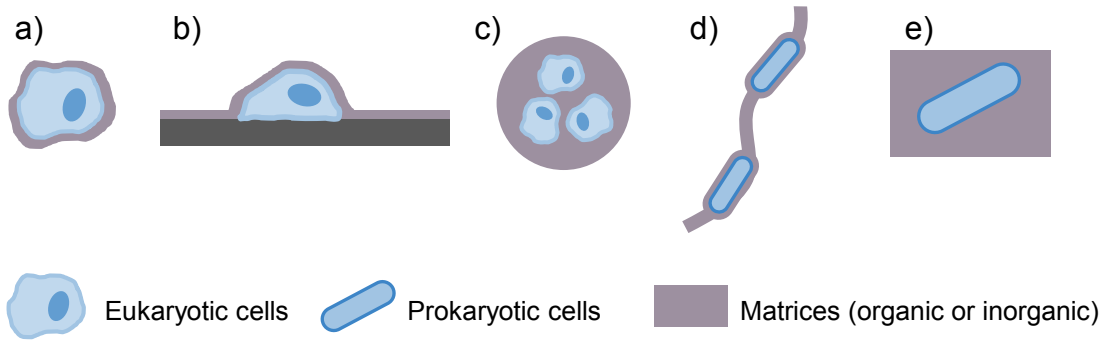

Figure I.9: Cells can be immobilized within matrices with varied geometries such as shells[110] (a), films[111] (b), beads[6] (c), fibers[112] (d) and gels[113] (e).

The choice of the composition of the matrices and the desired structure influences the requirements in terms of process, which in turn must be adapted to preserve the integrity of the encapsulate.

I.2.a What is encapsulation?

To understand the role of material processing in encapsulation approaches, it is first necessary to give a brief definition of the term encapsulation itself. Encapsulation is a type of immobilization, where the encapsulated species is entrapped within a matrix, as opposed to binding where the object is attached on the surface of the material. Binding approaches can be based on a wide range of interactions, either physical (hydrophobic, ionic, Van der Waals) or chemical (covalent bonds). However, species immobilized by encapsulation may be subjected

to further binding (for instance covalent). The distinction between simple binding and encapsulation is therefore not always clear, for instance when objects are immobilized on the pores surface within a porous material. The distinction may however be made not based on the final location or interactions between the immobilized object and the matrix, but rather based on the processing and shaping of the material. Sheldon[114] defined immobilization as attachment on a prefabricated support, while encapsulation requires formation of the matrix itself in presence of the encapsulate (see Figure I.10).

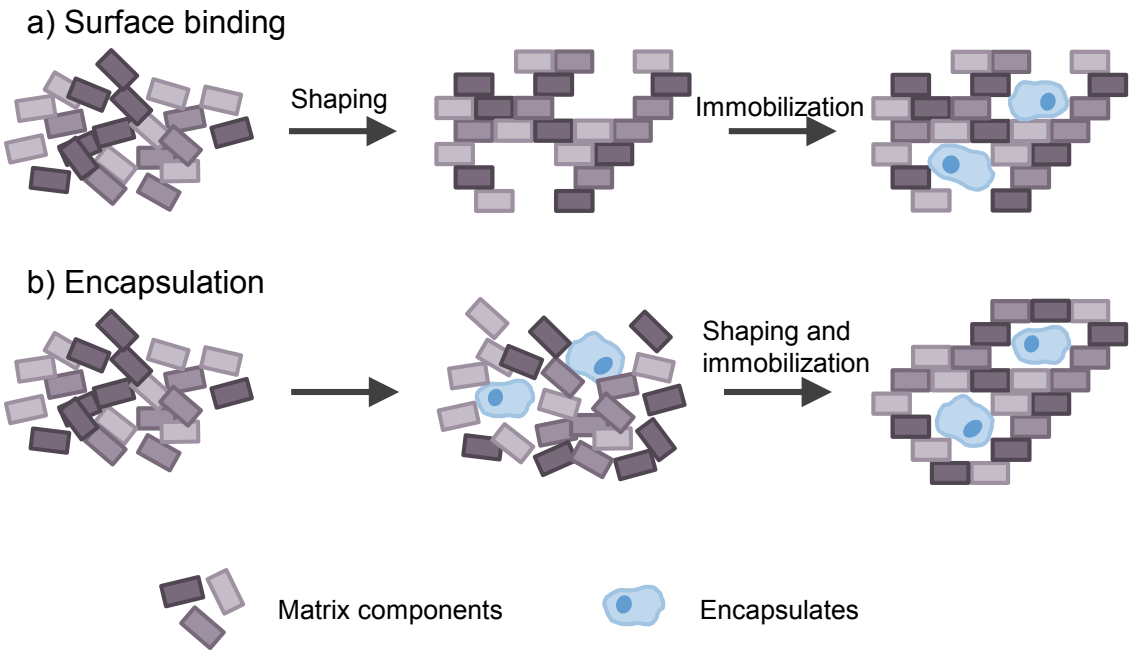

Figure I.10: In encapsulation approaches the immobilization matrix is formed directly around the object to immobilize (b), contrary to surface binding where the object is attached to a pre-existing support (a).

Immobilization and encapsulation techniques may be applied to a wide range of species, besides whole cells, with different goals, advantages and drawbacks. This includes encapsulation of simple molecules such as drugs or more complex ones (small polypeptide, DNA, various protein and enzymes), single cells (for instance animal cells or cells from higher plants) as well as whole organisms (microalgae, fungi, bacteria etc…).

Immobilization technologies were initially developed for enzymes with potential in the chemical industry. The need for greener and less solvent-consuming processes highlighted the interest of enzyme-based chemical synthesis[115]. First commercial use of immobilized enzymes was reported in Japan in the late 60s for racemic resolution of L-methionine[116]. Initial goals were to design efficient enzyme-based reactions and immobilization of enzymes proved to be efficient for thermal stabilization[117] of enzymes and long term storage[118]. In addition immobilization provides advantages for handling as well as to separate enzymes from products, resulting in increased reusability[119]. The drawback to immobilization of enzymes is often a drop in intrinsic activity compared to free enzymes, either due to modification in the structure of the enzyme or to diffusion limitations[120]. This may however be compensated by

the increase stability and reusability of immobilized enzymes[121]. Since these initial attempts, enzymes have been immobilized within a variety of materials (both organic and inorganic) and for a wide range of syntheses[122].

The knowledge about enzyme immobilization has been extended for encapsulation of a wide range of objects ranging from simple molecules or biomolecules to complex proteins and finally to whole cells and microorganisms. The variety in the type of encapsulates is due to the growing number of applications seeking to take advantage of Nature's efficiency while ensuring stability and reusability. But when considering encapsulation, especially for sensitive entities such as cells and microorganisms, there are also some limits. One key aspect when encapsulating living cells regards their long term viability. It is necessary to design matrices allowing the necessary substrates and nutrients to reach the encapsulated object[7]. When considering entrapped microorganisms, it may also be necessary to address the possibility of cell division since the cells are physically constrained within the matrix[123].

Encapsulation can actually be applied to very simple structures such as single molecules. In this prospect, the most relevant example of application is probably drug delivery[124]. In this case encapsulation in a well-chosen matrix may allow for the protection (for instance from pH variations in the digestive track) of the drug molecule until it reaches the intended delivery site. Another main advantage of drug encapsulation is the control it confers over delivery kinetics. Such delivery systems have also been used for more complex and also more sensitive molecules and biomolecules such as proteins[125,126] (for instance growth factors[127]). Encapsulation is now also regarded as a possible option for cell delivery[128,129]. In this case encapsulation may provide a valuable protection against immune response, since the encapsulating matrix can be tuned to act as a filtering membrane, allowing small molecules to go through while retaining larger molecules such as immunoglobulins[130,131]. Such approaches also lead to the design of artificial organs. Pancreatic islets have been entrapped in alginate as soon as 1980[4]. Encapsulation also allowed the design of artificial single cells, for instance by entrapment of DNA and protein synthesis machinery in alginate-silica-beads[132]. Another aspect of encapsulation relevant to biomedical applications is the design of sensors, one prominent example being the encapsulation of glucose oxidase as glucose sensor[133].

The use of sensors is however not limited to medical applications. Horseradish peroxidase has for instance been use as the functional unit in hydrogen peroxide sensors[134,135]. This system has been widely used as model for enzyme encapsulation, but other enzymes have also been used, for instance as a way to detect potentially harmful chemicals such as phenolic compounds[136]. Encapsulated whole cells, such as photosensitive plant cells or microorganisms sensitive to specific pollutants, have also been used for sensing[137].

Similar as the design of sensors, enzymes have also been used to design electrodes for applications in the domain of sustainable energy[138], but most popular encapsulates regarding the development of biological energy sources are whole cells. Both microalgae[139,140] and bacteria[141] have been extensively used as biocatalysts for fuel cells.

Various entities have also been encapsulated for applications in environmental science. Both enzyme[136] and cells (fungi[142], algae[143], bacteria[144,145]) have been used as sensors due to their high sensitivity and specificity. More than simple pollution monitoring immobilization technology has been used for bioremediation. Materials containing enzymes such as peroxidase have also proven to be of use for remediation of contaminants[146]. But conventional bioremediation is usually performed through the use of living organisms and especially microorganisms. The different cell types may benefit from immobilization from viability and stability point of view. As a result, various cellularized materials have been studied for remediation purposes, using biofunctional units such as bacteria[8,147,148], fungi[149], algae[150].
Encapsulation of biomolecules and cells is of use for a wide variety of applications from biomedicine to sustainable energy and environmental application. The main advantages of encapsulation are stabilization and protection of the encapsulated objects. Depending on the application, the matrix may also be tuned for permeability, to act as conductive material or be designed for controlled degradability for instance. Even if the encapsulated molecule or cell can be seen as the functional unit, as opposed to the matrix which is the structural part, both elements have significant influences on each other. As a result, the encapsulating matrix must be designed according to the targeted application and to the encapsulated entity. One key element of such designing process is the choice of the matrix composition.

I.2.b Encapsulation in biopolymers

Polymers and more specifically natural polymers (also called biopolymers) have been widely used for encapsulation of molecules, proteins (including enzymes) and cells (either eukaryotic or prokaryotic). Although biopolymers present some undeniable advantages from the encapsulation point of view, they also have some shortcomings from the material scientist's perspective.

I.2.b.i About biopolymers

Polymers are commonly referred to as biopolymer when they can be extracted or recovered from living organisms, whether they are animals (collagen)[151], plants (cellulose)[152], algae (agar)[151] and bacteria[153] (xanthan) or less commonly fungi (pullulan)[154]. Most of the commonly used biopolymers can be classified into the polysaccharide or protein categories. However it is worth mentioning that natural rubber (polyisoprene) or lignin (polyphenol) are also biopolymers.
The type of polymers present in an organism is dependent of the species, and even of the biological kingdom considered, even though they are no general and absolute rules. Plants and algae are generally composed of polysaccharides, although, as was mentioned earlier, lignin, one of the major components of wood is a polyphenol. On the other hand, most biopolymers in animals are proteins. One exception to this tendency is chitin which is a polysaccharide

mainly found in crustacean shells. Table I.3 is an overview of the most common biopolymers, their main sources and applications.

Table I.3: Sources and applications of most common biopolymers.

Type	Polymer	Main source	Applications	Ref.
Polysaccharides				
Anionic	Alginate	Brown seaweed	Food, biomaterials	155,156
	Agar	Red seaweed	Food, microbiology	157
	Carrageenan	Red seaweed	Food, cosmetics	158
	Pectin	Fruits (citrus, apple, beetroot…)	Food, beverage, biomedecine	159,160
	Xanthan	Bacteria	Food, cosmetics, pharmaceutic	161,162
Cationic	Chitin	Crustacean	Food, biomedecine	163,164
	Chitosan	Chitin derivative	Food, cosmetics, biomedecine	163,164
Neutral	Cellulose	Higher plant cell wall	Paper industry, biomedecine	152,165
	Starch	Corn, wheat, potato	Food, pharmaceutic	166167
Proteins				
	Collagen	Animals (cattle, porcine)	Biomedecine	168
	Gelatin	Collagen derivative	Food, biomedecine	168
	Fibroin	Silk (spider, moth)	Biomedical	169
	Zein	Corn	Textile, coatings	170
Polyphenol				
	Lignin	Wood	Paper, chemistry	171,172
Polyisoprene				
	Rubber	Hevea	Automobile, consumers goods	173

Contrary to synthetic polymers or proteins, polysaccharides (extracted from plants for instance) are often polydisperse. If the monomeric units corresponding to the various polysaccharides and the overall structures are generally well known, the fact that these polymers are extracted from natural sources induces variability in the structural composition. In fact biopolymers are usually rather families of macromolecules[151,174], with variabilities in structure or length depending on the source but also on the extraction methods and possible post treatments. This variability does not however impede the use of biopolymers for a large range of applications. Food industry is a major consumer of biopolymers, especially polysaccharides[175], due to their wide availability and general low cost. Polysaccharides such

as agar, alginate, pectin or xanthan are very widely used in the food industry either as stabilizing, emulsifying, gelling and thickening agents. Proteins are also of interest for the food industry. Gelatin is for instance one of the most commonly used gelling agents. But biopolymers have also been largely used for biomedical applications, from drug delivery to tissue engineering and surgery[168,176]. In this case, the intrinsic biocompatibility of natural polymers is a decisive advantage. Other industrial activities such as textile or paper are also important users of biopolymers such as cellulose and lignin[152,171]. Here the biopolymers are mainly used for their structural features.

Use of biopolymers is a general trend in many domains due to the growing demand for alternatives to synthetic polymers (especially petrol based ones). The need for eco-friendly and sustainable alternatives is responsible for a renewed interest in biosourced and natural polymers.

I.2.b.ii Advantages and limitations of biopolymer encapsulation

Encapsulation technology has also taken advantage of the possibilities given by biopolymers[5]. In nature, biopolymers are often found as structural materials[177]. Polysaccharides such as cellulose or pectin are found in plant cell walls and provide mechanical support[178]. In animals cells are usually comprised in an extracellular matrix composed of proteins (*i.e.* collagen). Biopolymers' initial function is therefore to be an encapsulating matrix. As a result, biopolymers appear as ideal candidates for encapsulation technologies, especially for medical applications, due to their wide availability, low cost as well as their intrinsic bio and cytocompatibility and biodegradability.

For several decades, alginate has been one of the most popular biopolymers for encapsulation[179–182]. In addition to the previously mentioned advantages, alginate can be crosslinked by divalent cations (including calcium) by forming "egg-box" structures[183] as a way to yield self-supporting gel materials. Encapsulation in crosslinked alginate was first reported in 1980 for immobilization of pancreatic islets[4] but has since been used to encapsulate drugs[184], biomolecules[125], enzymes[185], mammalian cells[186], fungi (including yeast[187]), algae[188] and bacteria[186].

Even if alginate is by far the most commonly used biopolymer for encapsulation, it is however not the only one. Chitosan[189,190] or pectin[191,192] have for instance been considered for cells[193] or enzyme immobilization as well as drug delivery.

The common point to all biopolymers used for encapsulation is their gelling properties. Since the polymer is here intended to be used as a structural unit (most commonly as microcapsules), gelation is necessary to provide self-supporting matrices. The intrinsic softness and toughness of polymers are both an advantage and a drawback from the encapsulation point of view. It provides a suitable environment for living cell and may be advantageous for tissue engineering applications, but might be problematic for applications where the matrix should provide protection against mechanical solicitation. This issue is also

linked to the question of degradability and especially biodegradability. For most medical applications biodegradability is a great advantage, especially for controlled delivery over long periods of drug or even cells. But this advantage becomes a drawback for applications in other domains such as energy or environment, where the stability of the matrix can be crucial.
One approach to control and tune these aspects has been the use of polymer composites including two or more biopolymers with different properties[194]. From the processing point of view, several biopolymers have the great advantage of being hydrosoluble. This is invaluable for encapsulation processes since cells can be directly dispersed in polymer aqueous solutions prior to shaping of the material.
In short, biopolymers appear as ideal candidate for encapsulation due to their bio and cytocompatibility. They can be shaped through a wide variety of approaches, but they suffer from shortcomings in terms of stability and mechanical properties.

I.2.c Encapsulation in inorganic matrices

Another approach, quite opposite to the use of biopolymers, for the encapsulation of cells and biomolecules is the use of inorganic compounds. Cells and biomolecules have been encapsulated in a wide range of compounds including metal oxides[113,133,195], carbonates[196], or layered double hydroxides[148,197,198]. One of the most common medium for encapsulation in inorganic matrices however remains sol-gel silica.

I.2.c.i About sol-gel silica

Silica (silicon dioxide) is one of the most abundant oxides in soil, but can also be found in mineralized organisms such as diatoms. If silica (for instance fumed silica or fused quartz) can be obtained through high temperature processes, the possibility to obtain silica materials at low temperature from a solution of precursors has attracted attention for more than a century. In 1844 J.J. Ebelmen first reported the phenomenon of hydrolysis of alkoxides in presence of moisture[199]. It is only decades later, around 1930, that materials were actually made by sol gel techniques as thin film by Geffken[200] or aerogels by Kistler[201]. It is only at the end of the 60s that interest in sol-gel approaches actually grew significantly. Sol-gel chemistry has since been used in wide range applications and with several types of metal oxides (for instance based on titanium, zirconium or aluminum). Depending on the targeted application, various types of materials can be obtained through sol-gel. Sol-gel syntheses rely on polymerization of precursors (small molecules) to form a colloidal suspension of silica particle called “sol”. The inorganic polymerization can be further controlled to yield precipitation of the silica particles (Stöber process[201]) or to result in the formation of hydrated gels, where silica forms a percolating network. Such gels can be further processed to remove the solvent. Depending on the drying techniques it is possible to obtain aerogels which retain

the initial porous structure of the gel (for instance using supercritical drying) or more condensed xerogels (see Figure I.11).

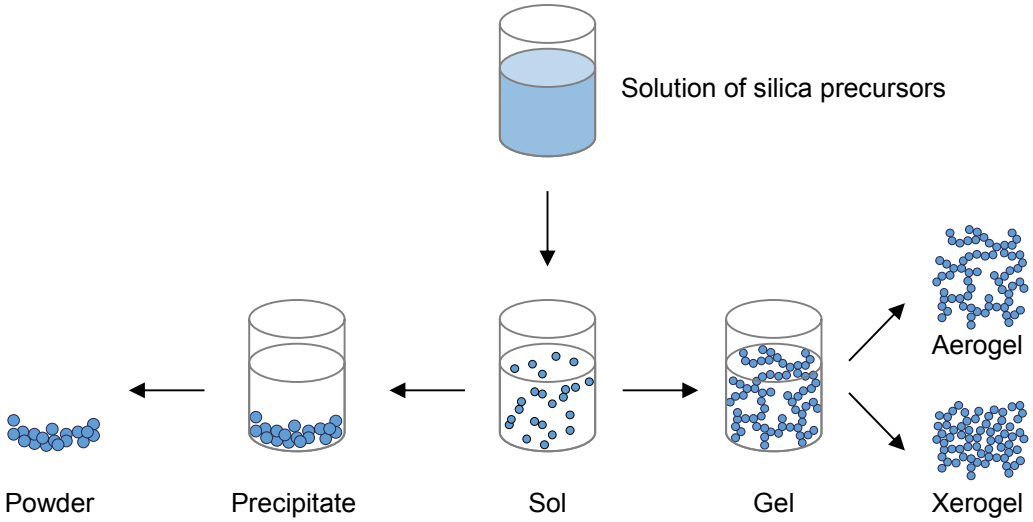

Figure I.11: Different types of silica-based materials can be obtained by the sol-gel process. Adapted from Owens *et al*[202].

Sol-gel processes are generally based on two main synthetic pathways: the alkoxide-based route and the silicate-based route. Synthesis of sol-gel based materials is commonly carried out using alkoxides, one of the most prominent examples being tetraethyl orthosilicate, also known as tetraethoxysilane (TEOS). Alkoxides can be functionalized by a wide range of reactive groups (including organic groups) as a way to tune the synthetic conditions and the final material properties. The formation of the inorganic polymer occurs in two steps (see Figure I.12). The monomers are first hydrolyzed. Total hydrolysis would result in formation of silicic acid, but in most sol-gel processes, hydrolysis is only partial. Hydrolysis may be catalyzed either by acidic or basic conditions. The hydrolysis is followed by condensation of the silicic acid to form oxygen bond resulting in the formation of oligomers and subsequently silica particles. Depending on the synthetic conditions, especially pH, nucleation or growth of the silica particles may be tuned resulting in different gel morphologies.

Another common synthetic pathway to obtain silica gels is the use of metal salts. One of the common precursors source for this approach are sodium silicates (waterglass) of general formula $Na_xSi_yO_z$. Sodium silicates can be found as solids or basic aqueous solutions, often as a mixture of various silicic oligomers. Gelling is obtained by neutralization of the suspensions resulting in the formation of a percolating network.

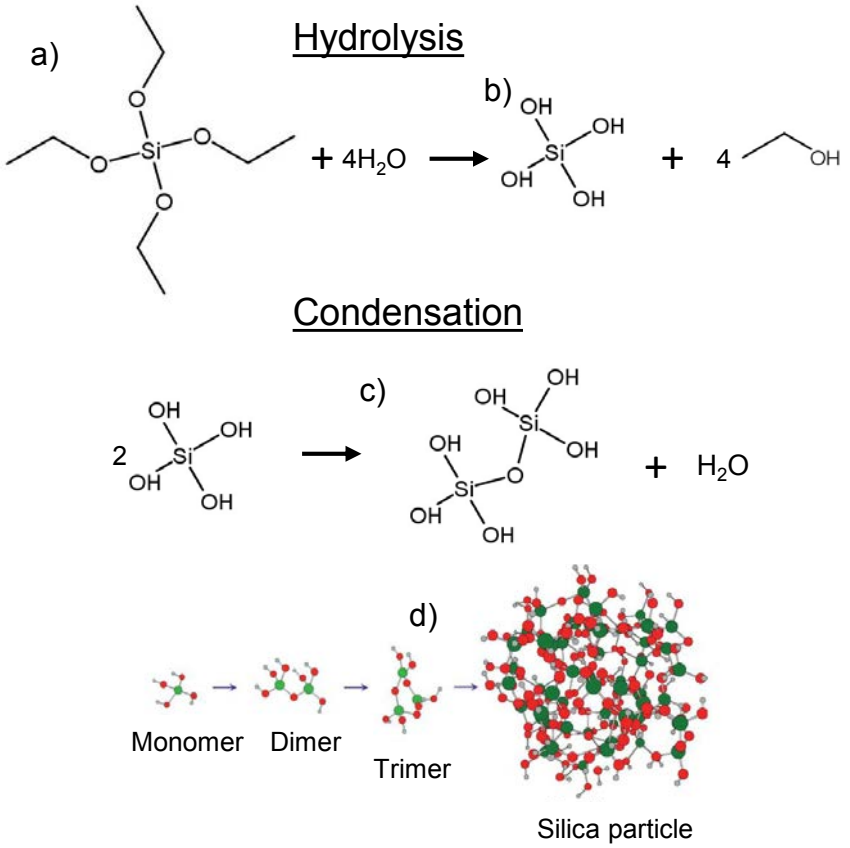

Figure I.12: TEOS (a) hydrolysis results in the formation of silicic acid (b). Silicic acid can then be condensed to form a silica network (c and d). Scheme d is reproduced from Wang *et al.*[203].

Both the alkoxide route and the aqueous route can be tuned in terms of gelling times, optical properties or mechanical behvior[137]. Parameters such as pH and temperature may have a significant influence regarding the gelation kinetics and the characteristics of the final material, but they are also of great importance for possible encapsulated biological entities.

I.2.c.ii Advantages and limitations of silica encapsulation

Given the mild conditions required for the formation of inorganic gels in sol-gel techniques, such materials have been used for immobilization of sensitive molecules such as dyes in 1955[204] or enzymes in 1971[205]. Silica gels have since been used for the encapsulation of various biological species including proteins[206], mammalian cells[207], plant cells[208], yeast[111], bacteria[113] or algae[209] (see Figure I.13). Fields of application include medicine (drug, protein and cell delivery[203,210]), biosensors[211] or environmental science[212].

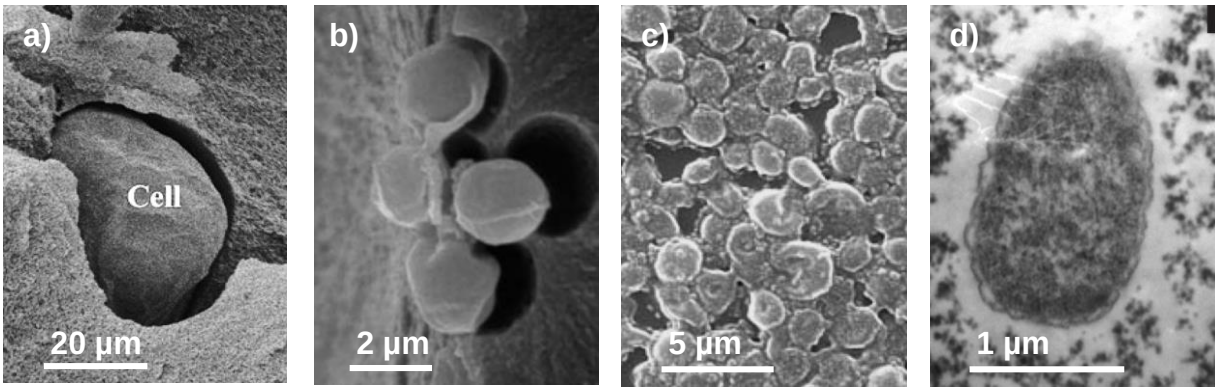

Figure I.13: a) SEM image of *Arabidopsis thaliana* plant cell in matrix prepared from sodium silicate and organosiloxanes (reproduced from Meunier *et al.*[208]), b) SEM image of *Chlorella vulgaris* algae TMOS-based network (reproduced from Darder *et al.*[209]), c) SEM image of *Pichia pastoris* yeast cell in a sodium silicate based matrix (reproduced fromGuan *et al.*[213]), d) TEM image of *Escherichia coli* in a gel prepared from LUDOX and sodium silicate in presence of glycerol (reproduced from Nassif *et al.*[113]).

Even though it is mainly part of the mineral world, silica has been used in the world of living organisms as protective shell by diatoms, which can be seen as form of encapsulation. Silica gels can therefore be seen as good candidates in the search of matrices for hosting living organisms. Cytocompatibility of silica has been demonstrated for a wide range of organisms, but the encapsulation process itself must also be designed carefully to prevent any deleterious effect to the encapsulated entity.

Sol-gel syntheses have the significant advantage of being conducted at low temperature (for instance at room temperature or 37°C, which is compatible with many cells). But depending on the chosen synthetic pathway, some other parameters are likely to induce toxicity. One of the most used precursors for sol-gel synthesis is TEOS. This precursor is widely available and can easily be hydrolyzed and condensed to form silica gels. However, ethanol is produced during the hydrolysis of TEOS, which is likely to be harmful to most cells. Use of alkoxides in general is subjected to the same limitation with production of the corresponding alcohols (methanol for tetramethyl orthosilicate, propanol for tetrapropyl orthosilicate etc…). Furthermore, hydrolysis of alkoxide is usually conducted under acid or basic condition, which can be highly deleterious for cell viaility.

One proposed way to deal with this issue is to resort to a two-step encapsulation. The chosen alkoxide is first hydrolyzed under conventional conditions. The formed alcohol is then removed and the sol is brought to neutral pH before addition of the considered cells[214,215]. Gelation takes then place to entrap the cells within the silica matrix. Alkoxide precursors themselves have also been modified to prevent release of harmful alcohol in order to ensure compatibility of the encapsulation process[216–218].

The use of the aqueous sol-gel route may be another alternative since gelation can be carried out at neutral pH and without production of alcohol[207,219,220]. This approach however implies the presence of high salt contents. Well-defined silica colloids (*e.g.* LUDOX®) have been added to silicates in order to form silica gels while maintaining low salinity. This however

results in lower stability of the gels. Such colloidal particles have therefore been associated with silicates to combine stability and low salinity[113].
Immobilization within a silica matrix (gels, films or dry porous materials) of biomolecules[221] or cells[212] has proven to be of interest regarding protection of the encapsulated objects for various applications. This however requires careful design of the encapsulation process since harmful by-product or physico-chemical conditions may be encountered. Immobilization within hard and brittle materials is however not very common in nature, since cells are usually entrapped within polymeric extra cellular matrices, which are often soft and tough materials. One way to combine the durable protection provided by silica matrices with the enhanced compatibility of biopolymer matrices is the design of hybrid materials for encapsulation.

I.2.d Encapsulation in hybrid matrices

Both organic and inorganic compounds have been used for the encapsulation of cells and microorganisms. Each type of compound possesses its own advantages and drawbacks from the functional and structural points of view. Another approach for encapsulation consists in combining organic and inorganic moieties in order to design materials with tailor-made properties (for instance in terms of mechanical behavior or processing options).

I.2.d.i About hybrid materials

In general the term hybrid refers to the mixture of two components with different properties. It is used in biology (for instance in botanic) to refer to mixing of two different species, often as a way to yield new or enhanced characteristics. In recent years it has also been used in the automobile domain to refer to cars combining two different energy sources as a way to combine sustainability and performances. Hybridization can therefore been seen as a way to take advantages of two different moieties (in terms of physico-chemical properties for instance) in order to gain new properties or enhanced properties.
The term hybrid is often implicitly used to refer to organic-inorganic hybrids. A distinction must be made between hybrid materials and composites materials. The most commonly accepted definition for composite materials is the association of a dispersed phase within a continuous phase (or matrix). The term hybrid is generally used to describe materials where the components are mixed at the nano or molecular scale. This may consist in a homogeneous blend or in a nano-scale dispersion. In this last case, hybrids are sometimes described as nanocomposites. Hybrid materials are commonly separated into class I and class II hybrids. In class I materials interactions between the two moieties are weak (hydrogen, Van der Waals, ionic etc..) while class II materials are characterized by covalent or ionocovalent bonds[222].
Creation of hybrid constructs can also be a way to finely tune physico-chemical properties of the final material such as mechanical and thermal behavior, stability, density, permeability, optical properties, hydrophobicity, biocompatibility etc…[223].

One of the major advantages in the design of hybrid materials is the flexibility it offers through the choice of the components themselves, but also due to the wide range of possible processing techniques. As a result of such versatility, hybrid materials have now become ubiquitous. They have been used in domains as varied as energy, health, housing, micro-electronics, micro-optics and environment.

In the domains of environmental science and medicine, a type of hybrid in particular has attracted a lot of attention. Hybrid materials based on biopolymers as organic moiety, also called bionanocomposites[224], present the advantages of conventional hybrids in terms of tunability and enhanced properties, but here the biocompatibility and biodegradability inherent to biopolymers may also be exploited. The addition of an inorganic moiety allows for control over the main limitations of biopolymers (low mechanical strength and low stability)[225]. From the processing point of view one type of inorganic compounds has been especially favored. Metal oxides in general and more specifically sol-gel processes seem especially relevant for controlled synthetic approaches of metal oxide-biopolymer hybrids[226]. Among this family of compounds, silica based materials are especially prominent.

From a structural point of view, silica-biopolymer hybrids are distributed between two extreme organizations.

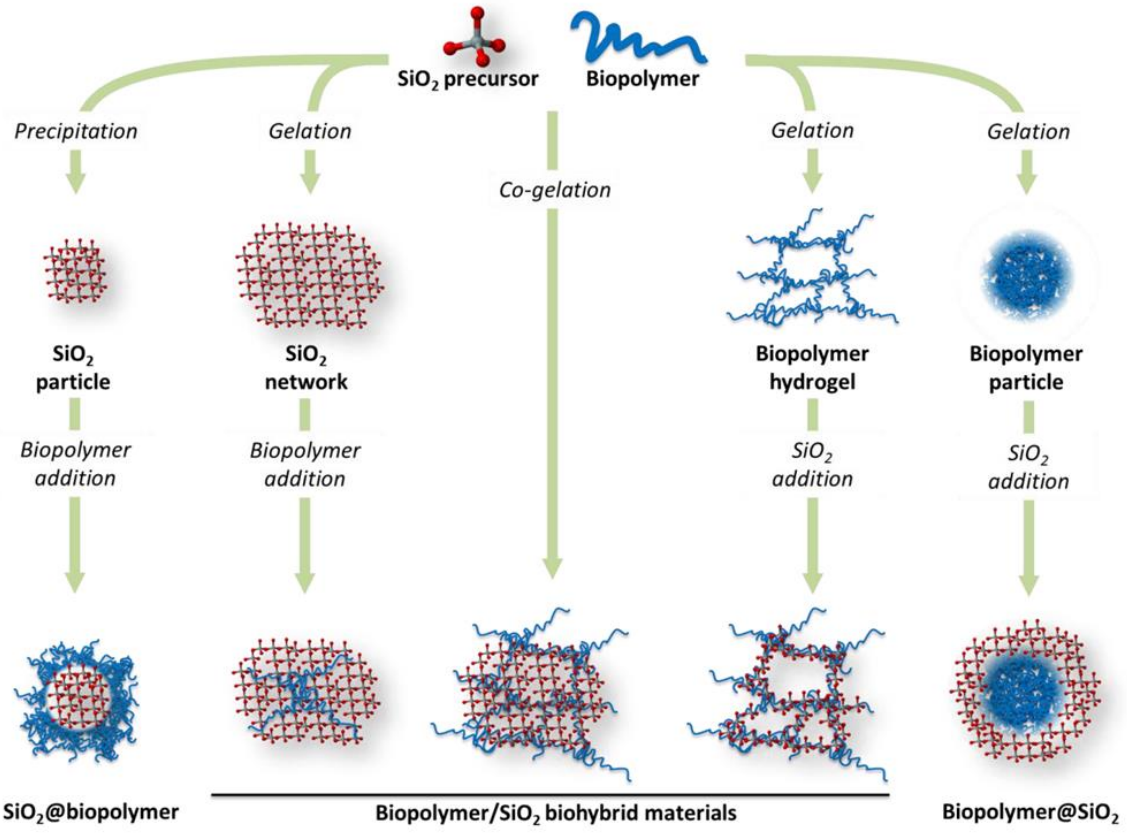

Figure I.14: A wide range of architectures can be obtained for silica-biopolymer hybrids. Reproduced from Christoph *et al.*[227].

On the one end of the spectrum are the materials composed of a biopolymer matrix in which the inorganic moiety is dispersed. On the opposite end of the spectrum are inorganic matrices containing a biopolymer phase. Core-shell particles (either biopolymer@silica or silica@biopolymer) can be seen as specific cases of hybrid compounds, although they do not constitute a material from the macroscopic point of view. Control over the gelation of both the inorganic and organic moieties is key to obtain the desired architecture (see Figure I.14).
As was mentioned previously, one of the most widely used biopolymers is alginate, mainly due to its wide availability, non cyto-toxicity and gelling properties. This trend is also found in the design of silica-biopolymer where silica-alginate constructs have been used for numerous applications[228,229]. Silica has however also been associated otherbiopolymers including pectin[230], chitosan[231] or collagen[232]. The nature of the biopolymer is of paramount importance since it has a direct influence on the interactions between the organic and inorganic moiety, which in turn is determinant for both the structure and function of the final hybrid material[233].
Since both composition and shaping of the hybrid materials have significant impact on their final properties and characteristics, these two aspects represent keys to design tailor-made materials for specific applications.

I.2.d.ii Use of hybrid matrices for encapsulation

Silica-biopolymer hybrids and nanocomposites are especially favored for applications in medicine or environmental science. The flexibility, tunability and biocompatibility of silica-biopolymer hybrids make them excellent scaffolds for cell growth[234]. In addition the use of nanocomposites is a good way to control the mechanical characteristics of the materials without significant changes of the surface chemistry, which is of great importance for cell growth[235]. Silica-biopolymer bionanocomposites have also been used in depollution applications as adsorbing materials[236]. The use of silica and biopolymers ensures good eco-compatibility since both components are present in nature.
Hybrid biopolymer-silica matrices have also largely been used as encapsulation matrices for various biological entities. In this case the system become even more complex since they comprise an inorganic and an organic structural moieties, as well as the biological functional entity.
Advantages of encapsulation in silica-biopolymer hybrids are similar to the ones mentioned for the individual moieties concerning stabilization and protection. However combination of the organic and inorganic moiety usually allows for a minimization of the shortcomings while preserving or enhancing the advantages. Such materials may for instance have the advantages of the biopolymers in terms of bio and cytocompatatibility, but with enhanced mechanical properties provided by the silica moiety. Parameters such as the stiffness or the biodegradability of the material, as well as the general geometry (beads, fibers, monoliths etc…) and morphology (porosity or architecture of the different phases) must be tailored

depending on the targeted application. In addition to the tuning of the structural part, the functional entity (enzyme, animal cells, plant cells, microorganisms) must also be chosen according to the desired application.
First encapsulations in hybrid matrices were performed using enzymes, immobilized within alginate bead and subsequently coated with silica[237]. Such encapsulation provided protection against thermal and chemical denaturation, while the presence of silica ensured mechanical robustness. This type of system has since been used for the encapsulation of various biomolecules and cells[6]. The synthetic pathway itself could be tuned using bioinspired silica deposition[131]. Alginate-silica bead have further been used for immobilization of bacteria[238], mammalian cells[239], fungi or microalgae[240]. However depending on the targeted application other biopolymers can be associated to silica as encapsulating matrices (including chitosan[117], collagen[241], xanthan[242] or pectin[243]). Applications for silica-biopolymer-based biohybrids range from protein and cell delivery[241], energy production[244] or biosensing[245] to environmental science[8,246].
Despite the wide range of available biopolymers and the flexibility of the available processing techniques, most encapsulation routes require gelation of the biopolymer, often as micro beads[247]. The functional entities remain encapsulated within hydrated gels, which may be problematic from storage and handling point of view. In addition, in the case of immobilized cells, the porosity of the matrix is essential to provide the encapsulate with necessary nutrients. This is especially relevant for applications in environmental science, where it is essential that the substrates diffuse to the functional encapsulated species. For such devices, the micro and mesoporosity is important to allow molecular diffusion while preventing cell leaching.

I.2.e About encapsulation of living organisms in hybrid materials for soil bioremediation

As was demonstrated, encapsulation is a widely applicable strategy. Encapsulation processes can be characterized and classified depending on several criteria including the nature of the encapsulate, the nature of the matrix or the targeted application. These different interrelated aspects must be considered in the design of an encapsulation strategy.
This work focuses on the elaboration of cellularized hybrid materials for soil bioremediation.
The relevant domain of application (environmental science), the type of encapsulate (metabolically active microorganisms) and the class of matrix (hybrid materials) have all been separately addressed in various works. The combination of these three specific characteristics have however more rarely been reported.
Encapsulation processes have been used for environmental science in two main ways: for the development of sensors[143] and for bioremediation strategies. The bioremediation approaches may rely on the encapsulation of enzymes[146], but the use of encapsulated cells is most commonly reported. A wide variety of organisms (mostly bacteria and algae) relevant to bioremediation have been encapsulated in either organic (including gellan-gum[248], polyethylene oxide/polycaprolactone/polyethylene glycol composites[147] or polyethylene

glycol and poly(vinyl alcohol) fibers[249]) or inorganic matrices (mainly silica[250,251], but also layered double hydroxides[148] for instance). Encapsulation in hybrid materials has been widely developed for enzyme immobilization. Examples of microorganisms relevant to bioremediation encapsulated within hybrid materials are however scarce.

The bacteria *Pseudomonas luteola* has been immobilized in alginate-silica beads for the remediation of Reactive Red 22[8]. Similarly, cyanobacteria *Nostoc calcicola* was entrapped in silica-coated alginate beads for metal adsorption[246]. An alginate-silica matrix was also used for the immobilization of *Stereum hirsutum* to remediate malachite green[149]. The efficiency of these functional materials was however assessed for water treatment. *Pseudomonas fluorescens* encapsulated within alginate-bentonite clay nanocomposite[109] was reported to have enhanced survival rates in soil, but the potential of the cellularized material for bioremediation was not assessed.

One of the main difficulties regarding the use of encapsulated microorganisms for soil bioremediation is related to diffusion limitations and substrate transport. The use of a porous encapsulation matrix could be beneficial to favor such phenomena.

I.3 Encapsulation by freeze-casting

Freeze-casting has been used for a few years to design porous material and more specifically materials with an oriented porosity. Such a structure can be a way to favor capillary mass transport within the material.

I.3.a Shaping using ice as a template

I.3.a.i About freeze-casting

Freeze-casting is a processing technique relying on the use of ice-crystals as templates for the shaping of porous materials. Due to the very low solubility of most compounds in ice, freezing of a solution, suspension or slurry usually results in a segregation phenomenon. As a result the particles or solutes are repelled and concentrated by the growing ice crystal. The phenomenon has for instance been described in the literature through the observation of freezing seawater[252], but such behavior is actually ubiquitous in nature[253]. While the templating capabilities of growing ice may be deleterious in many cases (for instance damages caused to soils and roads in winter or freezing of cells[254]), it represents an interesting tool from the material scientist's perspective. First reports of the use of ice crystals as a way to shape materials dates from 1954[255], but the technique of freeze-casting (which has also been called ice-templating, freeze-gelation or even ice segregation induced self-assembly[254]) has mainly attracted attention during the last decade (Figure I.15).

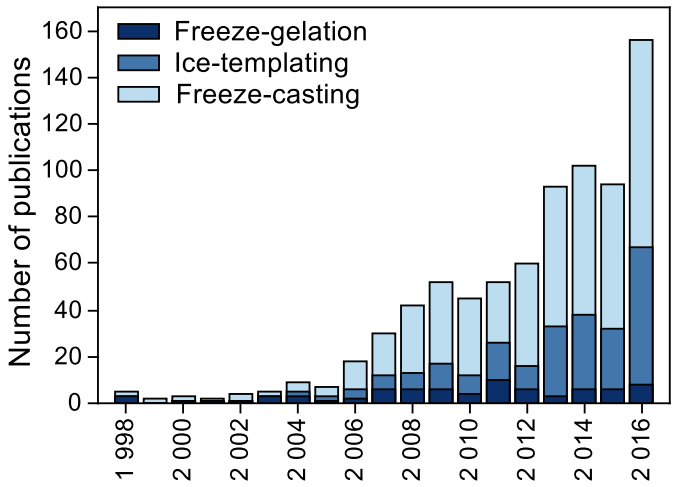

Figure I.15: Number of publication related to the keywords freeze-gelation, ice-templating and freeze-casting. Results collected from Web of Science database (retrieved in July 2017).

Freeze-casting is indeed an easy-to-implement way to obtain porous materials. One of the specificities of freeze-casted materials is that oriented porosity can be obtained using the appropriate freezing-setup. Another advantage is that it can be used for processing of a wide variety of materials, from ceramics and metals to polymers. The principle is to freeze a solution, suspension or slurry in order to grow ice-crystals which are subsequently sublimated

to free the desired porosity. Due to the low solubility of most compounds in frozen water, segregation occurs during freezing resulting in the formation of ice crystals on the one hand (which will become the pores after drying) and of the pore walls shaped by the growing ice crystals on the other hand (see Figure I.16).

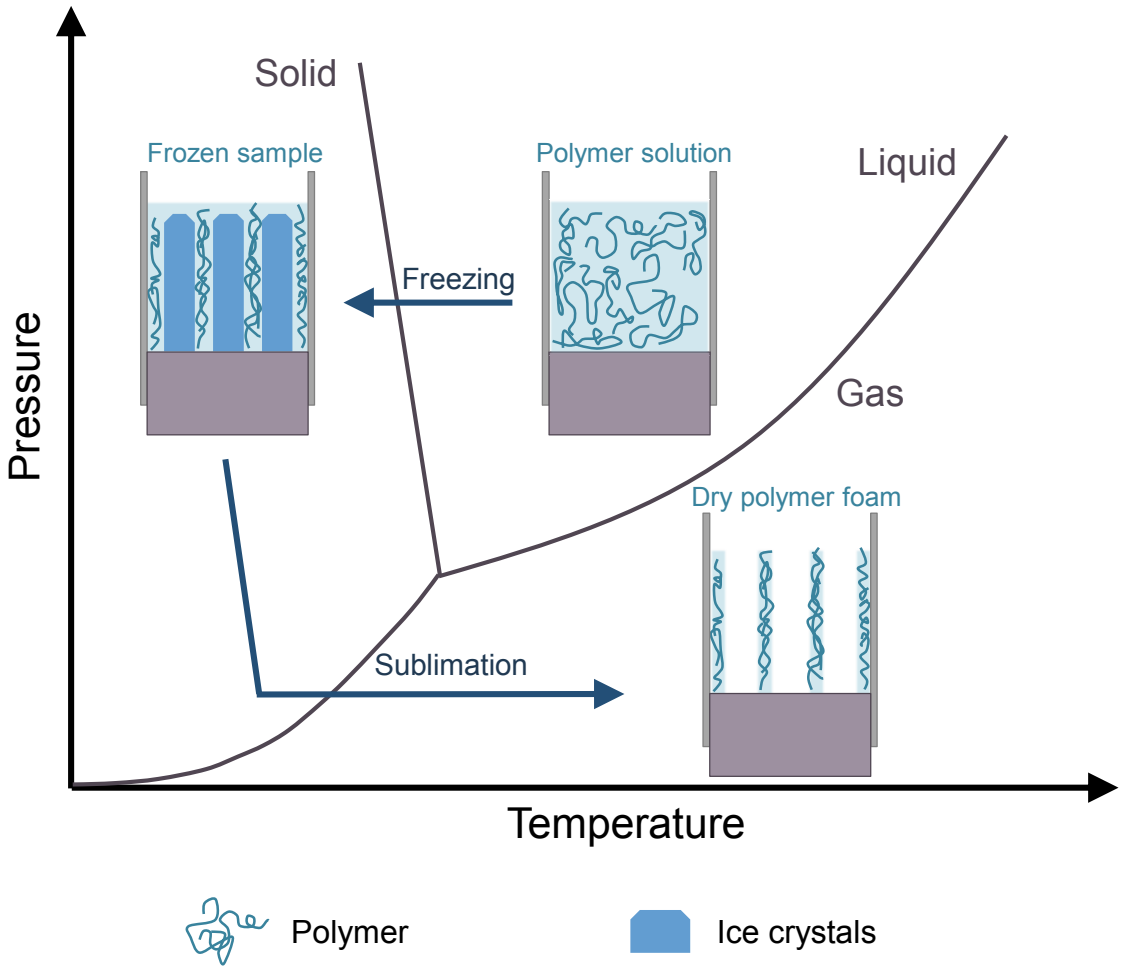

Figure I.16: Polymeric porous materials can be obtained by unidirectional freezing and subsequent lyophilization of and aqueous polymer solution. Adapted from Deville[256].

One of the major advantages of ice-templating is the control it confers over the pore morphology of the final material. The porous structure can be tuned through a wide variety of parameters which can depend on the setup used (control of the temperature gradient) but also on the composition of the frozen solution or suspension (solvent, particles size, additives etc…).

The shape and orientation of the pores can be tuned by controlling the ice nucleation and growth. In order to obtain aligned and oriented porosity a temperature gradient must be established within the sample. A simple way to obtain such gradient is to plunge samples in a liquid nitrogen bath at a chosen speed. In this case however the cooling temperature is set to -196°C. A common freeze-casting setup is therefore composed of a heat conductive material (copper, aluminum etc…) in contact with a cold source (such as liquid nitrogen)[257]. Addition

of a heating resistance allows for precise control of the heat-conductive element's temperature. The desired solution or suspension is poured in a mold and put in contact with the cold finger to establish a temperature gradient. As a result ice-crystals will nucleate at the interface with the cold element and grow along the temperature gradient (see Figure I.17). Although such setup is commonly used, it is far from being the only possible configuration. For instance systems with two cold sources have been used for better control of the temperature gradient[258,259].

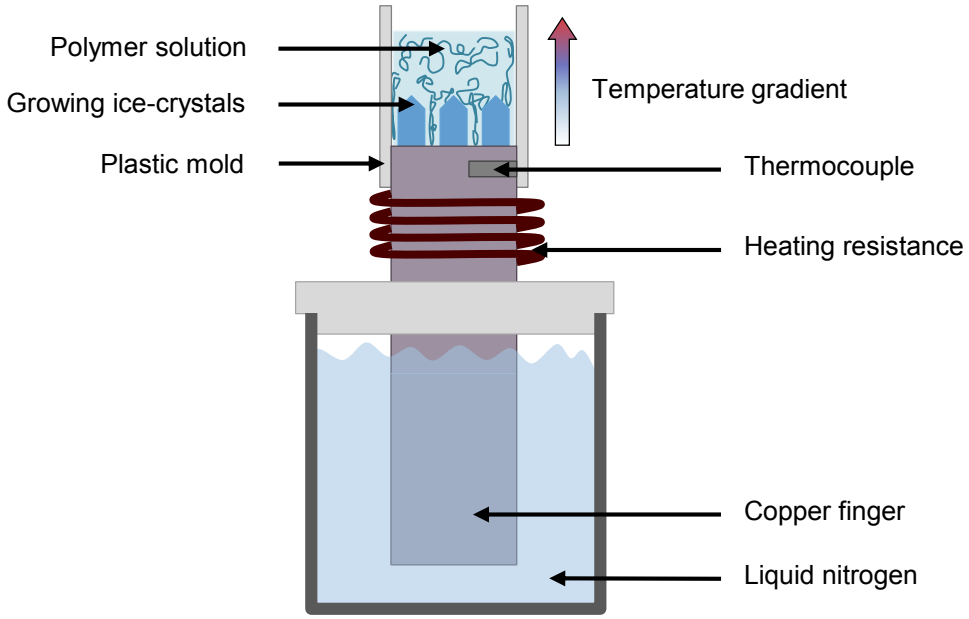

Figure I.17: Unidirectional porosity can be obtained by applying a chosen temperature gradient to the sample.

Use of such a setup allows for a precise control of the temperature both in time (a chosen temperature ramp can be applied) and space (the orientation of the gradient is well defined). The temperature gradient has a direct influence on the freezing-front velocity which is key to the control of the size of the pores[260]. In addition to the influence of the temperature gradient, freezing-front velocity is also largely dependent on the thermal properties of the solidified phase, that is to say on the composition of the initial solution or suspension[257]. Formulation of the initial slurry is key to control the freezing front velocity, but may also influence a wide range of characteristics likely to modify the final porous structure.

As mentioned previously, ice-templating can be used with a wide variety of compounds since it mainly relies on physical interactions. It has for instance been used for shaping polymer solutions[261], or more recently for metals[262]. The method has also been extensively used for shaping of porous ceramics, including silica[263] and alumina[260]. Depending on the interactions between the templated colloids, further sintering or densification may be required after sublimation of the ice-crystals to yield satisfying mechanical properties. Use of a binder (for instance polymer in ceramic slurries) may also be a way to obtain structural integrity of the materials[264]. All the components of such complex suspensions must be carefully selected in order to ensure control over the desired pore morphology.

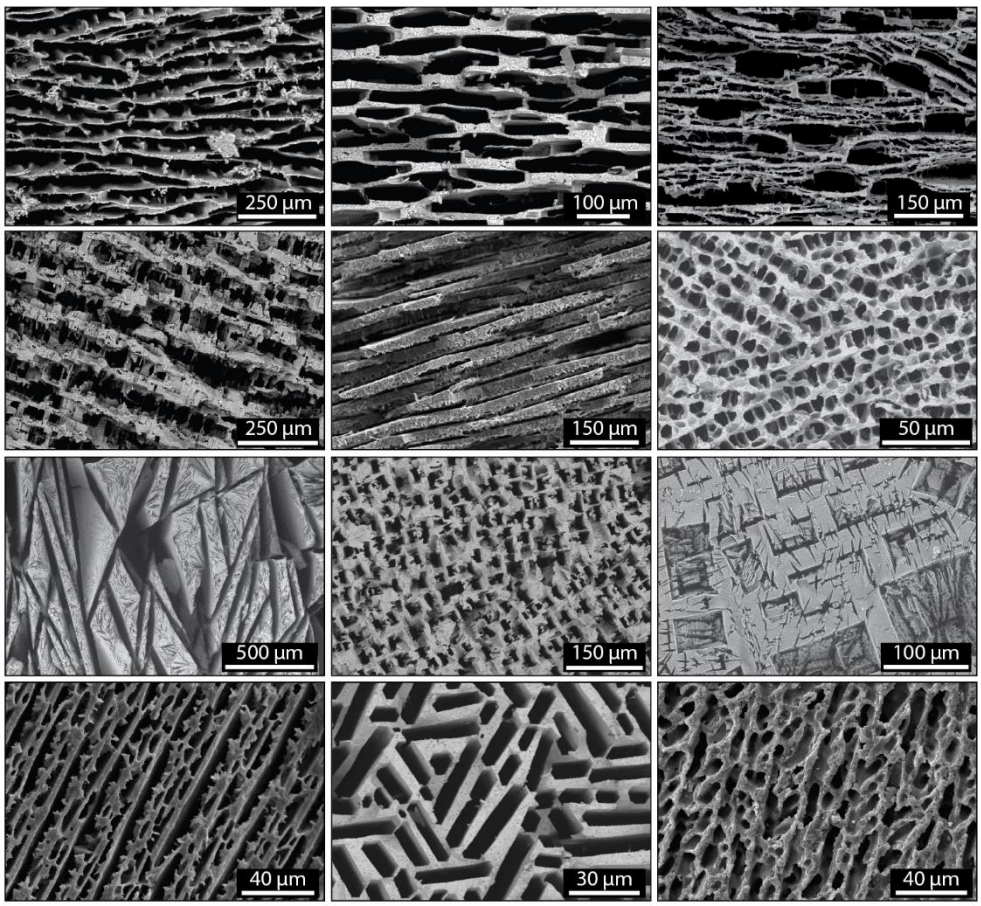

Figure I.18: A wide variety of morphologies can be obtained for freeze-casted porous ceramic by tuning the formulation of the initial slurry (solvent, binders, dispersants, solid loading and pH). Reproduced from Deville[265]

The first element to be selected is the compounds on which the material will be based (for instance the type of polymer or of ceramic). The chemical composition is relevant since it may affect interactions between the colloids, as well as the particle-solvent interactions. The chemical nature of the freeze-casted components is however far from being the only relevant parameter. Figure I.18 illustrates the variety of morphologies which can be obtained for ceramics by changing parameters such as solvent, binders or solid loading.

The characteristics of the particles themselves are also critical in the morphology of the final material. Most commonly, such particles are hard (as is the case of ceramics), but it is also possible to apply freeze-casting to soft particles (such as polymer particles or even cells). In the case of ceramic processing, which has been one of the most studied materials, the properties of the slurry are very dependent on the size[266], shape[254,267] and density of the particles. Usually these parameters are chosen in order to prevent sedimentation phenomena, although these can be taken advantage of to create gradients within the final porous material. Regardless of the nature of the colloids, another crucial parameter is the concentration (or solid loading) within the initial slurry[268]. It may influence the final density (and mechanical properties) of the material, but is also relevant to the freezing process itself since it is likely to modify the viscosity or freezing point of the liquid sample.

Water is most often used as the solvent to disperse polymer or ceramic particles. Use of dispersant is often required to obtain stable suspensions. The nature of the solvent used is one of the most important parameter in the design of freeze-casting systems, since it largely influences the crystal nucleation and growth, which is the driving force of ice-templating. In the case of water, one of the most commonly observed morphology is composed of lamellar and well aligned pores, often organized in orientation domains[269]. In some cases, this can be linked to the hexagonal crystallographic structure of ice and to the fact that ice growth is favored along the a axis compared to grow along the c axis[256] (see Figure I.19), however depending on the composition of the initial suspension and freezing conditions, ice growth mechanisms are often much more complex. Depending on the ice growth, morphologies such as microhoneycombs can also be obtained[270].

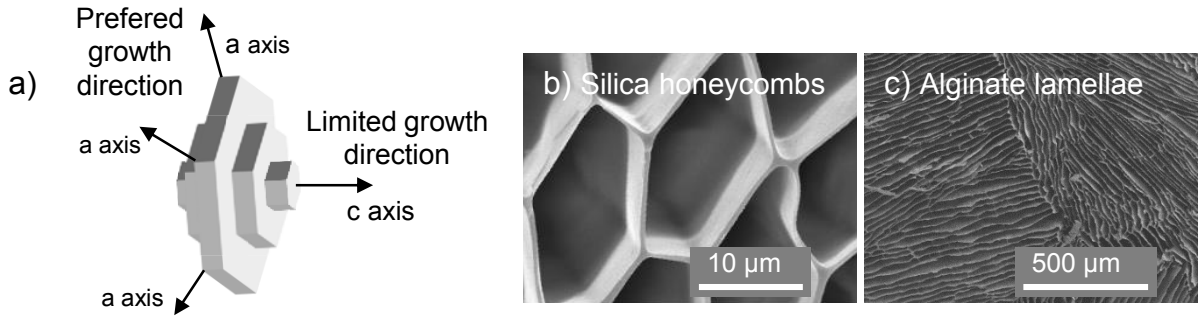

Figure I.19: (a) Hexagonal ice crystals grow preferentially along the a axis resulting in honeycomb (b) or lamellar (c) pore morphologies. (a) reproduced from Deville[256], (b) reproduced from Mukai *et al.*[271], (c) reproduced from Christoph *et al.*[187]**.**

The presence of additives[272] such as dispersants, common cryoprotectants (sucrose[273], glycerol[274]) or binders (such as polymers[275,276]) is likely to modify the ice nucleation and growth and therefore the porous structure of the material. It is however difficult to predict the effect of such modifications[277] since the additives are likely to impact many parameters simultaneously (ice growth, viscosity, freezing point etc…). The use of a different solvent may also provide access to original shapes of pores. Camphene-based freeze-casting has for instance been used to obtain dendritic pore morphologies[278,279]. Fishbone-like structures have been obtained by freeze-casting in liquid carbon dioxide[280].

The ice growth can therefore be tuned through a variety of approaches, but ice nucleation and the initial stages of growth are also of tremendous importance for the final morphology. Ice undergoes a non-lamellar growth phase before attaining a steady-state growth regime. A transition from an initial planar ice front to a lamellar ice morphology results from destabilization of the solid-liquid interface due to the accumulation of solutes at this interface. As a result, areas with different pore morphologies can be observed close to the interface with the cooling element[260]. Such morphology heterogeneities have been minimized by modifying conventional freeze-casting setup by the introduction of a tilting angle of the cooling element[281]. Importance of the interface with the cooling element has also been demonstrated through modulation of the final pore morphology thanks to patterning of the cold finger[273].

In short, a large number of often interrelated parameters (both from the setup and formulation points of view) are susceptible to influence the porous morphology of the final materials. The comprehension of their influence is key[282] to gain control in the precise design and tuning of materials with a wide variety of structures.

I.3.a.ii Range of application

As mentioned previously, ice-templating processes can be applied to a wide range of compounds[283] to yield a great diversity of structures. Such versatility has opened the way for the use of freeze-casting in many applications. Each class of materials has its own specificities in terms of shaping even if the principle (use of ice crystals as templates) remains the same.

One of the major uses of freeze-casting techniques is for shaping of ceramic compounds[256] (including alumina[260,284,285], silica[271,286], titania[287,288], zirconia[289,290], clays[291,292], calcium phosphate[293] and hydroxyapatite[294–296]). Polymers, and water soluble polymers in particular, have also extensively been shaped though ice-templating. In this case, instead of a suspension of hard particles, the frozen medium is a solution of dispersed macromolecules. The interest of the use of macromolecules is that the lyophilized materials are usually self-supporting and do not require further treatment. Examples of freeze-casted polymers include biopolymers (alginate[297], cellulose[298,299], chitosan[300], collagen[301], gelatin[302] or silk[303]) but also synthetic polymers like poly(vinyl alcohol)[304,305] or poly(lactide-co-glycolide)[305]. Carbon-based materials have also been shaped by freeze-casting to yield ultralight aerogels with conductive properties, for instance using multi-walled carbon nanotubes[306,307] or graphene[308,309]. Metals have also been shaped through ice-templating, either from metal particles[262] or metal precursors[310]. As is the case for ceramic particles, the choice of the particles and dispersants is crucial for the control of the final porosity of the material in order to avoid sedimentation. In the case of metals however, the question of oxidation must also be considered for metals such as iron[311], titanium[262] or copper[312] but can be avoided using stable metals (gold[313], silver[314] or stainless steel[315] for instance).

Some of these materials can be shaped individually, but in some cases it may prove interesting to combine them. Polymers have for instance been added to ceramic suspensions[264,275] (as binder or in order to modify the final morphology). But the combined use of different component can also be a strategy for the elaboration of composite materials (either by simultaneous ice-templating of the different moieties[292] or by freeze-casting of a structure and subsequent infiltration[314]). Such composites may have original architectures[259] or properties[316] (for instance mechanical behavior[317] or conductivity[318]).

Such diversity opens the ways for uses in fields ranging from biomedical application to energy, environmental science or housing materials. Ceramic based materials are for instance of interest when high mechanical, thermic or chemical stability is required. This includes, among many other applications, thermal insulation[290,319], catalytic supports[287] or biomaterials[296]. Biopolymer[304,320] or biopolymer-based composites[234,321] porous materials

have been largely favored for applications in biomedicine. The use of scaffold with an aligned porosity is particularly interesting for cell oriented growth[322]. Ice-templated materials have also be used in the environmental domain, for instance as absorbents[323–325].
Freeze-casting has proven to be a widely applicable technique for shaping numerous compounds. The process can be tuned through a variety of parameters (setup, freezing rate, composition, presence of additives, type of solvent etc…). The versatility of this technique which is both straightforward and highly tunable has allowed for the design of materials with tailor-made properties (chemical interactions, mechanical behavior, thermal stability etc…) for specific applications.

I.3.b Freezing and drying cells

Freeze-casting can be applied to many compounds, including polymers and inorganic moieties, commonly used for biomolecule or cell encapsulation (for instance alginate[297] or silica[326]). The aligned porous structure of the materials has proven to be interesting for various applications since it may provide oriented support for cell growth or facilitate mass transport in adsorption mechanisms. Furthermore, most freeze-casting approaches use water as solvent which is an advantage from the cytocompatibility point of view.
Freeze-casting therefore appears as good candidate for original encapsulation procedures. There are however only few examples of encapsulation of biological entities within freeze-casted materials, which may partly be attributed to the challenge that is the freezing of biological entities.

I.3.b.i Encapsulating cells by freeze-casting

Requirements are different for encapsulation of simple molecules such as drugs, biomolecules (including proteins) or cells (animal cells, plants cells, microorganisms such as yeast or bacteria).
Polymer-based freeze-casted materials have been used for entrapment and release of drug[304,327,328]. Control of the porosity and morphology of such structures allows for good control of the release rates (by erosion of the matrix or swelling and dissolution of the drug), which is a key feature of most drug delivery devices. In the case of water soluble drugs entrapment can easily be achieved by dispersing the drug molecules in the initial suspension. Freeze-casting has also been used for the encapsulation of more complex molecules such as enzymes[329] by ice-templating of a PVA-protease mixture. In this case the structure of the matrix can be tuned as a way to maximize mass transport which could be of great interest for the design of high-yield bioreactors. As is the case for drugs, the homogeneous encapsulation of enzymes is facilitated by the fact that the molecules can be efficiently dispersed in the aqueous carrier solution (often polymer)[330]. In the case of enzymes however, the molecules are much more sensitive to their environment and the composition of the matrix must be

designed to preserve the structure and enzymatic activity (for instance by using a polymer moiety). The issue of preservation is even more essential when contemplating the encapsulation of more complex structures such as liposomes[331] or cells.
Bacteria in particular have be entrapped in freeze-casted ceramic[332], multiwalled carbon nanotubes[307] or polymer structures[10]. From a structural point of view entrapment of cells is not as straightforward as it may seem. Cells can be seen as soft and deformable particles to be entrapped between the growing ice lamellas. Mechanisms of sedimentation, entrapment or rejection by an advancing ice-front have mainly been studied in the case of ceramic particles[257], but the general mechanisms can be extended to the case of soft particles such as cells or bubbles[333]. Such behavior strongly depends on various parameters such as the ice front velocity, the viscosity of the carrier solution, the size and density of the particles or the interaction between the particles and the ice front (see Figure I.20).

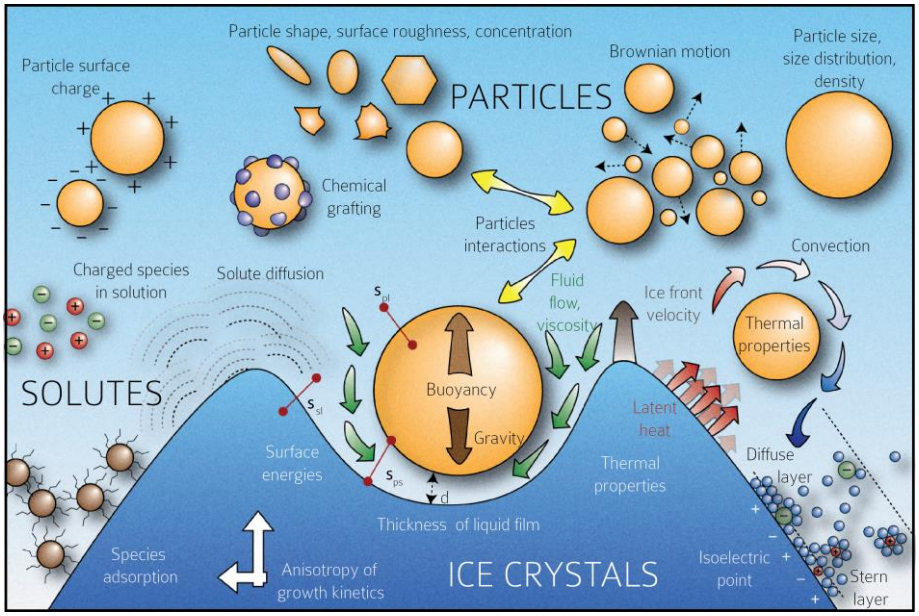

Figure I.20: Interaction between the freezing front and particles are influences by a wide variety of parameters. Reproduced from Deville[267].

Growth of ice-crystals is responsible for shaping and formation of pore walls, but the counterpart to this templating effect is the application of non-negligible mechanical constraints on the cells[334] which may prove highly deleterious to their viability. As a result, cells have been pre-immobilized in alginate beads to ensure better cell survival through the encapsulation process[10,307]. Immobilization in such cytocompatible biopolymer may also be of use to prevent damages due to freezing and drying. From a microbiological point of view freezing and lyophilization of living cells is far from being free from consequences for the cells, as can be attested by the extensive efforts invested for several decades in understanding and optimization of cryopreservation[335].

I.3.b.ii Freezing cells

Freezing is a highly deleterious phenomenon to most living organisms. Nature has devised strategies to deal with this issue in a few species exposed to extreme temperatures[336] such as insects, and some amphibians or reptiles[337]. If such behavior remains exceptional, the observation and understanding[338] of the underlying phenomena have open the way for the development of advanced cryopreservation strategies.

Two main sources of damage have been identified as consequence of freezing: formation of intracellular ice, which induces structural cell damages and rise in extracellular solute concentrations during external ice formation which may result in cell dehydration, significant cell shrinkage and membrane changes. Common cellular protection strategies include the secretion of cryoprotective molecules such as glucose[339] or glycerol[340]. Sufficient concentration of such cryoprotectants in cells may prevent excessive cell shrinkage due to osmotic dehydration during the formation of extracellular ice. Another strategy consists in the limitation or control of ice crystals formation through to the use of proteins (antifreeze proteins[341]). The action mechanism for these proteins is however not fully understood. In this case, the efficiency does not rely on high solute concentration but rather on specific interactions with ice. Several classes of freeze-protecting proteins have been identified with different behaviors. They may for instance induce controlled ice nucleation to prevent random ice crystal formation or be bound to ice crystals to tailor ice growth. Another effect observed was the presence of a thermal hysteresis, resulting in lower freezing point despite low protein concentrations.

The use of cryoprotective agents has been mimicked for the preservation of a whole variety of cells including mammalian cells[342,343], plant cells[344,345] or microorganisms[346,347]. Even if cryopreservation protocols must be tailored the specific targeted species, the general principles and strategies are similar. A distinction can be made between two main routes[348]. In conventional cryopreservation, focus is put on the control of ice formation and growth. In vitrification approaches, the goals is to completely prevent the formation of ice crystals.

In conventional cryopreservation, the most common way to preserve the cells is through the use of cryoprotectants, from which glycerol is the most prominent example since its first use in 1949[349]. The action of glycerol (and other intracellular cryoprotective agents such as DMSO) relies mainly on two effects: the increase of intracellular solute concentration induces a freezing-point depression thus limiting the formation of intracellular ice, and these high concentrations prevent osmotic imbalance during concentration of extracellular solutes during ice formation and subsequent cell shrinkage. It has also been proposed that one possible cause for cell injury during freezing is related to the increase of intracellular salts concentrations up to toxic levels due to dehydration of cells[350]. By preventing excessive dehydration of the cells, glycerol could therefore limit the rise in salt concentration and subsequent toxic effects. The efficiency of such cryoprotective agents therefore relies both on their capacity to efficiently penetrate cells and on the control of their possible toxicity

In addition to the presence of cryoprotective agents, another key element in the control of survival in cryoprotective strategies is the freezing rate[351]. Since injuries are highly dependent on osmotic phenomenon, the kinetics of water diffusion through the cell membranes has a heavy influence on the cryoprotection efficiency. At high cooling rates, water cannot permeate through the membrane quickly enough to compensate osmotic unbalances. The remaining intracellular water has higher chemical potential and become increasingly supercooled, ultimately resulting in the formation of intracellular ice. On the other hand, at sufficiently low cooling rates, water diffuses out of the cells and freeze-externally[352]. However if dehydration of the cells is too important, the previously mentioned effects of cell shrinkage and increased salt concentration may result in cell damages (see Figure I.21). Due to these antagonistic effects, an optimal cooling rate must be found to minimize intracellular ice formation, while maintaining non-toxic intracellular solutes concentrations. Such optimum is usually dependent on the type of cells due to the diversity in intracellular composition but also in the nature of the cell membranes.

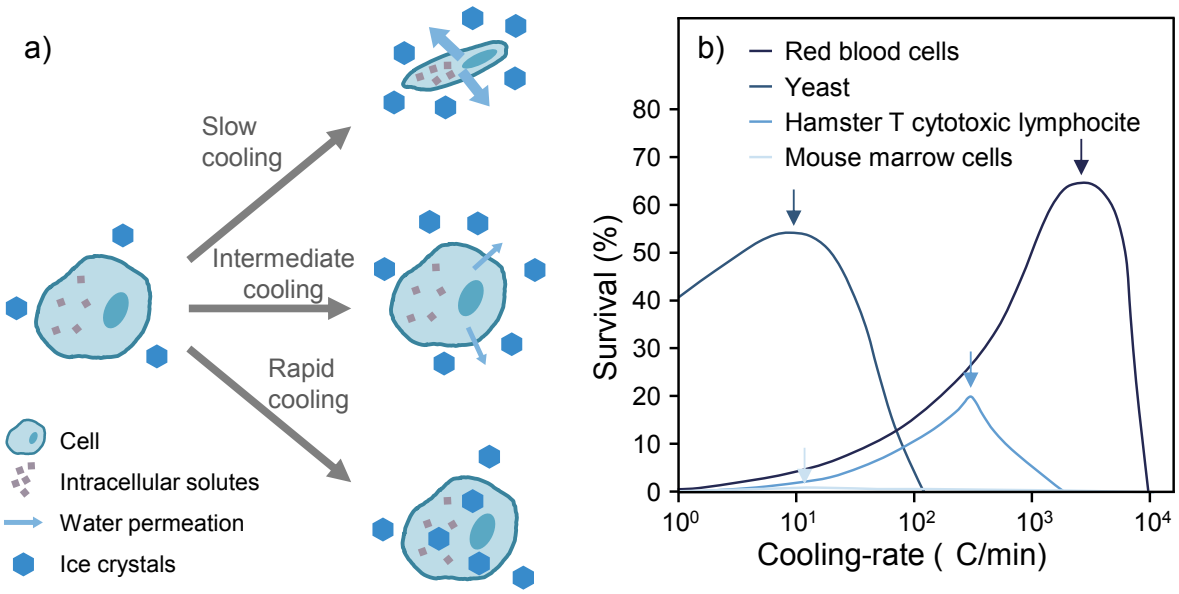

Figure I.21: High cooling rates may induce formation of intracellular ice while too slow rates may result in cytotoxic intracellular solutes concentration (a). A cell dependent optimal cooling rate can be found to minimize these effects (b). (a) adapted from Mazur[352], (b) adapted from Pegg[348].

Some cryoprotective agents such as sucrose, trehalose or polyethylene glycol (called non-penetrating cryoprotectants) are able to protect cells from freezing damages through different mechanisms, since they are not capable of permeating through the cell membrane[346]. Their main pathway of action therefore relies on the control of external ice nucleation (for instance on the formation of smaller ice crystals) to minimize mechanical constraint. Another possible action of such compounds is the modification of water diffusion kinetics[353] which also modifies the ice crystals formation and may help in preventing high osmotic imbalances.

A different approach in cryopreservation consists in fully avoiding freezing by vitrification of the intracellular water. Condition for water vitrification are however not easy to obtain. Both

high intracellular solute concentrations and very high cooling rates are required (see Figure I.22). A critical cooling rate, which depends on the total solute content of the solution, can be defined as the rate above which ice nucleation kinetics is too slow for freezing to occur[354].

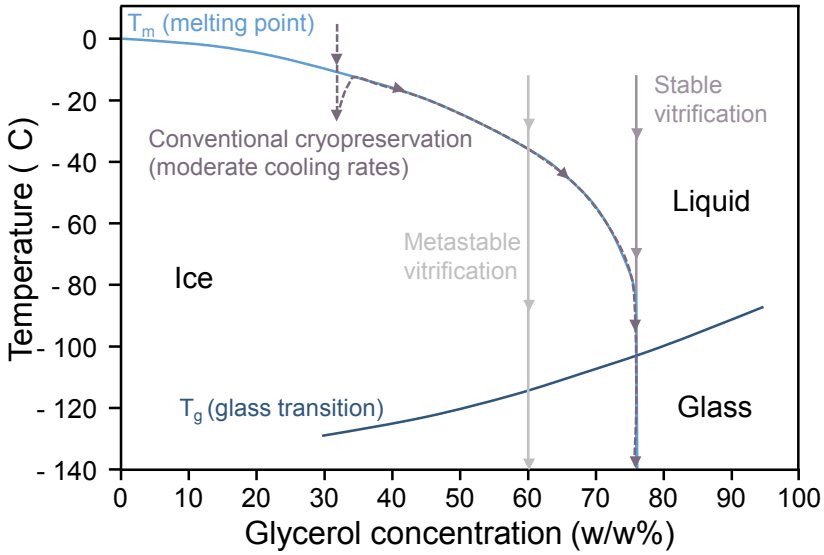

Figure I.22: Vitrification requires high cryoprotectant concentrations and very high cooling rates. Adapted from Fahy *et al.*[355].

Vitrification has the advantage of completely preventing the formation of intracellular ice crystals which could be damaging to the cells, without need for dehydration and subsequent elevation of the intracellular solutes concentrations[356]. As a result, there is no need to find an optimal cooling rate, which is of great interest for the preservation of multicellular units or whole organs. The downside is however the necessity to use high initial cryoprotectant concentrations which may be concerning both in terms of toxicity and of osmotic pressure.

Since freezing is generally used as a tool for long term preservation for further use, it is essential to consider not only the freezing process but also the return of the cells to their initial state. This includes thawing and removal of the cryoprotectants. In both cases the conditions must be carefully chosen. Thawing rate has proven to be just as important as the freezing rate[357]. Cryoprotectant removal is usually performed by washing with a solution with lower concentration in the considered cryoprotective agents. Concentrations must be adjusted carefully in order to prevent osmotic shock.

Another approach for the preservation of cell is not the inhibition of cellular activity through the use of very low temperature, but rather by the completed cell dehydration.

I.3.b.iii Drying cells

Freeze-drying has also been used a way to preserve and store proteins[358] and cells (animals[359], plants or microorganisms[360,361]) as well as virus (vaccines[362]). The main advantage of this

approach is the cost efficient storage and facility in transport and handling, since dry cells do not need to be kept at very low temperature such as frozen cells.

Freeze-drying consist in the freezing of a cell suspension and subsequent lyophilization under high vacuum. As a result the cells and organisms subjected to freeze-drying must actually face two types of stress: freezing and subsequent drying. The drying step itself is usually composed of primary drying, which is the sublimation of ice crystals under high vacuum and secondary drying which consists in the removal of bound water[363].

Optimization of processes for freeze-drying must therefore take in account both sources of damage. Effects of freezing have been extensively studied for conventional cryopreservation. It is however much more difficult to assess the effects of the drying step alone, since it is always preceded by a freezing step. In addition these effects can be interrelated which means that survival and damages must be considered across the whole process[364]. Optimization of the freeze-drying process however usually consists largely in optimization of the freezing conditions (formulation of the suspension and freezing rate).

As a result, cells are usually dispersed in solutions containing common cryoprotective agents. However some compounds also display specific lyoprotective features. Formulations may contain both cryo and lyopreservatives or single compounds which present protective effect during both freezing and drying. Common protective agents used in freeze-drying include trehalose, sucrose or glycerol as well as skim milk. As mentioned previously, some cryoprotectants are capable of permeating through the cell membranes and accumulate in the intracellular medium. Most of these compounds are highly hydrophilic. Such capability to retain water may provide advantages during the drying process[346].

As is the case for conventional cryopreservation, the freeze-dried species must be returned to their original hydration state prior to use. Even if only water has been removed from the cells during ice sublimation, better results are usually obtained with more elaborate rehydration media (for instance saline)[365].

Conclusion

Living organisms and microorganisms in particular have proven to be interesting tools for the depollution of soils. Bioremediation approaches have been investigated for the treatment of soils containing various common pollutants such as PAH, pesticides or even heavy metals. The limitation of such strategies is usually the intrinsic sensitivity of living organisms.

Encapsulation of cells and microorganisms in various matrices has proved to be an efficient way to design functional materials. Entrapment of metabolically active species usually allows for enhanced stability, reusability or recovery of the cells. Entrapment matrices and encapsulation protocols must be designed in order to satisfy imperatives from a structural as well as structural point of view. These requirements can be met by tuning the composition of the material, as well as the shaping processes. Use of hybrid or composite materials is a good way to combine the cytocompatibility of materials such as biopolymers with the stability of inorganic materials such as silica.

Freeze-casting is a shaping process relying on the formation of ice crystals to act as template for the design of porous materials with complex and controlled architectural features. This technique has been of great interest to the material scientists' community due to its versatility and tunability. Morphological control can be gained throughout control of compositional parameters (nature of the compounds, shape of the particles, type of solvent used, presence of additive etc…) or by modifying processing parameters (type of setup, freezing rate etc…). Controlled freeze-casting techniques have been used for the design of complex composites architecture, in particular including various particles in a well-structured matrix.

In order to apply such a method to the encapsulation metabolically active microorganisms, the challenge of living organisms must be addressed. Conventional strategies include the addition of cryoprotectants but also tuning of the freezing-rate, which can easily be controlled in ice-templating approaches.

As a result freeze-casting could prove to be a valuable tool in for the encapsulation of cells in biopolymer macroporous materials with an oriented porosity and in hybrid macroporous materials. This processing approach could be used both as a way to control the structural features of the material and as way to control the functional aspects of cell encapsulation.

Cellularized hybrid materials with an oriented porosity could be of great interest for environmental applications. Entrapment of microorganisms with bioremediation capabilities could be a decisive advantage in depollution strategies of contaminated soils, as a way to introduce efficient exogenous microorganisms while ensuring stability and preservation against potentially harmful conditions for the metabolically active microorganisms, as well as preventing their dispersion.

Chapter II : Pectin as a supporting structure

Introduction

As mentioned before, the conception of a hybrid material containing microorganisms was considered as a two-step process: formation of a biopolymer scaffold containing the targeted cells and coating with a silica layer. The structural properties of the material were first investigated in absence of cells, while keeping in mind the fact that the designed material is intended to be used as cell-host matrix and that the shaping process must be adapted to cellular encapsulation.

The first objective was the elaboration of a dry macroporous biopolymer-base material. The characteristics of the biopolymer structure were investigated using ice-templating techniques. Both the formulation of the initial polymer solution and the freezing setup were explored as possible levers on the pore morphology. The influence of the porous structure was in turn assessed over the macroscopic properties of the material such as mechanical wetting behavior.

II.1 A few words about pectin

First and foremost, the material must be compatible with living microorganism, which implies the use of a non-toxic compounds, solvent and shaping process. This points towards the use of natural polymers (also known as biopolymers)[5] such as polysaccharides (for instance alginate[4], chitosan[190], starch[366], or pectin[192]), or proteins[367] (collagen and its derivative gelatin, silk fibroin, keratin). These types of polymers are especially widely used in the medical domain for applications as varied as drug delivery, wound dressing, scaffolds [156]. The food industry is also one of the main consumers of biopolymers[175] as stabilizing, gelling or thickening agents, but they are actually used in almost every domain including packing, textile or paper industry[368].

Pectin is a polysaccharide found mainly in the plant cell primary wall, especially in young tissues and fruits[369]. The best known, and most commonly used pectin sources are apple pomace and citrus peels [370,371], but pectin can actually be found in a wide variety of plants including tomato, carrots, beet root, apricots mango or even sunflower[174]. Pectin plays a role in the mechanical behavior of the cell wall[178] and more largely in the texture of the plant or fruit[372] which implies the presence of various pectic substances depending on the location, type and maturity of the cells within the plant. Even in single cells, a distribution of structural domain can be observed[373]. As a result pectin, or rather pectins, are very complex to characterize and no simple or general structure can be given. It is however possible to identify specific recurrent regions and structures, from which the three most common are homogalacturonan (HG), rhamnogalacturonan I (RG-I)[374] and rhamnogalacturonan II (RG-II)[375] (see Figure II.1).

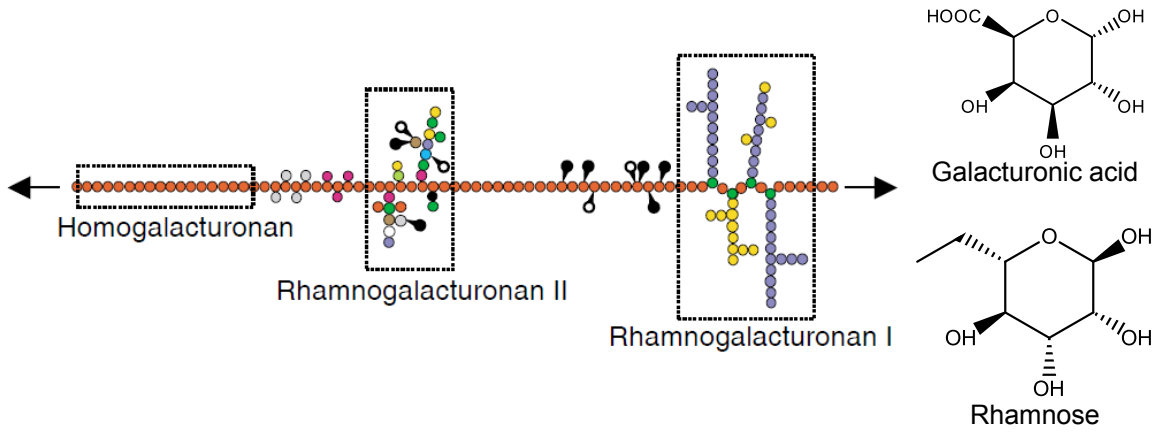

Figure II.1: Pectins are a family of mainly linear polymer based on covalently linked galacturonic acid. Oligosaccharide side chains of different length may also be present, containing the following residues : Galacturonic acid (●), rhamnose (●), apiose (●), fucose (●), aceric acid (●), galactose (●), arabinose(●), xylose (○), glucuronic acid (○), ketodeoxymanno-octulopyranosylonic acid (●).
Depending on the pectin source different levels of methylation ( ) and acetylation ( ) can be observed.
Reproduce from Willats *et al.*[160]

HG is a linear polymer composed of a chain of 1,4-linked α-D-galacturonic acid (GalA). This chain may be partially esterified of acetylated depending on the source, extraction method and subsequent treatment. RG-I consists in alternating residues of rhamnose (Rha) and galacturonic acid (GalA) (α-D-GalA-1,2-α-L-Rha-1,4). Neutral side chains can be attached on the Rha residues, most often 1,4-β-D-galactan or 1,5-α-L-arabinan. RG-II, also called substituted homogalacturonan, is the most complex and variable of these three structures[174]. Contrary to what the name rhamnogalacturonan II suggests, the backbone of this structure is made of homogalacturonan[160] but is substituted with a wide variety of side chains. In reality, most pectins present several of these well identified structures[376] and as a results the polymers are commonly accepted as heterogeneous sequence of simple HG regions ("smooth" regions) and more substituted regions[377,378] ("hairy" regions). It has however be proposed that the HG regions might themselves be side chain to the RG-I regions[379].

Since pectin is mainly used in the food industry[371], especially as a gelling or thickening agent, structural characteristics influencing the gelling properties of the pectin are of great importance. There are however some applications in other domains, which may call upon various other properties of the pectin chains. As mentioned, food industry [380] and medicine or pharmaceutical industry [381,382] are the most prominent users of pectin based materials, but there are also reports in environmental science, for instance as adsorption materials[383,384]. The pectin based materials may adopt various forms such as gel bead [385], films [386], three dimensional scaffolds [387] and dry porous materials [388]. Regardless of the targeted application, it is necessary to understand the relationship between the structure of the pectin and its physical properties, in order to choose to best candidate for desired function.

The chains of HG or RG may be methylated and/or acetylated which may have and influence on interchain interactions. For this reason, pectin are commonly separated according to their degree of methylation (DM) into highly methoxylated pectins (HM) with a DM above 50% and low methoxy pectins (LM) with DM inferior to 50%. HM pectins are able to form gel in acidic conditions in presence of high sucrose content[389]. This is typically what happens in the confection of jams. LM pectin can also form gels but under different conditions. In this last case, the presence of divalent cations such as Ca^{2+} is required. A proposed explanation is the formation of an "egg-box" structure[390], similar to the one observed upon crosslinking of alginate[183]. It is however necessary to remember that pectins are complex and heterogeneous polymers, which results in complex molecular interactions and macroscopic behaviors. For this reason the two previously cited gelation mechanisms are not completely independent and calcium proved to be able to modulate gelation of HM pectins[391]. In addition, several parameters can influence the gelling properties of pectins, including pH, chain length, temperature and type of divalent cation[392].

The degree of acetylation also plays a major role in the gelling properties of pectin[393], since the presence of the functions may sterically hinder formation of the gels. This is one of the proposed explanations for the limited gelation capabilities of pectin extracted from beet root compared to citrus or apple pectins[394]. The properties of pectins extracted from beet root pulp

[395,396] can be modified depending on the extraction conditions [397] and post-treatments [398] in order to make it compatible with conventional gelling conditions. This however makes the beet root pectin less competitive than citrus or apple pectins. As a result, this type of pectin is not commonly used in the food industry and it largely remains an unexploited by product of the sugar industry. Beet root pectin has however its own specificity, namely the presence of ferulic residues [399] which may confer a possibility to crosslink the pectin[400] in order to obtain gels.

In this work we chose to use a shaping technique that does not rely on the gelling properties of pectin, but takes advantage of its polymeric nature and of its solubility in water.

II.2 Ice-templating or the use of water to shape materials

II.2.a Comparison of different freezing-conditions

Ice templating is a simple way to obtain dry porous materials. Besides its simplicity, one of the main advantage of the technique is its versatility since it can be applied to components ranging from polymers[304,320] to ceramics[256] and metal[262], as well as various composites[234,319,321].

The general idea is to freeze a solution (or suspension) in order to form ice crystals which will serve as templates for the final porosity. As ice crystals grow, solutes are segregated from the solvent (often water), which results in the formation of the future pore walls around the newly grown ice crystals. The latter are then removed by sublimation to free the porosity. This method can be used to shape many different raw materials, since the vast majority of solutes have a very low solubility in ice. The limit then resides in the capacity of the material to retain its shape after removal of the ice crystals. One possibility is to add a sintering step as is the case for the shaping of ceramics. In the case of pectin freeze-casting, the dry foam obtained after lyophilization is self-supporting, but it is important to highlight the fact that this network is not crosslinked, and that any contact with liquid water results in the dissolution of the polymer structure.

The method for the formation of a macroporous pectin foams may seem straightforward: freezing of an aqueous solution of the polymer and freeze-drying of the sample. However, many parameters must be taken in account including the formulation of the initial solution (concentration, possible additives), the freezing conditions (freezing-rate, geometry) and the drying conditions. In order to link the processing parameters to the final foam morphology[297], four different freezing conditions were explored. As a first approach, 4 mL samples were placed in polyethylene cylindrical molds of 19 mm in diameter and subsequently frozen in conventional -20°C and -80°C laboratory freezers. Samples of the same size were obtained by plunging the molds containing the pectin solution into a liquid nitrogen bath. These three approaches were compared with the freeze-casting technique, where a chosen temperature ramp was applied to the sample in contact with a heat conductive element (copper) at a precisely set temperature.

Material and methods

Influence of the freezing conditions was assessed on aqueous solutions of pectin at 40 g/L.

The pectin used was kindly supplied by Estelle Bonnin and Catherine Garnier at the Biopolymères Interaction Assemblages laboratory at INRA Nantes and was extracted from sugar beet pulp. The dry powder was used without further treatment.

Pectin solutions were prepared by dissolution of the powder in deionized water and stirred overnight at room temperature. The resulting viscous solutions were then frozen by various

methods described hereafter and subsequently freeze-dried in a Christ Alpha 2-4 LD freeze-dryer for 48 hours, under 0.05 mbar vacuum.

The samples frozen in laboratory freezer were typically 4 mL samples of 40 g/L pectin solution placed in polyethylene cylindrical molds of 19 mm in diameter. The samples were left overnight in the freezer either at -20°C or -80°C before drying. To obtain samples frozen at -196°C, similar samples were directly plunged into a liquid nitrogen bath for around 5 minutes (until no ebullition of the liquid nitrogen was visible).

Various samples were obtained by the freeze-casting technique. As previously described, the freeze-casting method aims at providing a controlled temperature gradient, in order to freeze the sample at a controlled rate and with a specific orientation.

The homemade setup (see Figure II.2 *and Annex p 209) is composed of three copper rods (Ø = 15 mm), plunging in a liquid nitrogen tank for half their length. Each rod is equipped with a heating resistance linked to a PID thermocontroller. A thermocouple is place about one centimeter bellow the top of the central copper rod. Typical cooling profiles include a 3 min equilibration step at 20°C and a cooling ramp at a rate between 1°C/min and 10°C/min. When the temperature reaches -60°C, temperature remains constant until the frozen sample is removed. Cylindrical polypropylene mold can be adjusted on top of the rods to pour the pectin solutions.*

Scanning Electron Microscopy (MEB) observations were performed on Hitachi S-3400N SEM. The samples were sputtered with 20 nm of gold and observed under 3 to 4 kV acceleration and 30 µA probe current.

The OrientationJ plugin to the Fiji software was used to obtain orientation distributions and mapping. (OrientationJ, java plugin for Fiji/ImageJ, written by Daniel Sage at the Biomedical Image Group, EPFL, Switzerland[401]*).*

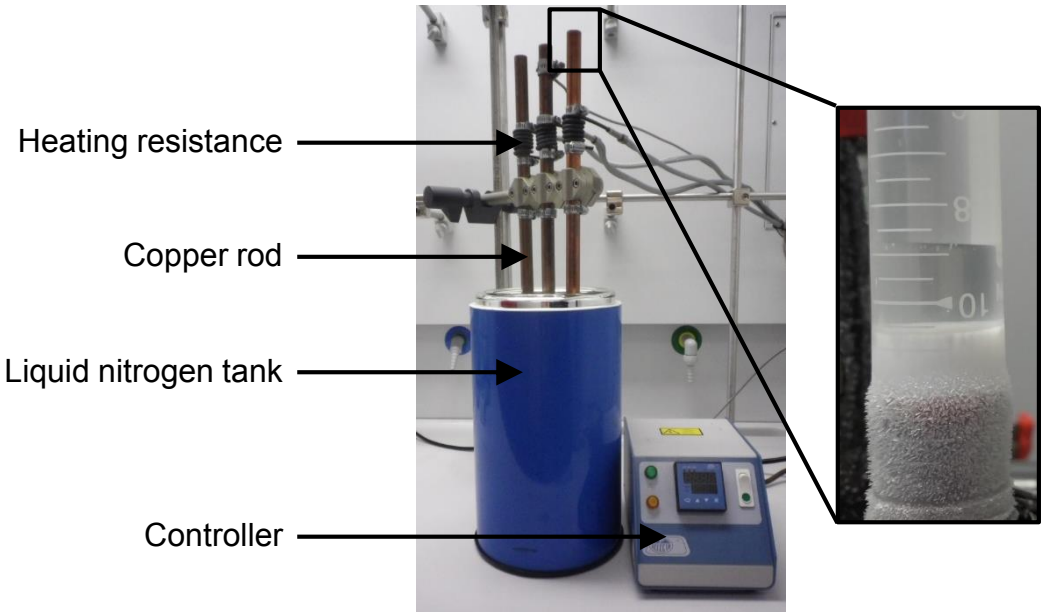

Figure II.2: The homemade freeze-casting device is composed of three copper rods plunging in a liquid nitrogen tank to provide cooling and equipped with heating resistances. The temperature is set through a PID thermocontroller. A polypropylene cylindrical mold can be affixed on top of the copper rod.

To understand the influence of the freezing method over the morphology and properties of the final material, it was necessary to pinpoint the differences between these methods. To characterize each freezing condition, the temperature at the core of the samples were monitored by a thermocouple during the whole freezing process (from a few minutes to four hours). Figure II.3 displays theses temperatures (full line) as well as the target temperature (dotted line), which was either the temperature of the freezer, liquid nitrogen bath, or the temperature at the top of the copper rod (in the case of freeze-casted samples).

The first three conditions (freezers at -20°C, -80°C and liquid nitrogen bath) can easily be compared due to the very similar setups (one fixed target temperature, same type of mold and anisotropic source of cold). The main changing parameter is the targeted temperature (-20°C, -80°C or -196°C), but the geometry of the setup was the same. In this last case, the temperature follows a linear gradient along the axis of the cylindrical mold. In addition, the targeted temperature is not fixed, but is a ramp with a chosen slope (in this case 10°C/min). In other terms the temperature can be controlled both spatially and in time.

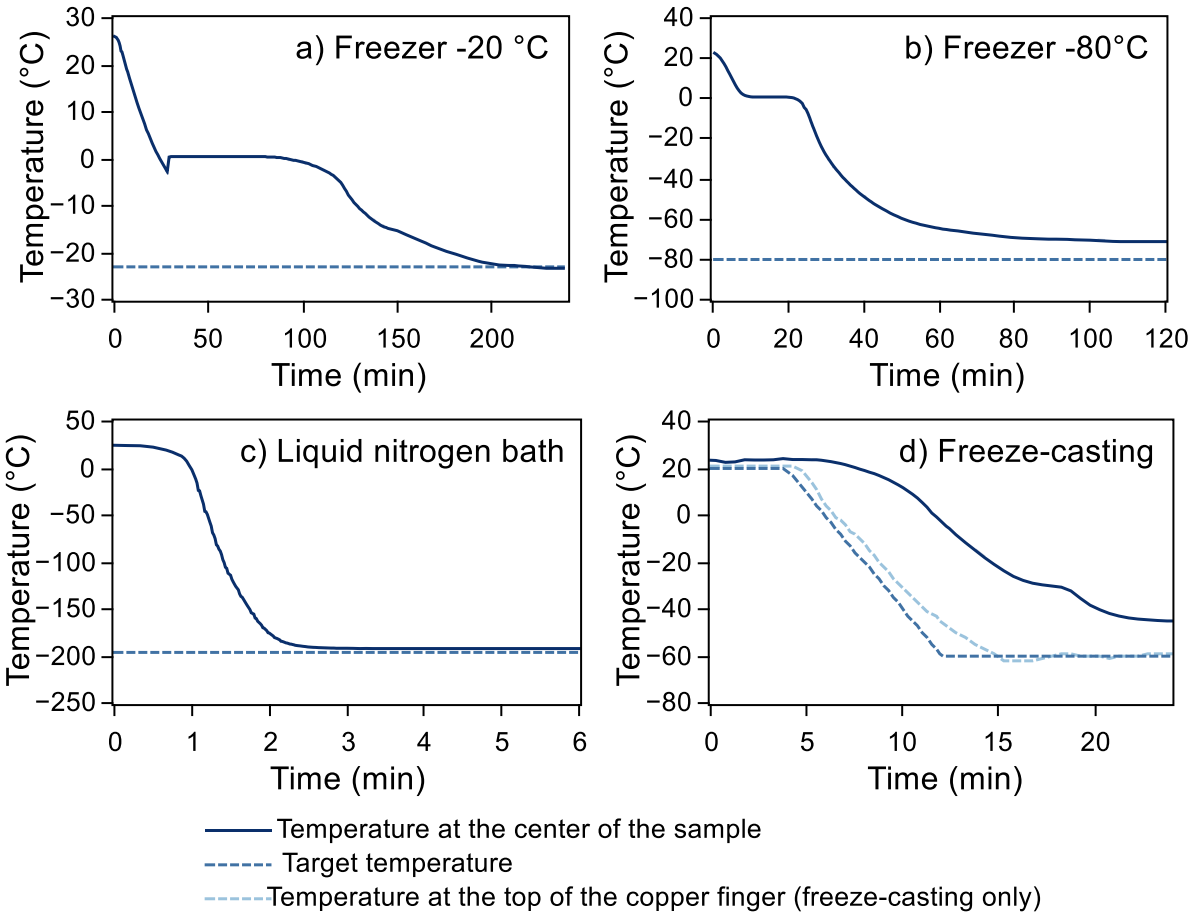

Figure II.3: The temperature profiles obtained in -20°C (a) and -80°C (b) conventional freezers are similar. A slight delay in cooling can be observed in the sample obtained in liquid nitrogen (c). The temperature profile for the freeze-casted sample (d) is very different since the targeted temperature is set to follows a ramp.

For the samples frozen in laboratory freezer the temperature profiles are similar. After an initial cooling period, the temperature remains constant. This corresponds to the actual phase transition in the sample, and the growth of the ice crystals throughout the sample. After complete freezing of the sample, the temperature at the core of the sample decreases down to the target temperature. At lower temperature (-80°C) the initial cooling rate increases (3,6 °C/min in the -80°C freezer *vs* 1,2 °C/min in the -20°C freezer) and the phase transition time decreases (around 10 min at -80°C *vs* 50 min at -20°C). When the samples are plunged in liquid nitrogen, a delay is observed before initial cooling (at 243°C/min). With the freeze-casting technique, the temperature at mid height of the sample follows the imposed temperature ramp, but with a slight shift (5 minutes). In this case, the cooling rate is 7.2 °C/min (theoretical ramp was of 5°C/min). To explain these variations, it is necessary to link them to the final morphology of the material, as a way to understand the relation between these temperature profiles and the ice growth.

II.2.b Influence on the pores morphology

Different morphologies can be observed at the macroscopic scale (see Figure II.4). The sample obtained at -20°C has a homogeneous aspect and no significant difference can be observed between the longitudinal and transversal views. The sample obtained at -80°C looks less homogeneous, with small striations visible on both the longitudinal and transversal views, but no clear orientation is noticeable. Slight iridescence can be seen in samples obtained in a liquid nitrogen bath (oriented in a radial fashion) and by freeze-casting (in the longitudinal direction).

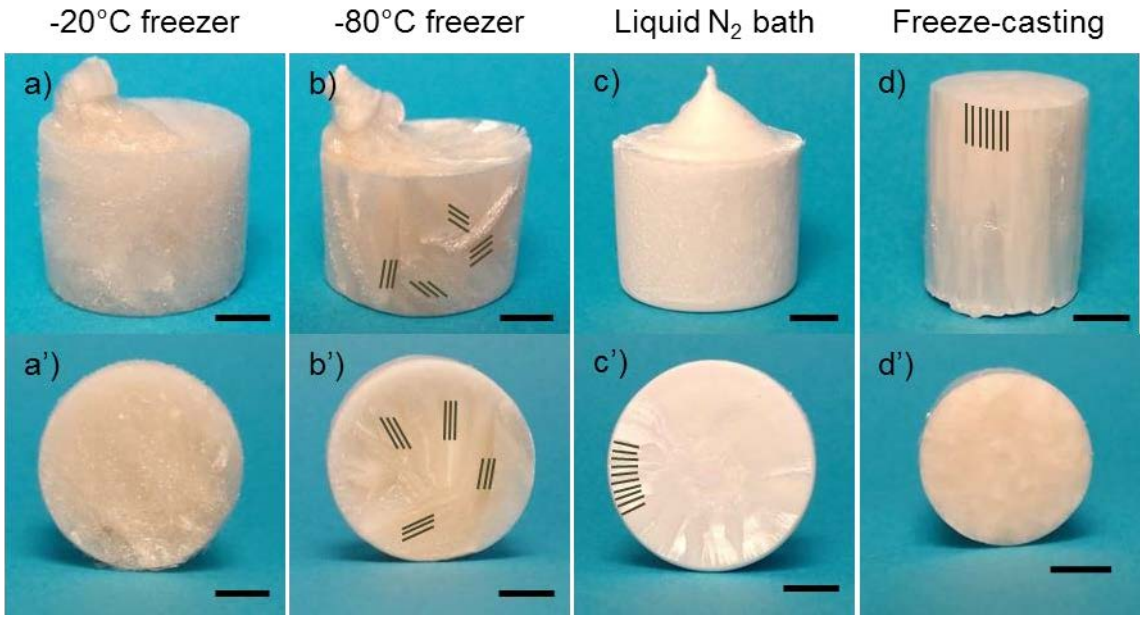

Figure II.4: The sample obtained in a -20°C conventional freezer (a and a') looks homogeneous. The sample obtained at -80°C (b and b') displays non-aligned striations. The sample obtained in a liquid nitrogen bath (c and c') shows radially arranged structures. The freeze-casted sample (d and d') shows longitudinal iridescence. Scale bars: 5 mm.

The morphology of the samples was further investigated by Scanning Electron Microscopy (SEM). Each sample was cut and observed in transversal and longitudinal directions (see Figure II.5). Samples obtained at -20°C and -80°C present similar morphologies in both directions. The sample prepared in liquid nitrogen however present a strong anisotropy. An oriented porosity can be observed on the longitudinal section. A mapping of the pores directions (see Figure II.6) reveals a radial organization of the pores in the case of the samples prepared in liquid nitrogen. The same analysis on foams obtained in freezers at -20°C and -80°C shows no specific orientation of the pores.

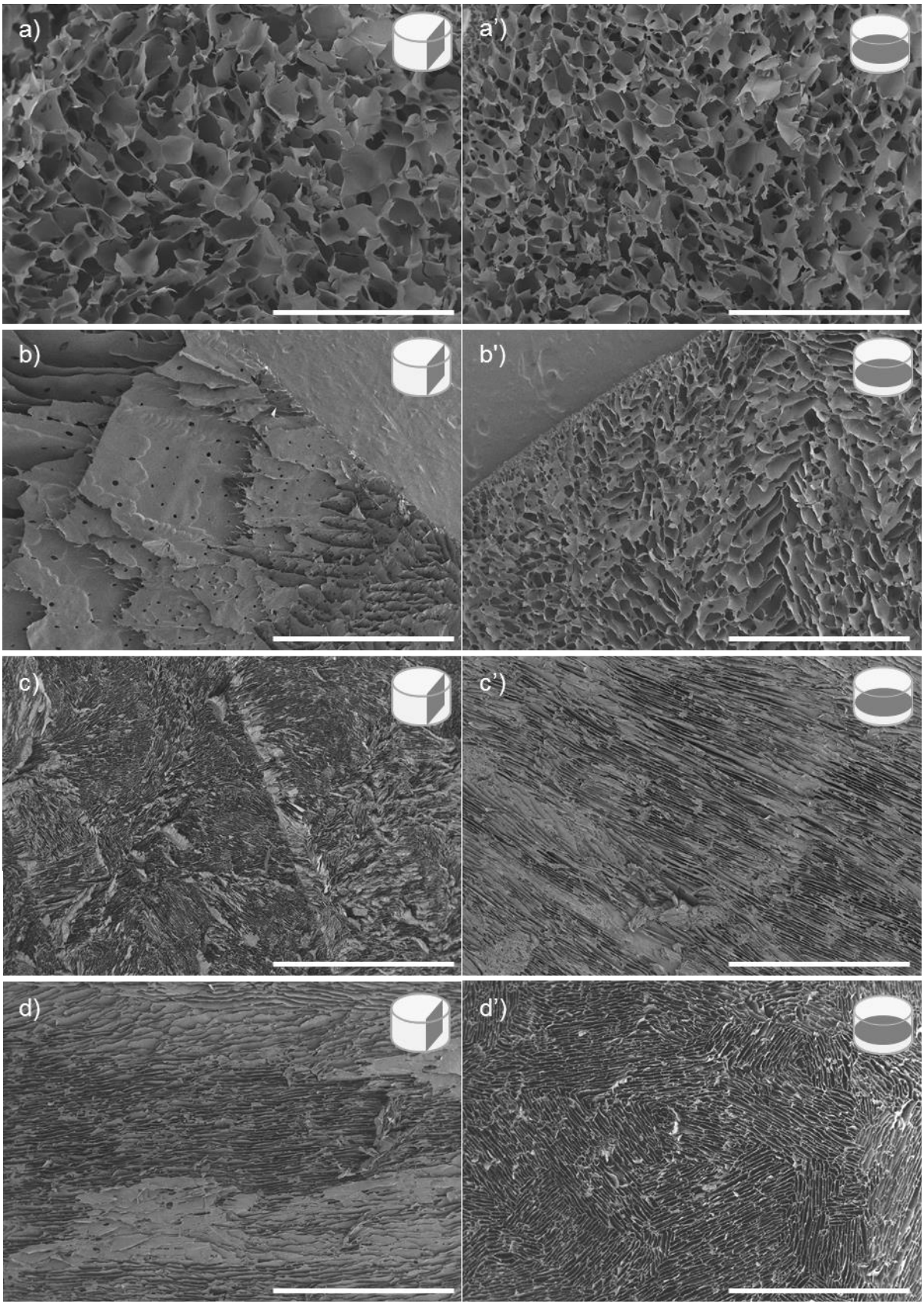

Figure II.5: SEM observation reveals differences between longitudinal (a, b, c and d) and transversal slices (a', b', c', and d'). Pore are anisotropic in samples obtained at -20°C (a and a'). Pores seem slightly elongated in samples obtained at -80°C (b and b'). Both samples obtained in liquid nitrogen (c and c') and freeze-casted samples (d and d') show well aligned and oriented pores. Scale bars: 1mm.

The pore morphology can directly be linked to the ice crystals formation. The ice growth behavior can be inferred from the temperature profiles presented in Figure II.3. The presence of a temperature plateau and moderate initial cooling rates for the samples prepared at -20°C and -80°C (see Figure II.3 a and b) seems to indicate that there is no or limited temperature gradient inside the sample. The cooling rate is slow enough for the temperature to remain homogeneous thorough the sample. The whole sample reaches transition temperature at the same time, resulting in simultaneous nucleation of ice in the whole volume, which corresponds to the plateau in the temperature profile. As a result, ice crystals grow in an anisotropic fashion (see Figure II.7 a), resulting in non-specific ice crystal shapes, and therefore in non-specific, non-aligned pores. It is however noticeable that the pores in the material obtained at -80°C, so presumably with a higher temperature gradient, are slightly elongated.

To investigate the influence of a temperature gradient, samples were prepared by immersion in a liquid nitrogen bath. In this case, the temperature at the core of the sample remains stable before dropping sharply (see Figure II.3 c). This might be due to the presence of an important temperature gradient between the core and the sides of the sample. It is probable that ice crystals nucleate almost immediately when the sample is plunged into liquid nitrogen, but only in the outer regions of the sample. Due to the radial temperature gradient, the ice crystals then grow in a radial fashion inside the sample (Figure II.7 b). This organization of the ice crystals results in the observed orientation of the pores. The absence of a plateau at the transition temperature supports the idea that when the center of the sample freezes, the rest of the sample is already frozen. It might be noted that the actual gradient is not strictly radial, since the sample is plunged entirely in liquid nitrogen. A vertical component to the gradient must therefore be present at the top and bottom of the sample, resulting in a slight tilting of the pores.

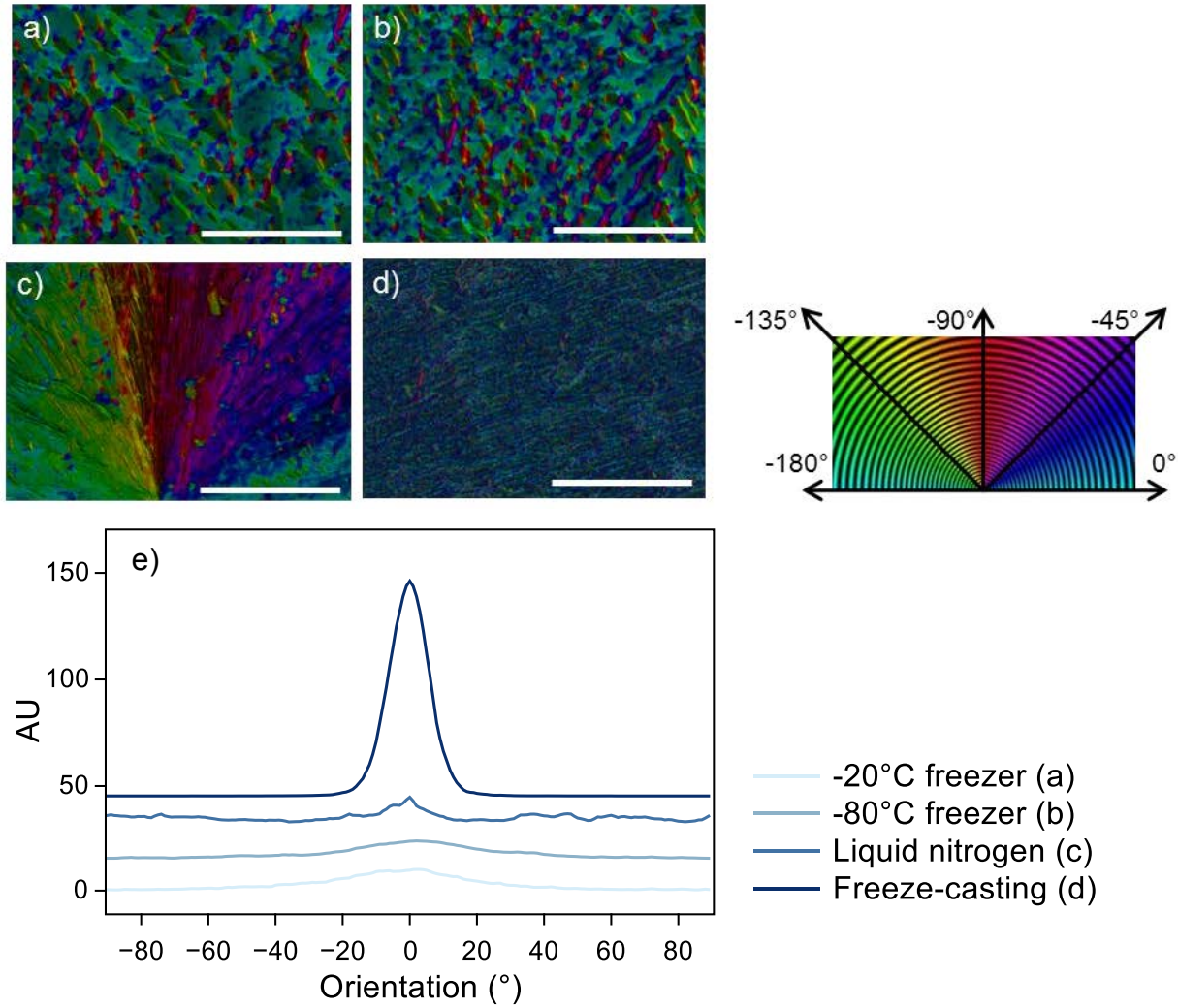

Figure II.6: Mapping of the pore orientation in SEM images of samples obtained at -20°C (a) and -80°C (b) in conventional freezer reveal no specific orientation. Cross sections of samples obtained in a liquid nitrogen bath (c) reveal a radial organization. Longitudinal cuts freeze-casted samples (d) also reveal oriented porosity, but all pores are aligned. Pore orientation distribution confirms these observations (e). The pore orientation distributions were centered on 0° for clarity. Scale bars: 500µm.

The presence of a temperature gradient inside the liquid sample is responsible for the orientation of the final porosity, however, in the case of freezing with a liquid nitrogen bath, there is no control over this gradient which strongly depends on the mold geometry. To gain better control over the pore morphology, samples were prepared by freeze-casting. This method confers control over the orientation of the temperature gradient, as well the kinetics of the ice growth. By placing the sample in contact with a cooling element at the basis of the cylindrical mold, it is possible to induce a longitudinal temperature gradient. The temperature in the region directly in contact with the cooling element closely follows the imposed temperature ramp. The temperature in the middle region of the sample (where the thermocouple was placed) however follows the cooling ramp with a certain delay (see Figure II.3 d). As soon as the temperature of the cooling element reaches the transition temperature, ice crystals nucleate in the bottom region of the sample. The crystals then grow along the temperature gradient, which is to say along the cylinder axis (Figure II.7 c). SEM observation

of a cross section (Figure II.5 d) reveals the presence of a lamellar structure, where the pores are organized in orientation domains. This lamellar structure is characteristic of materials obtained by freeze-casting of aqueous solutions or suspensions and is the direct consequence of the crystallographic properties of ice[256].

The observation of the longitudinal section (see Figure II.5 d') reveals that all the pores follow a common direction along the direction of the temperature gradient. This translates into the presence of a single well defined peak in the pore orientation distribution (see Figure II.6).

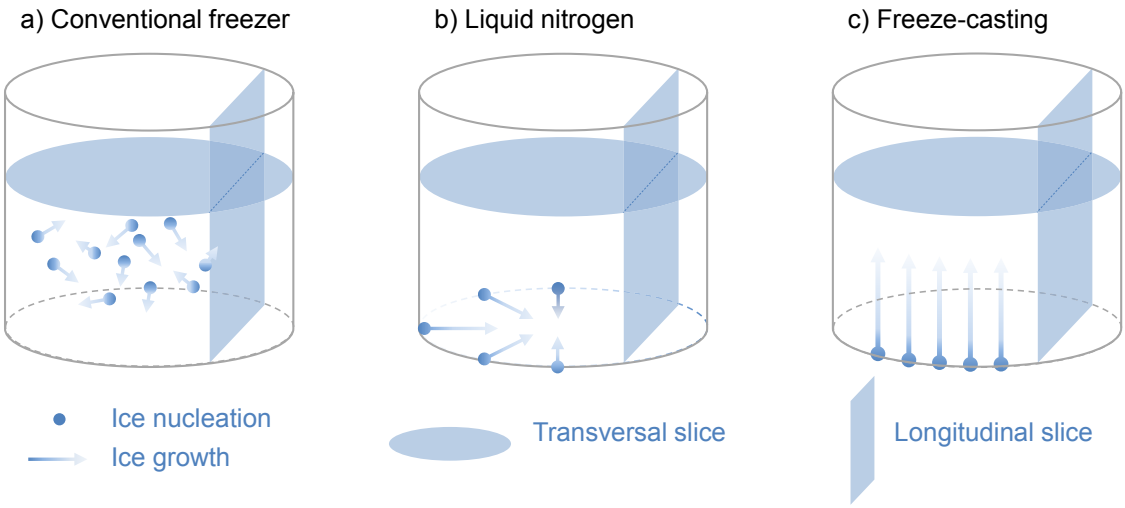

Figure II.7: Ice grows in different ways according to the freezing technique. In conventional freezers (-20°C and -80°C) nucleates homogeneously and ice grows in an anisotropic fashion (a). When plunged into liquid nitrogen ice nucleates in the outer region of the sample and grows radially towards the center of the sample (b). With freeze-casting process, ice nucleates at the interface between the copper and the sample and grows upward in a channel-like manner (c).

Both the temperature profiles and morphology observations allowed for the identification of three different types of ice growth, which are summed-up in Figure II.7. The presence of a temperature gradient, as is the case for samples obtained by dipping in liquid nitrogen or freeze-casting, induces the oriented growth of ice crystals and therefore the formation oriented pores. Freeze-casting presents the further advantage of precisely controlling the direction and amplitude of this temperature gradient.

II.2.c Influence on mechanical behavior

The control of the freezing conditions influences the morphology of the material, which in turn has an influence on the physical properties of the foam. The mechanical behavior of the samples obtained by the four different freezing methods was assessed under compression.

Material and methods

Mechanical behavior under compression was assessed using an Instron 5965 traction and compression device. Cubes of 1 cm³ were cut in the different samples. Samples were compressed up to a 50% strain, at a constant displacement rate of 1 mm/min. Charge was measured in function of displacement and corresponding stress and strain were calculated. Five replicates were used for each measurement.

Two orthogonal compression directions were used on 1 cm³ samples: along the cylinders axes (axial compression) and perpendicularly to the cylinder axes (radial compression). When applicable, these directions were specifically chosen along or orthogonally to the pores of the material. For the -20°C and -80°C samples axial compression (Figure II.8 a) was to considered orthogonal to the pores and radial compression (Figure II.8 b) was considered along the pores by comparison with the liquid nitrogen samples. In the case of the freeze-casted samples however, axial compression (Figure II.8 c) was along the pores and radial compression (Figure II.8 d) was orthogonal to the pores.

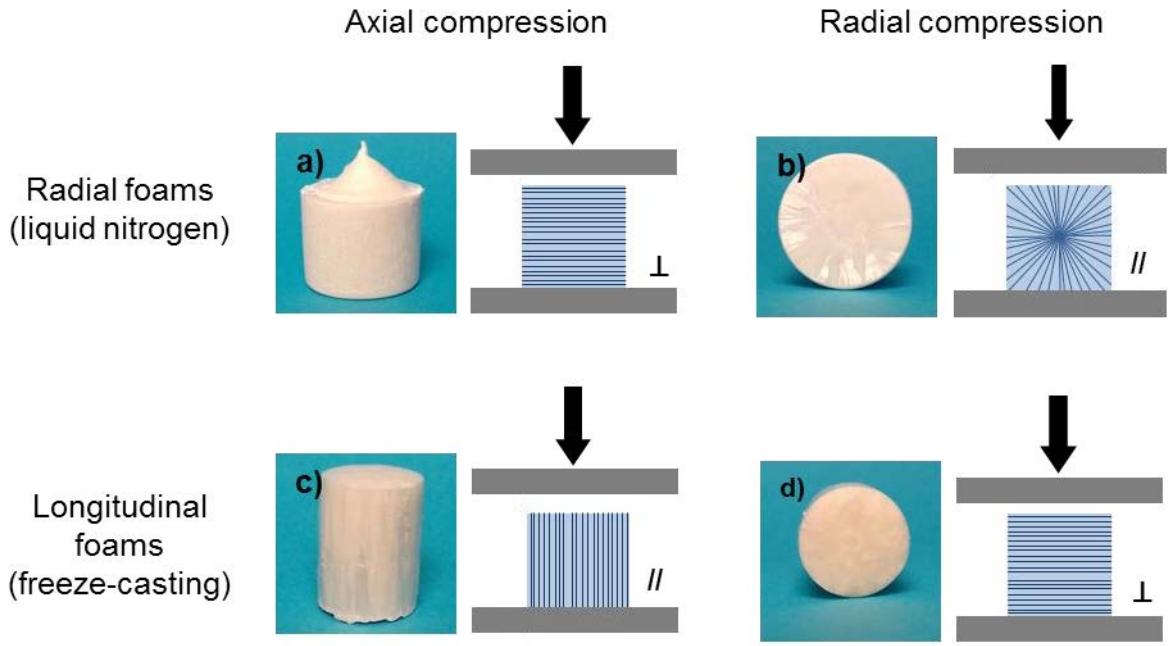

Figure II.8: Samples were cut down to 1 cm³ cubes and the mechanical behavior was assessed under compressive strength. Samples were solicited under axial (a and c) and radial (b and d).compression.

Figure II.9 shows the stress/strain behavior for materials with various pore organizations and the values for Young's modulus and compressive strength are summed up in Table II.1. An anisotropy ratio was calculated by comparing the Young's modulus measured in the direction of the pores (//) and perpendicularly to the pores (⊥).

$$Anisotropy\ ratio = \frac{E_{\perp} - E_{//}}{E_{\perp}}$$

Compared to the other materials, the sample prepared by freeze-casting displayed a highly anisotropic behavior. When compressed in the direction of the pores, this material has a Young's modulus of 2,8 MPa, which is typical for polymer foams of this density[402]. However under compression orthogonal to the pores, the Young's modulus drops to 125 kPa. This strong mechanical anisotropy is the direct consequence of the structure anisotropy described earlier.

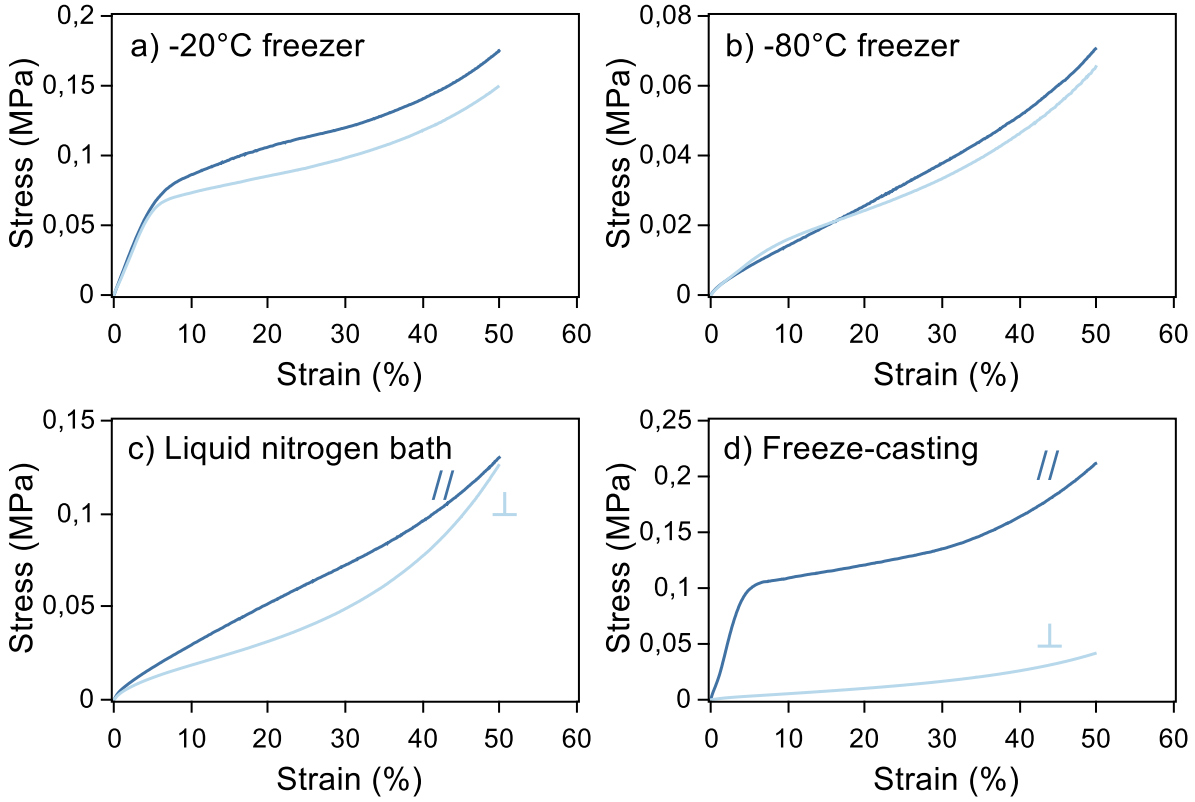

Figure II.9: Samples obtained with conventional freezing at -20°C (a) or at -80°C (b) present no significant mechanical anisotropy. Foams obtained with liquid nitrogen (c) present an oriented porosity, but the mechanical behavior is quite similar in both directions. The sample obtained by freeze-casting (d) show both higher Young's modulus and compressive strength when compressed along the pores.

The cellular materials with no specific orientation have no or little mechanical anisotropy (see Figure II.9 a and b and Table II.1). The Young's modulus in both directions are in the same order of magnitude (between 1,1 and 1,5 Mpa for the -20°C freezing *vs* 0,3 Mpa for the -80°C freezing). The observed difference may be attributed to the slightly elongated shape and more lamellar structure of the material prepared at -80°C.

The radial structure (sample obtained using a liquid nitrogen bath), despite having a specific pore orientation, displays no mechanical anisotropy. This might be attributed to the fact that the compressive tests are not really performed directly along the pores but rather on a distribution of orientations, due to the radial organization. The apparent mechanical behavior therefore results from a mean over several orientation including compression along the pores but also orthogonal compression (see Figure II.8 b).

Table II.1: Young's modulus and compressive strength for foams obtained from freezing of 40 g/l aqueous pectin solutions under various freezing conditions.

	Conditions	Freezing rate (°C/min)	Anistropy ratio	Young's modulus (MPa)	Std dev (MPa)	Compressive strength (kPa)	Std dev (kPa)
Compression orthogonal to the pores (⊥)	-20°C freezer	1.2	28.9	1.07	0.50	65	17
	-80°C freezer	3.6	19.4	0.27	0.10	NA	NA
	Liquid nitrogen (-196°C)	243.3	21.0	0.49	0.09	NA	NA
	Freeze casting at 10°C/min	7.2	95.2	0.13	0.03	NA	NA
Compression along the pores (*//*)	-20°C freezer	1.2	28.9	1.50	0.47	67	34
	-80°C freezer	3.6	19.4	0.34	0.15	NA	NA
	Liquid nitrogen (-196°C)	243.3	21.0	0.62	0.78	NA	NA
	Freeze casting at 10°C/min	7.2	95.2	2.61	0.65	92	2

The morphology can be linked to the mechanical behavior which is a good indication to assess the physical properties of the material. Another relevant information regarding the considered application is the wetting behavior, where oriented or channel like pores seem to be a definitive advantage.

II.2.d Influence on the wetting behavior

By the use of a controlled version of the ice-templating process, a unidirectional cellular pectin-based material was obtained. This oriented porosity could be useful in soil depollution applications as a way to maximize substrate transport *via* capillary phenomena.

Material and methods

Wetting behavior of the foams was assessed by impregnation of the foams with a solution of Disperse Red 1 at 0.2 g/L in absolute ethanol. The impregnation was recorded on camera and images were analyzed the ImageJ software. Wetting profiles were obtained by separating the impregnated regions from the dry ones by the "Threshold" function. The images were then assembled thanks to the "Reslice" function and the profiles were extracted by the "Find Edges" and "Save XY Coordinates" functions.

Initial wetting rates were measured from the slope of the profile during the first 1.5 sec of impregnation.

To highlight the influence of the porosity orientation, cellular pectin materials with a radial structure (obtained in a liquid nitrogen bath) and with a longitudinal porosity (obtained by freeze-casting) were subjected to the capillary ascension of a solution of Disperse Red 1 in absolute ethanol. The analysis of the images provided the corresponding wetting profiles (Figure II.10). The materials were impregnated both along and orthogonally to the pore orientation as was the case for compression. In the case of radial foams, alignment of the impregnation direction with the porosity could not really be obtained due to the distribution of orientations.

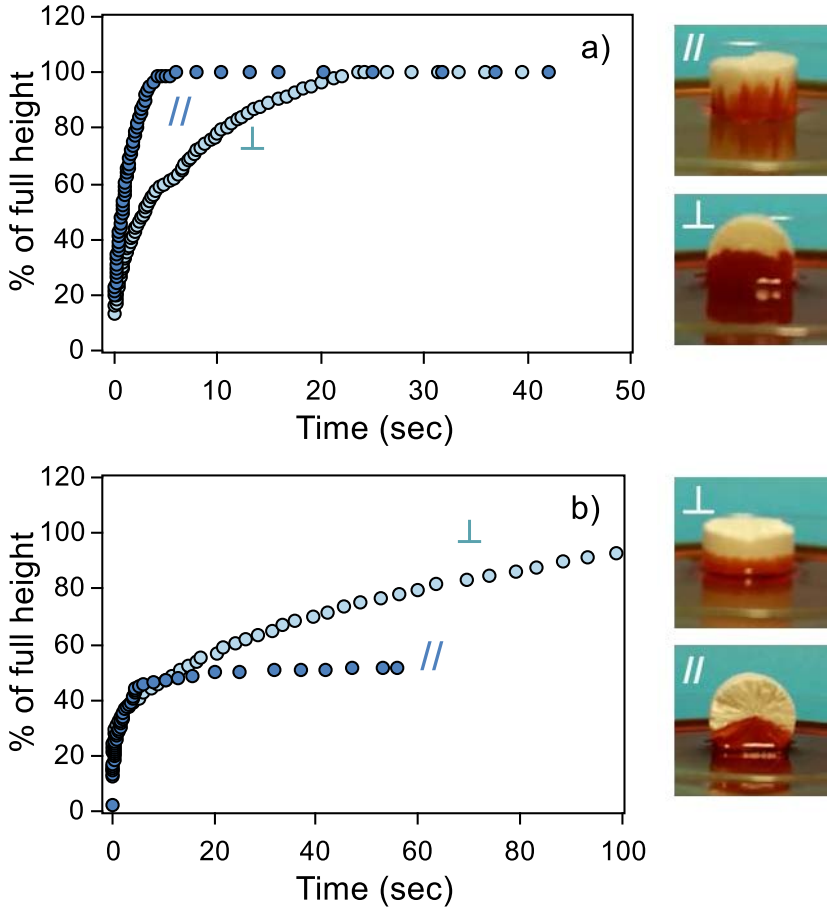

Figure II.10: Foams obtained by freeze-casting (a) show very different wetting behavior compared to radial foams obtained by ice-templating in liquid nitrogen (b). Mass transport seems to be more efficient in freeze-casted foams.

Table II.2 compiles the initial wetting rates for radial and freeze-casted foams. As expected, the capillary ascension was much faster along the material's pores. However it is interesting to notice that the radial foam is quickly impregnated up to 50% of its total height, but then the impregnation is drastically reduced. Due to the distribution of orientations, the wetting cannot occur along the porosity throughout the whole sample, and as a result the full wetting of the foam is a combination of longitudinal and orthogonal wetting regimes.

In the case of freeze-casted samples, further control of the wetting properties may be gained by taking advantage of the slight pore size gradient usually observed in samples[403].

Table II.2: Initial wetting rates are higher when impregnation occurs along the pores of the foam. Freeze-casted foams have higher initial wetting rate both along and perpendicular to the pores

Type of pores	Impregnation along the pores	Impregnation perpendicular to the pores
Axial porosity (a)	2.3	1.4
Radial porosity (b)	1.6	0.8

Both the foams obtained by plunging into liquid nitrogen (radial foams) and the freeze-casted materials (with a longitudinal porosity) may have significant interest from an application point of view based on their mechanical and wetting behavior. They were further investigated in terms of fine tuning of the morphology.

II.3 Variations around foams obtain with a liquid nitrogen bath

The freezing method has a direct influence on the morphology of the foams and macroscopic properties, but it is also possible to tune these by formulation of the initial solution and variations of the processing parameters.

II.3.a Influence of the polymer concentration

The morphology of radially oriented foams obtained by plunging polymers solutions into a liquid nitrogen bath can be modified by changing the composition of the initial solution. This may refer to the nature of the polymer itself, to the presence of various additives but also more simply to variations in the concentration of the polymer.
Samples were prepared from pectin solutions at various concentrations, which proved to have a direct influence on the pore morphology, as can be seen in SEM cross sections (see Figure II.11).

Material and methods

Solutions of various pectin concentration (40, 45, 50, 55 and 60 g/L) were prepared by dissolving beet root pectin in deionized water. Solutions were stirred under magnetic agitation a few hours at 40°C to facilitate dissolution of high pectin contents. About 1.8 mL of solution was poured into 2 mL cryotubes (about 0.8 cm in diameter and 3 cm in height). The samples were plunged into liquid nitrogen for a few minutes and immediately vacuum dried for 24 h.
Cross sections were cut with a scalpel and sputtered with 20 nm of gold for SEM observation.
The SEM pictures were analyzed with the ImageJ software for pore morphology characterization. Pore dimensions were determined on 150 separate measurements. Pore wall thickness was estimated by performing 5 measurements on 4 different pore walls.
Pore size characteristics are presented as box-and-whiskers plots (see Annex p 202).

The most direct way to characterize the morphology of the pore walls is the measure the pores width, or in other term, the space between two pectin layers. (Figure II.12 a). It is also possible to measure the pore walls thickness (Figure II.12 b). It must however be noted that these values are less statically relevant that pore width due to the limited number of measurement performed. In addition both pore width and pore wall thickness measurements may be subjected to slight perspective errors since SEM pictures are never taken perfectly orthogonally to the sections. They can however give a good order of magnitude for these dimensions and information about general tendencies in size variations.

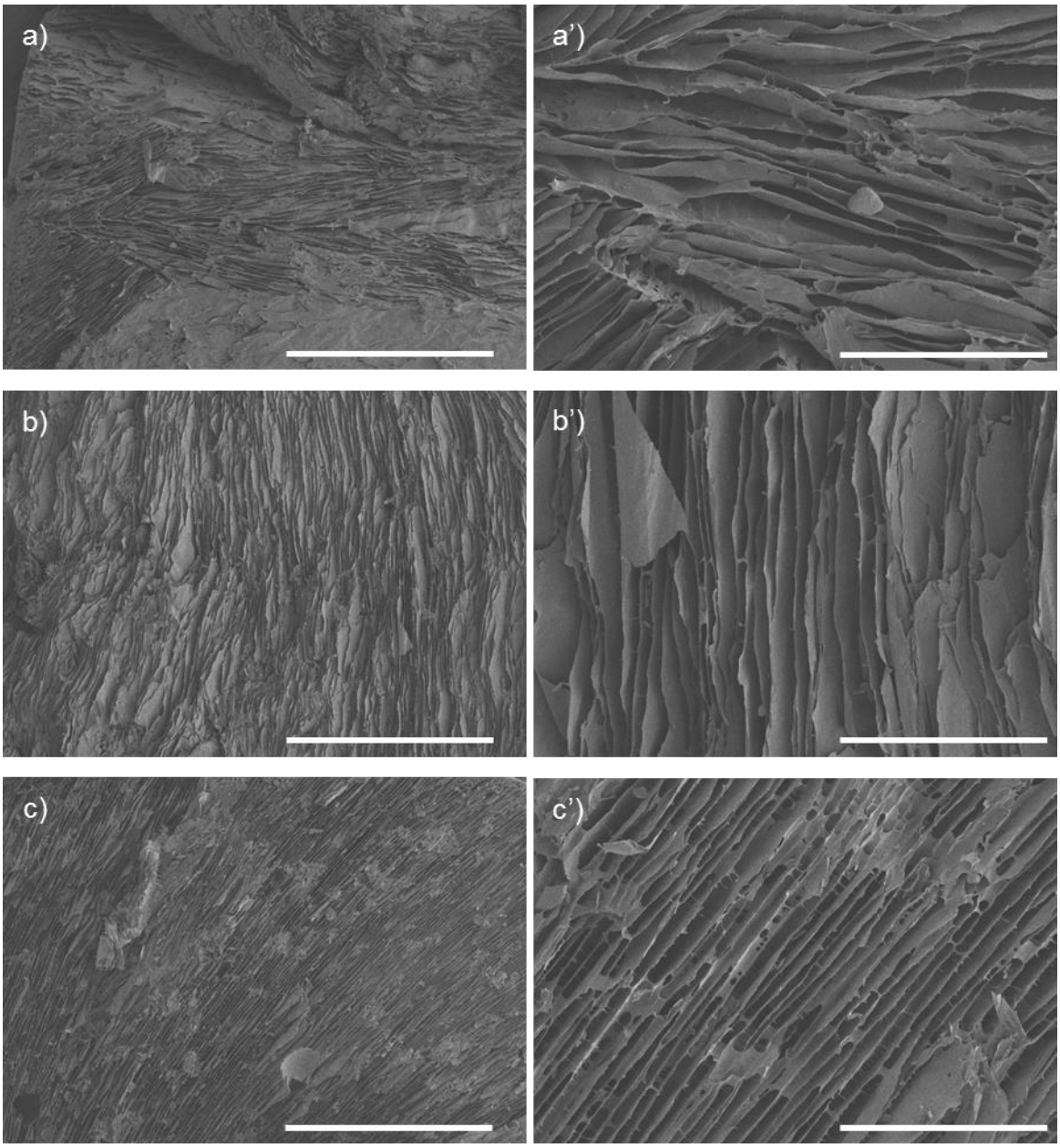

Figure II.11: Foams prepared at 40 g/L (a and a') display wider and less ordered pores than foams prepared at 50 g/L (b and b') and 60 g/L (c and c'). Scale bars: 500 µm for a, b and c, 100 µm for a', b' and c'.

Pore wall thickness and pore width are linked but it is difficult to highlight a simple relation between these two dimensions, because there are many other parameters to take in account, including the pore length, the total polymer content, the pore wall density as well as the total number of pores. Assuming similar pore walls densities and a constant polymer concentration, smaller pores (*i.e.* smaller ice crystals) would mean more pore and therefore more pore walls, resulting in thinner pore walls. On the other hand, if a constant number of pores is assumed, as well as a constant pore wall density, thicker pore walls may be expected at higher pectin concentration.

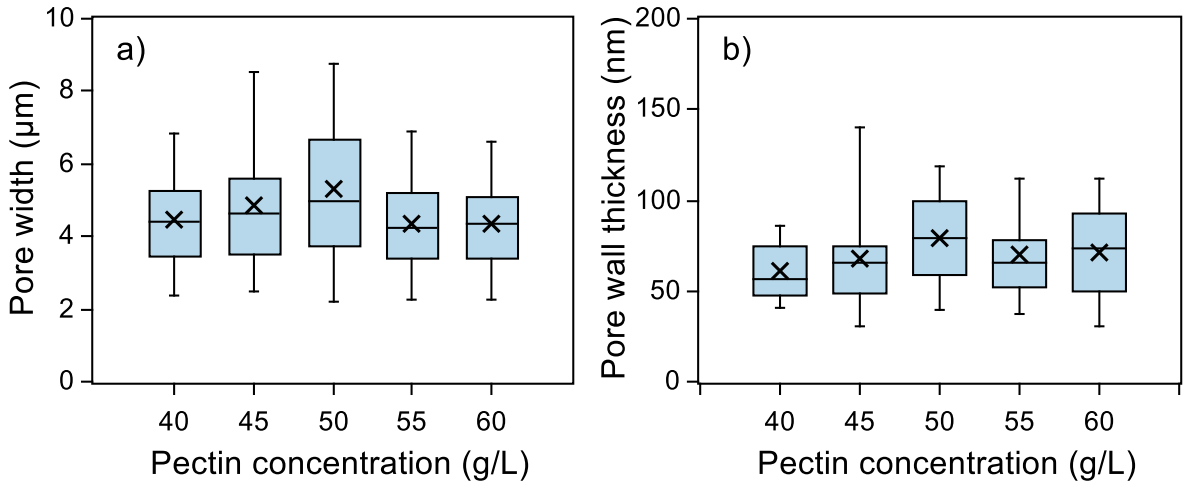

Figure II.12 : Pore width (a) and pore wall thickness (b) are not significantly different when the polymer concentration changes.

But in reality it is difficult to modify one of these parameters without changing the others. As a result, there is not clear variation over the concentration range considered (40 to 60 g/L in pectin) for the pore width or pore wall thickness. This may be due to the fact that several parameters are changing at the same time, possibly compensating each other. For a more comprehensive evaluation of the influence of the pectin concentration, it would be interesting to study foams prepared at lower concentrations. However, for too low concentrations (below about 10 g/L), it might be difficult to obtain self-supporting materials due to the lack of a dense polymer network to form the pore walls. Higher pectin concentrations induce higher solution viscosity, which may involve the presence of higher mechanical constraints during the ice growth, thus limiting the formation of ice-crystals. Direct interactions between the polymer and the ice surface may also influence the ice growth. For considered range of concentrations however, no significant pore width change was monitored (see Figure II.12 a).
No significant pore wall thickness variation can be observed (see Figure II.12 b). As mentioned earlier, higher concentrations may be expected to result in thicker pore walls. But smaller, and therefore more numerous, pores implies more pore walls, which may therefore be thinner.
If the width of the pores or the pore wall thickness does no change dramatically when the concentration changes, the organization of the pores is modified, as can be seen at higher magnification (Figure II.11 a', b', c' and d'). Higher pectin content seem to result in more ordered and more regular pores. Although cutting of the samples for observation in SEM may slightly alter the aspect of the pores, it is clear that the pores are better aligned in the foams obtained at 50 and 60 g/L than the foam at 40 g/L.

II.3.b Influence of the addition of a reheating step

Beside the pore size, another important aspect of the pore morphology is their interconnectivity. It has been reported that the solvent nature may be able to tune this

aspect[280]. In this case however, the aimed application must be taken in account. Since the material is to be used as a host for microorganisms, it is essential to use nontoxic solvent such as water. Instead of modifying the formulation of the initial solution, the tuning of the pore morphology was investigated through processing parameters.

Material and methods

Foams were prepared in the same way as previously described by dissolving 40 g/L of pectin in deionized water, and stirring overnight at room temperature. 1.8 mL of the solution was poured into 2 mL cryotubes, which were plunged into liquid nitrogen for a few minutes.
Half the samples were immediately put to dry in the freeze-drier, and the other half was left 5 minutes in a 0°C bath and subsequently freeze-dried.
Transversal slices were cut and sputtered with 20 nm of gold for observation in SEM microscopy.

Figure II.13 presents the aspect of foams obtained by plunging a pectin solution in liquid nitrogen and drying the obtained samples. A reheating step up to 0°C was added to study the influence of the initial temperature of drying.

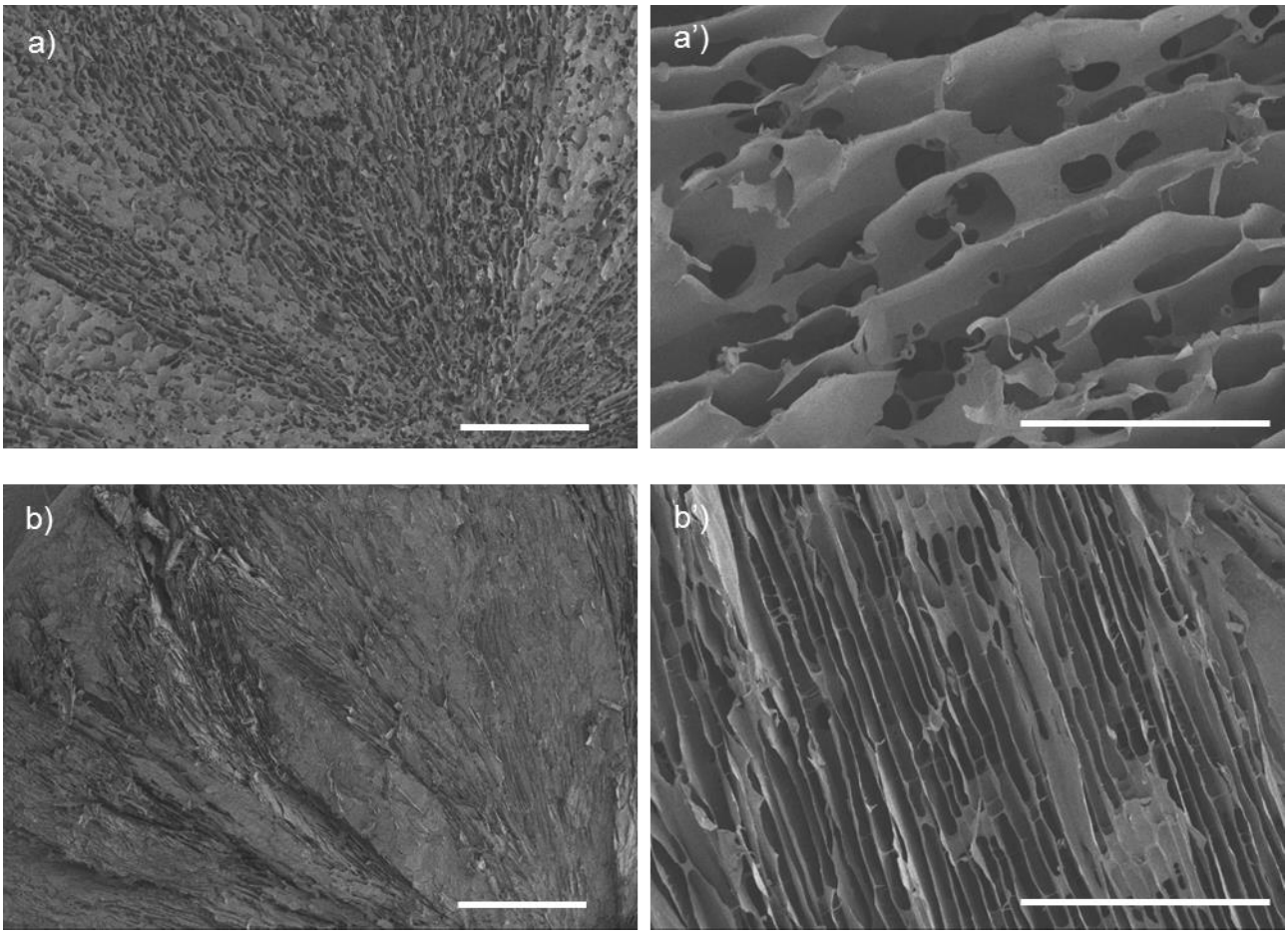

Figure II.13: When sample are reheated prior to drying (a and a') pores are bigger and more interconnected than when sample are dried immediately after freezing (b and b'). Scale bars: 500 µm for a and b, 100 µm for a' and b'.

When the samples are reheated the morphology of the foam changes dramatically. Pores become much wider (about 200 µm) as can be seen in Figure II.13 a', while pores are only 5 µm wide in the case of the foams obtained by drying immediately after freezing (see Figure II.13 b'). When the samples are reheated, interconnections between adjacent pores appear. The diameters of these openings range from 100 and 300 µm. The general radial organization is however preserved as can be seen at lower magnification (Figure II.13 a and b).

Pore interconnections have been reported in materials obtained by ice templating, but they generally result from the use of solvents yielding highly dendritic structures upon freezing. In presence of specific composition[404] or additive[274,405], or with different solvents[280] a large array of pore morphologies may be obtained. They result in pore interconnections which are generally finely controlled and well organized. In this case however, ice-formation is strictly similar between the two samples. The protocol only differs after complete freezing of the sample. Some level of reorganization in the ice network upon reheating may occur and the formation of interconnections might be due to the partial thawing of the ice crystal and subsequent local dissolution of the pectin walls. Samples are however put under vacuum before complete melting of the sample.

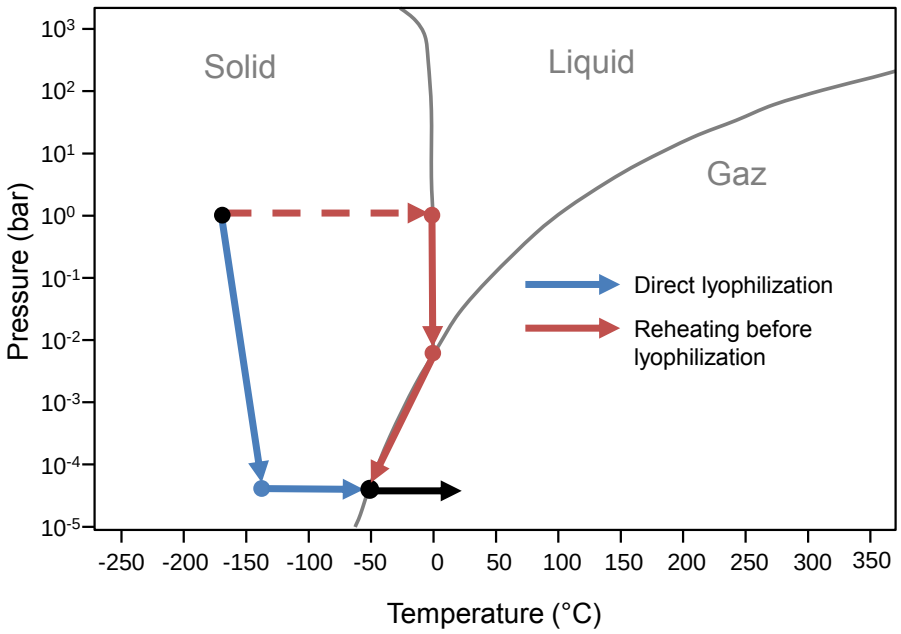

Figure II.14: In samples dried directly after freezing (blue arrow) pressure drops below the triple point and the ice undergoes sublimation which results in lamellar pore walls. When the initial temperature of the sample is higher (red arrow), the sample crosses the melting line. However, since the pressure quickly drop, only small regions have time to melt and dissolve the pectin walls.

When samples are placed in the freeze-drier directly after freezing, pressure drops to 0.05 mbar in a few minutes, which is below the pressure of water triple point (6.1 mbar). Although the sample temperature slowly rises again, the phase transition that the sample undergoes is sublimation (Figure II.14, blue arrow) and not thawing. When the sample is reheated slightly below 0°C, the sample is subjected to partial melting before the pressure reaches a value sufficiently low to ensure ice sublimation. (Figure II.14, red arrow). The repartition of the

interconnections may be attributed to locally higher solutes concentrations at the surface of the pectin wall, resulting in the local lowering of the ice melting point and subsequent dissolution of small regions of the pectin wall. The change in pore width may however suggests complete thawing and re-freezing of the ice lamellas, resulting in a rearrangements of the pore walls.

Other variations of this drying step may be designed. For instance drying of the sample inside the original mold or in a larger container also has an influence on the pore interconnectivity. Such interconnections may present a significant interest regarding the targeted application as a way to ensure good substrate exchanges all throughout the samples. The method however presents the serious drawback of being difficult to precisely control. It relies on a fragile equilibrium between partial thawing of the pore walls and preservation of the general structure. This implies the necessity to control the temperature in the sample, which may prove extremely versatile depending on the sample size and geometry, and results in very low reproducibility. A more controlled way to tune the pore morphology would therefore be to control not the fate of the ice crystal before sublimation, but the growth of ice crystal themselves.

II.4 Tuning of freeze-casting conditions

Although the method of ice-templating by plunging into liquid nitrogen has the great advantage of being very easy to implement, it does not provide sufficient control over the ice growth itself. As mentioned earlier, the freeze-casting technique confers control over the geometry of the temperature gradient, and therefore over the pore orientation, but it also allows for a control of the freezing-rate as a way to modulate the ice growth, and therefore the pore size and morphology[273].

II.4.a Influence of the solution concentration

In order to gain control over the material morphology, key parameters must be identified all along the synthetic path. The first step of the material preparation is the formulation of the aqueous pectin solution. As a result, it may seem logical to start tuning the material properties through the composition of the initial solution. Depending of the type of polymer used, the morphology of the pores may vary significantly[187,261,300,304,320,322]. However, even a change of concentration for a given polymer may have an influence on the aspect of the pores as can be seen in Figure II.15.

Material and methods

Solutions at different concentrations (20, 30, 40 and 50 g/L) in pectin were characterized with a MCR 302 Anton Paar rheometer. The solutions were stirred under magnetic agitation overnight at room temperature. Measurements were performed under cone-plane geometry, with a 24.969 mm diameter, 1.0110° angle and 50 µm truncation. Viscosity was measured as a function of shear rate, between 1 and 100 s^{-1}.

Samples were prepared for each concentration by freeze-casting of 3mL in 15 mm diameter mold, at 10°C/min and dried for 48 h at 0.05 mbar.

Cross sections and longitudinal sections of the foams prepared at different pectin concentrations were cut and sputtered with 20 nm of gold for SEM observation. SEM images were analyzed with Fiji software and the OrientationJ plugin.

Cubes of 1x1x1 cm were cut to assess the mechanical behavior under longitudinal compression (compression in the direction of the pores). Each measurement was repeated on 5 different samples.

To assess the efficiency of liquid transport within the foams, samples obtained from different concentrations were put in contact with a 0.2 g/L solution of Disperse Red 1 in ethanol. Impregnation was recorded and the images were analyzed using Fiji software to extract the wetting profiles.

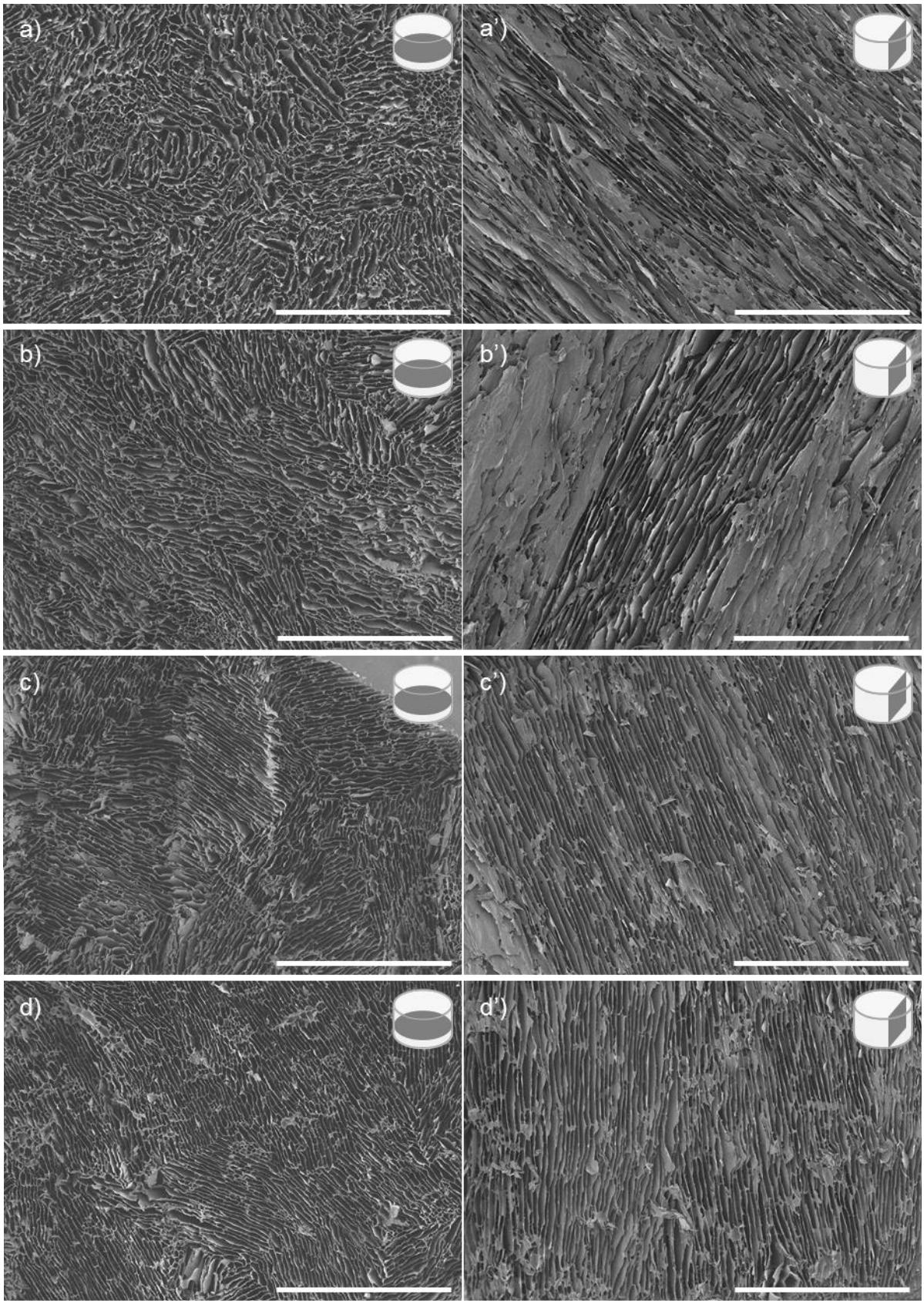

Figure II.15: Pores in foams obtained from solutions at 20 g/L (a and a') and 30 g/L (b and b') are wider and shorter, as well as less organized than pores in materials freeze-casted from 40 g/L (c and c') and 50 g/L (d and d') pectin solutions. Scale bars: 500 µm.

For pectin concentrations between 20 and 50 g/L, the same aligned morphology can be observed from longitudinal sections (see Figure II.15 a', b', c' and d'). However, cross section SEM images (see Figure II.15 a, b, c and d) display notable differences.

At low pectin concentration, the pore, though unidirectional (see Figure II.15 a' and b'), do not present well-ordered lamellar porosity. The orientation domains of well-aligned pore can only be seen for higher polymer content. Increase in polymer concentration induces an increase in the order of the porosity. This might be due to higher mechanical constraints in highly concentrated solutions.

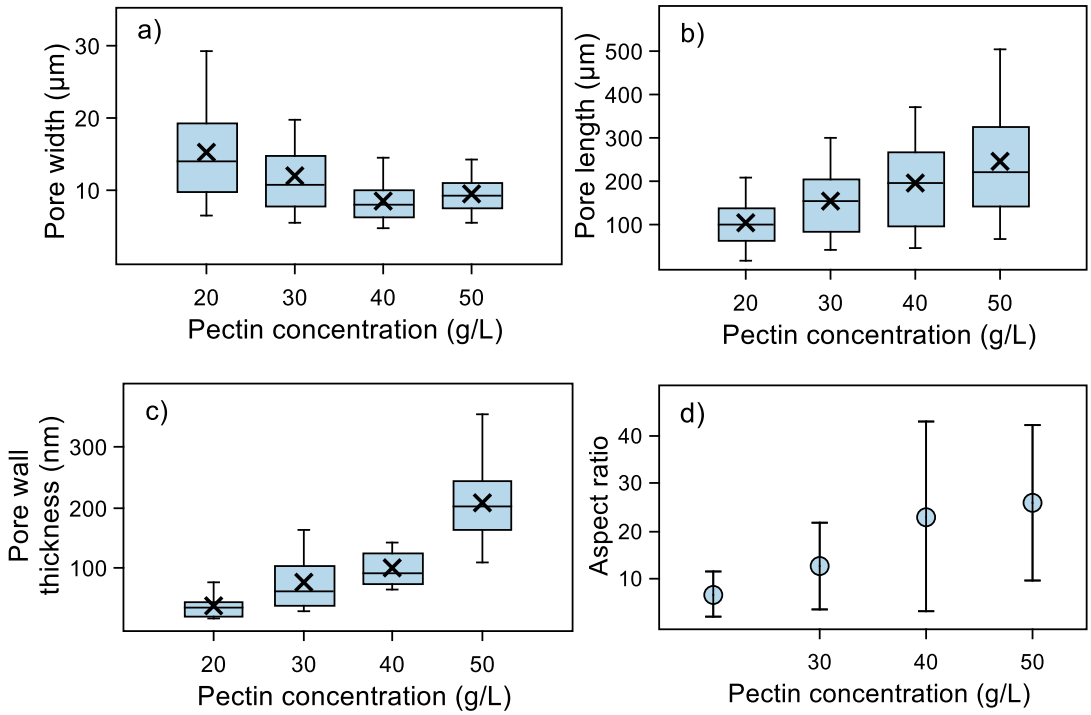

Figure II.16: At higher concentration, pore exhibit narrower (a) and longer (b) pores, as well as thicker pores (c). Variations in width and length of the pore results in a significant shift in the pore aspect ratio (d).

The preferential growth of ice in certain directions has a direct influence on the aspect ratio of the pores (see Figure II.16 d). Analysis of the SEM cross section also revealed a significant modification of the pore sizes (see Figure II.16 a and b). Lower pectin densities are responsible for wider (pores range from 8.5 to 15.3 µm) and shorter pores (from 104 to 245 µm). Pore walls are also thinner (from 39 to 208 nm) when the initial concentration in polymer is low. The larger pores, which also means a reduce number of pores since the overall size of the sample does not change, as well as the thinning of pore walls can be linked to the lower amount of polymer available for the formation of the walls when the initial solution has low pectin content. But variation in solutes concentrations also influence the liquid/solid interface, since both the viscosity and freezing points are modified by the solute concentrations.

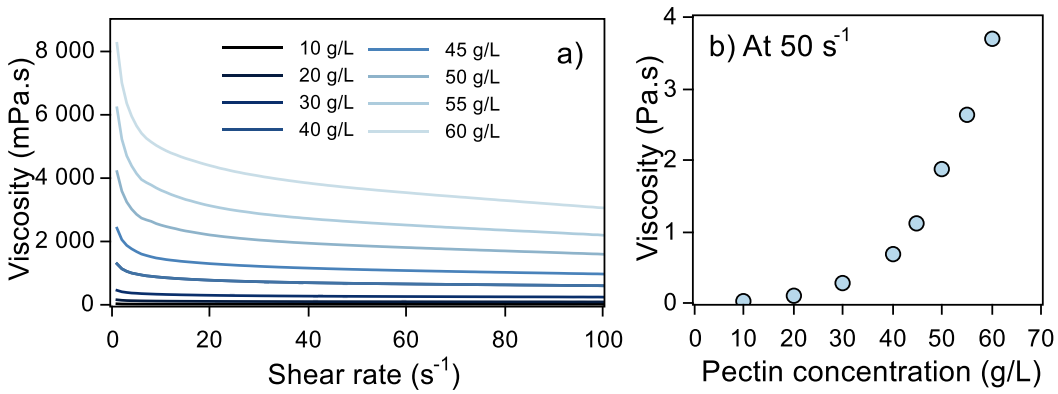

Figure II.17 : Higher polymer concentrations result in higher viscosity (a). Above a critical concentration (40 g/L) the polymer chains are percolating resulting in sharp viscosity increase (b).

Another parameter to consider is the variation in viscosity of the polymer solution according to concentration (see Figure II.17). Low concentration solutions exhibit lower viscosity, as a result, ice growth is less mechanically constrained which results in larger ice crystals and therefore larger pores.

Once again, the tuning of the cellular structure can be directly linked to the control of mechanical behavior. As may be expected, the materials prepared from higher concentration solutions exhibit higher Young's modulus, compressive strength and toughness (see Figure II.18 and Table II.3). The changes in the initial solution concentrations correspond to the variation in the porous materials final density. As was documented by Ashby and coworkers[402], Young's modulus tends to increase with apparent density, regardless of the type of material. Young's modulus measured for these materials (between 1 and 5 MPa) are typical for polymer foams with density ranging from 20 kg/m^3 to 50 kg/m^3. The stress-strain profiles show typical behavior for polymer foams, with an initial elastic behavior (up to about 7% strain), followed by a plastic deformation plateau (between 7 and 40% strain). The material then undergoes a densification, which translate in a strain increase beyond 40% deformation.

Table II.3 : Mechanical characteristics of foams obtained by freeze-casting at 10°C/min from pectin solutions at various concentrations under compression along the pores direction.

Concentration (g/L)	Density (kg/m^3)	Std dev (kg/m^3)	Young's modulus (MPa)	Std dev (MPa)	Compressive strength (kPa)	Std dev (kPa)
20	23.7	1.3	0.97	0.17	20	2
30	31.3	1.5	1.13	0.25	58	1
40	40.7	1.2	2.91	0.76	115	6
50	48.5	1.9	4.96	2.05	185	8

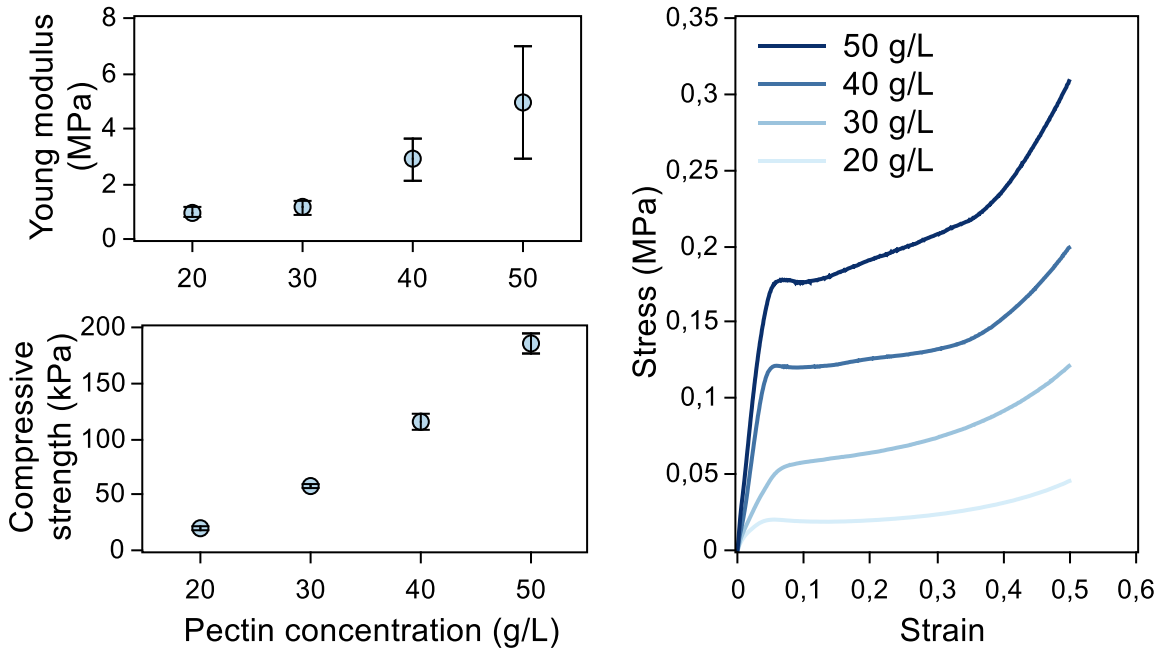

Figure II.18: Higher pectin concentrations result in higher apparent density which results in higher Young's modulus and compressive strength

Materials with different densities follow the same general profile, however the yield strength changes significantly (variation between 20 and 186 kPa). This might be linked to the changes in pore walls thickness mentioned previously.

The wetting behavior of the foams was assessed by impregnation of 1 cm high foams using a solution of Disperse Red 1 in ethanol (see Annex p 213). Despite differences in the pore size, the wetting profiles were similar for the samples prepared from pectin solutions at different concentrations. All samples were impregnated in less than 0.5 s.

As mentioned previously, both the initial solution and the actual processing parameters can be tuned to modulate the pores morphology. One of the major advantages of the freeze-casting technique compared to simple dipping in liquid nitrogen is the possibility to control the cooling rate of the sample as a way to control the structure of the foam.

II.4.b Influence of the freezing-rate

The freeze-casting technique provides a control of the temperature gradient in terms of kinetics thanks to the use of a controller to set a specific cooling rates. This parameter has a direct influence on the pore morphology (see Figure II.19).

Material and methods

A solution of pectin at 40 g/L was prepared from beet root pectin and deionized water and stirred overnight at room temperature.

Samples of 3 mL were prepared in 15 mm diameter molds. Three cooling rates were used: 1, 5 and 10°C/min. The samples were then lyophilized for 48h.

SEM observations were performed on transversal and longitudinal slices, sputtered with a 20 nm gold layer.
Mechanical behavior was assessed under longitudinal compression on 5 replicates of 1 cm^3 cubes.
Wetting behavior was assessed by impregnation of the foams by a solution of Disperse Red 1 in absolute ethanol. The capillary ascension was filmed and the images were analyzed thanks to Fiji software to recover the wetting profiles.

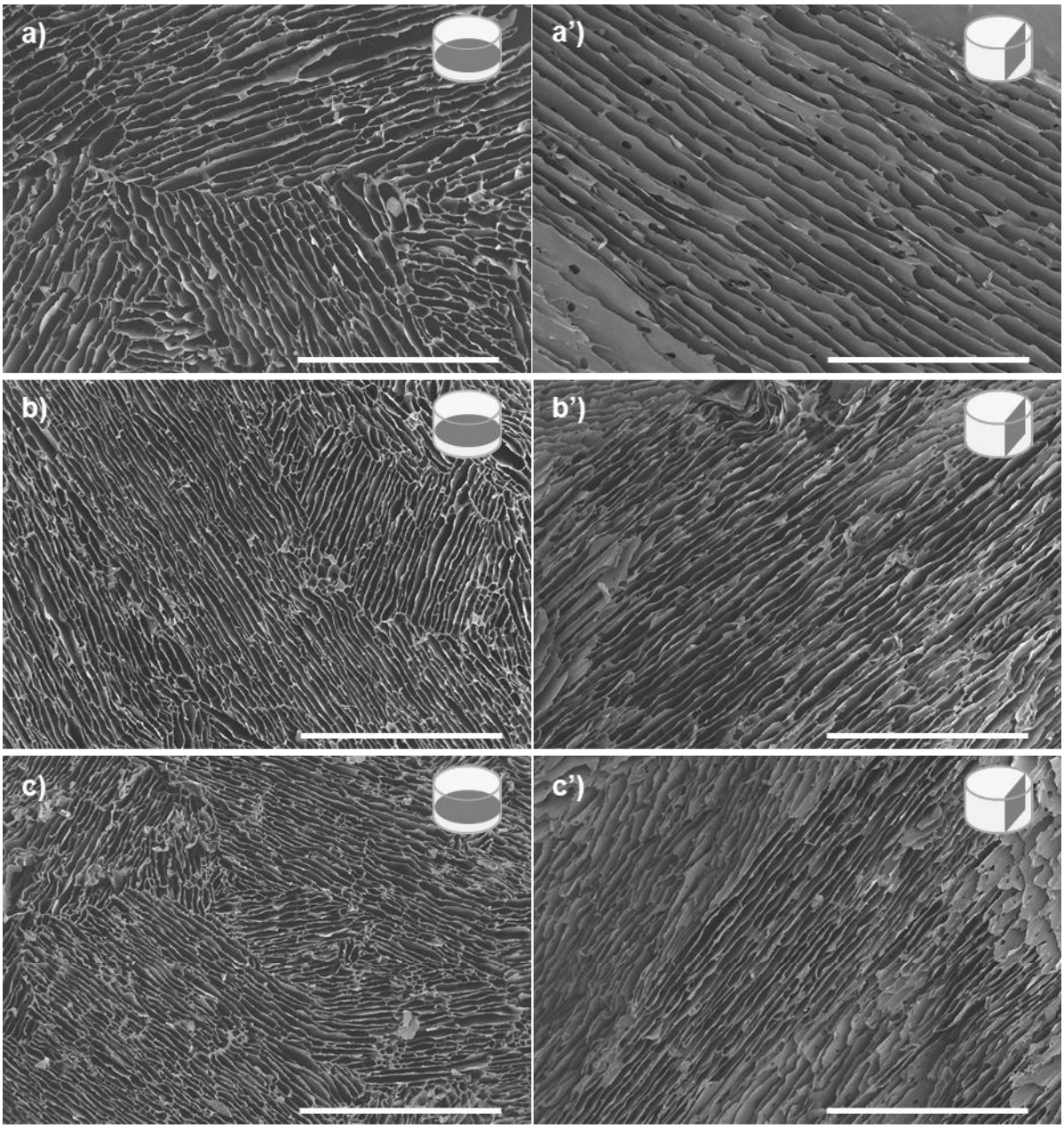

Figure II.19: Transversal (a, b and c) and longitudinal (a', b' and c') SEM observations of foams obtained by freeze-casting of 40 g/L pectin solutions at different freezing rates show common oriented and lamellar porosities. The general morphology is similar for foams obtained at 1°C/min (a and a'), 5°C/min (b and b') and 10°C/min (c and c'), however pore size varies. Scale bars: 500 µm.

The materials are characterized by a lamellar structure, where the elongated pores are organized in several domains of same orientation. The orientation analysis (see Figure II.20 d) allows for a better discrimination of these alignments. Regardless of the cooling rate, several wide peaks can be observed on the cross section distribution chart (Figure II.20 d), which correspond to the different lamellar domains. Analysis of the pore orientation distribution also reveals that the longitudinal alignment of the pores is not modified by the change of cooling rate. The orientation distribution in longitudinal sections (see Figure II.20 e) displays a single and narrow peak. The width at mid-height of the peaks show no significant variation (respectively 17°, 13° and 14° for cooling rates of 1°C/min, 5°C/min and 10°C/min). The freeze-casting technique therefore proves to be applicable with variable sets of parameters, while preserving the key feature of oriented porosity.

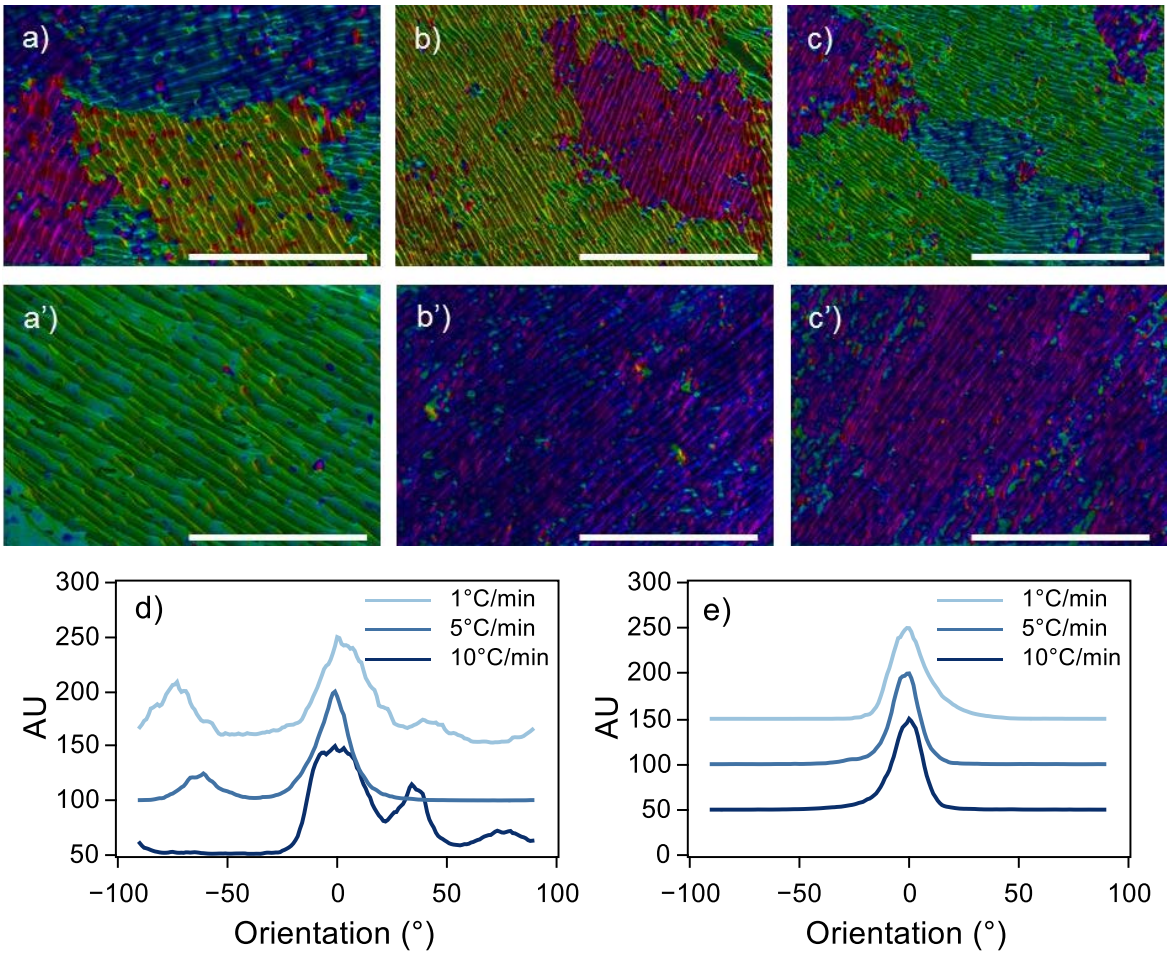

Figure II.20: Foams obtained at 1°C (a and a'), 5°c/min (b and b') and 10°C/min (c and c') have similar, well aligned morphologies. Observation of transversal slices (a to c) show several orientation domains resulting in the presence of multiple peaks in the orientation distribution. Orientations domains appear larger at low cooling rates. (d). Mapping of the pores orientation on longitudinal slices (a' to c') reveals perfectly aligned pores which translates into single well defined peaks in the orientation distribution (e). Scale bars: 500µm. Orientation distribution curves were normalized, centered on zero and an offset was applied for clarity.

Even though the general organization of the porosity is the same regardless of the cooling rate, the SEM pictures of cross sections (see Figure II.19 a to c) reveal slight pore size variations.

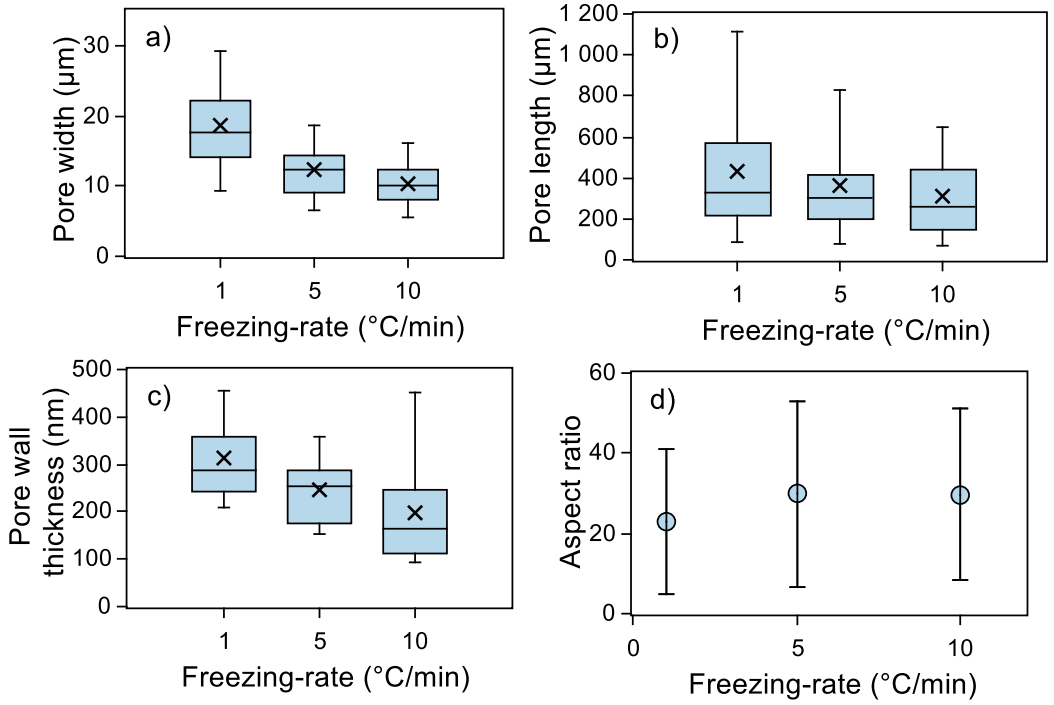

Figure II.21: Faster cooling results in narrower (a) and shorter (b) pores, but the aspect ratio does not change dramatically (d). The pore wall thickness decreases (c) at higher freezing rate.

Figure II.21 presents the variations in pore width and length, as well a as pore wall thickness, in function of the freezing-rate. Mean pore length varies from 309 µm to 428 µm when the cooling rate decreases. The large standard deviations for these values must however be underlined. This may be explained by the length variations observed in each orientation domain. A more significant parameter to describe the cellular material's morphology might therefore be the pore width which presents smaller deviations. The pore width mean values range from 10,4 µm at 10°C/min to 18,7 µm at 1°C/min. Slower freezing is responsible for the formation of larger ice crystal. The resulting pores after freeze-drying are therefore wider. A decrease in the pore wall width can also be observed at high cooling rates (see Figure II.21 c) (200 nm at 10°C/min vs 312 nm at 1°C/min). All these samples have a similar density, so that when the number of pores per cm² increases (*i.e.* when pores are smaller), the amount of polymer available for each pore wall decreases, resulting in thinner pore walls.

Contrary to samples prepared at different pectin concentrations, in this case the apparent density of the foams is similar although the morphology of the pore and the pore wall thickness are different.

These small structural changes have no clear influence on the mechanical properties of the foams. Values for Young's modulus and compressive strength are presented in Figure II.22 and Table II.4.

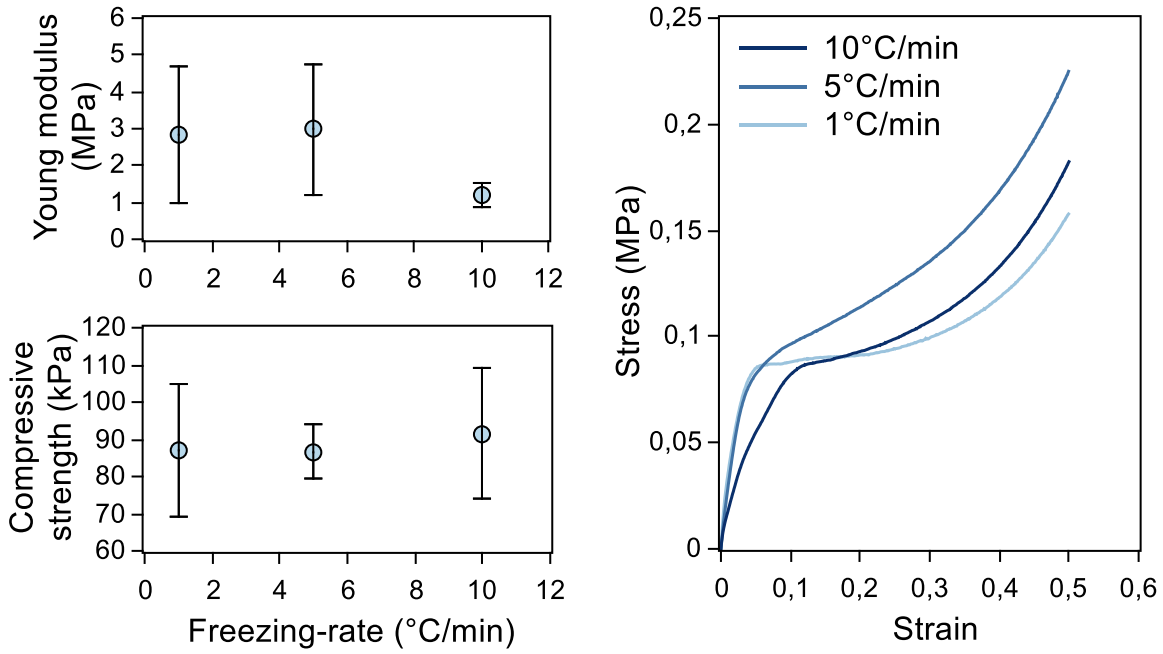

Figure II.22: No significant changes in mechanical properties can be seen in samples prepared at various freezing rates.

Table II.4: Mechanical characteristics of foams obtained from pectin solutions at various freezing rates under compression along the pores direction.

Freezing-rate (°C/min)	Young's modulus (MPa)	Std dev (MPa)	Compressive strength (kPa)	Std dev (kPa)
10	1.21	0.32	91	18
5	2.98	1.70	87	7
1	2.84	1.84	87	18

Young's modulus values are around 3 MPa and compressive strength are about 0,1 MPa while are typical values for polymer foams[402]. A slight drop in Young's modulus can be observed at 10°C/min, but remains within the standard deviations of the measurements at 1°C/min and 5°C/min.

The wetting behavior of the foams was assessed with foams prepared at different freezing rates (see Annex p 213). No significant change in the wetting profile could be observed, all the samples were fully impregnated in less than 0.5 s.

Modifications of the freezing-rate had a significant influence on the pore morphology and size (smaller and better-organized pores at higher freezing rates). The macroscopic properties of the foam such as the mechanical behavior or the wetting properties were however not impacted.

Conclusion

Ice templating proved to be an efficient way to shape beet root pectin. Pectin solutions were processed into porous dry foams thank to freeze-drying.

Various freezing methods were compared and proved to yield various pores morphology which has a direct influence on the macroscopic properties of the foam such as mechanical or wetting behavior, which are of great importance from the application point of view.

Freezing in conventional freezers yielded anisotropic pores, but freezing in liquid nitrogen and freeze-casting resulted in the formation of oriented porosity, respectively organized in a radial or longitudinal fashion.

The freeze-casting technique confers control over processing parameters such as the freezing rate. Other parameters like the polymer concentration may also be modified in order to tune the pores morphology. Characteristics such as pore width or pore wall thickness can be modified in order to control the macroscopic properties of the foam. The oriented porosity, which is the key feature of this pectin-based cellular material is however preserved.

The shaping of the polymer is the first step toward the elaboration of a hybrid material destined to host living organisms (see Figure II.23). Good comprehension of the various processing parameters which may also have an influence on the viability of the encapsulated species will be essential in the design of the encapsulation protocol in order to accurately evaluate and predict their influence on the foam morphology.

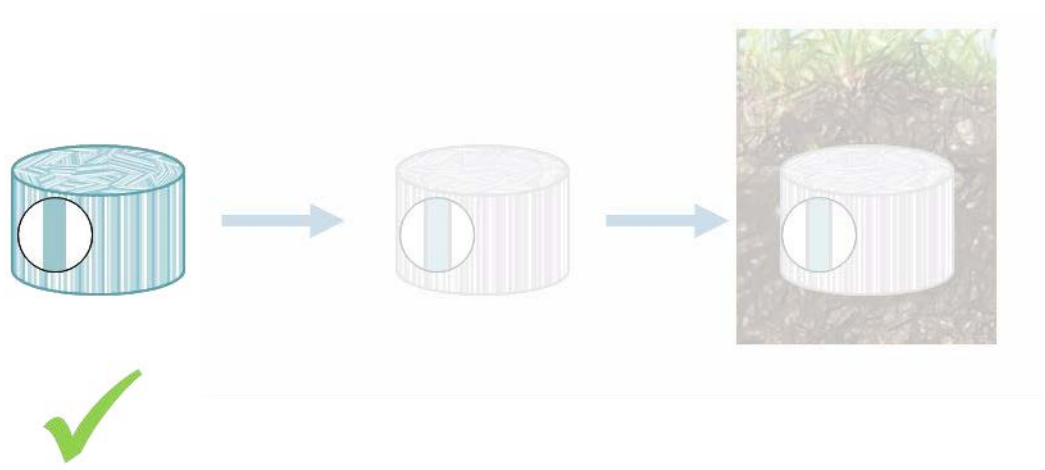

Figure II.23: Pectin macroporous foams with unidirectional porosity and tunable pore size were obtained by freeze-casting.

Chapter III : Design of a biopolymer-silica hybrid porous structure

Introduction

Pectin foams with unidirectional porosity may represent an interesting asset in the design of a device for soil depollution, since they should favor mass transport of the targeted pollutant through capillary phenomenon. Pectin was chosen in particular for its non-cytotoxicity and water solubility, which are essential for hosting living organisms. The water solubility of pectin, though being an advantage from the encapsulation perspective, may be problematic from the structural point of view, since the material is destined to be implanted in soils. The water content of the considered soils is likely to dissolve the pectin structure rendering the device inefficient. One option to prevent such dissolution of the foam is to coat the polymer with an inorganic material capable of ensuring its structural integrity in a hydrated state.

Silica appears as a good candidate to play the part of the inorganic moiety in such a hybrid foam. It is both eco-friendly (silica is a major component of soils) and non-cytotoxic to the considered microorganisms (silica gels have been used for bacteria encapsulation[113]). Another advantage of silica is the fact that it can easily be obtained through sol-gel processes, which can be performed at low temperature and under mild conditions. Such considerations are essential, since the silica coating is meant to be applied on pectin foams containing living bacteria. A vapor phase sol-gel silica deposition method to coat macroporous pectin foam with a silica layer was developed and optimized, as a way to prevent dissolution of the structure upon contact with water.

III.1 Silica coating using vapor deposition

III.1.a About sol-gel and gas phase deposition

This developed vapor phase silica deposition technique is based on sol-gel chemistry of tetraethyl orthosilicate (TEOS) (see paragraph I.2.c.i, p30). TEOS is one of most commonly used sol-gel silica precursors. Alkoxides in general have been used for applications ranging from industrial coatings[406,407] to encapsulation matrix for sensitive biomaterials[111,408]. Typically, TEOS can be hydrolyzed with water in a liquid phase, and can then be condensed to form the inorganic polymer network. Both acidic and basic conditions may be used to catalyze hydrolysis, resulting in different morphologies and properties[409].
In several applications, formation of thin and homogeneous layers of silica is crucial. One way to obtain such materials is to use vapors of silica precursors as a way to precisely control the amount of reactive species involved. Early gas phase deposition techniques have been developed for microelectronic devices[410] and involved use of high temperatures[411] under oxidizing conditions. Alternative methods including use of plasma or ozone[412] have been used to gain better control over the silica layer properties and characteristics. These methods are commonly referred to as chemical vapor deposition (CVD), but many variations have been described regarding deposition conditions (including temperature, pressure, precursors or activating species). However for specific applications such conditions were not suitable, especially when living cells were involved[413]. Classical sol-gel techniques, which have the great advantage of being usable at low temperatures, were therefore adapted to gas phase deposition techniques[414]. Such methods have been especially efficiently used for immobilization of various structures (from lipids[415] to various cells[210,416,417]) with thin silica layers. Silica precursors (most commonly TEOS or TMOS) have also been deposited on a wide variety of substrates, including polysaccharide hydrogels, in order to yield hybrid matrices for cell encapsulation[418,419].
This approach was therefore chosen for the coating of the pectin-based foams.

Materials and methods

In a typical coating experiment, pectin macroporous foams were prepared as previously described. 40 g/L beet root pectin solutions were frozen either by dipping in liquid nitrogen (hereafter noted radial foams) or by freeze-casting at 10°C/min (hereafter noted freeze-casted foams), and subsequently vacuum dried at least 24h at 0.05 mbar.
Foams were maintained in a desiccated atmosphere until further use. Before silica deposition, pectin foams were weighted (initial mass was noted m_i). Silica deposition in vapor phase was performed in a closed vessel (see Annex p 210) containing an aqueous solution of HCl at 5 wt%, saturated with NaCl (typically 17 mL of 37 wt% HCl was introduced in 133 mL of deionized water and 60 g of NaCl was added). Samples were placed on a perforated plate. Vials of tetraethyl orthosilicate (TEOS) were introduced (typically 4 vials containing 10 mL of TEOS). The deposition chamber was then sealed and maintained at 30°C. After chosen

deposition times (ranging from a few days to several weeks), samples were removed from the closed vessel and maintained 24h at 30°C in an open container and subsequently at least 24h in desiccated atmosphere at room temperature. Samples were weighted again and this value was considered as the final mass (note m_f).
As a first approach, mass gain was assumed to correspond to the addition of silica. Weighing was therefore used as a straightforward way to assess silica content of the foams (noted $\%_{SiO2}$).

$$\%_{SiO2} = \frac{m_f - m_i}{m_f} \times 100$$

where $\%_{SiO2}$ is the weight mass percentage of silica, m_i the initial polymer mass, m_f the final mass.

Pectin foams were put in contact with an atmosphere containing TEOS vapors, HCl and water to ensure hydrolysis and condensation. At 30 °C NaCl saturated aqueous solutions are expected to yield 75.6 % of relative humidity[420]. Presence of HCl at 5 % may however slightly modify this value. Azeotropic point for HCl/H_2O mixture is for a 20 % HCl content, which means that solution and atmosphere composition might vary slightly over time. Direct pre-hydrolysis of the liquid TEOS in the initial vials may confer better control over the stoichiometry of TEOS and water, as well as a precise pH control. This would however lead to the rapid condensation or at least formation of oligomers in the vials. The resulting mixture would not be volatile enough to ensure vapor phase deposition of the reactive species on the surface of the foams. In this setup, hydrolysis and condensation occur directly on the polymer surface, resulting in the progressive and controlled formation of a silica layer. The drawback to this precise control is that small amounts of precursors are reacting, resulting in a slow formation of the silica layer.
It might be argued that higher processing temperatures may be of interest in speeding the process up (all depositions were performed at 30°C). Use of higher temperatures may allow for higher saturation vapor pressure of TEOS, resulting in larger amounts of available molecules on the pectin pore walls. In addition kinetics of hydrolysis and condensation are temperature dependent. Higher temperatures may however not be compatible with cell survival. Furthermore part of the water and acid contained in the atmosphere of the deposition chamber will eventually be dissolved directly in the liquid TEOS vials, resulting in slow hydrolysis of the liquid precursor. Higher processing temperature would likely result in quicker gelation of the precursor solution.
Other parameters may be of importance in the coating kinetics, such as the volume of precursor available, but also the geometry of the vials and more specifically the surface of exchange between the atmosphere of the container and the liquid. A large volume of TEOS with a very small exchange surface would likely not be efficiently deposited. For this reason it was preferred to divide the volume in several vials, to maximize the liquid/gas interface.

Similarly, composition of the aqueous acid solution may have a significant influence on the deposition kinetics, just as pH control is essential in classic liquid sol-gel chemistry.
In short this silica deposition technique which seems simple and straightforward is in fact very sensitive to a wide range of parameters and must therefore be carefully optimized in order to yield reproducible and controlled silica coating. Several sets of coating conditions were therefore applied to different models of foams.

III.1.b Deposition on radial foams

Efficiency of the vapor phase deposition process was first assessed on pectin foams prepared by dipping in liquid nitrogen. For these samples the pore morphology was organized in a radial fashion and pores were interconnected. This type of sample has the advantage of being quickly and easily prepared, and could therefore be produced in large batches which allowed for the screening of various processing parameters.

III.1.b.i Observation of the silica layer

The first step in the validation and optimization of the described coating technique was to assess and characterize the presence of silica in the samples exposed to vapors of TEOS.

Material and methods

Radial foams were prepared as previously described in Chapter II. An aqueous solution of pectin at 40 g/l was prepared under magnetic stirring at room temperature overnight. About 1.8 mL of solution was poured in cryotubes, which were immerged in liquid nitrogen for a few minutes. The samples were slightly reheated to ensure pore interconnection and subsequently vacuum dried for 24h.
Samples were then placed for 14 days in the deposition chamber described in paragraph III.1.a . The samples were left 24 h at 30°C and 24 h at room temperature in a desiccated atmosphere before final weighing.
Slices were cut and sputtered with 20 nm of gold for SEM observation.
Slices were sputtered with 20 nm of carbon before EDX analysis.
Samples were crushed for FT-IR spectroscopy observations on Perkin Elmer Spectrum 400 FT-IR/FT-NIR Spectrometer equipped with Universal ATR sampling accessory.

The first and most direct ways to assess the presence of silica after contact with vapors of TEOS was to weigh the samples before and after the treatment. Mass gain may be attributed to the formation of silica species on the surface of the sample. Weighing of the samples confirmed the presence of a mass increase up to about 50 % of the total mass after 14 days.

A simple method to identify the nature of the added material is the use of FT-IR spectroscopy (see Figure III.1). Spectra were measured for samples with various mass additions (samples were left for different times in the deposition chamber). A sample of pectin not exposed to vapors of TEOS was used as control.

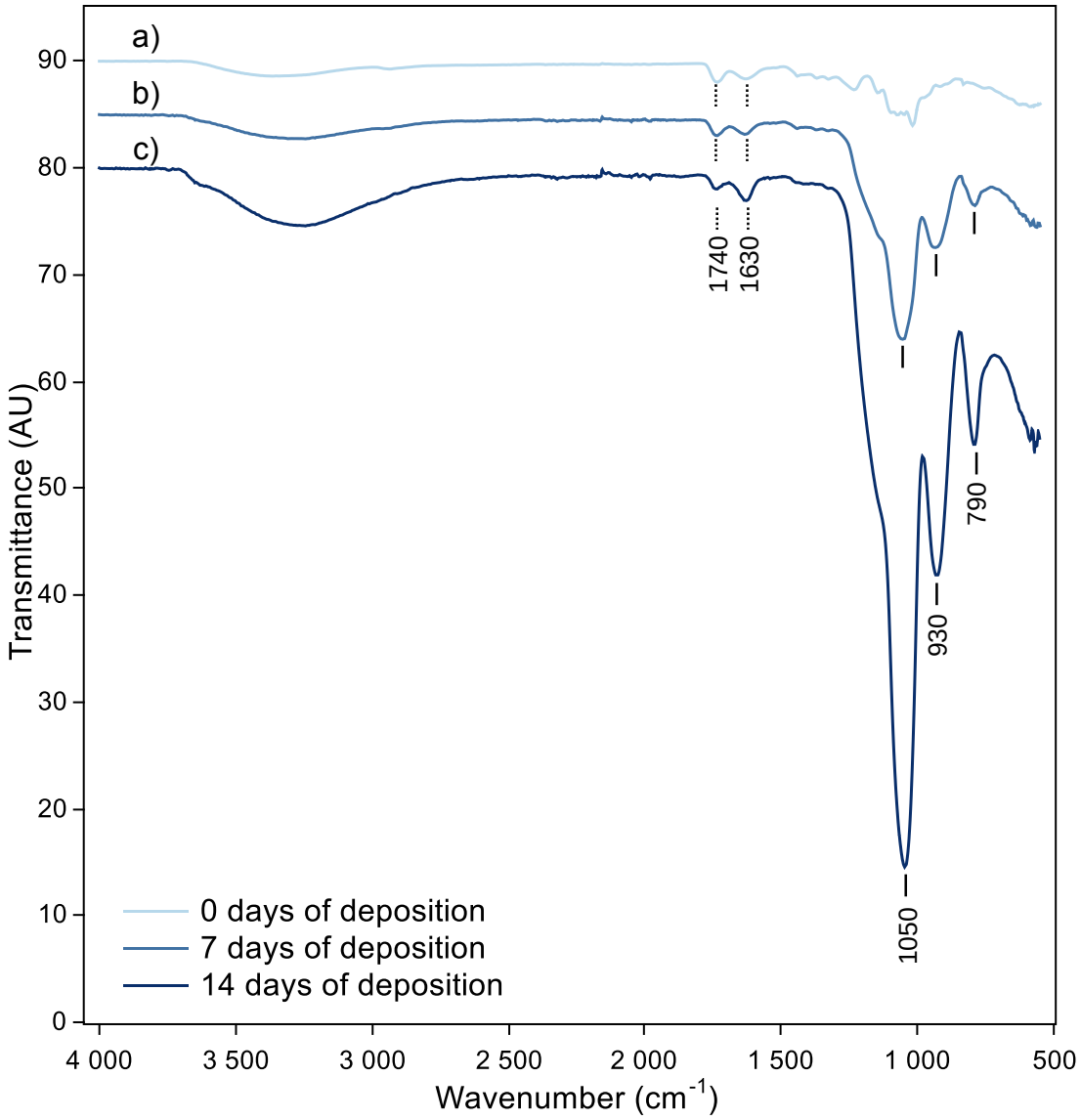

Figure III.1: After foams were exposed to TEOS vapors for 7 days (b) or 14 days (c), new peaks appear in the low wavenumber region compared to samples of pectin alone (a). These peaks are characteristic of silica. An offset was applied to the transmittance curves for clarity and the curves were normalized to the $\nu_{C=O}$ = 1740 cm^{-1} peak.

The wide but not very intense peak observed in all samples around ν_{O-H} = 3400 cm^{-1} can be attributed to stretching of O-H bonds. Such functions may be present in both pectin and silica and can therefore not be used as a mean of identification of the material corresponding to the mass increase.

Two small peaks are common to the three samples (at 1740 cm^{-1} and 1630 cm^{-1}). The peak at $\nu_{C=O}$ = 1740 cm^{-1} could be due to the stretching vibration of the C=O bond of acetyl esters in pectin[421].

Since the pectin scaffold is common to the various samples, this peak is likely to remain unchanged after silica deposition. As a result $\nu_{C=O}$ = 1740 cm^{-1} was used as reference for normalization of the spectra.

Interestingly three defined peaks appear at lower wavenumbers after the deposition step. These peaks can be correlated with typical silica signals. Peaks around ν^{a}_{Si-O} = 1070 cm^{-1} and $\nu^{s}_{Si-O-Si}$ = 800 cm^{-1} have been attributed to stretching of Si-O-Si bonds, as the asymmetric stretching and symmetric stretching of the oxygen atoms respectively[422]. A peak around ν_{Si-OH} = 930-950 cm^{-1} may be attributed to stretching of Si-OH bonds. The literature values are slightly shifted but small variations have previously been reported depending on the density of the silica network[423] and condensation state of the TEOS silica precursor[424]. Additional shift may be attributed to the type IR spectroscopy detection method (use of an ATR module). This series of bands are nonetheless representative of the presence of silica within the foams exposed to TEOS vapors. The intensities of these specific peaks increased with prolonged deposition time, which is consistent with the measured mass increases. The presence of silica within the samples after the deposition process was confirmed. This analysis was not quantitative, but supported the hypothesis that the mass increase is due to the presence of silica. In further experiments, mass gains were considered as the silica content of the samples.

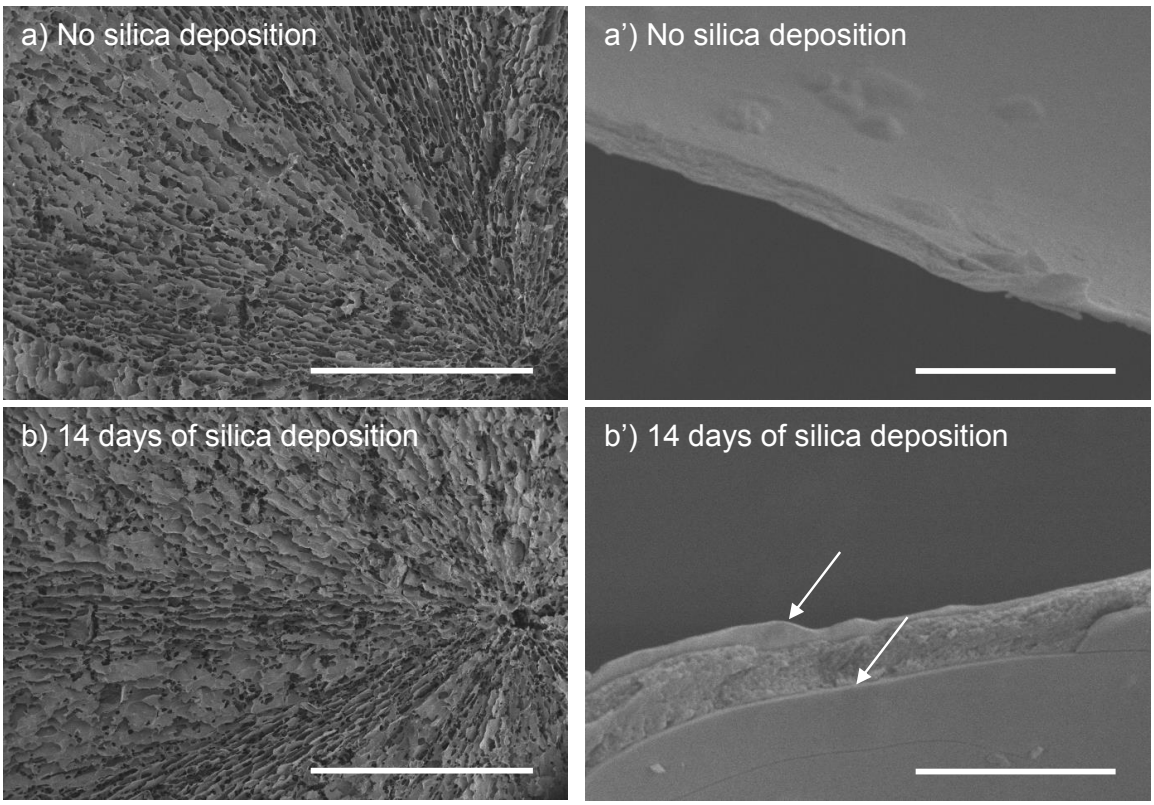

Figure III.2: Samples with no silica (a) and with 58 $\%_{SiO2}$ (b) present identical general morphologies. At higher magnification a smooth layer can be observed on both sides of the polymer pore wall (b') for the sample containing silica. Scale bars: 1 mm for a and b, 3 µm for a' and b'.

The silica coating was further characterized by SEM. As can be seen in Figure III.2 a and b, the general structure of the materials is not altered by exposition to TEOS vapors, despite acid conditions and about 75% of humidity. At higher magnification (Figure III.2 a' and b') a significant difference between the two samples can be observed. After silica deposition a smooth layer can be seen on both sides of the initial pectin wall, which is likely to correspond to the mass increase previously mentioned.

To confirm the composition of the deposited layer, energy dispersive X-Ray spectroscopy (EDX) was performed on a samples exposed 14 days to silica vapors (see Figure III.3).

Element analysis showed the presence of silicon and oxygen. The presence of oxygen may not entirely be attributed to the formation of a silica layer since it is present in large amounts in the pectin itself. Silicon is however likely representative of the presence of silica.

The homogeneity of the silica layer was confirmed by mapping of the oxygen and silica.

The proposed method for addition of silica to pectin foams was therefore validated. This method may however be optimized through various parameters (deposition time, temperature, geometry of the deposition chamber etc…) in order to tune the silica layer itself.

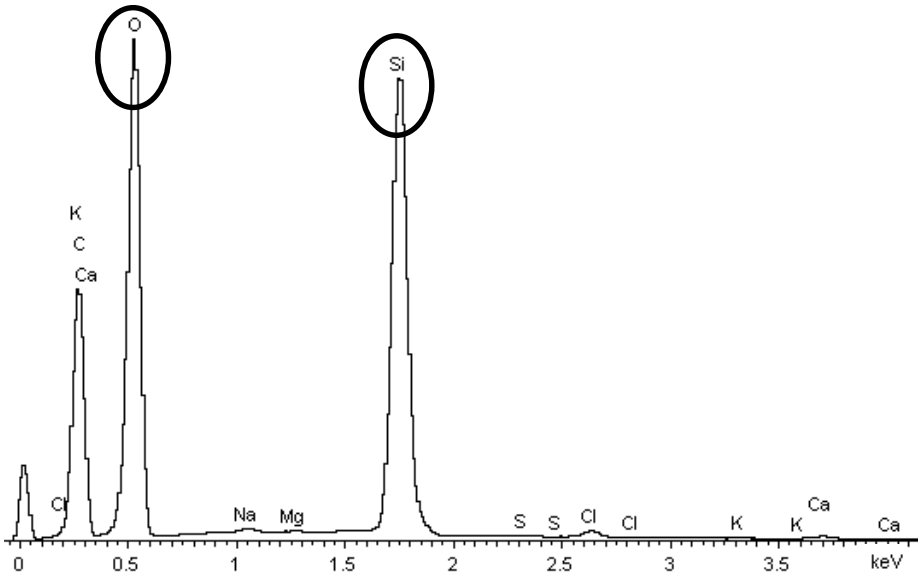

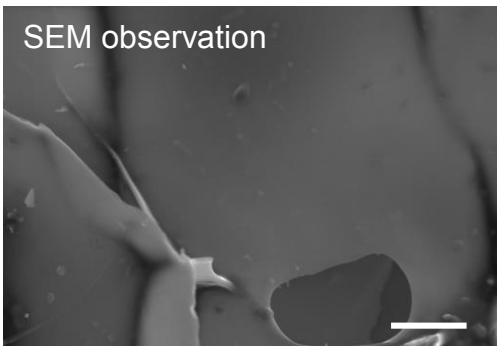

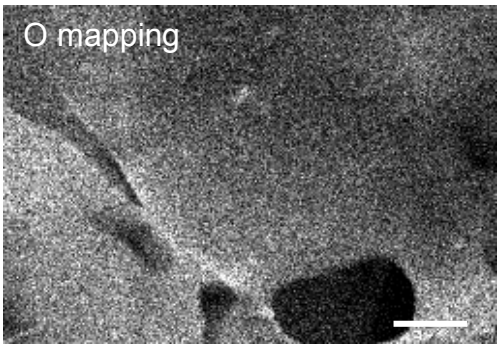

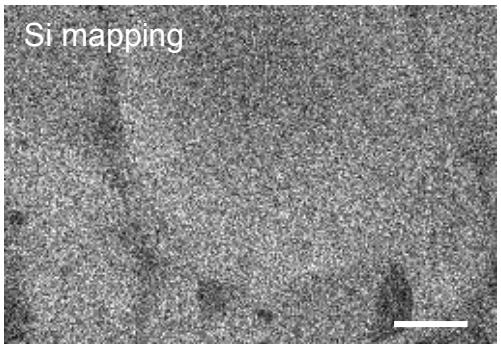

Figure III.3: Element analysis confirms the presence of both oxygen and silicon within the sample (a). Element mapping seems to indicate homogeneous repartition of the silica layer on the pectin pore walls (b). Scale bars: 10 µm.

III.1.b.ii Tuning of the silica layer

To gain further control over the deposition of the inorganic moiety on the polymer foam, samples were exposed for various times to vapors of TEOS as a way to yield various silica contents.

Material and methods

The deposition conditions used were the same as previously described. 1.8 mL freeze-dried pectin foams were prepared and weighted. The samples (about 59 ± 2 mg) were placed in the deposition chamber described in paragraph III.1.a . Samples were removed after various deposition times (between 1 and 15 days). Samples were dried 24h at 30°C and 24h at room temperature in a desiccated atmosphere before final weighing.

Samples were cut and sputtered with 20 nm of gold for SEM observation.

Figure III.4 g present the mass gain depending on the deposition time.

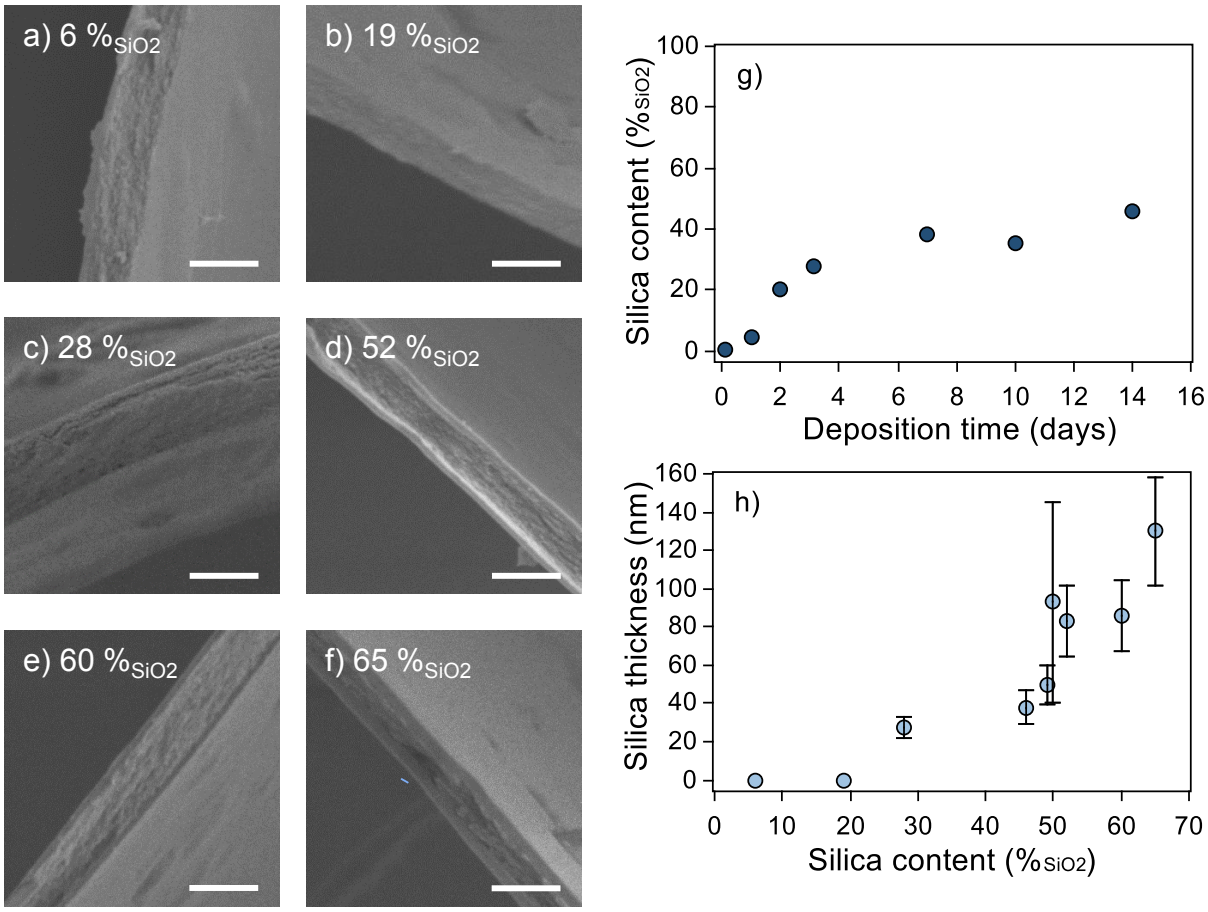

Figure III.4: Silica content can be increased by prolonged exposition to TEOS vapors (g), a plateau is reached after about one week. SEM observation of samples with different silica contents reveals the presence of silica layers of different thicknesses (a to f) which vary according the silica content. Scale bars: 1µm.

Sample masses increases between 0.3 mg and 60 mg in a 15 days-time span, which correspond to mass percentages between 0.5 $\%_{SiO2}$ and 46 $\%_{SiO2}$. Mass gain is important during the first few days, but reaches a plateau after longer expositions (after about one week). Such phenomenon might be a combination of saturation of the deposition and condensation of the silica precursors in the vials, resulting in lower volatility. All foams used were of the same size and mass, as a result deposited mass variations and silica mass percentage variations are equivalent. Samples were further characterized by SEM imaging.

Figure III.4 present SEM images corresponding to the samples exposed to TEOS vapors for various times. Up to 2 days of deposition no silica layer is visible with this observation technique. At higher silica content a smooth layer can be observed on both sides of the pectin walls. Thickness of the silica layer varied according to the silica content (see Figure III.4 h). These thickness values must however be considered with caution. The statistical relevance is questionable since only 5 measurements were taken on only two different pore walls. As a result the values do not take in account possible heterogeneities within the samples. It must also be noted that pictures cannot always be taken strictly perpendicularly to the exposed edge of the pore walls, which may result in some perspective bias in the measurements. The vapor phase deposition method proved efficient in adding the desired inorganic moiety to the pectin-based foams. Various deposition times allowed for tuning of the silica content and thickness of the silica layer. Several other parameters are however likely to influence the deposition process.

HCl concentration, presence of NaCl and the volume of introduced TEOS were modified in order to assess the robustness of the addition of silica (see Annex p 214). Silica contents were polydisperse after only 7 days of deposition, but the dispersion was reduced after 14 days of silica deposition. Modification of parameters such as HCl concentration, the presence of NaCl or the modification the TEOS volume did not significantly modify the deposition kinetics.

As a result, chemical vapor deposition of TEOS proved to be an efficient way to add silica to pectin foams. The polymer porous scaffolds were coated with a tunable and homogeneous layer of silica and the process proved to be efficiently reproducible and robust.

III.1.c Coating of unidirectional foams

Preparation of macroporous pectin foams by dipping in liquid nitrogen has the advantage of being quick and adapted to large batches of samples. However, as mentioned in Chapter II, this method implies very high cooling rates, which, as will be discussed in Chapter IV, might be problematic from the encapsulation perspective. As a result the vapor phase was also applied to freeze-casted pectin foams.

Material and methods

Freeze-casted foams were prepared from 3 mL of 40 g/L pectin solutions, frozen unidirectionally at 10°C/min and subsequently vacuum dried at 0.05 mbar for 24h. The resulting samples were cut to 1.5 cm high cylinders and placed in the deposition chamber previously described. A 5 wt% aqueous solution of HCl, with 400 g/L of NaCl was used to ensure hydrolysis. Four vials containing 10 ml of TEOS were introduced in the closed vessel. Coating was performed up to 16 days at 30 °C/min. After removal from the deposition chamber samples were left 24 h at 30 °C and 24 h at room temperature in a desiccated atmosphere to remove excess humidity before weighing.

Silica content on pectin foams with unidirectional porosity (obtained by freeze-casting) was first assessed based on the mass gain. Freeze-casted foams were exposed for various times to TEOS vapors and Figure III.5 present the deposition profile compared to silica coating of radial foams (obtained by dipping in liquid nitrogen). In both cases a plateau can be observed after about a week. In the case of unidirectional foams however the maximum silica content appears much lower (about 15 $\%_{SiO2}$) compared to radial foams (about 40 $\%_{SiO2}$). The maximal mass increases were about 23 mg and 40 mg for freeze-casted and radial foams respectively.

Beside the structural differences between the two types of samples (unidirectional porosity *vs* radial porosity), the considered foams also have different volumes. Since two parameters (morphology of the porosity and mass of the samples) are changed simultaneously, it is however difficult to identify their respective influence.

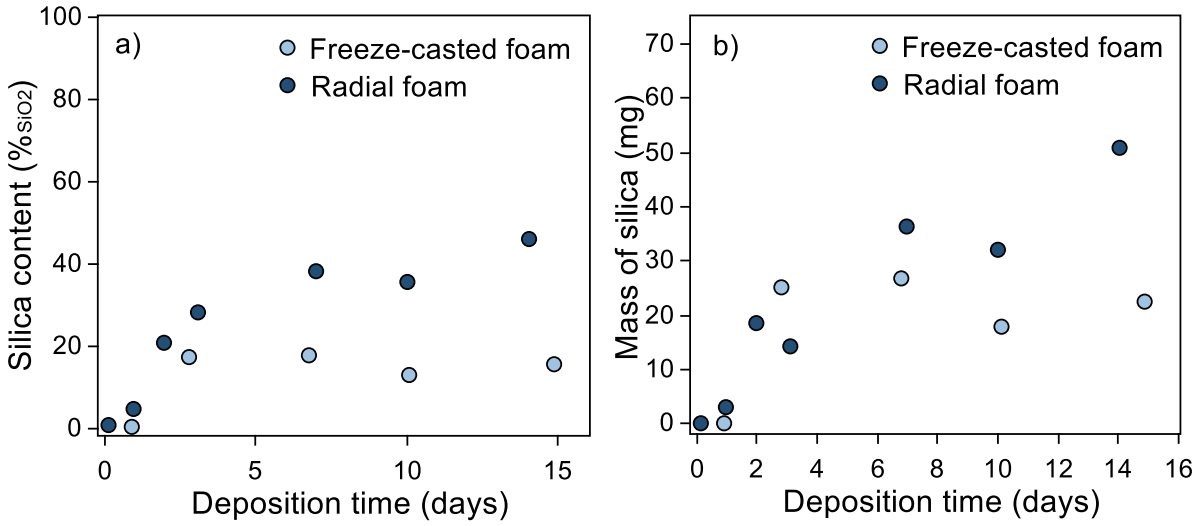

Figure III.5: Plateau in the silica content can be observed on both freeze-casted and radial foams (a). The final deposited mass is higher for radial foams (b).

In order to discriminate between these two effects, another series of silica deposition was performed on samples prepared with a single technique (freeze-casting) but cut to different sizes (and therefore different volumes).

Material and methods

Pectin foams were prepared by freeze-casting at 10°C/min, from a 40 g/L polymer solution. The samples were vacuum-dried and kept under desiccated atmosphere until further use.

Samples were cut to 8.2 mm, 4.3 mm or 1.7 mm (mean value on triplicate samples). They were placed in the deposition chamber previously described (see Annex p 210) and left 10 days at 30°C in presence of 4x10 mL of TEOS and 150 mL of 5 wt% HCl with 400 g/L of NaCl. After removal from the closed vessel samples were left 24 h at 30 °C and 24 h at room temperature in a desiccated atmosphere. Final weight of the samples was used to determine the silica content.

Silica deposition in vapor phase on freeze-casted foams seemed less efficient in yielding high silica content, or thick silica layers. Thin layers or incomplete layers of silica may not be able to protect efficiently the pectin scaffold against dissolution. In order to investigate the reason of this low efficiency, the influence of the mass of the samples was evaluated.

As can be seen from Figure III.6 a, the final relative silica content ($\%_{SiO2}$) decreases proportionally to the thickness of the foam (from 62 $\%_{SiO2}$ to 28 $\%_{SiO2}$). Another way to interpret this set of data is to say that the added mass of silica is constant (about 19 mg), regardless of the initial thickness of the foam (see Figure III.6 b)

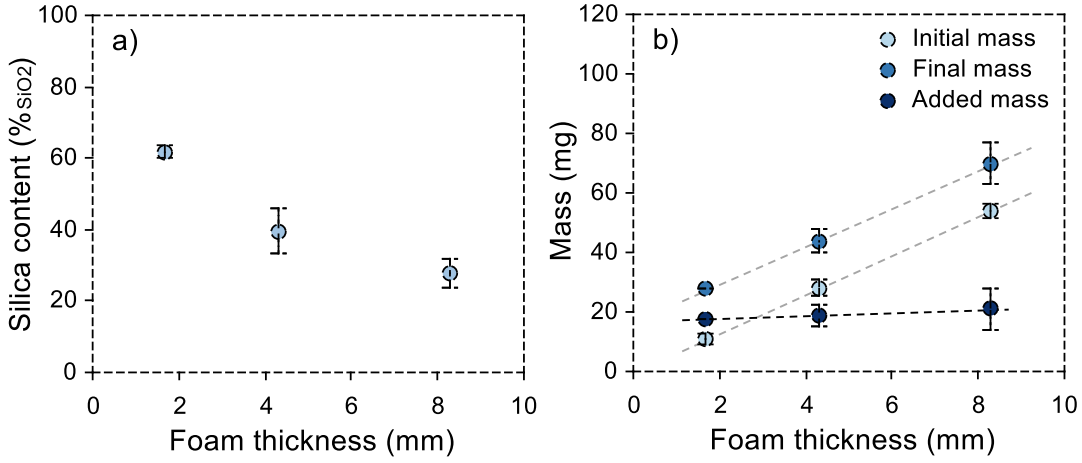

Figure III.6: Silica mass percentage decreases with sample thickness (a). Initial and final mass are proportional to the sample thickness, but the added silica mass is similar for all samples (b).

All the samples were prepared with the same method (freeze-casting). As a result all samples have the same diameters and densities. As a consequence the volume of the samples, their mass and their thickness are proportional. The thickness of the foam appears as an especially relevant criterion in the understanding of the silica deposition phenomena due to the oriented porosity of the foams.

The concentration in silica precursors (and other reactive species such as water) is assumed to be homogeneous throughout the deposition chamber. The flow of reactive species from the chamber to the inside of the foam is also assumed to be constant and is assumed to occur only through the cross section of the samples. Since the diameter of the foams is independent of their volume (or thickness), the exchange surface is also independent of the volume of the foams (assumed to be equal to the sum of the top and bottom surfaces of the cylinders, which is about 3.5 cm^2). With similar flows and exchange surfaces, the total mass of precursors within the foams for a given time is therefore independent of the sample's thickness, which is consistent with the measured silica masses (see Figure III.7).

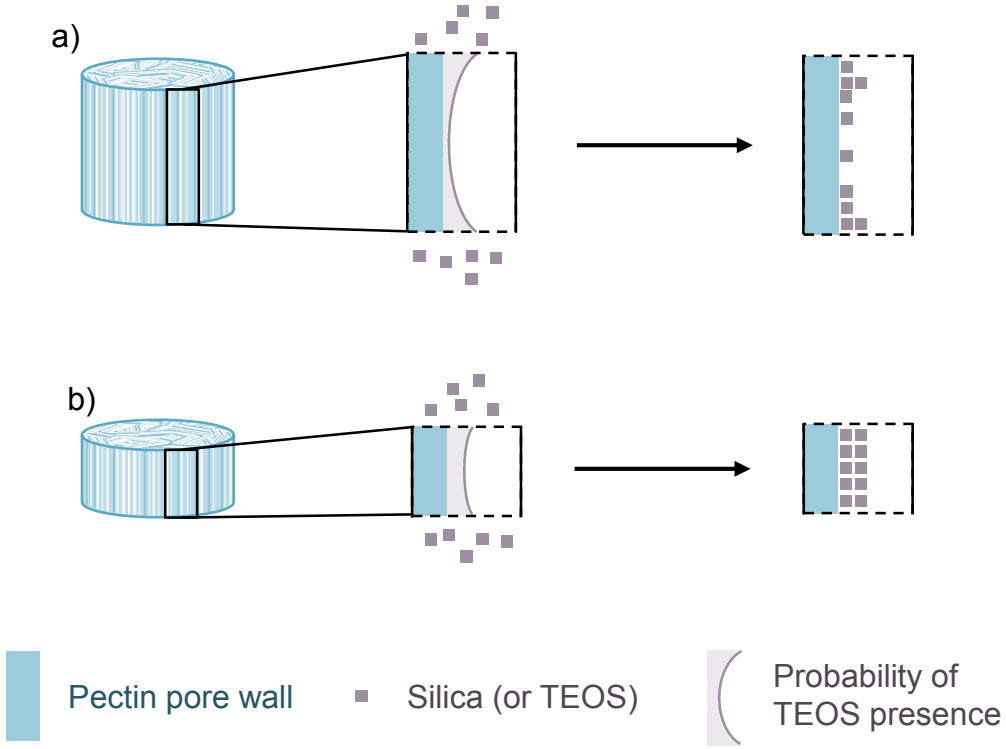

Figure III.7: Silica precursor flow is assumed to be independent of the foam volume. Since all foams have the same diameter, similar masses enter the foams in a given time. As a result the added masses are similar, but the relative mass content (or thickness of the silica layer varies. Silica layer is likely to be more homogeneous in thin foams (b) than in thick samples (a) due to diffusion limitations.

In addition, the use of thicker samples is likely to result in less homogeneous silica layer due to diffusion limitations. If a constant free mean path is assumed for precursors within the foams, the probability of presence of precursors diminishes at the center of the foams. As a result, silica layers may be thicker in the upper and lower regions of the foams. In the case of thinner samples, the variations in this probability are likely to be limited resulting in more homogeneous silica layers.

It seems that the volume of the sample is also a way to tune the final silica content of the hybrid foam (or in other terms the thickness of the deposited silica layer). In the case of foams with an oriented porosity however, more than the total volume, the diameter of the foams (rather than the total volume) appear to be determinant in setting to total introduced silica mass.

III.1.d Characterizations

Once the deposition conditions were set, the resulting hybrid pectin-silica foams were characterized with various methods.

Material and methods

Pectin foams were prepared by freeze-casting of a 40 g/L polymer solution at 10°C/min and vacuum drying.

Samples were cut to 2 mm to 4 mm of thickness to ensure high silica contents. Deposition times were modified to tune the silica content.

Thin slices were cut after silica deposition and coated with 5 nm of platinum for SEM-FEG observation (SEM-FEG Hitachi SU-70).

Samples were dehydrated in PFA 8% and fixated with glutaraldehyde and osmium and subsequently immobilized in epoxy embedding medium(see p 200. 50 nm to 80 nm slice were cut with LEICA EM UC7 microtome and contrasted with uranyle acetate for TEM observation on Cryomicroscope Tecnai spirit G2.

About 10 mg of crushed samples were heated up to 1200°C at 5°C/min under air for thermogravimetric analysis (TGA) analysis (on Netzsche STA 409 PC Luxx thermal analyzer).

Samples about 5 mm thick with silica contents between 11 $\%_{SiO2}$ and 52$\%_{SiO2}$ were compressed along the pore direction to 50% of strain at a constant displacement rate of 1 mm/min using Instron 5965 traction and compression device.

The silica layers were first observed in microscopy. SEM-FEG images of freeze-casted pectin foams coated with 48 $\%_{SiO2}$ and 60 $\%_{SiO2}$ are presented in Figure III.8 a. Two thin silica layers can be observed on the sides of the pectin pore walls. The measured thicknesses are 23 nm for the sample containing 48$\%_{SiO2}$ and 32 nm for the sample with 60 $\%_{SiO2}$. These values can only give an order of magnitude for the thickness of the silica layer due to the previously mentioned bias of perspective and limited statistical relevance. The aspect of the layers themselves appears slightly different compared to observation made on gold coated samples. Initial observations on gold coated samples revealed very smooth layers. Here however the silica layers appear granular. This difference may be due to the fact that sputtered gold particle are bigger than sputtered platinum particle and may therefore hide some of the topological details of the observed layer.

TEM observations were performed on samples embedded in resin. 10 measurements of the thickness of the silica layer where performed on 5 separate pore wall images for each sample. For a 47 $\%_{SiO2}$ silica content, pore walls had a mean thickness of 18 ± 12 nm, while at 34 $\%_{SiO2}$ the silica layers were 8 ± 3 nm thick. The high standard deviations for these values illustrate the inhomogeneities within a single sample. Despite these wide distribution, values are statistically different (at $p < 0.05$) which is consitant with the layer thickness-silica content dependance described in III.1.b.ii.

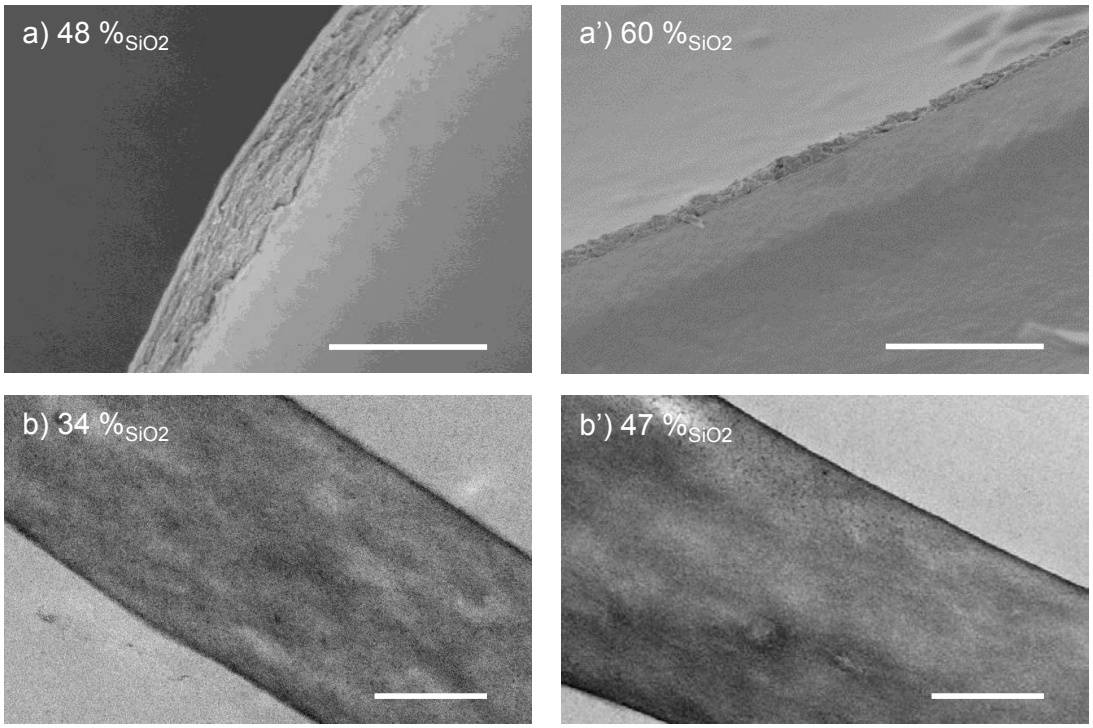

Figure III.8: SEM-FEG observation of sample coated with 5 nm platinum reveal the presence of silica layers with a granulose aspect on the pectin pore walls (a and a'). Measurement of silica thicknesses on TEM images (b and b') confirms the links between silica content and layer thickness. Scale bars: 1 µm for a and a' and 200 nm for b and b'.

Microscopy analyses allowed for direct observation of the silica layers. To further characterize the hybrid samples, they were analyzed by TGA. As mentioned previously, the added mass after the silica deposition process was assimilated to silica content. Pectin and silica are however both highly hygroscopic. When samples were left at ambient humidity, it is likely that non negligible amounts of water were adsorbed on pectin and silica. Mass percentage losses for sample with different silica contents ($0\%_{SiO2}$, $15\%_{SiO2}$ and $43\%_{SiO2}$ measured by weighing) are presented in Figure III.9. The purely organic sample (Figure III.9 a) shows the degradation of the pectin moiety. A first mass loss can be observed between 70°c and 120°C, which represents about 10% of the total sample mass. This is likely due to desorption of water. Similar mass losses can be seen in samples containing silica (Figure III.9 b and c), in the same temperature range and representing the same mass percentage. A second mass loss can be observed between 200°C and 450°C corresponds to calcination of the pectin. In presence of silica, this mass loss also starts at 200°C but occurs up to 510°C, which may correspond to a partial stabilization of the pectin structure. After calcination, the residual masses were 3%, 23% and 36% respectively for samples with $0\%_{SiO2}$, $15\%_{SiO2}$ and $43\%_{SiO2}$ apparent silica content. These values were normalized to remove the contribution of water mass. As a result the non-calcined fractions of the dry samples are 3%, 25% and 41% respectively. It seems therefore that the silica contents determined by simple weighing of the samples are slightly shifted compared to the actual inorganic contents. They remain however indicative of the variations between different samples and of the order of magnitude of the inorganic fraction.

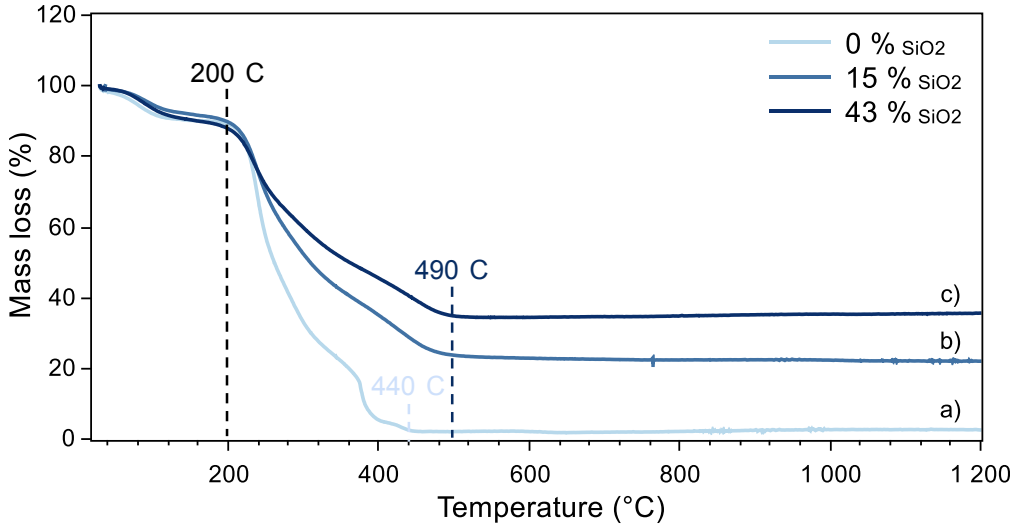

Figure III.9: TGA of samples with 0 $\%_{SiO2}$ (a), 15 $\%_{SiO2}$ (b) and 43 $\%_{SiO2}$ (c) (as measured by weighing). Loss of mass due to water desorption can be observed in all samples, but residual mass percentage after calcination of pectin vary according to the apparent silica content.

Even if weighing does not allow for precise determination of the actual silica content, it remains a direct and widely applicable, as well as non-destructive technique. It was therefore kept as a further reference to compare silica content between samples, keeping in mind that the actual mass values might be shifted.

Silica was added to the pectin foams primarily to ensure protection against dissolution of the structure. However addition of inorganic material to the polymer foam is likely to modify other properties of the material, including its mechanical behavior. Figure III.10 presents the stress/strain curves as well as Young's modulus and compressive strength depending on the silica content. Up to about 20 $\%_{SiO2}$ the mechanical properties of the material appear similar to the characteristics of the pectin alone samples. As expected, higher mass percentages of the inorganic moiety result in stiffer inorganic material. The addition of silica also results in higher compressive strengths (see Table III.1).

Table III.1: Young's modulus, compressive strength and densities for foams with various silica contents.

Silica content ($\%_{SiO2}$)	Apparent density (mg/cm^3)	Young's Modulus (MPa)	Compressive strength (kPa)
0	41.0	1.3	145
12	50.7	1.1	140
17	48.8	1.0	147
24	58.9	1.3	179
28	59.2	2.4	186
32	51.9	2.1	204
43	76.2	3.4	287
52	85.4	4.8	336

The general aspect of the stress/strain curves is also modified by the presence of silica. At low silica content (less than 20%$_{SiO2}$) the curves are similar to pectin alone foams. This corresponds to the limit silica content necessary for SEM observation of the silica layer and could be attributed to the limit to the formation of a fully percolated silica layer. At higher silica content small irregularities appear. They may be attributed to localized failures of the silica layer, as they strongly resemble the behavior described for porous inorganic materials[316,425].

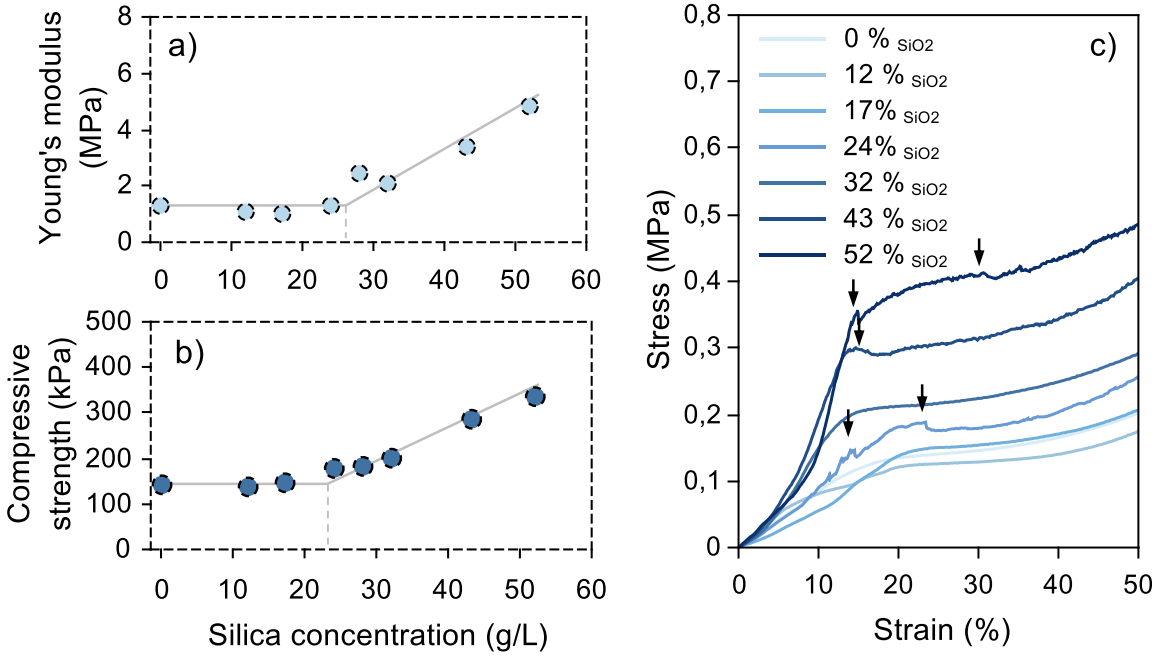

Figure III.10: Young's modulus (a) and compressive strength (b) are similar up to 20 %$_{SiO2}$ and increase for higher silica content. Similarly stress/strain curves for foams with silica contents up to 20 %$_{SiO2}$ (c) have similar general aspects. At higher silica content, signs of silica failures appear (black arrows).

The samples can be seen as a series of pores walls composed of several layers of materials (silica-pectin-silica) with different mechanical behaviors (see Figure III.11). This corresponds the structure of a lamellar composite, in which case a rule of mixture can be applied[426]. Due to variations in chemical composition in the pectin chains, the surface of the polymer walls is likely to present slight heterogeneities, in particular in terms of hydrophobicity and charge. As a result, silica deposition mechanism may be assumed to start by preferential deposition of the silica where interaction with the pectin substrate is more favorable and then be extended across the durface. At low silica content, the silica is likely to be organized as localized patches rather than a fully percolating layer. As a result the mechanical behavior is governed by the pectin structure. At higher silica content, the applied stress is distributed on materials with different Young's modulus, but same strain is applied. Since $E_{silica} > E_{pectin}$ most of the stress will be sustained by the silica layers, and the mechanical behavior will strongly resemble behavior of a fully inorganic material.

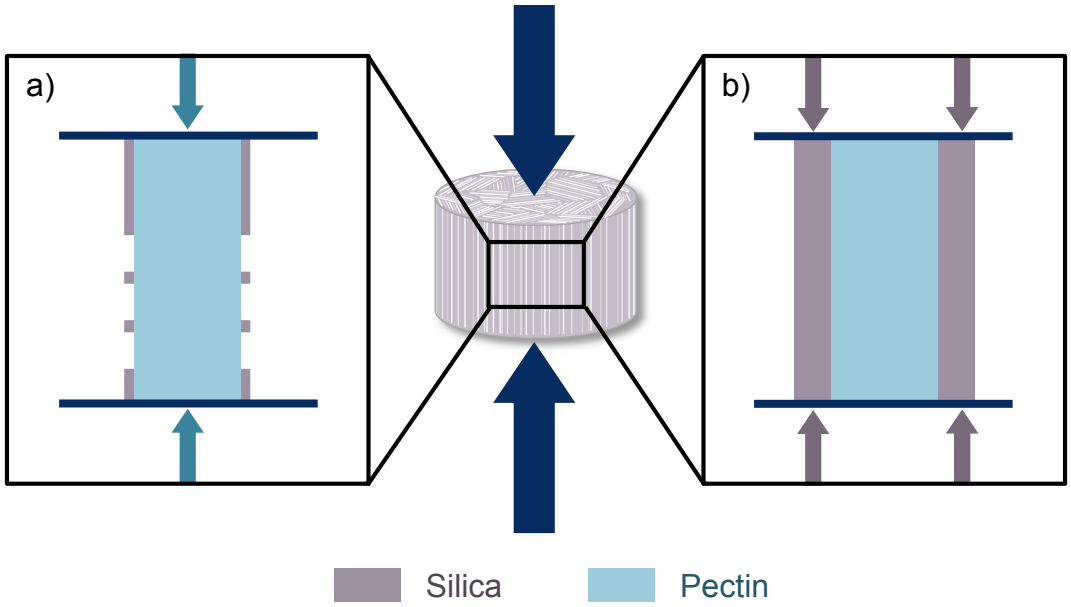

Figure III.11: In samples with no percolating silica layers (a) the applied stress is mainly supported by polymer (E_{pectin}). At higher silica content (b) the same strain is applied to both components. Since $E_{silica} > E_{pectin}$ the overall stress is mainly representative of the silica layers.

This simple model may explain the general differences observed both on the typical mechanical values (Young's modulus and compressive strength) as well as the aspect of the stress/strain curves. By using vapors of silica precursor (TEOS), it was possible to efficiently cover the polymer pore walls of the previously described foams with a homogeneous silica layer. The method proved efficient and reproducible and silica layers could easily be observed and characterized. The thickness of the layer could be tuned either by changing the deposition time, or the geometry of the samples. The goal of this addition of an inorganic moiety to the polymer scaffold was to ensure that the initial pore structure is retained and that the material does not dissolve when used in the conditions of the targeted application. The behavior of the material was therefore assessed in different model conditions.

III.2 Behavior of the hybrid material in a typical soil

III.2.a Influence of the silica content on ageing

The hybrid porous material is meant to be used in polluted soils as a host matrix for metabolically active bacteria. Non-negligible water contents are expected in such environments, which is likely to result in rapid dissolution of a material solely composed of pectin. The presence of a silica layer all across the polymer pore walls should however limit this phenomenon.

III.2.a.i In liquid medium

The behavior of the hybrid material was initially assessed in liquid medium, as this represents the "worst case scenario" if the targeted environment is a highly hydrated soil.

Material and method

Macroporous foams were prepared by freeze-casting at 10°C/min from an aqueous solution of pectin grafted with rhodamine isothiocyanate (RITC) (see Annex p 208). The samples were vacuum dried and various contents of silica (0 $\%_{SiO2}$, 22 $\%_{SiO2}$ and 37 $\%_{SiO2}$) were added to the polymer foams.

The samples were plunged in 15 mL of water and left under elliptic agitation at room temperature. Supernatants were regularly sampled and centrifuged to remove any material debris. Pectin content was deduced from UV-vis spectrometry at 558 nm (see calibration in Annex p 208). Silica concentration was assessed by the silico-molybdic method[427] *(see Annex p 208). Visual aspect of the supernatants was also monitored. All assays were performed in triplicate.*

Figure III.12 hybrid foams displaying very different behaviors depending on the silica content. When samples were made of pectin alone (Figure III.12 a), the material rapidly swelled and appeared to be fully dissolved after only 24h. In presence of about 22 $\%_{SiO2}$ (see Figure III.12 b) the material retained its general shape up to 13 days but signs of partial dissolution could be observed after 22 days. Finally the sample containing 37 $\%_{SiO2}$ (see Figure III.12 c) appeared to retain its structure even after 22 days in water. As might be expected, it seemed that higher silica contents are more efficient in preventing pectin dissolution.

To characterize more precisely the kinetics of foam ageing in water, the composition of the supernatant was followed over 3 weeks. As can be seen in Figure III.13 a, the pectin content of the supernatant increased sharply for the pectin only sample within the first few hours. Over longer periods (see Figure III.13 a') the pectin concentration in the supernatant appeared to drop slightly, which might be due to sedimentation or aggregation phenomena. It is also possible that some rhodamine bleaching occurred over the 3 weeks considered period.

Immersion of hybrid materials (22 $\%_{SiO2}$ and 37 $\%_{SiO2}$) resulted in a small increase of pectin concentration in the supernatant which remains stable over 3 weeks. Higher silica content resulted in lower pectin content in the supernatant.

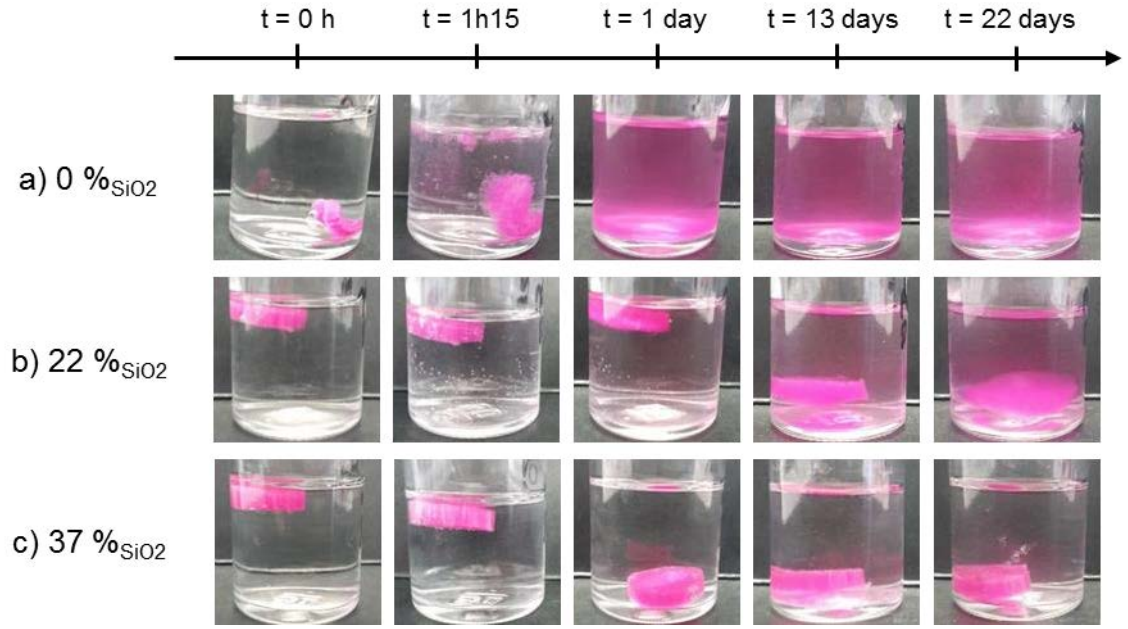

Figure III.12: Pectin foams are rapidly dissolved in water (a). Addition of silica is efficient in preventing the foam dissolution. Samples with high silica content (c) seem to retain their structure over longer period than materials with lower silica content (b).

Aging kinetics regarding silica layers (see Figure III.13 b and b') are slightly different. Trace of silica could be detected in the supernatant of the foams composed of pectin alone. This may be explained by the fact that the assay were conducted in glass vials and should therefore be considered as a baseline signal. Another possible explanation could be the presence of a small silica amounts in pectin. In a counter intuitive manner, silica concentrations were higher in the supernatant of samples with lower silica content. The different silica contents were obtained by exposing the samples to vapors of TEOS and HCl for various times. These different deposition times have an influence on the overall silica content but might also be responsible for variations in the condensation state of the silica layer (confirmation might be obtained by solid state NMR). Higher condensation of the silica network may limit the dissolution rate of the layer, which might explain the difference observed between the two ageing profiles for hybrid foams. The considered silicon concentration values must however be considered with caution. The silicomolybdic method used for titration is indeed only efficient for detection of monomeric units of silicic acid. To minimize bias due to this limitation, all supernatant samples were diluted to fit the observation range and kept under stirring for 24h before titration was performed, but it cannot be excluded that part of the silica content may not have been detected.

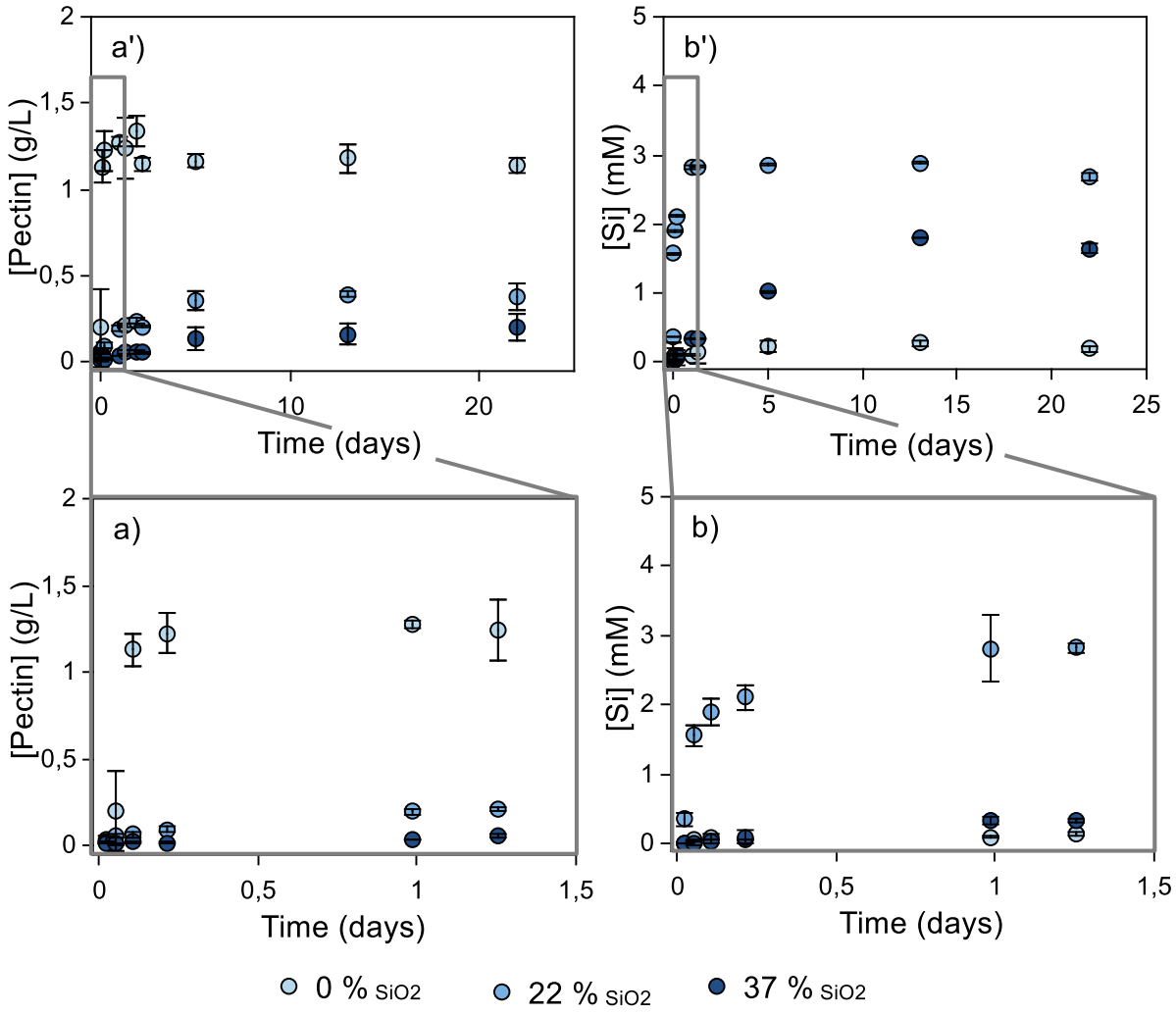

Figure III.13: Pectin concentration increases sharply for samples with no silica in the first few hours (a) and remains stable afterwards (a'). Silica concentration increases faster for supernatant of samples with lows silica content (b').

Addition of silica seems efficient in preventing dissolution of the pectin foams. As mentioned previously, it is likely that under a critical silica content (around 20%SiO2) the silica does not form a fully percolating, resulting in exposed pectin areas which can directly be dissolved. In addition thin silica layers are likely to be more prone to defects than thicker layers, possibly resulting in leaching of the pectin core of the walls (see Figure III.14). On the contrary thick silica layers are likely to efficiently protect the pectin structure against dissolution. Thickness of the silica layer is in addition susceptible to modulate the diffusion of water and therefore the rehydration kinetics of the pectin foams.

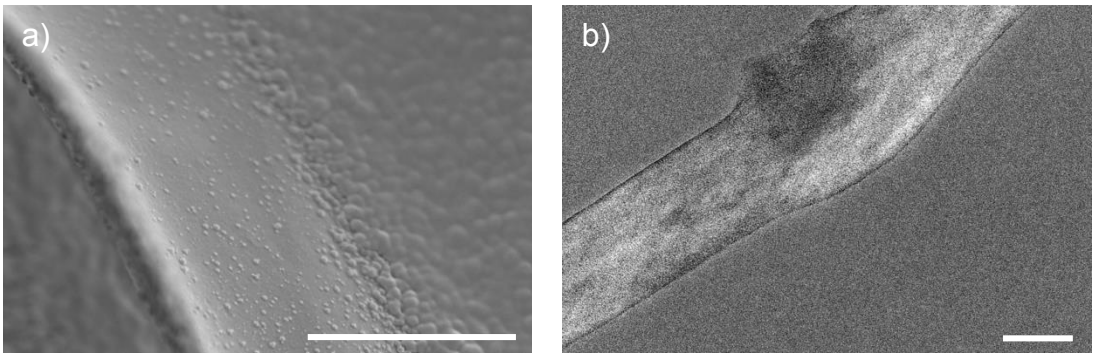

Figure III.14: Non-percolating silica layers (a) or defects in the silica layer may result in dissolution and leaching of the pectin pore wall. Scale bars: 2 µm for a and 200 nm for b.

Effects of rehydration may however not be the only possible source of material ageing in soil. For instance, these assays do not take in account possible degradation by endogenous microorganisms, which is likely to occur in soil. To assess such behavior, hybrid foams were introduced in reference soil samples and monitored over several weeks.

III.2.a.ii In soil

Behavior of pectin-silica hybrid foams was assessed in a reference soil (upper horizon silt loam Luvisol, see details in Annex p 204) over 5 weeks in order to identify possible biodegradation mechanisms.

Material and methods

Samples were prepared as previously described by freeze-casting and lyophilization of a pectin solution and subsequent deposition of silica by exposition to vapors of TEOS.
Ageing in soil assays were performed at Laboratoire de Géologie de l'ENS in collaboration with Pierre Barre.
Foams were placed in 110 g of soil rehydrated by 118 mL of deionized water (see Annex p 211). The soil used was upper horizon (0-30 cm) of a silt loam Luvisol sampled at the Versailles INRA station (see composition in Annex p 204). Samples with different silica content (0 $\%_{SiO2}$, 25 $\%_{SiO2}$, 34 $\%_{SiO2}$ and 39 $\%_{SiO2}$) were place in separate vials and incubated at 20°C (4 samples were used for each silica content). Samples were removed after 1 day, 6 days, 20 days and 37 days.
After various stays in soil, samples were dehydrated by immersion in successive baths of increasing ethanol content (20 %, 40 %, 60, 80 % and 100 %) and left to dry 24h at room temperature. Cross-sections and longitudinal slices were cut and sputtered with 20 nm of gold for SEM observation.

Visual aspect of the foams after various residency times in soils is presented in Figure III.15. Behavior of the materials in soils is consistent with observation made in water. Samples purely composed of pectin (see Figure III.15 a) quickly lose structural integrity.

After only 24h, the sample appears much smaller and after one week it can barely be distinguished from the surrounding soil. Addition of 25 $\%_{SiO2}$ seems to slow down the degradation process, however significant contractions can be observed after 20 days and 37 days. Higher silica content (34 $\%_{SiO2}$) seems to protect slightly more efficiently the structure, but the general evolution of the material is similar to the one observed for samples at 25 $\%_{SiO2}$. For 39 $\%_{SiO2}$, the sample appears to remain stable over more than 5 weeks.

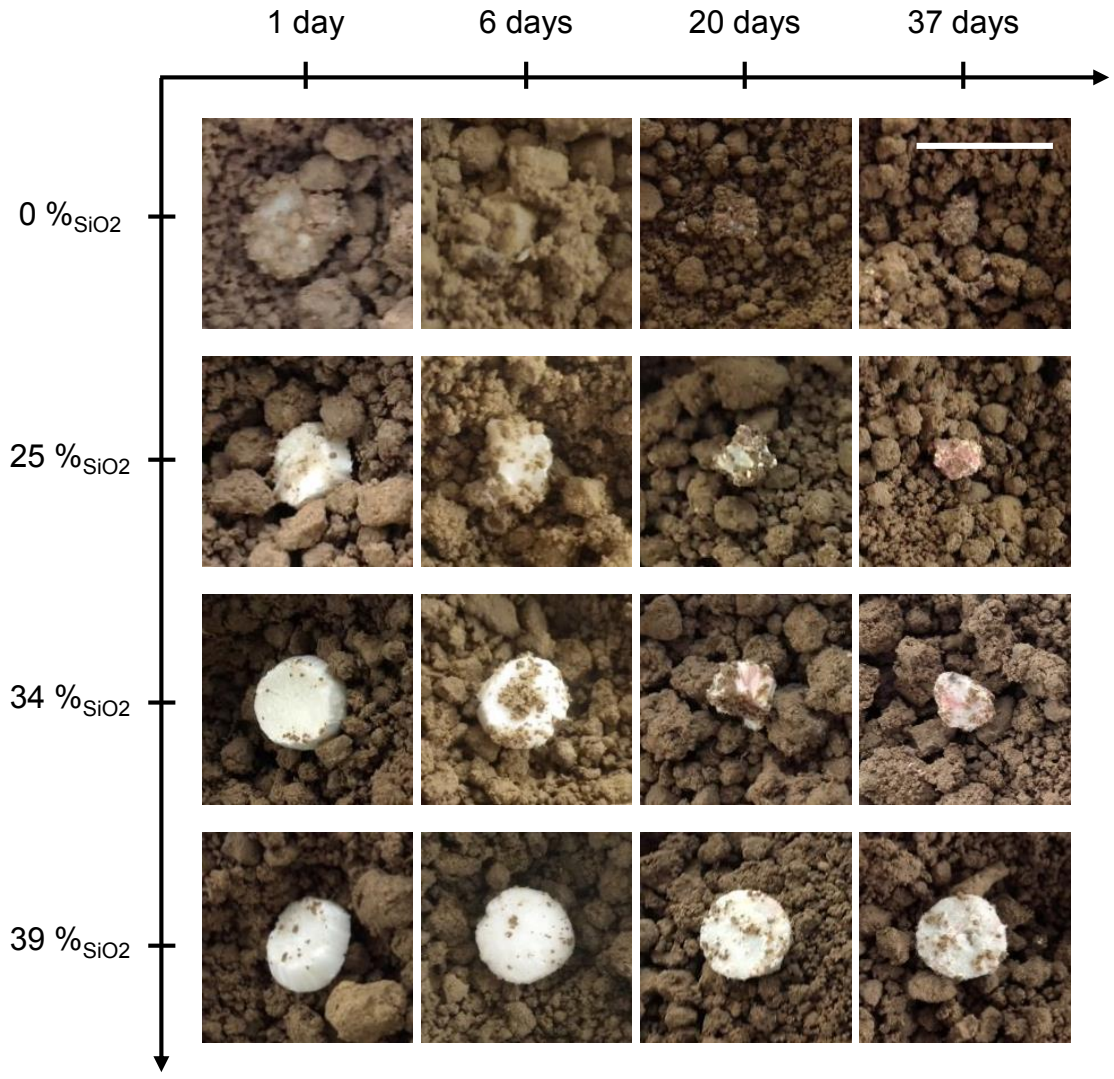

Figure III.15: High silica contents appear to efficiently protect hybrid porous foams against macroscopic loss of structure. Scale bars: 2cm.

From the application point of view, preservation of the macroscopic structure is important to prevent leaching of the encapsulated bacteria. However preservation of the pore morphology may also be necessary in order to insure capillary mass transport of the pollutant within the material. Evolution of the porous structure was therefore followed through SEM observation (see Figure III.16). As might be expected, changes in the porous structure follow the macroscopic features described previously. Foams with no silica rapidly lose their porous

structure. No significant morphology can be observed, even after only one day in soil. This might be due to rapid rehydration and subsequent dissolution of the pectin pore walls. With 20 $\%_{SiO2}$, the shape of the foam can still be distinguished, but the porous pattern seems however largely disrupted. At higher silica contents (34 $\%_{SiO2}$ and 39 $\%_{SiO2}$) the oriented and aligned pores can still clearly be observed, even after 5 weeks in soil.

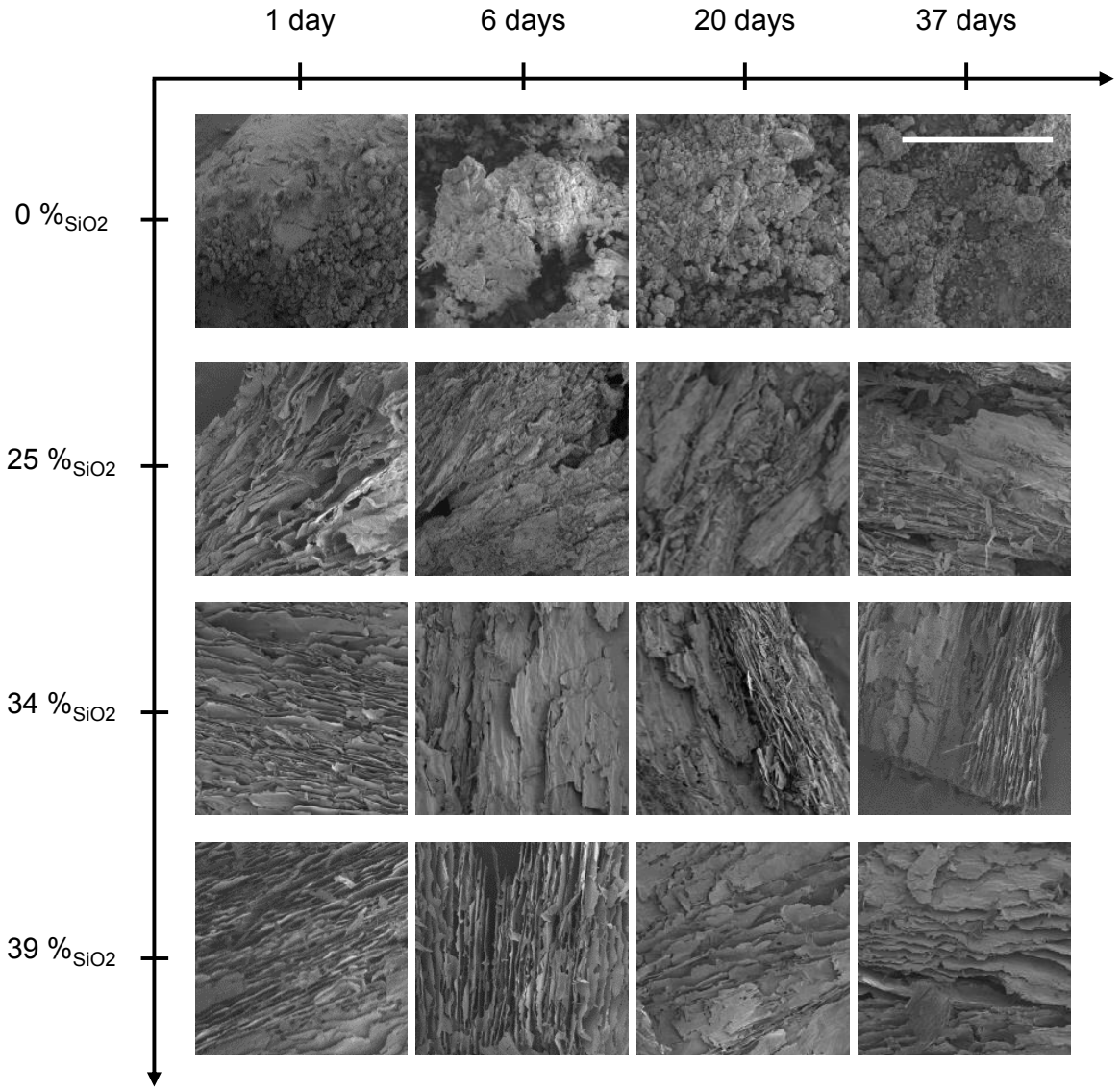

Figure III.16: In absence of silica (a), no porosity can be observed in the remaining material. Low silica content (b) allows for better retention of the general foam structure, but the characteristic oriented porosity appears to be damaged. A high silica contents (c and d), the initial porosity appears to be efficiently preserved. Scale bars: 500 µm.

Assays in both liquid medium and in soil seem to indicate that a minimal silica content or thickness of the silica layer is necessary for efficient protection of the pectin structure. This might be linked to the fact that no clear silica layer could be observed in SEM below 20%$_{SiO2}$. Similarly no significant changes of mechanical properties were observed for samples

containing less than 20%$_{SiO2}$. This may indicate that at low silica content, silica does not form a full layer, which is not sufficient to prevent the dissolution of the pectin pore walls.
The hybrid materials obtained through a two-step process (freeze-casting to obtain a pectin scaffold and silica deposition) appear to be able to sustain prolonged stays in soil. The targeted application is the use of these materials as host matrix for metabolically active microorganisms as a way to degrade pollutants in soil. Interactions between the soil, the contaminants and the matrix, as well as diffusion aspects are keys to the efficiency of the functional material. Foams were therefore introduced in soil containing dye as model pollutant.

III.2.b Behavior in polluted soil

The final goal is to introduce metabolically active species within the pectin pore walls as functional units. The matrix itself may however have a contribution to the depollution process though adsorption of the pollutant. Pectin has been widely used for adsorption of metallic species. In this case however the targeted pollutants are rather organic species such as hydrocarbons, pesticides or dyes. Dyes represent a good laboratory scale model due to the fact that they are both easy to handle and easy to detect and characterize. In addition some dyes species have been proven to be efficiently adsorbed on both pectin-based [428,429] and silica-based[430,431] materials.

III.2.b.i In liquid medium

Adsorption properties of the hybrid foams were first assessed in aqueous solution and compared to the adsorption properties of soil. Reactive Black 5 (hereafter noted RB5), an anionic dye mostly used in textile industry, was used as a model pollutant.

Material and methods

Hybrid foams were prepared as previously described by freeze-casting and drying of a pectin solution (see Annex p 209) and subsequent silica deposition by exposure to TEOS vapors (see Annex p 210).
Three different adsorbents were used:10 %$_{SiO2}$ and 20 %$_{SiO2}$ hybrid foams and the previously mentioned soil example (silt loam Luvisol sampled at the Versilles INRA station). 50 mg of soil or one foam (between 28 mg and 50 mg) were exposed to an aqueous solution of Reactive Black 5 at 20 mg /L (see Figure III.17*).*
The volume of solution was adapted so that the total dye mass was equivalent to 0.2 % of the sample mass. Each assay was performed in triplicate. Samples were left in contact with the aqueous dye solution 24h at 25°C under static conditions.

Dye concentration was assessed by UV-vis spectroscopy at 598 nm (see calibration in Annex p 207). Supernatants were centrifuged 10 min at 5000 rpm and one volume of PBS 2X was added to ensure constant pH for all measurements.
Discoloration rates were calculated as follows:

$$\%_{discol.} = \frac{[RB5]_f}{[RB5]_i} * 100$$

where $\%_{discol.}$ is the discoloration rate, $[RB5]_i$ is the initial RB5 concentration and $[RB5]_f$ is the final RB5 concentration.

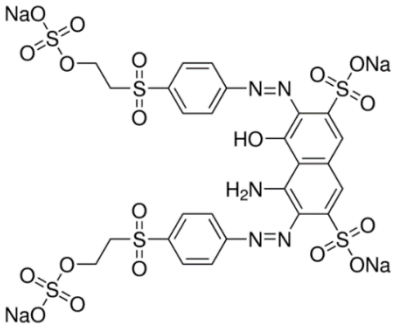

Figure III.17: Chemical structure of Reactive Black 5.

Visual assessment of the different samples (see Figure III.18) shows significant discoloration of the solutions in presence of hybrid foams. The foams themselves become bright blue.

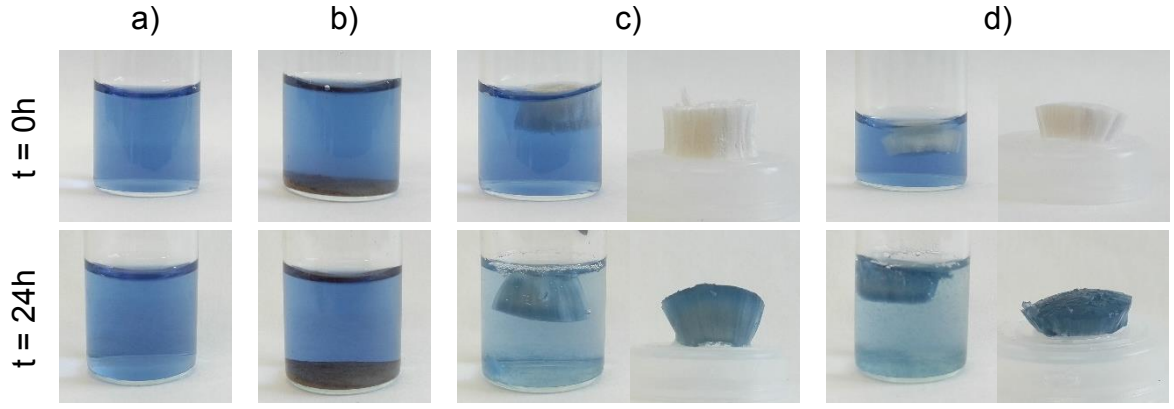

a) RB5 control in water [RB5] = 20 mg/L
b) RB5 in water + soil
c) RB5 in water foam (10 $\%_{SiO2}$)
d) RB5 in water foam (20 $\%_{SiO2}$)

Figure III.18: No discoloration of the RB5 solution can be observed from contact with 50 mg of soil (b) compared to the aqueous control solution (a).The addition of hybrid foams with 10%$_{SiO2}$ (c) or 20 %$_{SiO2}$ (d) results in the apparent discoloration of the supernatant and in the coloration of the foams themselves.

Discoloration was quantified by UV-vis spectroscopy. As can be seen in Figure III.19, RB5 final concentrations are similar for the aqueous control and the sample in presence of soil. RB5 solutions exposed to pectin-silica hybrid foams were significantly discolored (65 ± 5 %

and 62 ± 5 % of discoloration for foams with 10 $\%_{SiO2}$ and 20 $\%_{SiO2}$ respectively). Dye concentrations for assays with the foams at 10 $\%_{SiO2}$ and 20 $\%_{SiO2}$ were not statistically different. The silica content of the hybrid foam does therefore not seem to have a significant effect on the adsorption properties of the foam. Both samples have however relatively low silica contents due to their thickness (which limits the maximal relative silica content as was demonstrated in III.1.c p 100. Higher silica contents may have more pronounced effect.

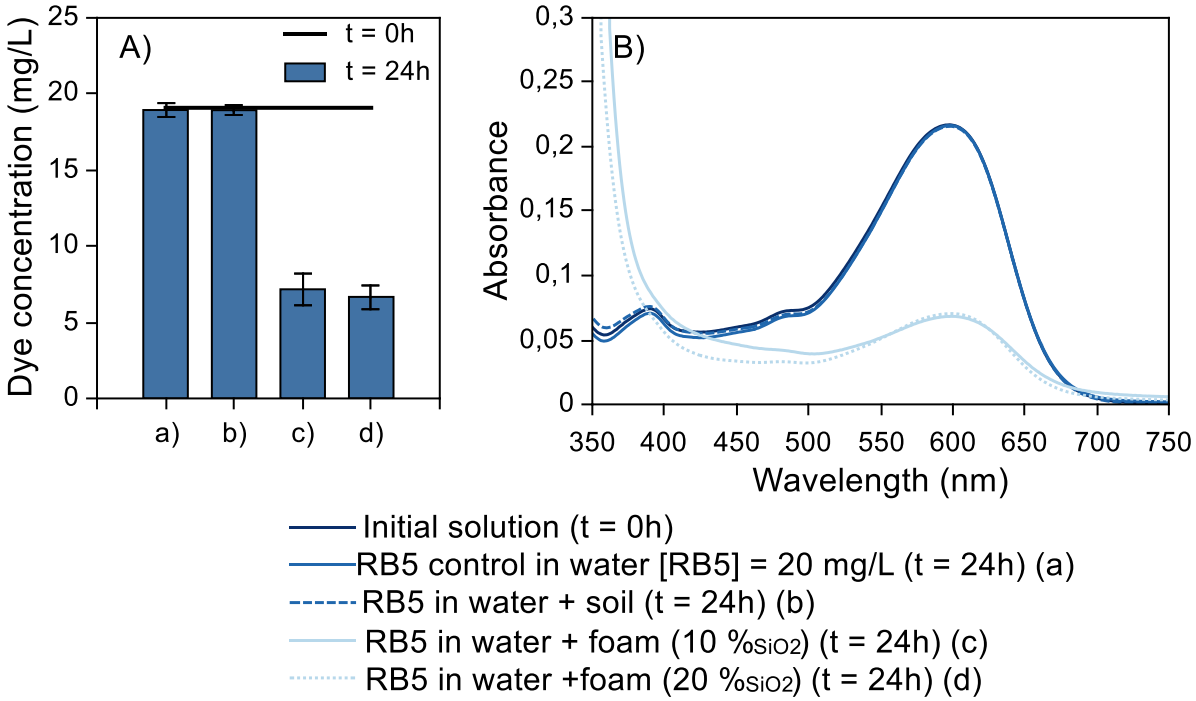

Figure III.19: Control RB5 solution (a) and solution in contact with 50 mg of soil (b) do not present any significant discoloration. In presence of foams containing either 10 $\%_{SiO2}$ (c) or 20 $\%_{SiO2}$ (d), about 60 % of discoloration can be observed.

It might be assumed that the discoloration can entirely be attributed to adsorption phenomena. Since the assays were performed at 25°C, in deionized water and over 24h only, degradation of the dye by microorganisms from the soil or water may be neglected.

Dye mass loading on the foams was therefore directly calculated from the concentration difference between the initial and final supernatants:

$$q = \frac{\left([RB5]_i - [RB5]_f\right) * V_{RB5}}{m_{sample}}$$

Where q is the dye loading, $[RB5]_i$ the initial RB5 concentration, $[RB5]_f$ the final RB5 concentration, V_{RB5} the added volume of aqueous RB5 solution and m_{sample} the mass of the foam sample.

Dye loadings were found to be 1.2 ± 0.1 mg_{dye}/g_{foam} for both hybrid samples Soil itself is likely to have some adsorption properties toward the RB5. However in this case, both use of low dye concentrations and of small quantities of soil for adsorption may have prevented

detection of this phenomenon. It is however likely that bigger amounts of soil may adsorb significant dye masses.

III.2.b.ii In soil

Efficiency of the pectin-silica porous material for discoloration of a RB5 loaded soil was assessed by introducing 10 $\%_{SiO2}$ foams in 5 g of soil saturated by a RB5 solution.

Material and methods

Hybrid foams (about 35 mg) were prepared accordingly to the previously described process (freeze-casting and drying of pectin and silica deposition). Mean silica content on the triplicate samples was 12 ± 1 $\%_{SiO2}$. Samples were placed in 5 g soil saturated by 3.5 mL of 0.1 g/L of RB5 aqueous solution. The total mass of dye represents about 1 % of the foam mass and 0.007 % of the soil mass.

Controls were performed in triplicate with an aqueous solution of RB5 at the same concentration without soil and with soil saturated by the same solution but with no foam. Soil was also put in contact with water containing no dye to establish a baseline.

After 24h at 25°C under static conditions, 3.5 mL of PBS 2X were added to each sample to simulate rinsing *water and 2 mL of supernatant were centrifuged 10 min at 5000 rpm and UV-vis spectra were measured.*

Visual observation of the supernatants (see Figure III.20), which can be seen as the equivalents of rinsing water in an actual polluted sites, show a significant difference between the system containing only soil (Figure III.20 c) and the system containing a foam within the soil (Figure III.20 d). The efficiency of the device seems to be confirmed by the fact that the initially white foam is blue after 24h in the dye loaded soil.

a) RB5 control in water $[RB5]_i$ = 100 mg/L
b) Water + soil
c) RB5 in water + soil
d) RB5 in water + soil + foam (10 $\%_{SiO2}$)
d') Foam after adsorption

Figure III.20: Apparent color of the control sample (a) does not seem to change after 24h at 25°C. The control performed by putting water containing no dye in contact with the reference soil results in a slight yellowish coloration of the supernatant (b). Supernatant of the soil where a pectin-silica foams was introduce (d) appear lighter than the sample containing only soil (c). This is confirmed by the blue coloration of the foam itself (d').

Concentration variations were assessed by UV-vis spectroscopy. Absorbance was measured at 598 nm. Contribution of the yellow coloration due to the soil was removed based on the control sample. Both concentrations in rinsing water from soil with and without foam where significantly lower than the initial concentration. Discoloration rates were found to be 82 ± 1 % and 57 ± 1 % respectively. Dye adsorption was therefore significantly more efficient in presence of pectin-silica hybrid foams. In this case, due the presence of larger amounts of soil, it was possible to measure the absorbed mass of dye on the soil, which was found to be 0.038 mg_{dye}/g_{soil}. In comparison the dye loading of the foam, which weighed only about 0.35 mg, was estimated to be 2.28 mg_{dye}/g_{foam}. This value was calculated assuming that the amount of dye adsorbed on soil was the same in presence and in absence of the hybrid foams.

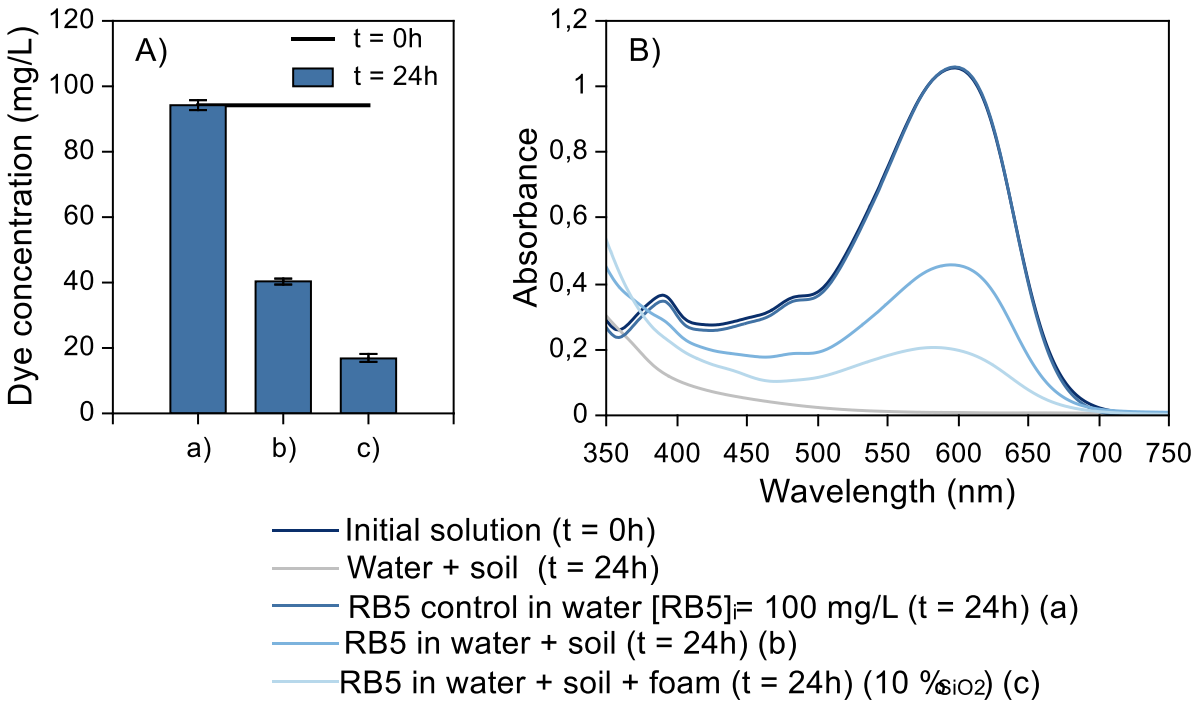

Figure III.21: The control solution is stable in water over 24h (a). Part of the dye content is adsorbed on the soil (b). Discoloration of the rinsing water is significantly improved in presence of a hybrid foam (c).

The pectin-silica material seems in itself to be efficient in depolluting a real soil-based system. A large amount of pollutant is adsorbed on the foam which results in a diminution of the apparent concentration in the rinsing water. Even if it is difficult to assess with this set-up, the foam is also likely to diminished the amount of dye adsorb on the soil particles by displacement of equilibrium.

Conclusion

Macroporous pectin foams were coated with silica through sol-gel chemistry. The specificity of the process relied on the use of vapors phase silica. This method allowed for efficient and controlled deposition of a silica layer, without any modification of the porous structure of the pectin scaffold. The silica appeared homogeneously distributed on the pectin pore wall surface and silica thickness could be controlled through two main processing parameters (deposition time and sample morphology).

Such a pectin-silica core shell structure could be of interest for various applications besides soil depollution. Fine control over the silica layer could prove useful in tuning the diffusion properties of the material. This could for instance be useful for the design of controlled drug delivery vehicles (control of the diffusion of drugs encapsulated within the pectin structure through the silica layer). The resulting hybrid foam proved to have enhanced stability both in liquid medium and in a typical soil example, which is crucial from the application perspective (see Figure III.22).

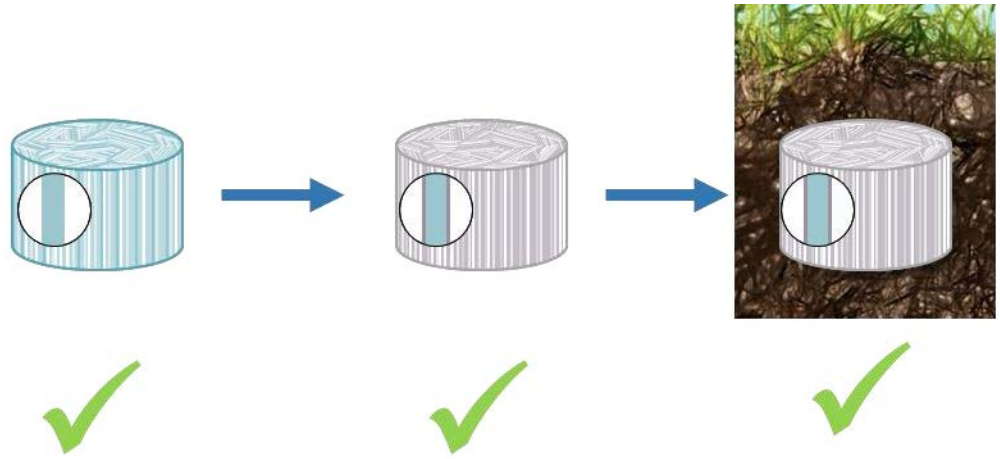

Figure III.22: Pectin foams where efficiently coated by a silica layer. Structural integrity of the materials was retained after several weeks in soil.

More importantly the material proved efficient in adsorbing a model pollutant (Reactive Black 5 dye) up to about 2 mg_{dye}/g_{foam}. These values are low compared to materials conventionally used for adsorption processes such as activated carbon[432,433]. The hybrid pectin-silica materials are however not meant to be used as simple adsorption devices, but as host matrix for microorganisms with pollutant-degrading capabilities. The fact that the dye could efficiently diffuse from a model environment and be adsorbed within the porous material is very encouraging regarding the depollution capabilities of this hybrid structure.

Chapter IV : Encapsulation of microorganisms in macroporous foams

Introduction

Microorganisms[1,89] such as yeast[92], but also and more significantly bacteria[81,93], have been successfully used for the degradation of various types of pollutants[16,28,34]. One of the main limitations to the use of microorganisms in soils is their sensitivity to various parameters such as temperature, pH or ionic strength, which are much more difficult to control in soil than in a liquid suspension. In addition introduction and dispersion of exogenous microorganisms in a given ecosystem may result in significant disturbance of the local biodiversity.

Immobilization and more specifically encapsulation of the considered microorganisms within a solid have been contemplated as efficient ways to limit these possible drawbacks. Such matrix must be designed as a way to allow and facilitate diffusion and mass transport of the targeted contaminants while preventing leaching of the exogenous microorganisms within the soil (for instance by designing appropriate macro, meso and micro porosities). As a result the encapsulation process should allow for efficient entrapment of the living cells, preservation of their metabolic activity from the functional point of view, but also for shaping of the matrix itself from the structural point of view.

Freeze-casting has proven to be an efficient way to elaborate macroporous polymer-based materials and to gain control over their oriented porous structure. Freeze-casting of a suspension of microorganisms in the same biopolymer could be used as an encapsulation process to prepare cellularized porous bioactive materials. Ice-templating parameters such as the freezing rate are usually considered as levers from the structural point of view, for instance to control the final pore size. In this case they could also prove valuable in order to control physical entrapment and viability of functional units within the porous material.

In order to evaluate the feasibility of cell encapsulation in the previously described macroporous pectin foams, *Saccharomyces cerevisiae* was used as a model. This proof of concept was then extended by using *Pseudomonas aeruginosa*, which is a more relevant model from the point of view of bioremediation.

IV.1 *Saccharomyces cerevisiae* as a proof of concept

IV.1.a About *Saccharomyces cerevisiae*

Saccharomyces cerevisiae is part of everyday life for many people, since it is commonly used in the bakery and brewing industry. Besides these applications, *S. cerevisiae* is also part of the life of many microbiologists. It is often referred as the eukaryotic equivalent to *Escherichia coli*[434], being widely used as cell model. This yeast has the advantage of growing in various media, both in aerobic and anaerobic conditions, with rapid doubling time (90 min in rich medium)[435].

A common culture medium is yeast peptone dextrose (YPD), but cells suspensions can also be obtained by simple rehydration of lyophilized cells in water. In order to evaluate the viability of yeasts in suspension several techniques can be used. Plate counting on LB-agar gel is an option, though not very commonly used for yeasts. Metabolic activity assays are generally preferred, though the information obtained by that way is not exactly the same. Indeed the notion of cell viability can be difficult to define since some cells may still have a metabolic activity without being capable of replication (viable but nonculturable state)[436]. It is for instance possible to take advantage of the degrading capabilities of *S. cerevisiae* toward glucose, which is key in the brewing industry[437]. As a result, titration of the evolution of the glucose concentration, for instance by mean of a hexokinase assay kit, may provide information on the metabolic activity of the cells.

Another possible way to investigate the metabolic activity of *S. cerevisiae* is to take advantage of its enzymatic reducing properties. Methylene blue has been used to monitor cell metabolic activity thanks to the Methylene Blue dye Reduction Test (MBRT). It has been used both for prokaryotic[438] and eukaryotic[439] cells. Under oxidizing conditions, methylene blue exhibits a characteristic blue color, but its reduced form is colorless, which makes it an easy-to-use visual probe for reducing activity

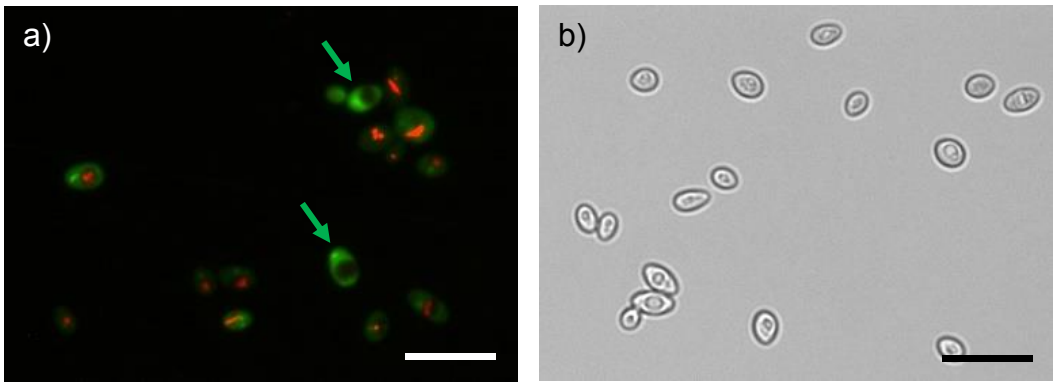

Figure IV.1: *S. cerevisiae* cells can easily be observed under optical microscope (b). The use of Live/Dead® staining kits (a) allows for easy discrimination between metabolically active cells with intravacuolar red staining and non-active cells with diffuse green staining (green arrows). Scale bars: 20 µm.

Due to their size (about 10 µm), *S. cerevisiae* cells can easily be observed by conventional optical microscopy (see Figure IV.1 b). This allows for the use of epifluorescence techniques to assess the viability of a yeast suspension, thanks to the use of Live/Dead® assay kits[440]. The fluorescent probe FUN1 penetrates the membrane of yeast cells regardless of their viability. Only metabolically active cells are capable of converting the dye from a diffuse green staining, to a red intravacuolar marking (see Figure IV.1 a).

IV.1.b Yeast encapsulation in a pectin foam

S. cerevisiae was encapsulated in a pectin matrix by simple freezing of a suspension of cells in a 40 g/L biopolymer solution plunged in a liquid nitrogen bath.

Material and methods

S. cerevisiae type II was obtained from Sigma-Aldrich under dry form.
Yeasts were rehydrated in water at 35 °C with chosen mass loadings and added to pectin solutions (final pectin concentration is 40 g/L and final yeast concentration ranged from 0 to 133.3 g/L). About 1.8 mL of suspension was poured into 2 mL cryotubes and the samples were plunged into liquid nitrogen for 5 minutes. The samples were then vacuum-dried overnight.
Dry foams similar to those, obtained in absence of cells were prepared as controls.
For SEM observation, transversal slices were cut with a scalpel and sputtered with 20 nm of gold.

Figure IV.2 gathers SEM images for pectin foams with three different cell contents (no cells, 33.3 g/L and 133.3 g/L). The thickness of the pore wall in absence of cells is inferior to 100 nm, which is smaller than the cell diameter (about 3µm). As a result the shape of the cell can easily be observed within the pore walls. With low cell contents individuals cells can be seen embedded in the pectin pore walls (see Figure IV.2 b'). The overall structure is slightly modified compared to non-cellularized foams, but elongated pores can still be seen (see Figure IV.2 b).
It is also possible to include higher cell contents in the initial suspension. This still results in a self-supporting macroporous material after drying, but the pores morphology is modified (see Figure IV.2 c). No clear pore orientation can be observed, and the pores appear much larger.
Upon closer look on the pore walls (see Figure IV.2 c') it is noticeable that they are actually mainly composed of cells. At intermediate concentrations, cells appear to be slightly more concentrated around the edges of the pores walls, which may be explained by the presence of different segregation rate during freezing for the cells and the polymer.
Assuming a similar density for the pectin powder and dry cells, an initial 33.3 g/L of cell content and 40 g/L of pectin concentration would account for a cell volume percentage of about 45% of the total dry wall volume. For a higher initial cell content (133.3 g/L) the cell volume fraction goes up to 77% of the pore walls. The cellularized materials with highest cell loadings could therefore be compared to ice-templated ceramic materials where solid particles

can be structured into porous materials. The structural integrity can be obtained through sintering (which is not applicable in the case of heat sensitive cells) or by using a polymer as a binder. In this case the cells could be considered as soft and deformable particle and pectin as the binder.

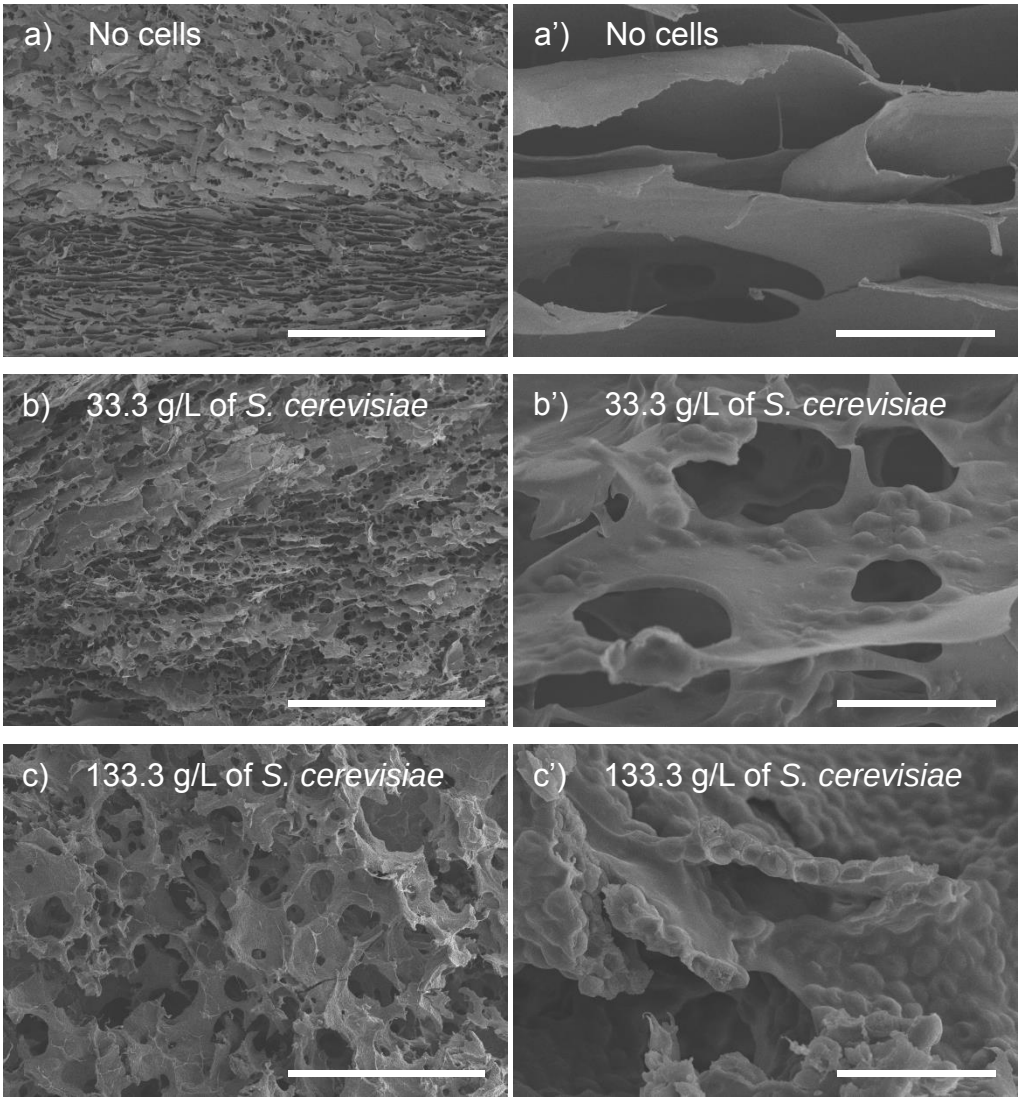

Figure IV.2: SEM observation of *S. cerevisiae* cells embedded in pectin foams. Foams with no yeasts (a and a') display an oriented porosity and lamellar pectin walls. The introduction of 33.3 g/L of yeast cells (b and b') in the initial suspension results in clearly visible cells embedded in the pore walls. At a 133.3g/L cell concentration (c and c') the general morphology of the foam is modified and the pore walls are mainly composed of cells. Scale bars: 500 µm in a, b and c, 20 µm in a', b' and c'.

For the targeted application, physical encapsulation of the cell is however not sufficient. The metabolic activity of the entrapped microorganism must be preserved in order to produce a depolluting device.

Material and methods

Yeast-containing foams were prepared as previously described and dispersed in water. Methylene blue was added. Volumes were adjusted to yield 33.3 g/l of yeast, 40 g/L in pectin

and 1.67.10^{-2} g/L in methylene blue. The suspensions were then maintained at 35°C until reduction of the methylene blue.
Discoloration rates were compared with samples prepared directly from fresh yeast, pectin and methylene blue at the same concentrations.

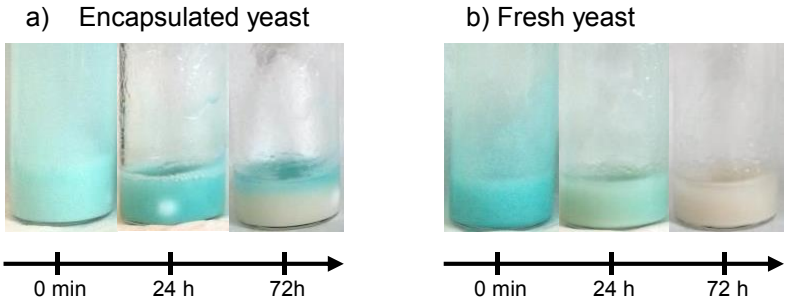

Figure IV.3: Yeast cells that were encapsulated in pectin foams (a) were able to discolor methylene blue when the foams were dispersed in water. The discoloration is however slower compared to samples prepared from fresh yeast suspension (b).

Even though discoloration is slightly quicker with suspensions containing fresh yeasts, the samples obtained from the yeast-containing foams are efficiently discolored after 72h. This suggests a drop in the amount of metabolic active cells due to the freezing and drying but a portion of the cells seem to remain active. One must however be careful in analyzing these results, since the discoloration mechanism is enzymatic. As a result enzymes may be trapped in the foams even though cells are dead, resulting in discoloration of the methylene blue. These result should therefore be correlated with other analytic methods, for instance fluorescence microscopy to confirm the cell viability.
S. cerevisiae is a common laboratory model since it is an easily cultivated, non-pathogenic, easy-to-observe and robust microorganism. It has been used for biosorption in bioremediation processes. It is however not commonly used for biodegradation, contrary to bacteria. Encapsulation of cells in ice-templated pectin matrices was therefore extended to *P. aeruginosa.* Such an organism is more relevant from a bioremediation point of view, but represents new challenges regarding encapsulation due to its sensitivity.

IV.2 Encapsulation of *Pseudomonas aeruginosa* in freeze-casted pectin foams

IV.2.a About *Pseudomonas aeruginosa*

Pseudomonas aeruginosa is gram-negative bacteria, capable of growing various environments (including water, soil, sediments) or hosts (plants, animals and humans). As a result of this adaptability, *P. aeruginosa* can be grown in a wide variety of conditions, in different media and at various temperatures. A commonly used growth medium is LB broth at 37°C[441], but this species can also be grow in minimal medium, in order to pinpoint the effect of specific carbon or nitrogen sources for instance. The versatility of *Pseudomonas* genus in general, and of *P. aeruginosa* in particular, regarding nutrient sources make them ideal candidates for bioremediation applications. These bacteria have been used for the degradation of a wide range of organic compounds (see Table IV.1).

Table IV.1 : Bioremediation capabilities of various *P. aeruginosa* strains. (*) corresponds to compounds mentioned in the REACH restrictions list (Annex XVII of REACH as retrieved from https://echa.europa.eu in July 2017)

Pollutants		Reference
Hydrocarbons		
	Hexadecane	442,443
	Crude oil	444–446
	Anthracene (*)	447
	Pyrene	448
	Phenanthrene	449,450
BTEX		
	Mixture	451
	Benzene, toluene, xylene	452
	Benzene	453
	Toluene (*)	454
Toluene derivatives		
	Dinitrotoluene	455
	Trinitrotoluene	456,457
Azo dyes		
	Direct orange 39	458
	Remazol black, methyl orange, benzyl orange	251
Phenol derivatives		
	Phenol	459
	Bisphenol A (*)	460
PCB		
	PCB	461
Pesticides		
	Tetramethylthiuramdisulfide	462
	Fenpropathrin	463

In brief, *P. aeruginosa* is a bacteria commonly used in microbiology laboratories. It is easy to handle due to its adaptability to various growth conditions and this same adaptability results in the common use of these bacteria in different bioremediation processes. Both these advantages make *P. aeruginosa* a good candidate for encapsulation in a soil depollution device.

IV.2.a.i Growth curves

Before any encapsulation attempt can be made, it is crucial to precisely characterize the growth of the specific considered strain. Growth of *P. aeruginosa* was monitored in LB medium at 30°C to identify its different growth stages.

Material and methods

P. aeruginosa ATCC® 27853™ strain was used from a storage agar plate (see Annex p 205 for preparation and storage).
One colony was pre-cultivated 24h at 30°C and 150 rpm in 10 mL of lysogeny broth (hereafter called LB medium) (see Annex p 204 on medium preparation). The pre-culture was then diluted by a factor of 50 (1.2 mL of pre-culture suspension in 58.8 mL of fresh LB medium) for culture in 75 cm² flasks at 150 rpm and 30°C.
Optical density (OD) was measured regularly by spectrophotometry at 600 nm.
Estimation of the number of viable cells was performed by plate counting at various cuture times (see Annex p 206 on plate counting).

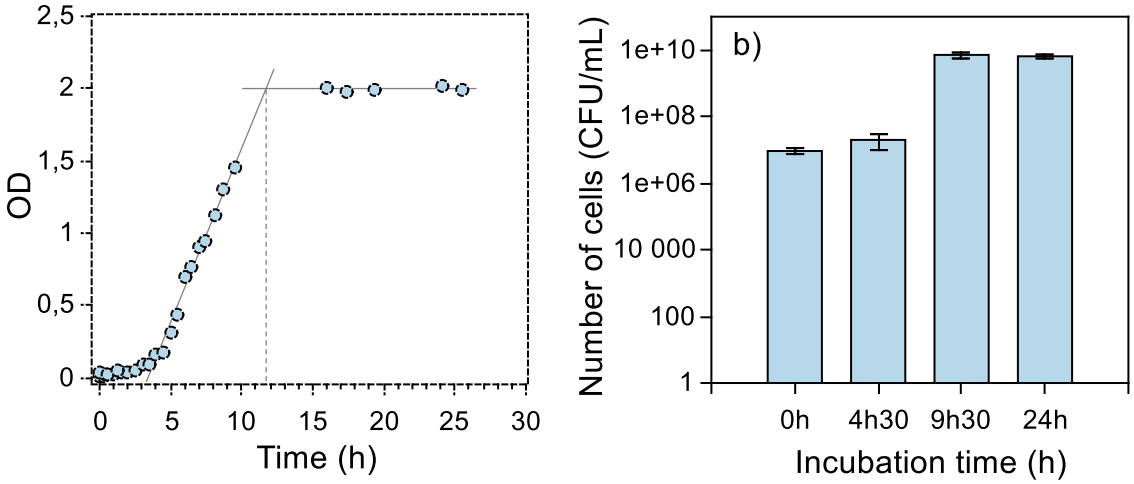

Figure IV.4: Growth curve for *P. aeruginosa* in LB medium at 30°C and 150 rpm (a) and corresponding number of CFU per mL at various incubation times (b).

Figure IV.4 presents the evolution of OD for a culture of *P. aeruginosa* in LB medium at 30°C and 150 rpm. A lag time of about 2h can be observed. The bacteria then enter the exponential growth phase. After about 12 h the OD reaches a plateau around 2, which corresponds to the stationary phase of the bacterial culture. OD was correlated to the number

of colony forming units (CFU) in the suspension. Similar cell concentrations were observed at 9h30 and 24h despite different OD. This might be explained by the presence non culturable cells in in the stationary phase suspension which may contribute to the OD.
Once culture conditions for *P. aeruginosa* were set, assays could be designed towards the encapsulation in the hybrid macroporous foams.

IV.2.a.ii Viability in pectin solutions

Before freezing, it is necessary to obtain a stable suspension of bacteria in the polymer solution. For practical and efficiency reasons, bacteria were not cultivated directly in the polymer solution, but rather grown separately and added to a pre-mixed polymer solution.

Material and methods

P. aeruginosa was cultivated as previously described in 75 cm² culture flasks at 30°C and 150 rpm, from a 1/50 dilution in LB medium of a pre-culture, itself inoculated from a single colony of P. aeruginosa.
In typical experiments, culture was maintained for 5h until 0.5 OD was reached. The 60 mL of culture medium were then centrifuged for 10 min at 5000 rpm and 20°C. The bacteria were then suspended in 3 mL of 0.22 µm filtered water (one twentieth of the original volume). The 3 mL of concentrated suspension were then added to 12 mL of a 50 g/L pectin solution.
Solutions of pectin were prepared in advance at 50 g/L to accommodate the addition of a small volume of cell suspension (one fifth of the final volume) and result in a final concentration of 40 g/L. Typically 12 mL of 50 g/L pectin solution were prepared and 3 ml of cell suspension were added to yield 15 mL of bacterial suspension in 40 g/L of pectin.
Solutions were prepared by adding a chosen mass of dry pectin powder in 0.22 µm filtered water. The mixture was left 24h at room temperature under elliptic agitation, but with not magnetic stirring.
Alternatively, pectin was dispersed in a 125 mM piperazine-N,N'-bis(2-ethanesulfonic acid) buffer (hereafter called PIPES) to stabilize pH closer to 7.. This yielded after addition of the cell suspensions a solution at 40 g/L in pectin and 100 mM in PIPES. The PIPES buffer solution was prepared by dissolving the desired amount of PIPES in a small volume of deionized water (typically 3.78 g for 100 mL of final solution), adjusting pH to 7 with 1M NaOH and adding water to reach desired volume and concentration (typically 125 mM).

In order to evaluate the cytocompatibility of pectin solutions towards *P. aeruginosa*, the number of colony forming units (CFU/mL) was compared for cells dispersed in water, in a 40g/l solution of pectin, in a 100 mM aqueous solution of PIPES and in a solution containing both 40g/L of pectin and 100 mM of PIPES. Plate counting was performed after 5 min and 24 h of contact (solutions were kept at 4°C in meantime) (see Figure IV.5). The pH of the solutions was measured in all solutions and was stable over 24 hours (pH = 5).

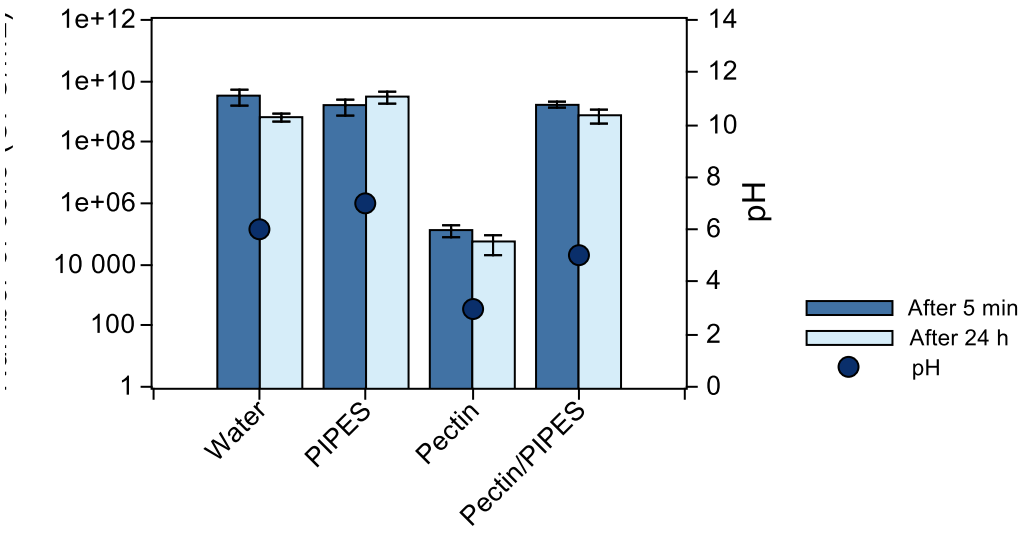

Figure IV.5: Bacteria in a 40 g/l solution of pectin undergo a drop in the number of CFU/mL. This may be explained by the acidic properties of the pectin which yield solutions at a pH around 3. The use of a PIPES buffer results in a number of CFU/mL similar to the control samples in water of aqueous solution of PIPES.

A significant difference between the pectin samples with and without PIPES buffer could be observed. The drop in the number of CFU in pectin solutions might be attributed to the low pH of the pectin solution (around pH 3), which is due to the acidic properties of the pectin, including carboxylic acid residues. The addition of PIPES buffer at 100 mM stabilizes the pH around 5. Increase of pH up to 7 might be beneficial for cell survival, but it would require addition of more concentrated buffer solutions. High solute contents may be problematic due to the sensitivity of bacteria to high osmotic pressures. It is all the more concerning, since the solutes introduced in the suspension tend to be concentrated by the freezing step of the shaping process. Since no significant changes in viable cell concentrations were monitored between the suspension in pH 5 pectin solution and pH 7 PIPES solution, compared to controls in water and aqueous solution of PIPES, the 100 mM buffer concentration was used in all further experiments.

As a result slight modification in the composition of the initial solution was efficient in preserving the viability of the cells in suspension. It was however mentioned in Chapter II, that a modification of the formulation of the initial solution has a direct influence on the morphology of the encapsulating matrix. Samples with no cells but in presence of PIPES buffer were prepared for SEM observation.

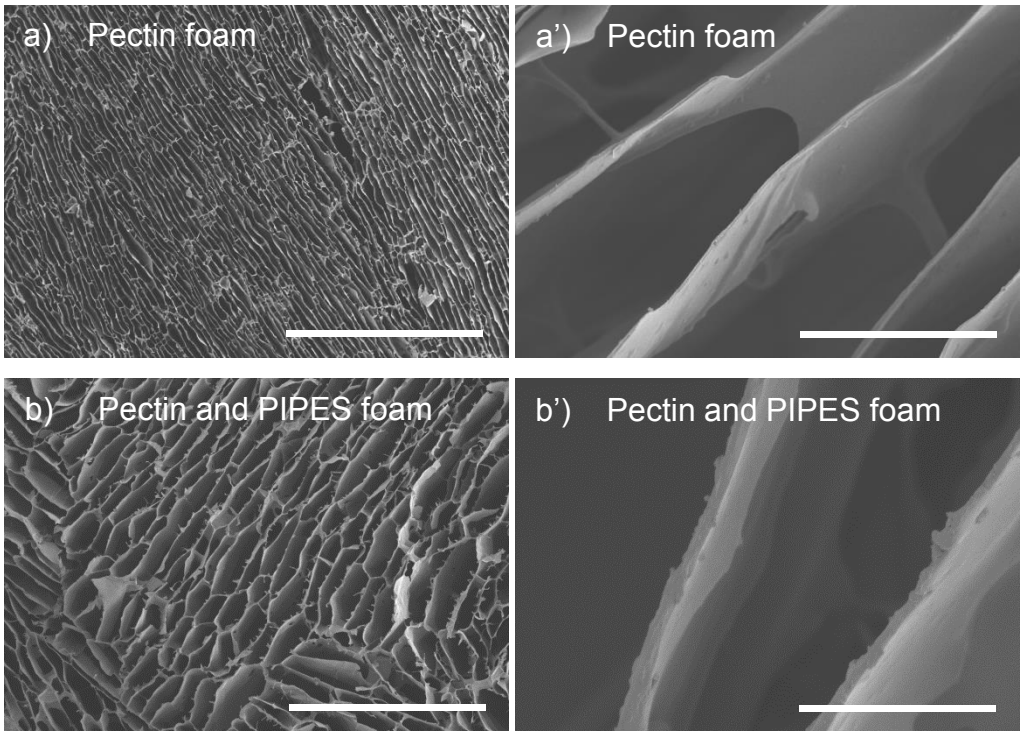

Figure IV.6: SEM observations of foams prepared from different pectin solutions. Samples prepared from a solution composed of 40 g/L of pectin and 100 mM of PIPES buffer (b and b') present larger pores and thicker pore walls compared to foam prepared from 40 g/L pectin solutions (a and a'). Scale bars: 500 µm for a and b, 20 µm for a' and b'.

Foams were prepared from pectin solutions at 40 g/L in water (Figure IV.6 a) and from solutions of pectin in PIPES buffer at 100 mM (see Figure IV.6 b). A significant difference in pore size was noticeable (Table IV.2). In presence of PIPES, the pore width almost doubles. The pore length is however smaller, which results in a large change in the pore aspect ratio. Another significant change is noticeable in the pore wall thickness. The addition of the solute at high concentration significantly modifies the pore morphology, which may be due to interaction with ice crystals thus modifying ice growth[273].

Table IV.2: Pore morphology with and without PIPES buffer in the initial pectin solution.

Samples	Pore width (µm)	Std dev (µm)	Pore length(µm)	Std dev (µm)	Aspect ratio	Std dev (µm)	Pore wall thickness (µm)	Std dev (µm)
Pectin at 40 g/L, 5°C/min	12	4	366	258	30	13	0.2	0.1
Pectin at 40 g/L PIPES at 100 mM, 5°C/min	25	13	202	74	8	5	1.5	0.4

A 100 mM concentration in PIPES corresponds to a mass concentration about 30 g/L, which must be compared to the 40 g/L concentration in pectin. Added solutes may indeed modify the ice growth by adsorbing preferentially on specific crystallographic surfaces and hinder the growth in one direction. But the PIPES also modify the pH of the initial solution, which changes from about 3 to 5. This has a direct influence on the pectin chains themselves, and is especially likely to influence the carboxylic acid functions which may be at least partially deprotonated. As a result the interaction between the pectin chains could be modified which may result in variations in the physico-chemical properties of the initial solution such as viscosity. As a consequence the ice growth during the freezing step can be modified, resulting in changes in the pore morphology, but also the pectin wall density and thickness.
A stable bacteria suspension in pectin is only the first step toward the encapsulation of living organisms in macroporous foams. This suspension must then be shaped, by the use of ice-templating as previously described. The resulting material must then be coated by silica in order to obtain a suitable material for the targeted use in soils.

IV.2.b Encapsulation of *Pseudomonas aeruginosa* in freeze-casted pectin foams

Bacteria cells can be entrapped in macroporous pectin foams by freezing of a cells suspension in 40 g/L of pectin. The ice growth results in the formation of pores after vacuum drying. The bacteria cells are incorporated within the cell walls during the formation of the ice crystals. This encapsulation is only possible due to a combination of various factors. Phenomena of particles sedimentation, rejection or entrapment have mainly been studied regarding solid ceramic particles. Such consideration can however be adapted and extended to soft particles such as bubbles or cells[333]. The fate of a particle in front of a freezing front is influenced by a wide variety of parameters. The first risk is sedimentation in the initial suspension. In the case of cells, such phenomenon is prevented by the fact that the cell density is close to the density of the suspending medium (the polymer solution). During the progression of the ice front, the fate of the particles (or cells) is mainly governed by two phenomena : the repulsive force due the different interactions energies between the particle, the solid and the liquid and the viscous drag exerted by the liquid displaced by the advancing front that pushes the particle towards the ice front[257]. As a result any parameter modifying one of these two aspects is likely to influence the encapsulation efficiency. For instance the chemical nature of the particle or the presence of additives in the liquid phase may significantly modify the surface interactions. On the other hand modifications of the solution viscosity or of the speed of the ice-front are likely to modify the regime and characteristics of the flow around the particles.
In the case of cell encapsulation, the particles (*i.e.* the cells) are about 1 µm in size and are dispersed in a pectin solution at 40 g/L, which has a viscosity around 1 Pa.s. These conditions are compatible with the immobilization of the cells directly inside the pectin walls. The shape of the cells under the pectin layer may be observed in SEM (see Figure IV.7), providing that the pore walls are thin enough. In some instances, the bacteria may be directly seen within the pore wall section, depending on the way the samples are cut.

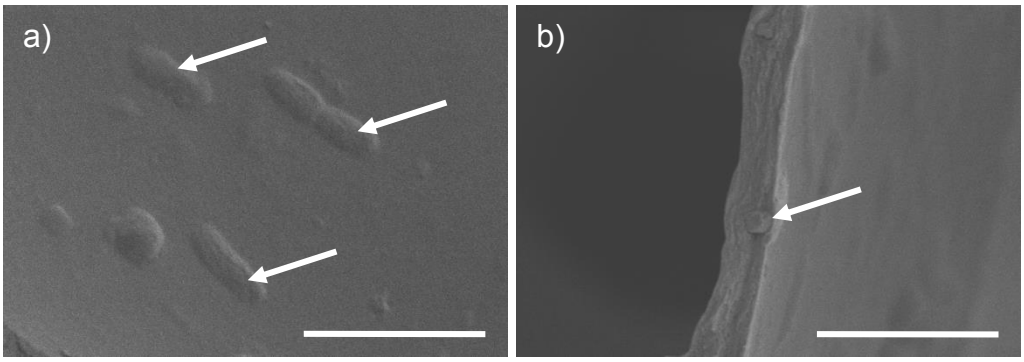

Figure IV.7: SEM observation of cellularized pectin foams. The shape of the bacteria can be seen under a thin pectin layer (a) and some cells be directly observed within the pore wall (b). Scale bars: 3 µm.

As pointed out earlier, physical encapsulation of the cell is essential but in order to be efficient, the shaping process must be compatible with the survival of the bacteria.

IV.2.b.i Influence of the freezing-rate

The ice-templating shaping process involves freezing of living cells. If freezing of living cells as a mean of encapsulation in a polymeric matrix has not been widely documented, there are extensive studies both regarding freezing of cells for preservation in the frozen state and freeze-drying of cells for preservation in a dry state[335] (see I.3.b , p45).

Two main deleterious effects of freezing on living cells have been identified. Formation of intracellular ice may result in disruption or destruction of the cellular membranes. The formation of extracellular ice is usually deemed as less deleterious to the cells[348], but may however induce significant mechanical stress on the cells[334]. The formation of extracellular ice also results in the concentration of the extracellular solutes, which in turn may induce dehydration of the cells. This may result in strong shrinking and deformation of the cells, but also in a rise of intracellular solutes to toxic levels. Common cryopreservation strategies include the use of cryoprotectants such as glycerol and control of the applied cooling rates. In both cases the goal is to adjust the osmotic balance between the intra and extracellular medium in order to prevent formation of intracellular ice while maintaining non-toxic solutes concentrations. Introduction of molecules (such as glycerol) capable of penetrating the cell membrane may indeed help to balance the rise in external solute concentration. Influence of the freezing rate has also proven to be crucial. High cooling rate limit the diffusion of water through the membrane and may result in supercooling of the internal wall which is responsible for the formation of intracellular ice. On the other hand if cooling rates are too low, water permeation may result in high intracellular solutes concentration which could be damaging to the cells[352]. As a result an optimal cooling rate can usually be found to maximize cell survival. Such optimum is however cell dependent since it may be influenced by different types of membrane or intracellular solutes concentrations. It is also likely to be modified by the composition of the freezing medium[348].

In this work however the freezing conditions are quite different from conventional cryopreservation. It must first be pointed out that no common cryopreservative is used during freezing. The freezing medium however contain a polysaccharide, which may act in a similar way as non-penetrating cryoprotective agents by tuning the formation of extracellular ice[346]. The presence of the polymer as an encapsulating layer may also provide protection against mechanical solicitation during freezing.
In addition to the stress of the freezing step, the encapsulated cells are also exposed to high vacuum (0.05 mbar) during lyophilization. A few studies[360] have been published regarding the freeze-drying of microorganisms, but generally they are freeze-dried from concentrated cell suspensions in order to obtain a powder for cell storage and not for encapsulation in a matrix, which may induce significantly behavior, particularly in terms of mechanical solicitation. In order to assess and optimize survival rates during encapsulation in pectin through freeze-casting, *P. aeruginosa* cells were frozen at various speeds and the numbers of CFU were compared.

Material and methods

P. aeruginosa was cultivated in LB medium up to 0.5 OD (about mid exponential phase) at 150 rpm and 30°C. The cell culture (typically 60 mL) was centrifuged 10 min at 5000 rpm and dispersed in one twentieth of the initial culture volume in water (typically 3 mL). This suspension was introduced in a pectin and PIPES solution to yield a 40 g/L concentration in pectin, 100 mM in PIPES, and a cell concentration equivalent to 4 times the initial culture (about 2.10^8 CFU/mL). The suspension was then frozen and subsequently vacuum dried. Part of the samples were directly thawed after freezing (30 mins at 30°C) in order to dissociate the effect of the freezing step from the drying step.

Cooling rates of 1°C/min, 5°C/min and 10°C/min were applied by freeze-casting. As a comparison point, samples were prepared by direct dipping in liquid nitrogen to yield a 250°C/min cooling rate.

The survival rates were compared between the samples frozen and thawed and the sample frozen and dried overnight. Thawed samples were diluted and spread on LB-agar plates and incubated at 37°C for 24h. Dry samples were dispersed in five times their volume of water and successive dilutions were prepared. Three samples were prepared for each cooling-rate and each dilution was plated in triplicate. The initial number of cells introduced was measured and slight variations were measured (between 1.10^8 and 1.10^9 CFU/mL). To facilitate comparison between the cooling rates the number of CFU *in frozen and thawed samples, and frozen and dried samples, the number of surviving cells were normalized to an initial number of cells of 1.10^9 CFU/mL.*

Figure IV.8 presents the number of CFU in samples frozen at different cooling rates. The number of CFU is only one type of indication regarding the viability of the encapsulated bacteria. The notion of survival regarding single cell organisms is complex[436], since some

cells may be incapable of multiplying while retaining a metabolic activity. Other complementary technique may be applied to investigate the viability of encapsulated cells, but plate counting remains a simple and widely applicable technique which will further be used as reference. As a result, the expressions survival rate or viability will be used as the number of CFU.

The samples obtained at 1°C/min, 5°C/min and 10°C/min were all processed by freeze-casting, with the same setup and are therefore strictly comparable. The device used is however unable to yield higher cooling rates and in order to assess the effect of very high cooling rates (around 250°C/min) samples were prepared by dipping in liquid nitrogen. These samples are therefore only an indication of the survival rates at theses freezing rates, but it must be kept in mind that the geometries are not strictly comparable, which might also have an influence on the survival of the cells since the mechanical constraints are different.

Samples frozen and thawed were compared to samples frozen and dried, as way to dissociate the effects of freezing and drying. However it is impossible to fully separate these two effects, or rather, it is impossible to assess the effects of freezing alone, since samples must necessarily be thawed before counting the number of CFU. As a result it is only possible to compare the combined effects of freezing and thawing to the combined effects of freezing, drying and rehydration.

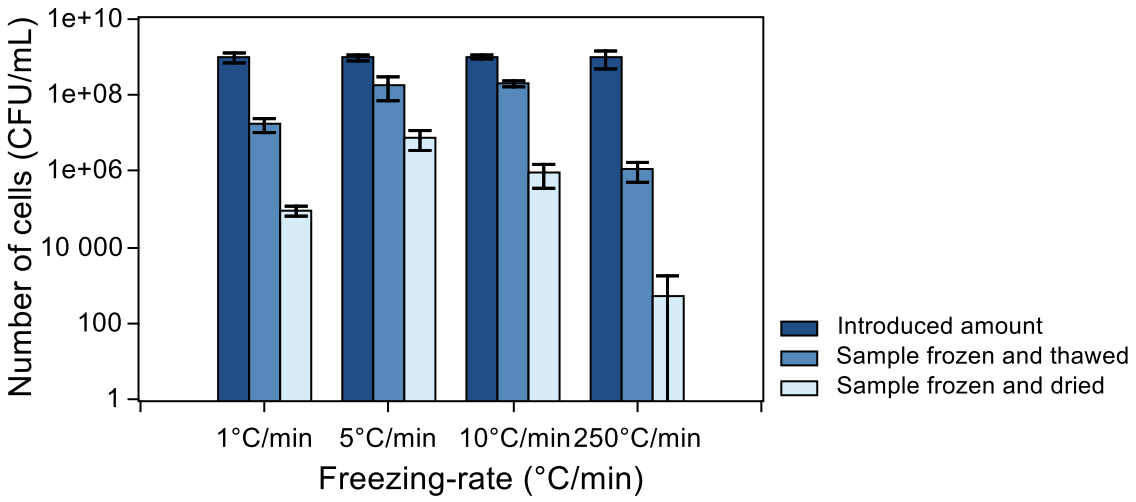

Figure IV.8: Freezing and thawing of the sample result in higher survival rates than freezing and subsequent vacuum drying. Optimal cell survival is obtained for a 5°C/min freezing-rate, which is slow enough to allow cell dehydration and prevent formation of intracellular ice, but fast enough to prevent limit high solutes concentration.

Freezing and thawing results in viability losses between 1 and 3 logarithmic units. Survival rates are similar at 5°C/min and 10°C/min (drop of 1 logarithmic unit). At 1°C/min a loss about 2 logarithmic units can be observed. At very high cooling rate, the lowest survival rate was observed (3 logarithmic units). As a result it seems that intermediary cooling rates yield higher survival rate which is in agreement with observations performed on cells suspension. It is however difficult to predict this optimal cooling rate, since there are large variations

depending on the type of cell[352].The survival rate after freezing and thawing represents only an indication of the influence of the freezing rate, but the most relevant information is the number of viable cells encapsulated in the dry macroporous matrix.
Regardless of the cooling rate, freezing and drying resulted in lower survival rates than freezing and thawing. After vacuum drying, the effects of the freezing rate are even more noticeable. Here again, the viability loss cannot be strictly attributed to the freezing and drying steps, but also to the rehydration conditions. It has indeed been shown that the medium used for cell rehydration has a significant influence on survival rates[365]. At 1°C/min about 10^5 cells are capable of forming colonies per milliliter of the initial suspension; at 5°C/min this value increases to 10^7 CFU/mL, but decreases to 10^6 CFU/mL at 10°C/min and even down to less than 10^3 CFU/mL at very high cooling rate. After drying, the presence of an optimal freezing rate is clearly visible. The highest number of CFU is observed for freezing at 5°C/min. Even if the drying conditions are strictly identical, the prior freezing conditions have an influence on the survival during the drying phase. As the temperature rises again, presence of internal ice created during freezing at high cooling rate may induce further cell damage. Another source of possible damages is the fact that cells are subjected to mechanical constrains, both during freezing[334] and under a 0.05 mbar vacuum, which is likely to induce sharp drops in survival rates. The applied vacuum is identical for all freezing-rates, but the cells might have different sensitivities due to the different freezing conditions. In addition, freezing rates have an influence of the pore walls themselves, including their thickness. These structural variations may have a direct influence on the cell survival since the pectin wall provides a protection against mechanical damage.
In all further encapsulations assays, cooling rate was set at 5°C/min even though changing other parameter, such as the bacterial growth phase, may in turn slightly shift the optimal cooling rate due to possible changes in the cells properties. It was however assumed that this variation was limited. Once this critical processing parameter was set, the state of the cells themselves was modified to evaluate the growth conditions best suited to the encapsulation process.

IV.2.b.ii Influence of the cell growth phase and concentration

The physiological state of the cells (and therefore the growth phase considered) has a significant influence on their resilience to the encapsulation process. The effect of the growth phase must however be distinguished from the influence of the initial cell concentration. In order to assess the influence of these two different parameters, cells were grown up to exponential and stationary phase and concentrated or diluted to different levels prior to encapsulation.

Material and methods

A culture of P. aeruginosa was grown in LB medium at 150 rpm and 30°C. Bacteria were cultivated either for 5 h (up to a 0.5 OD, exponential growth phase) or 24 h (up to a 2 OD, stationary growth phase). The culture media were centrifuged and dispersed in water in order to yield suspensions at two distinct concentrations for each growth phase. The cells were then suspended in previously prepared pectin and PIPES solutions (final concentrations of 40 g/L and 100 mM respectively). 3 mL of each bacteria suspension in pectin were then freeze-casted at 5°C/min and vacuum dried at 0.05 mbar for 24 h.

The dry foams were then dispersed in five times their volume of water, and successive dilutions were prepared for plate counting. Three samples were prepared for each growth stage and concentration, and each dilution was plated in triplicate.

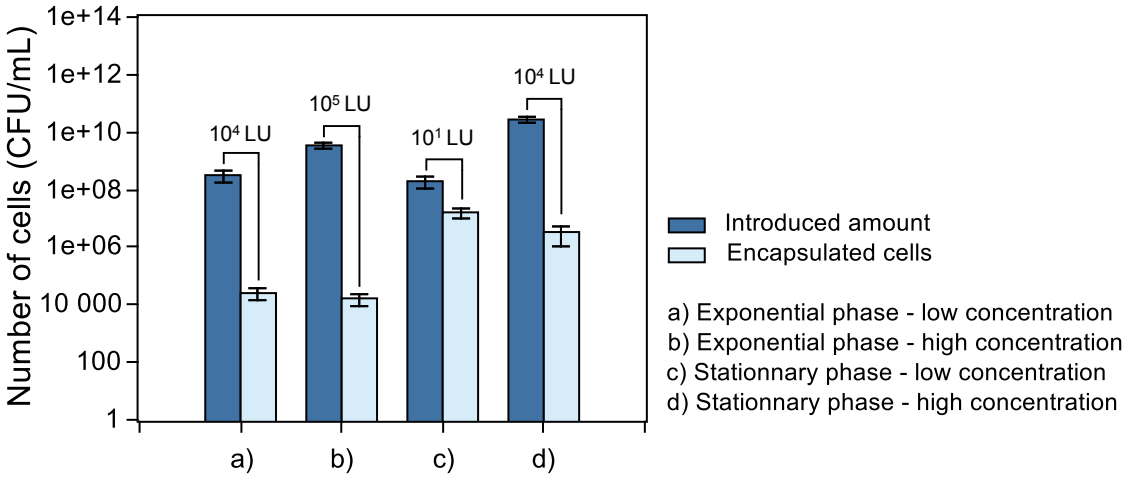

Figure IV.9: Cell in stationary growth phase (c and d) have higher survival rate than cells in exponential growth phase (a and b). When samples were prepared from the same cell culture but concentrated to different initial cell loadings, better survival rate were obtained from less concentrated suspensions. Cell losses are indicated in logarithmic units.

Figure IV.9 shows survival rates for encapsulated *P. aeruginosa* at different growth stages and different initial concentrations. At similar initial concentration (5.10^8 CFU/mL), cells encapsulated in stationary phase (Figure IV.9 c) have higher survival rates (5.10^7 CFU/mL) than cells encapsulated in exponential growth phase (5.10^4 CFU/mL, see Figure IV.9 a). This observation is consistent with previous studies performed on other bacterial and yeast species[347,464].

In order to ensure the highest efficiency for the final biomaterial, high initial cell concentrations may be of help. Cell cultures were concentrated to various levels to investigate the influence of cell concentration on survival. When larger concentrations of cell were introduced in the pectin solution, the final number of CFU (after freeze-casting and drying) were actually similar or lower than sample prepared from lower initial concentrations (see Figure IV.9 b compared to a and d compared to c). As a result introduction of less cells in the initial suspension actually yield higher rates of viable encapsulated cells.

IV.2.b.iii Long term survival

For encapsulated cells to be used in soil depolluting applications, the macroporous pectin foams must be coated with silica (see Chapter III). The silica coating provides protection against rapid degradation of the foam. The deposition process however requires contact with acidic atmosphere at 30°C for several days. In order to ensure complete encapsulation in the hybrid matrix, long term survival of the encapsulated cells must be assessed.

Material and methods

P. aeruginosa-loaded pectin foams were prepared as previously described. Bacteria were cultivated in LB medium and centrifuged, suspended in water and added to a pectin and PIPES solution. 3 mL of suspension were then freeze-casted at 5 °C/min and vacuum dried for 24 h. Cell loaded foams were cut into 4 equal parts and maintained 24 h in various conditions: at 4 °C and room humidity, 30 °C and room humidity and 30°C and a controlled 75 % humidity. One fourth of the foams were dispersed in water directly after drying and plated. Foams were also prepared and dried for 48h instead of 24 h.

As observed previously, several logarithmic units are lost in the encapsulation process (see Figure IV.10). After 24 h of drying the number of CFU drops from 10^9 CFU/mL to 10^6 CFU/mL. After only 24 h at 30 °C, regardless of the humidity level, no colonies could be observed after redissolution of the foams and plating. Slightly better results were obtained when the cell-loaded foams were kept at 4°C, but the number of CFU still dropped down to 10^4 CFU/mL after 24 h. However when the samples were left for 24 h supplementary hours under vacuum about 10^6 CFU/mL were counted, which is similar to the cell concentrations after only 24 h of drying.

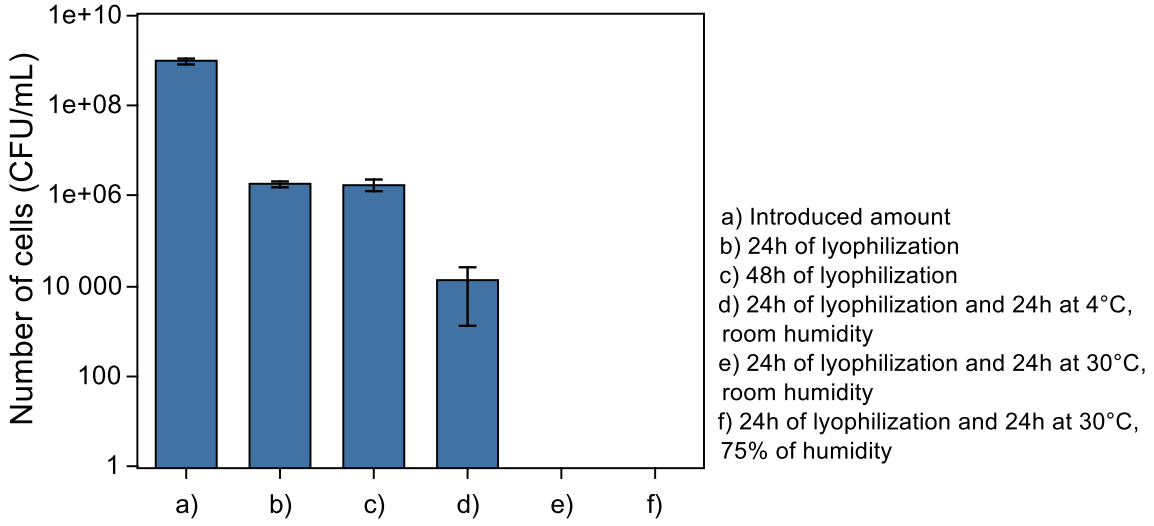

Figure IV.10: Dramatic losses in cell viability are monitored 24 h after the end of drying. At 30 °C (e and f) no CFU was observed, at 4°C (d) 10^4 CFU/mL were counted. Whether vacuum drying was carried out for 24 h or 48 h, similar survival rates were obtained (a and b). Values marqued with the same number of symbols are not significantly different (at $p<0.05$)

These observations highlight the crucial role of cell hydration in the long term survival. It seems that partial rehydration due to room humidity results in loss of viability, while complete rehydrated (when foams are immediately dispersed in water) present better survival rates. When cells are maintained under vacuum (completely dehydrated state) for 48h, the survival rates are similar to those obtained for shorter lyophilization times, which seems to indicate that once the initial drop in pressure has occurred, cells remain in a stable state. Higher survival rates were obtained when cells were maintained at 4 °C in a conventional fridge. This may be explained by a slowing of the cells metabolism, and maybe by a variation of humidity levels between the interior of the fridge and the 30 °C oven.
Regardless of the storage conditions, survival rates in pectin foams at long terms were not satisfactory. This is problematic regarding the global encapsulation strategy which includes silica deposition. The silica deposition method using TEOS vapors previously developed allowed for the formation of a homogeneous and well controlled silica layer on the pectin pore walls. This proved efficient in preventing the foam dissolution. The technique however required prolonged (several weeks) exposition of the foam to TEOS vapors at 30°C, which is not compatible with the survival of the encapsulated bacteria.

IV.2.c Influence of the presence of cryoprotective additives

A common strategy for optimization of cell survival in the frozen or dry state is the addition of cryoprotective[346] and lyoprotective agents[360]. These types of additive may be of help in the preservation of encapsulated cells over several days.

IV.2.c.i Influence on the encapsulation efficiency

Glycerol and trehalose were selected as possible protective agents during the freeze-casting and drying process. Influence of the presence of each additive or a combination of both was assessed regarding the survival rate of encapsulated *P. aeruginosa*, directly after drying and after 24h in a desiccated atmosphere. Glycerol was chosen as a typical cryoprotective agent, while trehalose has been used as protectant for preservation of bacteria during vacuum drying. Even if glycerol is expected to be especially efficient for protection during the freezing and trehalose might have a more significant action regarding lyophilization, it should not be excluded that each of these component may have an effect during the different stages of encapsulation. Additives were used separately and in combination in order to uncover potential synergic effects.

Material and methods

P. aeruginosa cells were encapsulated in pectin foams in presence of glycerol and/or trehalose (see Figure IV.11). Bacteria were grown in LB medium at 30°C and 150 rpm up to 0.5 OD. The culture was then centrifuged and dispersed in water, a 100 g/L solution of

trehalose, a 189 g/L (15 vol%) solution of glycerol or a 100 g/L trehalose and 189 g/L (15 vol%) glycerol solution. The cells were left 30 min at room temperature in theses suspensions and subsequently dispersed in a solution of 50 g/L of pectin and 125 mM of PIPES. The final suspension contained about 1.10^9 CFU/mL, 40 g/L of pectin and 100 mM of PIPES. The final additives concentrations were 20 g/L for trehalose and 38 g/L (3 vol%) for glycerol.
Cell suspensions were freeze-casted at 5°C/min and subsequently vacuum dried for 24 h.
Viability was monitored by plate counting. The number of CFU *was controlled in samples with various additives at three different stages: in samples frozen and thawed (30 min at 30°C), samples dispersed in water directly after 24h of vacuum drying and in samples kept 24h at room temperature in a desiccated atmosphere after drying. Three samples were prepared for each initial suspension composition and each dilution of dissolved foam was plated in triplicate.*

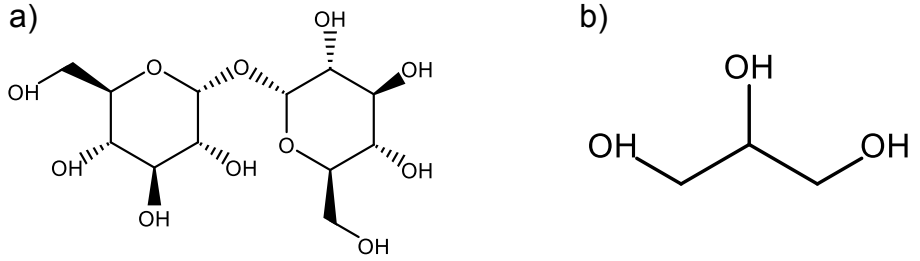

Figure IV.11: Trehalose (a) is a disaccharide commonly used in cryoprotection and as additive in preservation during drying. Glycerol (b) is one of the most commonly used cryoprotectant during freezing of several types of cells.

Figure IV.12 shows the number of CFU encapsulated cells at different stages of the shaping process. After freezing at 5°C/min and thawing, only a small loss of viability was monitored (less than 1 LU). After freezing and drying however, the presence of glycerol proved efficient in enhancing the cell survival rate.
Samples prepared with only pectin or pectin and trehalose (Figure IV.12 a and b) contained both around 7.10^5 CFU/mL, while samples with glycerol or a combination of glycerol and trehalose (Figure IV.12 c and d) were loaded with 4.10^6 CFU/mL and 2.10^6 CFU/mL respectively. The effect was even more noticeable after 24 h of storage. The samples were kept at room temperature in a desiccated atmosphere to prevent partial rehydration of the samples. Sample with no additives presented no detectable viable encapsulated cells after 24h. The presence of trehalose resulted in the survival of 2.10^3 CFU/mL, while addition of glycerol resulted in the presence of 6.10^4 CFU/mL after 24h. The combined effect of trehalose and glycerol yielded a 4.10^5 CFU/mL cell concentration.

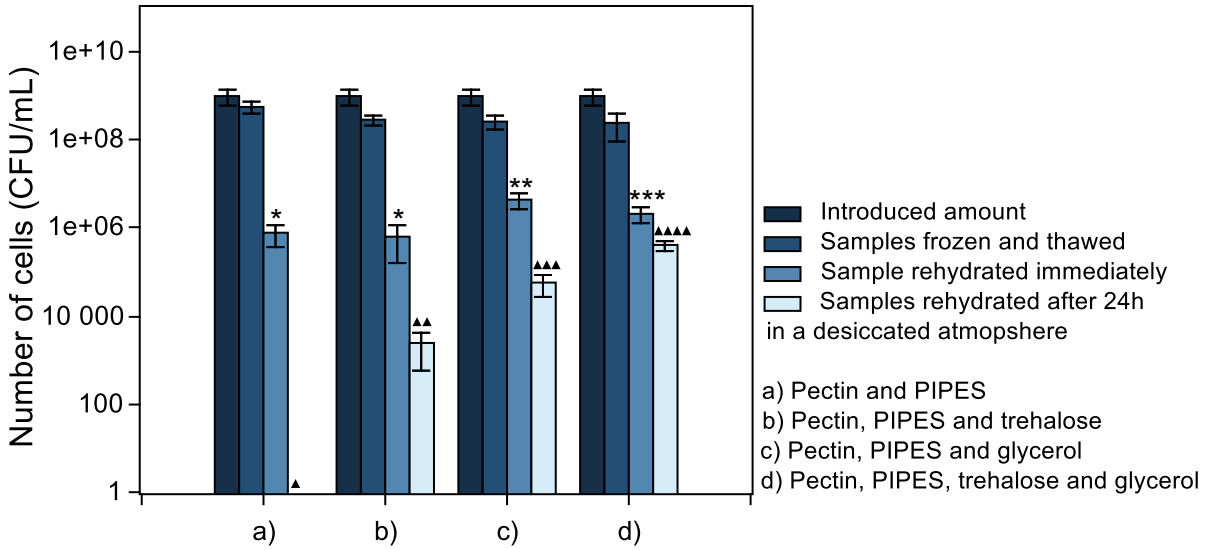

Figure IV.12: The number of CFU was assessed in various samples in presence of additives at different stages of the shaping process. No significant effect of the additives could be observed after freezing and thawing. After drying, similar survival rates were observed for samples containing no additives (a) and only trehalose (b). In the presence of glycerol the number of CFU was higher (c and d). After 24h at room temperature in a desiccated atmosphere, no cells capable of multiplying were observed in foams only composed of pectin. However the presence of additives greatly enhanced the survival rate, the best results being obtained in presence of both glycerol and trehalose. Values marked with different sets of symbols were compared for statistical significance. Values with the same number and type of symbol are not statistically different (at $p<0.05$).

After freezing and thawing, the addition of common cryoprotectants did not seem to modify the survival rate for encapsulate *P. aeruginosa.* The presence of pectin may be sufficient to provide protection against the main deleterious effects of freezing. After drying however, the presence of additives greatly enhanced the long term survival. Highest survival rates are observed for samples containing glycerol or glycerol and trehalose. Vacuum drying is usually composed of two separate steps: sublimation of the ice crystals and desorption of bound water. This second step usually requires gentle heating of the samples (up the about 20°C)[364], which was not performed in this case. In addition, intracellular water of cells immobilized within the pectin matrix is likely to be harder to desorb due to diffusion limitations. As a result, bound water might not be removed after the vacuum drying step. The presence of hydrophilic cryoprotectants (glycerol and trehalose) within the cells may be responsible for the protective effect towards drying[346], since higher amounts of bound water are retained.
This could prove decisive to maintain viable cells within the pectin foams throughout the silica coating process by exposure to vapors of TEOS, which requires long deposition times.

IV.2.c.ii Influence on the foam morphology

The presence of additives provides protection against viability loss, especially on the long run. These solutes are therefore beneficial to the functional part of the targeted depolluting device. Their influence on the structural part of the device must however not be overlooked, since presence of additives during freeze-casting usually results in morphological changes[272].

Material and methods

Foams with various additive contents (no additive, trehalose, glycerol or both glycerol and trehalose) were prepared as previously described, but with no addition of bacteria. Longitudinal and transversal slices were cut and sputtered with 20 nm of gold for SEM observation. Samples were maintained in a desiccated atmosphere between the end of drying and any further use.

Addition of trehalose at 20 g/L (Figure IV.13 c and c') does not induce significant morphology changes compared to foams prepared from pectin and PIPES alone (Figure IV.13 a an a'). Well oriented and aligned pore can be seen on longitudinal slices of both samples. The transversal section present typical elongated pores arranged in orientations domains. The addition of glycerol at 38 g/L (3 vol%) however significantly modifies the pore morphology. Samples containing pectin, PIPES and glycerol (Figure IV.13 b and b') are similar to samples composed of pectin, PIPES, trehalose and glycerol (Figure IV.13 d and d'). In both cases, some level of anisotropy can still be observed. Longitudinal slices show a lamellar pore wall arrangement, with well aligned pores. Transversal sections show a change in the pore aspect, which are not elongated but rather rounded. Pores are larger compared to samples with no glycerol, and more polydisperse in size. Foams prepared in presence of glycerol tend to be easily deformed during cutting of the samples. As a result the morphology observed in SEM may be slightly modified compared to bulk foams. In addition, foams containing glycerol tend to partly lose their structure when aged at ambient humidity. The pore walls tend to aggregate, resulting in a loss of porosity. This may be explained by a rapid adsorption of air humidity resulting in the rehydration of pore walls and subsequent loss of mechanical stability. As a result samples were maintained in a desiccated atmosphere until observation to prevent loss of structural features.

Trehalose and glycerol are both used as cryoprotective agents. Despite non negligible trehalose contents, no significant effect on the morphology could be seen. This might be attributed to the nature of trehalose which is a disaccharide (see Figure IV.11 a), and may therefore present common chemical properties with pectin which is a polysaccharide. Addition of glycerol however significantly changes the foam morphology. Glycerol presents high water affinity, which may explain the modification of the pore aspect. Pore present no specific elongation, but are rather rounded, which could be cause by interactions with glycerol preventing ice growth in specific directions. The pore walls themselves undergo changes in aspect and apparent mechanical behavior, which may be attributed to the presence of glycerol. Due to the high affinity of water and glycerol, dehydration of the polymer and glycerol mixture may be more difficult both during the formation of ice crystals and the vacuum drying. The resulting pore walls might have higher water content which may explain their tendency toward easy deformation and wrinkled aspect under SEM observation.

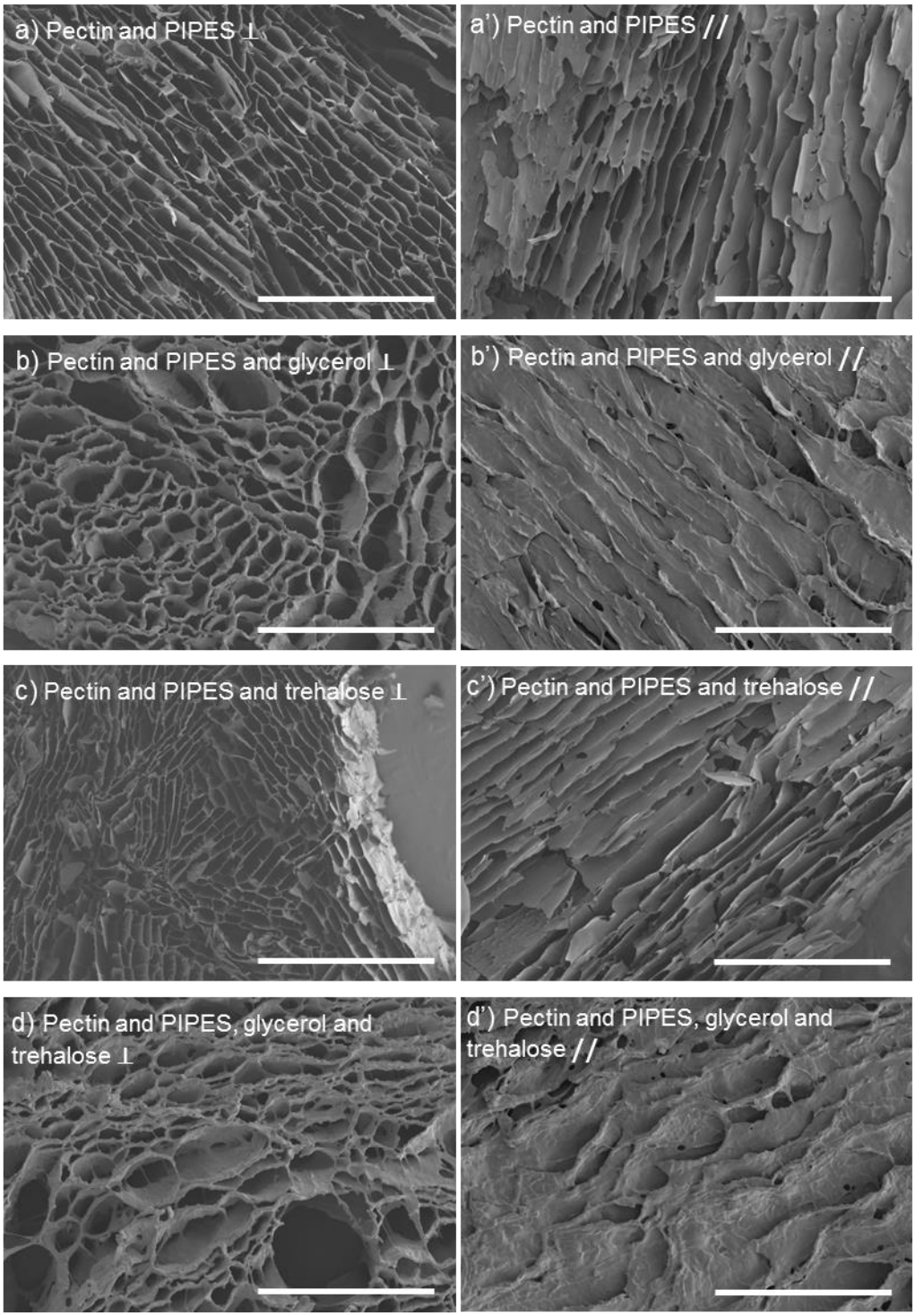

Figure IV.13: SEM observation of longitudinal (a', b', c' and d') and transversal (a, b, c and d) slices of pectin foams prepared in the presence of cryprotective agents. Foams containing 20 g/L of trehalose (c and c') have similar morphologies to foams containing no additives (a and a'). The addition of 3 vol% of glycerol (b and b') or a 30%vol glycerol and 20 g/L trehalose (d and d') mix result in a significant morphology change. Scale bars: 500 µm.

Addition of trehalose has no significant impact on the structure of the matrix, but used alone it has a limited impact on viability preservation. The best survival rates were observed in presence of glycerol, but this additive completely changed the structure and properties of the encapsulating matrix.

Conclusion

Encapsulation of cells in pectin foams may at first seem easy, as freezing and subsequent lyophilization of a simple cell suspension in a pectin solution results in the formation of a macroporous foam, with cells clearly visible within the pore walls. But this apparent simplicity uncovers a wide range of crucial parameters in order to yield a viable biohybrid material. Physical entrapment is only possible due to a combination of cells and suspending solution characteristics This encapsulation of cells is however not meant as a structural feature, but rather as the incorporation of functional units. This means that maintaining the cell metabolic activity is crucial. Assays with a robust and easy to handle model such as *S. cerevisiae* yielded encouraging results. This model was an efficient proof of concept, but regarding the targeted application, that is to say soil depollution, bacterial model are more relevant. Unfortunately, bacteria are also more sensitive. For this reason each step of the encapsulation process must be tailored to ensure optimal survival rate of the encapsulated species, in order to yield the highest possible metabolic rates in the final device. The initial formulation of the suspension media was composed of pectin and PIPES in order to efficiently control the pH and prevent cytotoxic effects after suspension of the cells in the biopolymer solution. During the freezing step, the cooling rate proved to have a significant influence on the survival rate. Damages caused by freezing have been observed in the domain of cell cryopreservation and are commonly attributed to two main effects: the formation of intracellular ice and the increase in solutes concentrations. The cooling rate has an influence on both these phenomena, since slow cooling yields dehydration of the cells, thus limiting the formation of intracellular ice. The counterpart of the dehydration is an elevation of the solute concentrations, sometimes up to toxic levels. As a result, an optimal freezing rate may be found, in order to prevent formation of intracellular ice, while maintaining reasonable solute concentrations. In the case of the encapsulation of *P. aeruginosa* in a 40 g/L solution of pectin in presence of PIPES the optimal freezing-rate was 5°C/min. But encapsulation in a biopolymer foam is only the first step toward the design of a depolluting device. As previously stated, foams need to be coated with a silica layer in order to withstand a prolonged stay in soil. The silica deposition process in vapor phase requires several days to obtain a coating thick enough to prevent the material degradation. It is therefore necessary to ensure survival at long term in the desiccated state. Unfortunately, cells entrapped in a simple pectin foam were not able to withstand a 24h storage. Addition of a common cryoprotective agent (glycerol) and of trehalose, which is known to preserve cells during lyophiliation, proved effective in enhancing the cell survival after 24h of storage. But this significant gain from the functional point of view was accompanied by major drawbacks from the structural point of view, since the porous structure was altered, and more importantly, foams became sensitive to aging at room humidity. As a result, even though the encapsulation in a biopolymer foam was successful, obtaining a hybrid pectin-silica foam containing living cells of *P. aeruginosa* proved difficult (see Figure IV.14).

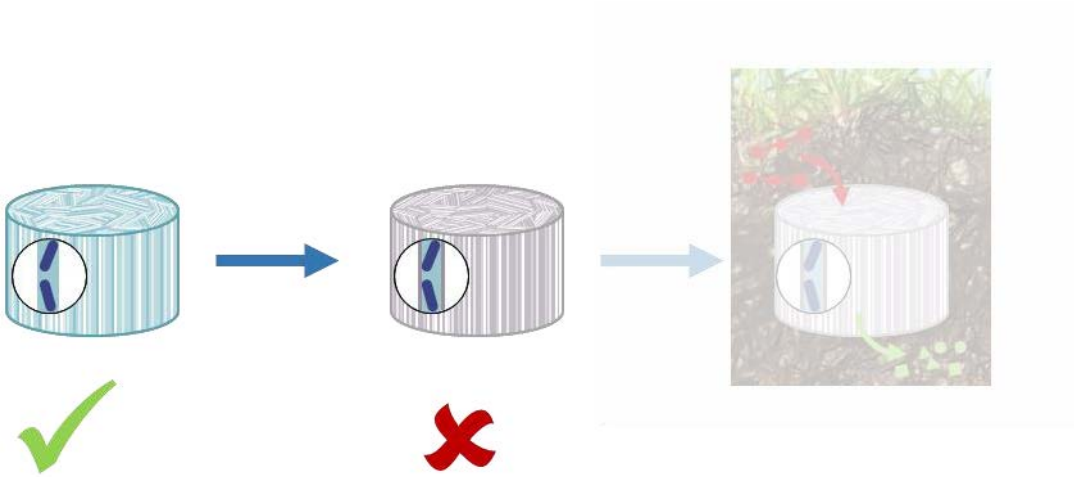

Figure IV.14: Encapsulation in pectin foam was achieved with about 10^7 CFU/mL after vacuum drying. However, viability at long term proved insufficient to allow vapor phase sol-gel silica deposition.

The crucial role of water regarding cell survival was however demonstrated. Use of pectin alone resulted in interesting structural features, but poor water binding properties, and therefore in low survival rates at long term. Addition of cryoprotective agents was efficient from a functional point of view since it enhanced cell viability, but resulted in unwanted structural changes. In order to combine, water binding and structural properties, encapsulation was attempted in another biopolymer.

Chapter V : From cell encapsulation to depollution

Introduction

Encapsulation in pectin-based porous materials was achieved by means of ice-templating. Storage of the cell-loaded materials however resulted in cellular death after short periods of time, which was incompatible with further processing of the foams into hybrid materials. The addition of cryoprotective agents was efficient from a functional point of view, since viable cells could be recovered after storage. From a structural point of view however, foams were significantly modified. Both structural and functional aspects are essential for the targeted application. The material must retain its integrity and oriented porosity to ensure mass transport of the pollutants while preventing dissemination of exogenous microorganisms in the soil. However if the encapsulated species are not metabolically active, the device will have limited remediation efficiency. In order to combine long-term cell survival and structural properties, encapsulation in another type of polymer was investigated. Alginate was chosen as an alternative to pectin. It is also a polysaccharide, commonly extracted from brown algae. It has however also been reported as part of bacterial biofilms, including in *P. aeruginosa*[465], which could be an indication of possible cytocompatibility.

Alginate has the advantage of being easily crosslinked in presence of divalent cations, which has made this biopolymer a very popular option for many encapsulation approaches[4,181]. Crosslinking of freeze-casted alginate foams may be a great advantage for depositionof silica through aqueous solution while preventing dissolution of the alginate structure. The optimization of the encapsulation in a biopolymer foam and subsequent silica deposition should result in a bionanocomposite where both the structure of the matrix and the encapsulated functional units are supporting the depolluting activity of the device. Such activity must be assessed on a model of pollutant.

Investigations in the domain of bioremediation have highlighted a wide range of pollutants susceptible of being degraded by given microorganism species and specific strains[1,466]. Application of the device for remediation of actual polluted sites would require in depth analysis and characterization of the site to determine the best suited organism or consortium for optimal remediation[467]. In this work the approach is however reversed since one specific microorganism was chosen to assess feasibility and efficiency of encapsulation. A model pollutant should therefore be chosen according to the encapsulated microorganism. The first and most crucial criteria to choose such model should be the capacity of *P. aeruginosa* to degrade it, but other parameters such as the methods of detection, availability or solubility of the pollutant for instance, should be taken in account. This pollutant is meant to work as a proof of concept for the targeted application. It should therefore be relevant in the context of bioremediation, but it must be remembered that laboratory conditions cannot fully represent natural polluted sites, and some experimental conditions may be chosen as a way to highlight remediation phenomena rather than to fully reproduce field conditions.

V.1 Alginate as an alternative biopolymer

V.1.a About alginate

Alginate is a polysaccharide usually extracted from brown algae (*Phaeophyceae*)[175], but a few bacterial species have been found to produce alginate polymers, including *P. aeruginosa*[468,469]. The vast majority of world production is used in food industry as stabilizers, emulsifiers and thickening or gelling agents[470]. However alginate has also been widely used in biomedical and pharmaceutical application for encapsulation of a wide range of molecules and biological species from drugs and enzymes to whole cells[125,179,184,188,419,471–473]. The high biocompatibility of alginate-based materials also make them ideal biomaterials[156,474]. It would however be impossible to give an exhaustive overview of the different uses of alginate since it has been one of the most popular biopolymers since it was first extracted by E. C. C. Standford in 1881.

Alginate is mainly composed of β-D-mannuronic acid and α-L-guluronic acid (see Figure V.1 a).

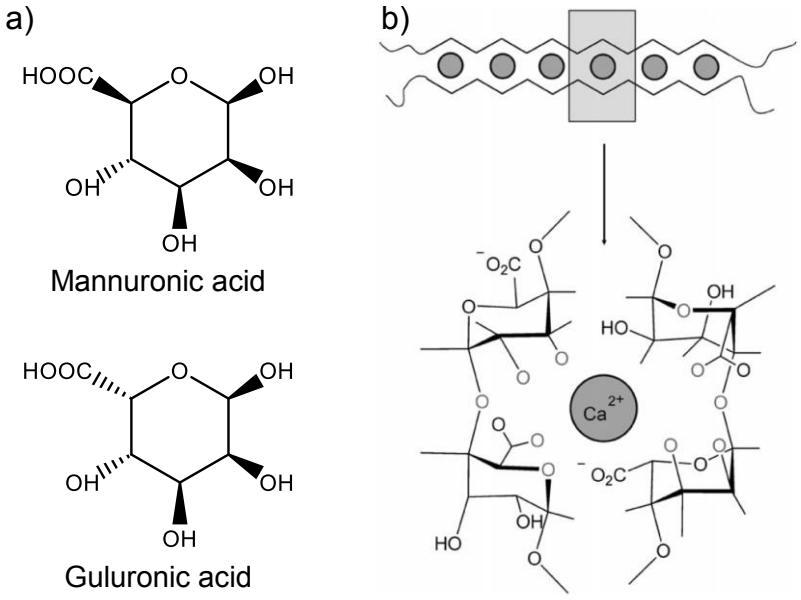

Figure V.1: Structure of β-D-mannuronic and α-L-guluronic acid, two main components of alginate (a). Alginate is capable of forming gel by binding of divalent cation in an "eggbox" configuration (b). (b) is reproduced from *Leick et al.*[475].

As is the case for many biosourced polymers, the structure of the alginate may vary considerably depending on the source and extraction conditions. This results in a wide range of possible physical and chemical properties. One of the most interesting and exploited properties of alginate is its capability to form gels in presence of divalent cations. The commonly accepted model regarding the ion binding properties of alginate is the so called "eggbox" structure proposed in 1973[183] (see Figure V.1 b). Gelation properties of alginate have been used to yield materials in a wide variety of shapes. The most common geometry is

the formation beads or capsules by crosslinking of alginate in a $CaCl_2$ bath[247]. But alginate gels have also been used as films or coating[476–478], sponges[479] and even fibers[480], sometimes in combination with other polymer. As mentioned earlier, use of alginate is very widely spread for many applications. Depending on the targeted application some of its properties, including the mechanical behavior or rheological properties, may not be entirely adapted. For this reason alginate has been associated with all sorts of materials from other natural[366,481–484] or synthetic polymers[485] to various inorganic compounds[228,229,238,486]. If gelling properties of alginate are extensively exploited for processing of this biopolymer, the material can also be shaped without gelation. Alginate has for instance been shaped thanks to ice templating processes in order to form porous materials[234,297,322].

V.1.b Freeze-casted alginate foams

Similarly to the approach used for the design of pectin-based foams, the structural aspects of alginate-based materials were first explored. Some parameters were however directly set according to the observations made in the case of pectin. Polymer concentration was set at 40 g/L and the materials were shaped exclusively using freeze-casting.

Material and methods

A solution at 40 g/L was prepared by dissolution of alginic acid sodium salt (15-25 cP at 1% in water, procured by Sigma-Aldrich) in deionized water. The viscous solution was then freeze-casted at different cooling rates. The resulting samples were vacuum dried at 0.05 mbar for 24h.

Cross sections and longitudinal slices were sputtered with 20 nm of gold for SEM observation.

Freeze-casted alginate foams appeared very similar at the macroscopic scale to pectin-based foams (see Figure V.2).

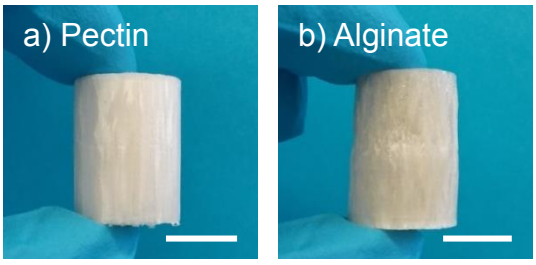

Figure V.2: Pectin-based freeze casted foams (a) and alginate-based freeze-casted foams (b) have very similar macroscopic aspects. Scale bars: 1 cm.

These similarities can also be found in the morphology of the pores (see Figure V.3). As is the case for pectin (see Chapter II), freeze-casting of an aqueous alginate solution results in the formation of a macroporous material, with oriented and well aligned pores. Such similarities

may be expected from the fact that both pectin and alginate are polysaccharide, with close chemical structures and functions. In both cases, polymers were used as 4 wt% aqueous solutions and the freezing setup and freezing rate were the same.

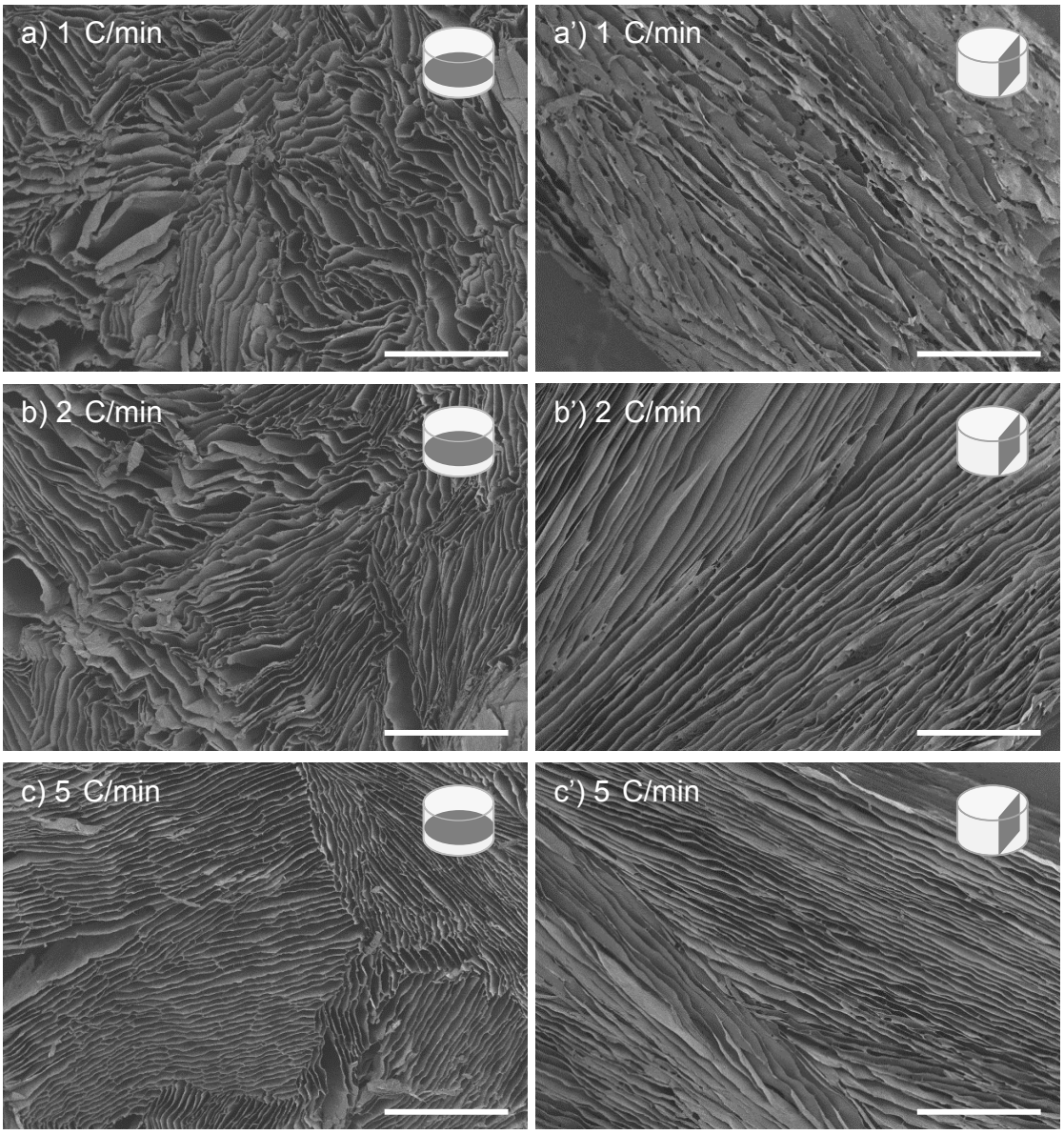

Figure V.3: Freeze casting of 40 g/L alginate solution result in macroporous foams with a pore morphology very close to the one observed in the case of pectin. When freeze-casting is performed at 1°C/min (a and a') pores are wider and shorter than with a 2°C/min freezing-rate (b and b'). At 5°C/min, (c and c') pores are narrower and better organized. Scale bars: 500 µm.

The pore width is of the same order of magnitude as for pectin foams (mainly between 10 µm and 50 µm). Like in pectin foams, the pore morphology can be modified thanks to processing parameters such as the freezing rate. As can be seen from Figure V.4, higher cooling rates result in smaller pores in alginate foams. This variation is consistent with observations made on pectin foams (see Chapter II). In the case of alginate, the pores obtained at low freezing-rates also appear less ordered. In other terms, the orientation domains observed in cross sections seem less extended.

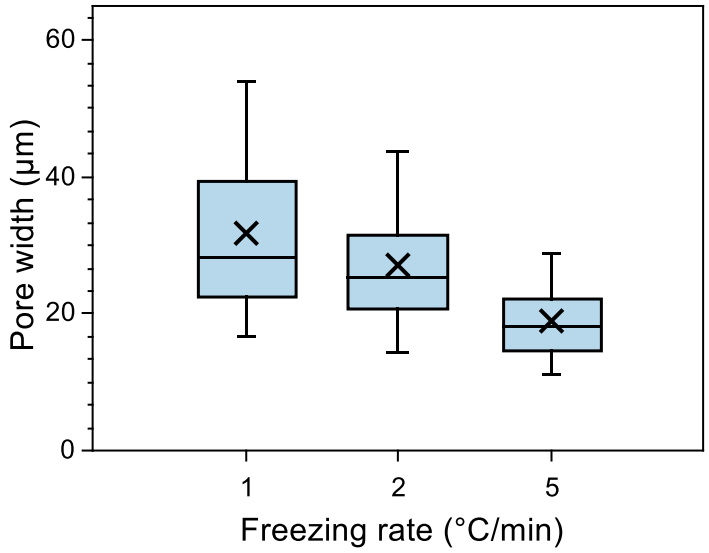

Figure V.4: Pore width decreases when higher cooling-rates are used during freeze-casting of alginate solutions. All values are significantly different (at $p < 0.05$).

As expected, alginate-based freeze-casted materials strongly resemble pectin-based foams. This confirms that alginate may be used as a suitable replacement for pectin in the design of a bionanocomposite for soil depollution.

V.1.c Encapsulation of *Saccharomyces cerevisiae*

Prior to encapsulation of *P. aeruginosa*, alginate was used as a matrix for encapsulation of *S. cerevisiae*[187]. The large size of the yeast cells allows for easy observation in microscopy and the robustness of the species makes for a good first step in the evaluation the functional aspects of encapsulation in alginate foams.

Material and methods

S. cerevisiae Type II was procured in the dry state from Sigma-Aldrich. Cells were dispersed in PBS (typically 1 mL) and added to Yeast extract Peptone Dextrose (YPD) medium (typically 20 mL). S. cerevisiae was grown 24h at 32°C under static conditions. The culture medium was then centrifuged (5 min at 1000 rpm) and the pellets were dispersed in PBS (typically 2 mL) and added to a 40 g/L alginate solution. The suspension was the freeze-casted at chosen cooling rates (1°C/min, 2°C/min and 5°C/min).

Viability was monitored by means of a glucose hexokinase assay kit. Briefly dry foams or thawed samples were dispersed in YPD and incubated 48h under static conditions at 32°C. Glucose concentration was then measured by means of glucose hexokinase assay kit and UV-vis spectroscopy. Positive controls were performed for suspensions of S. cerevisiae in PBS, alginate solution and negative control with blank alginate foams. Each assay was made in triplicate.

From the structural point of view, *S cerevisiae* cells were easily entrapped in freeze-casted alginate foams (see Figure V.5). The general structure of the foam was not altered by introduction of the cells, but at higher magnification, cells can clearly be seen within the polymer pore walls. The structural integrity of the cells themselves seems to be efficiently preserved.

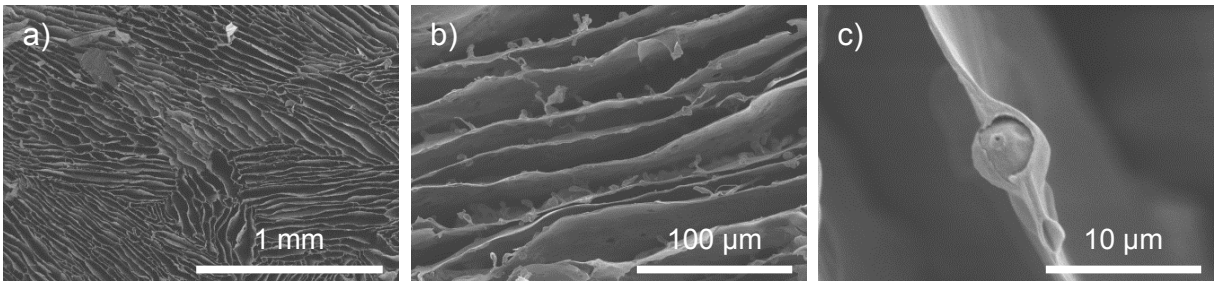

Figure V.5: Cell-loaded foams have the same general aspect as blank alginate foams (a). At higher magnification (b) cells can be observed in the pectin walls. Cells do not appear to lose structural integrity (c).

The cell viability was not monitored by plate counting as is common for bacteria, but rather by a metabolic assay. *S. cerevisiae* is capable of metabolizing glucose as is the case the fermentation process of beer[437]. As a result monitoring glucose content is indicative of cellular activity.

Initial glucose concentration in YPD medium was 20 g/L. The negative control indicates that this concentration remains stable after 48 h of incubation. Positive controls for cells suspensions in PBS and alginate are not significantly different (2.6 g/L and 2.5 g/L respectively which represent degradation of 87% of the initial glucose content). This illustrates the fact that alginate presents no cytotoxic effects towards *S. cerevisiae*.

Glucose concentrations, after incubation of cells dispersed from freeze-casted and vacuum dried foams, are higher than the ones obtained with positive controls, but are lower than the initial 20 g/L, which denotes significant metabolic activity after encapsulation in alginate. Samples prepared at 1 °C/min, 2 °C/min and 5 °C/min cooling rates resulting in degradation of 62 %, 53 % and 72 % of the initial glucose content respectively. However due to large standard deviations on the triplicate assays, these values are not statistically different from each other. This may indicate that freezing-rates in the considered range, which remains limited, have no significant influence on viability of encapsulated *S. cerevisiae* in alginate.

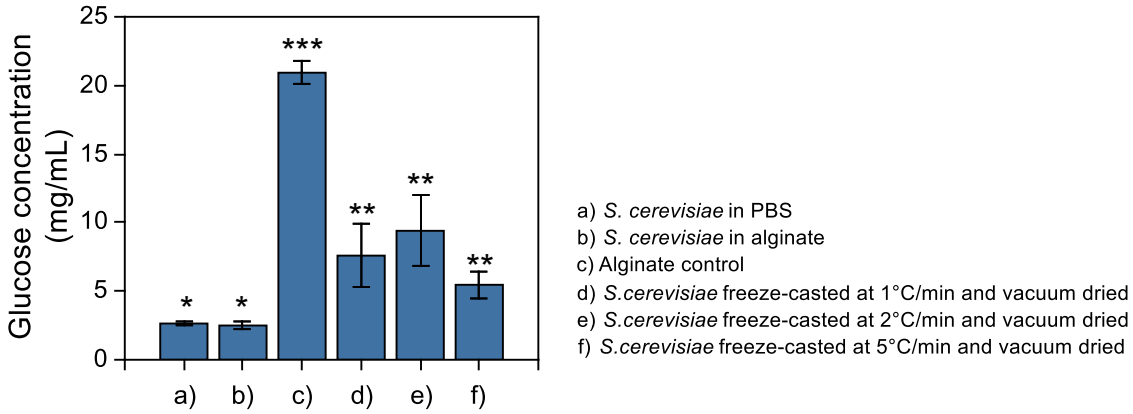

Figure V.6: Control cells in PBS (a) or alginate (b) are capable of degrading about 87% of the initial glucose content. Dispersion of alginate foams containing no cells (c) does not modify the glucose content. Dispersion of cells encapsulated in alginate foams obtained at either 1°C/min (d), 2°C/min (e) and 5°C/min (f) induces significant glucose consumption. Values marked by the same number of symbols are not statistically different ($p < 0.05$).

Encapsulation of *S. cerevisiae* confirmed that alginate could be used as a suitable material for encapsulation of microorganisms in a self-supporting, no cytotoxic, porous matrix. Encapsulation of microorganisms more relevant from the bioremediation point of view was then investigated, using *P. aeruginosa* as a model.

V.1.d Encapsulation of *Pseudomonas aeruginosa*

P. aeruginosa was successfully encapsulated in pectin biopolymer, however no viable encapsulated cell could be observed after 24 h of storage (see Chapter IV). Addition of common cryoprotective agents was efficient in preserving the viability of encapsulated cells, but the structural features of the matrix were greatly degraded. In order to prevent these issues encapsulation efficiency was assessed in different polymers.

V.1.d.i Encapsulation in various polymers

Material and methods

P. aeruginosa was cultivated as previously described. One colony was pre-cultivated in 10 ml of LB medium 24h at 30°C and 150 rpm. This pre-culture was then diluted by a factor 50 in LB medium and cultivated for 5h30 up to a 0.5 OD. The culture medium was centrifuged and pellets were dispersed in water. This suspension was then added to various polymer solutions in presence PIPES buffer. The final concentrations were 40 g/l in polymer and 100 mM in PIPES buffer. The polymer solutions were prepared in advance by dispersion of a chosen mass in 125mM aqueous solution of PIPES buffer and magnetic stirring overnight at room temperature (except for gelatin which was heated at 35°C). The following polymers were used: beet root pectin, sodium alginate, bovine gelatin and PVA Solutions were maintained at 35°C to prevent thickening and gelling of the gelatin solution.

3 mL of cell suspension were freeze-casted at 5°C/min and vacuum dried for 24h.
The resulting dry foams were immediately dispersed in water and successive dilutions were prepared and plated on LB-agar gels. The plates were incubated 24h at 37°C and the number of developed colonies was counted. Three foams were prepared for each polymer and each dilution was plated in triplicate.
Longitudinal and transversal slices were prepared and sputtered with 20 nm of gold for SEM observation.

Different polymers were chosen as possible alternatives to beet root pectin. Sodium alginate, like pectin, is a polysaccharide. Its structure and reactive functions are however different from pectin since it is composed of mannuronic acid and guluronic acid (while pectin is mainly composed of galacturonic acid and rhamnose). Gelatin was chose as another bio-sourced polymer, however it is not a polysaccharide like pectin and alginate, but a protein derived from collagen. PVA was chosen as a synthetic polymer, with known properties of biodegradability[487,488] and biocompatibility[489,490]. Solutions of these polymers at a concentration of 40 g/L in presence of 100 mM of PIPES were prepared and freeze-casted at the same rate (5°C/min) and subsequently lyophilized. Regardless of the polymer, self-supporting macroporous materials were obtained, but the pore morphology varied depending on the polymer as can be seen in Figure V.7.

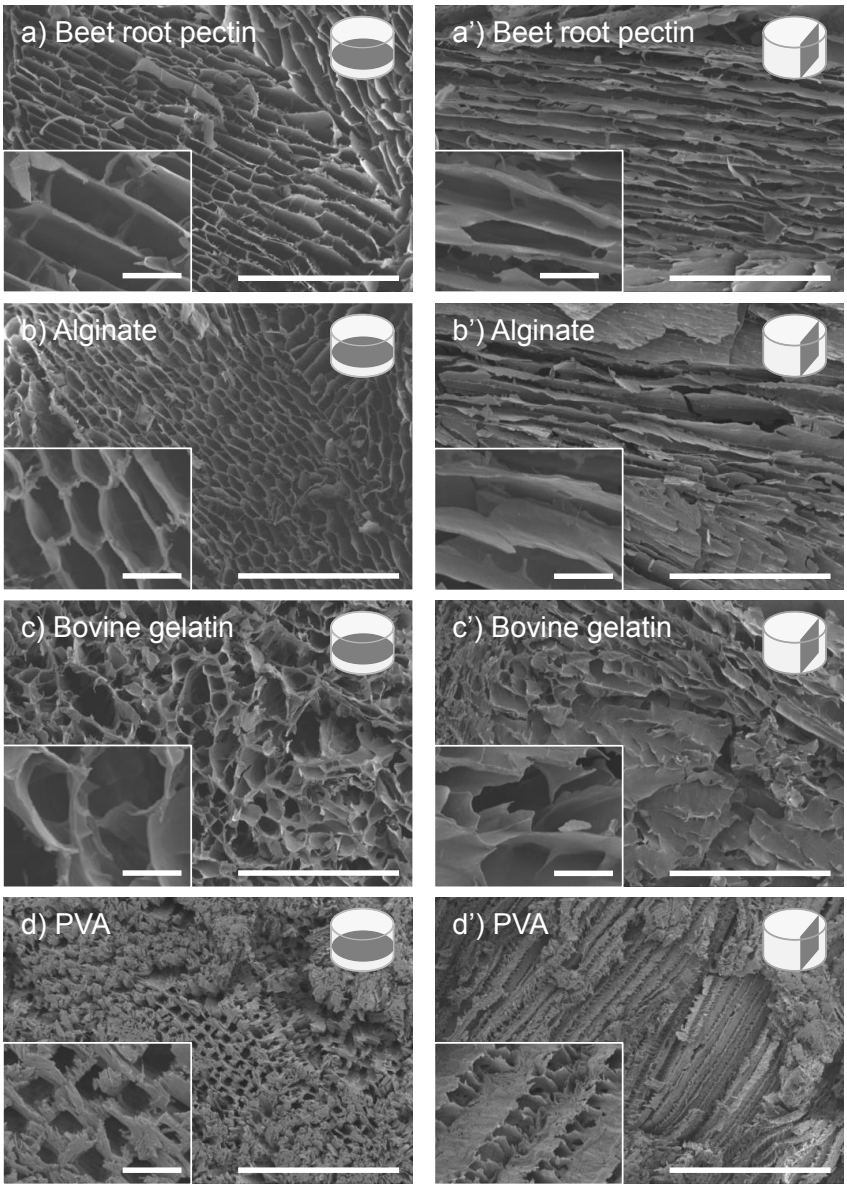

Figure V.7: Various solution of polymer freeze-casted at 5°C/min yield different pore morphologies. Beet root pectin (a and a') results well aligned and elongated pores. Alginate based materials (b and b') have a comparable morphologies, but with narrower and shorter pores. The porosity of gelatin samples (c and c') is not very well ordered. A degree of anisotropy can however be observed by comparison of cross-sections (c) and longitudinal slices (c'). The morphology of the PVA foams (d and d') is completely different with almost square-like and very regular pores. The alignment of the pores can be observed in the longitudinal section (d'). Scale bars: 500 µM for full images and 50 µm for inserts.

Morphology of beet root pectin based sample was described in Chapter II. Pores are oriented according to the applied temperature gradient. Pore walls have a lamellar aspect and are organized in orientation domains. Samples obtained from an alginate solution have a very similar morphology, but the pores are much shorter, or in other words more transversal bridges may be observed between the lamellar pore walls. All these samples were obtained in solutions containing PIPES buffer, which is likely to modify the ice growth.

Non-polysaccharide based foams displayed different morphologies. Materials obtained from bovine gelatin also displayed some level of anisotropy, however the pore alignment and order was greatly diminished compared to pectin or alginate based materials. Some higher level of

order have however been reported for ice-templated gelatin solution[268,320]. This low degree of orientation may be attributed to the presence of the PIPES buffer. In the case of PVA foams, the morphology is very different compared to the foams obtained from biopolymers. The pores are well aligned and oriented, but cross section uncovers almost square-like pores. Longitudinal section reveals the presence of numerous and regularly-spaced transversal walls. Such morphology is consistent with previously described PVA ice-templated macroporous materials[304].

All the observed structures appeared compatible with the targeted application and were used for encapsulation of *P. aeruginosa.*

Encapsulation efficiency was assessed immediately after vacuum drying. Cell-loaded foams were dispersed in water and successive dilutions were plated on LB-agar gels (see Figure V.8).

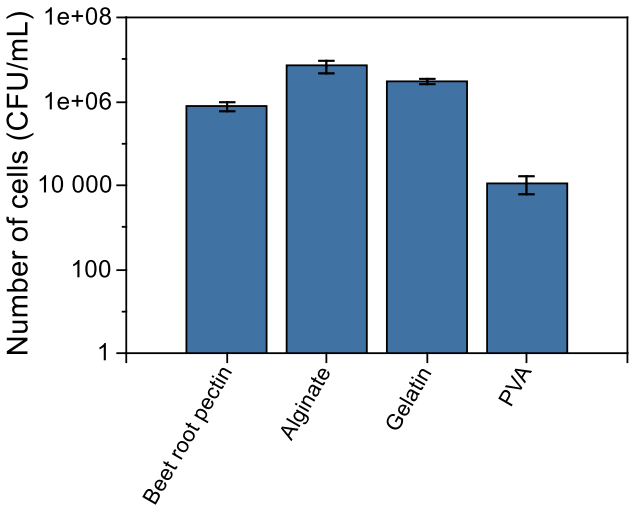

Figure V.8: Number of CFU/mL encapsulated in various polymers, from an initial introduced amount of 10^9 CFU/mL. Highest survival rates are obtained by encapsulation in alginate, gelatin or beet root pectin. About 10^4 CFU/mL were encapsulated in PVA foams. All values are significantly different (at $p < 0.05$).

Highest survival rates were obtained in alginate foams. About 7.10^6 CFU/mL were encapsulated in these foams which represents a loss of 2 LU. As a point of comparison 3 LU were lost during encapsulation in beet root pectin. Bovine gelatin also yielded high survival rates (around 3.10^6 CFU/mL). PVA and Citrus pectin resulted in significantly lower survival rates (10^4 CFU/mL and 10^3 CFU/mL respectively). Both alginate and gelatin appeared as suitable alternative to beet root pectin in terms of cell survival. Alginate however presents two major advantages compared to gelatin. First of all, alginate solutions are easier to handle from a processing point of view, since they do not gel at room temperature contrary to gelatin solution, which must be maintained at 35°C. From a structural point of view, alginate freeze-casted foams display a more controlled and organized porosity. As a result, alginate was selected for further investigation.

The main drawback for the use of pectin as the main component of the encapsulating matrix was the low survival rate after storage. *P. aeruginosa* cells were encapsulated in both pectin

and alginate foams in presence of PIPES buffer and the number of CFU was monitored at different stages (see Figure V.9).

Material and method

10^9 CFU/mL were introduced in initial solutions of pectin and alginate matrices, in presence of PIPES buffer to prepared cellularized biopolymer foams as previously described. Cell were cultivated up to a 0.5 OD, centrifuged and dispersed in solution of 40 g/L in polymer and 10 mM in PIPES buffer. 3 mL of the suspensions were freeze-dried at 5 °C/min and vacuum dried. The cell suspensions in polymers were maintained 24 h at 4 °C to assess possible cytotoxicity. After 24 h of lyophilization the samples were cut in two along the ice growth direction. One half was immediately dispersed in water, diluted and plated. The second half was maintained 24 h at room temperature in a desiccated atmosphere. The stored samples were then dispersed in water and plated. All LB-agar plates were incubated 24 h at room temperature before counting the number of colonies. Cells were encapsulated in three separates samples of pectin and alginate and each dilution was plated in triplicate.

The number of CFU/mL was similar in both pectin and alginate solution (with PIPES buffer) after 24 h of contact, which confirms that neither polymer have a cytotoxic effect at the considered pH. After encapsulation by freeze-drying at 5°C/min and vacuum drying, the number of viable cells encapsulated in the alginate matrix is significantly superior to the number of CFU/mL in pectin (6.10^6 CFU/mL and 2.10^6 CFU/mL respectively). The difference was even more noticeable after 24 h of storage under a dry atmosphere and room temperature. In pectin only about 500 CFU/mL were counted, with high variability between the triplicates, while alginate foam still contained around 4.10^5 CFU/mL.

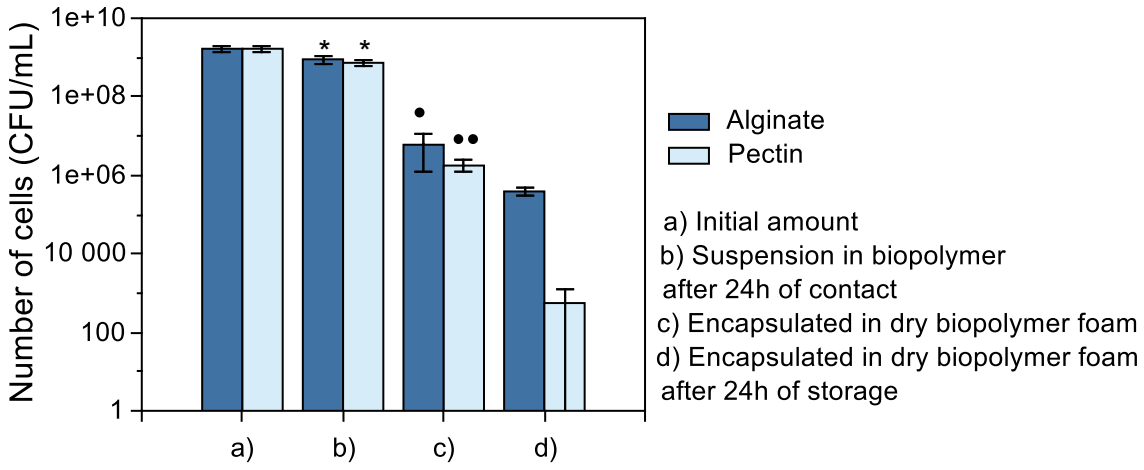

Figure V.9: Survival rates are similar for *P. aeruginosa* after 24h in suspension in solutions of 40 g/L of alginate or pectin in presence of 100 mM of PIPES buffer (b). After encapsulation in dry foams (c) survival was slightly higher when alginate was used as the encapsulating matrix. After 24h of storage in a desiccated atmosphere, the survival rate was very low in pectin (d). In alginate however, as much as 4.10^5 CFU/mL were still encapsulated after 24h of storage. Values marked by the same number of symbols are not significantly different (at $p < 0.05$).

A comparison of the survival rates in pectin and alginate highlighted the interest of the latter polymer for long term encapsulation, which could be an advantage during the silica deposition process. In order to further increase the potential final number of viable cells, several parameters were investigated in order to optimize the encapsulation process.

V.1.d.ii Optimization of the encapsulation conditions

In order to compare encapsulation in pectin and alginate, both polymers were dissolved in 100 mM PIPES. The presence of buffer is mandatory in the case of pectin (as was demonstrated in chapter IV, p130) due to the acidic properties of the pectin solution. An aqueous solution of alginate has however a pH close to 7 which should not be deleterious to *P. aeruginosa* viability. The influence of the growth phase was also highlighted during encapsulation in pectin (see chapter IV, p137). The influence of these two parameters (presence of PIPES and growth phase) on the encapsulation efficiency in alginate was therefore investigated.

Material and methods

P. aeruginosa was grown in LB medium up to 0.5 OD (exponential growth phase) and 1.9 OD (stationary growth phase). Cultures were centrifuged and pellets were suspended in appropriate amounts of water to yield about 5.10^9 CFU/mL. These suspensions were then added to solutions of alginate (final concentration 40 g/L) with or without PIPES buffer (final concentration100 mM). The introduced amount of cells was therefore 10^9 CFU/mL.
3 mL samples were prepared by freeze-casting at 5°C/min and subsequently lyophilized 24h at 0.05 mbar. Dry foams were immediately dispersed in water. The suspension were diluted and plated on LB-agar gels.

As can be seen in Figure V.10, successful encapsulation rates are higher for cells in stationary phase than for cells in exponential phase in alginate, regardless of the presence of PIPES. This is consistent with the observation made for this strain of *P. aeruginosa* encapsulated in pectin, as well as observations made for various bacteria species during freezing for preservation[347,464].

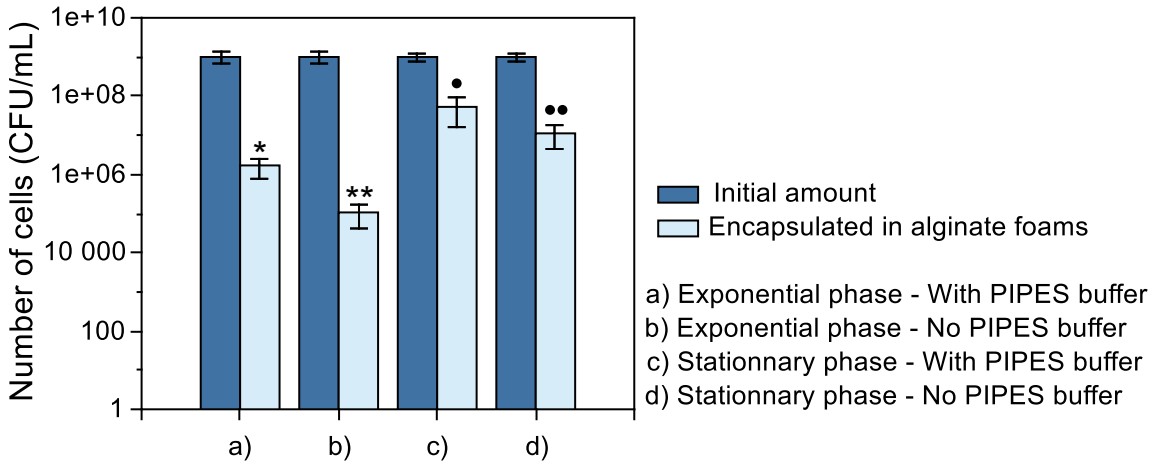

Figure V.10: Higher survival rates are observed for cell in stationary phase (c and d) compared to cells in exponential phase (a and b). The presence of PIPES (a and c) significantly enhances the survival rates. Values marked with different numbers of symbols are significantly different (at $p < 0.05$).

PIPES buffer was added to pectin solutions to regulate pH, since acidic conditions resulted in cell loss even before freezing. In the case alginate the aqueous polymer solution is neutral, which should render the use of buffer useless. Plate counting however reveals higher survival rates when cells are encapsulated in the presence of PIPES. PIPES is not used as a common cyoprotectant. Part of the efficiency of cryoprotective agents is however based on modification of the osmotic equilibrium between the intra and extracellular medium[348]. In this propect, introduction of PIPES could help in balancing osmotic pressures to prevent cell damages during freezing.

As a result the best encapsulation conditions for *P. aeruginosa* in alginate seem to be the use of stationary phase cells in an alginate/PIPES solution. Figure V.11 shows the amount of viable cells encapsulated in these conditions at various stages. No cytotoxicity of the solution can be observed after 24h of contact at 4°C. Freezing and thawing result in about 2.10^8 CFU/mL (with 1.10^9 CFU/mL introduced in the initial polymer solution), which is similar to the combined effects of freezing, drying and rehydration in water. When samples are maintained at room temperature in a desiccated atmosphere over 3 days, the number of viable cells drops to 5.10^6 CFU/mL. It is difficult to evaluate a minimal cell loading to predict functional efficiency of a cellularized material. Maintaining the highest number of viable cells throughout the various steps of the encapsulation however appears a good strategy to ensure maximal efficiency.

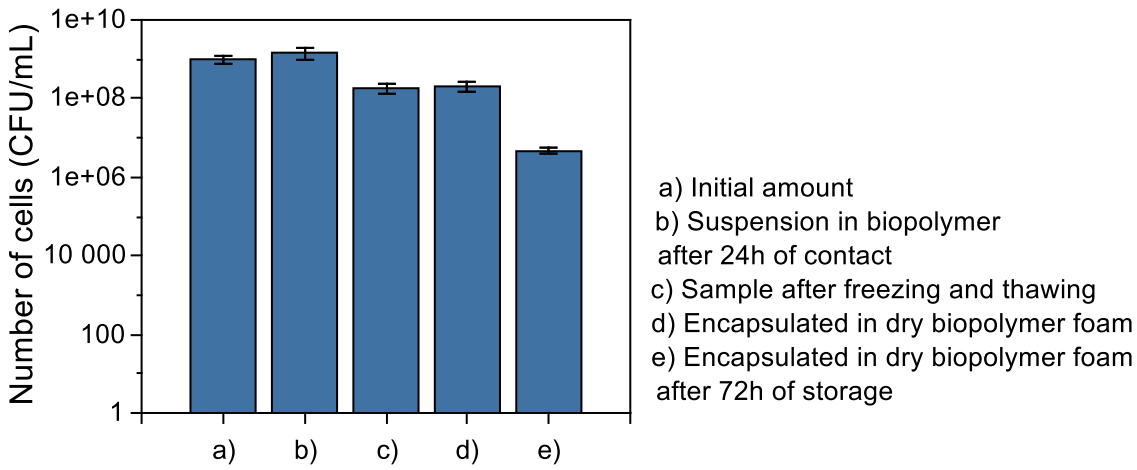

Figure V.11: 10^9 CFU/mL were dispersed in the initial alginate and PIPES solution (a). After 24h of contact (at 4°C) no loss of viability could be observed (b). After freezing and thawing (30 min at 30°C), about 20% of the cell were still capable of replicating (c). Similar survival rates were observed after freezing, drying and rehydration (d). Even after 3 days of storage, the alginate foam still contained about 5.10^6 CFU/mL (e).

The silica deposition through vapors of TEOS requires several days (up to two weeks) to yield a thick enough silica layer (see chapter III, p100), in the case of pectin foams. Deposition kinetics on alginate may however be modified, at least in the early stages, due to different interactions between the silica precursors and the polymer.

V.2 Encapsulation in a hybrid material

In order to yield fully functional bio-hybrid materials, usable in soils, the alginate foams must be modified to prevent dissolution in contact with water. As mentioned earlier, one possible way to ensure the durability of the material in soil is to coat the polymer scaffold with a thin layer of silica.

V.2.a Alginate-silica hybrid materials

V.2.a.i Vapor phase deposition

Pectin foams were coated by silica through a vapor phase deposition of TEOS. This method proved to be efficient in obtaining a thin and homogeneous controlled layer of silica (see Chapter III, p100). Vapor phase deposition has also been reported as a way to coat alginate beads[418]. The same technique was therefore assessed for silica coating of alginate porous scaffolds.

Material and methods

Polymer foams were obtained by freeze-casting of 40 g/L solutions of biopolymers (either beet root pectin or sodium alginate). The solutions were prepared by dispersing the polymer powder into deionized water and left under magnetic stirring overnight to yield homogeneous viscous solutions. 3 mL of solutions were then freeze-casted at 10 °C/min and vacuum dried 24 h at 0.05 mbar. Dry foams were cut to 1 mm thick discs and maintained 24 h in a desiccated atmosphere before weighting of the initial mass. The samples were then placed in a silica deposition chamber (see scheme in Chapter III) in presence of a 5 wt% HCl in water mixture saturated by NaCl and four vials containing 10 mL of tetraethoxysilane (also known as tetraethyl orthosilicate or TEOS). The deposition chamber was maintained at 30 °C and samples were removed after 4 or 10 days. The samples were left 24h at 30 °C and ambient humidity and 24 h at room temperature in a desiccated atmosphere. The samples were then weighted again and the relative mass gain was obtained by the following equation.

$$wt\%_{gained} = \frac{m_f - m_i}{m_f}$$

where m_i is the initial polymer mass and m_f is the final mass after various deposition times.
For SEM observations, samples were sputtered with 20 nm of gold. For energy-dispersive X-Ray spectroscopy (EDX) samples were sputtered with 20 nm of carbon.

Silica deposition was compared on alginate and pectin foams. The samples were placed simultaneously in the same deposition chamber. As was demonstrated in Chapter III, silica deposition tends to be faster on thinner discs. Deposition was therefore compared on 1 mm thick discs of pectin and alginate.

As can be observed in Figure V.12, mass gain was much higher on pectin-based foams, after the same deposition time. After 4 days, the amount of mass gained in the case of pectin was around 72 % of the final mass, while in the case of alginate it was only 12 %. After 10 days the mass gains were 82 % and 31 % for pectin and alginate respectively. This may indicate that in the case of pectin an almost saturated phase was already attained after 4 days, contrary to the alginate samples.

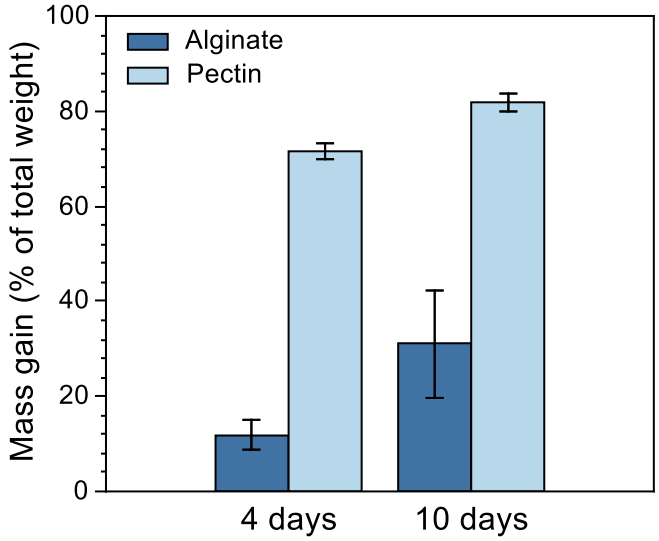

Figure V.12: After 4 days of silica deposition, mass gain represented around 70 % of the final mass in pectin samples, but only about 10 % in alginate samples. After 10 days of deposition the mass gain represented 80 % of pectin samples and 30 % of alginate samples.

The foams were observed in SEM after silica deposition. In the case of pectin a homogeneous and smooth layer of silica could be observed (see Figure V.13 a and a'). In the case of alginate however, heterogeneous square-like structures could be observed across the surface (see Figure V.13 b and b'). The shape of these structures points towards a crystalline material. In this case however we expect to obtain amorphous silica. In order to characterize the coatings on both pectin and alginate foams, EDX analysis was performed (see Annex p 219). The observed structures were sodium chloride, which was likely formed by interaction of the sodium contained in the alginate and the chlorine from the acidified atmosphere.

While a stay in an atmosphere saturated in silica precursors in presence of water and acid resulted in the rapid formation of a homogeneous layer of silica on pectin foam, the same process yielded very different result for alginate-based material. The mass gain was much slower in the case of alginate, which may be problematic with the view of coating a material containing living cells. Furthermore the added mass cannot be solely attributed to formation of a silica layer. These differences may be attributed to different interactions between the polymer and the silica precursors.

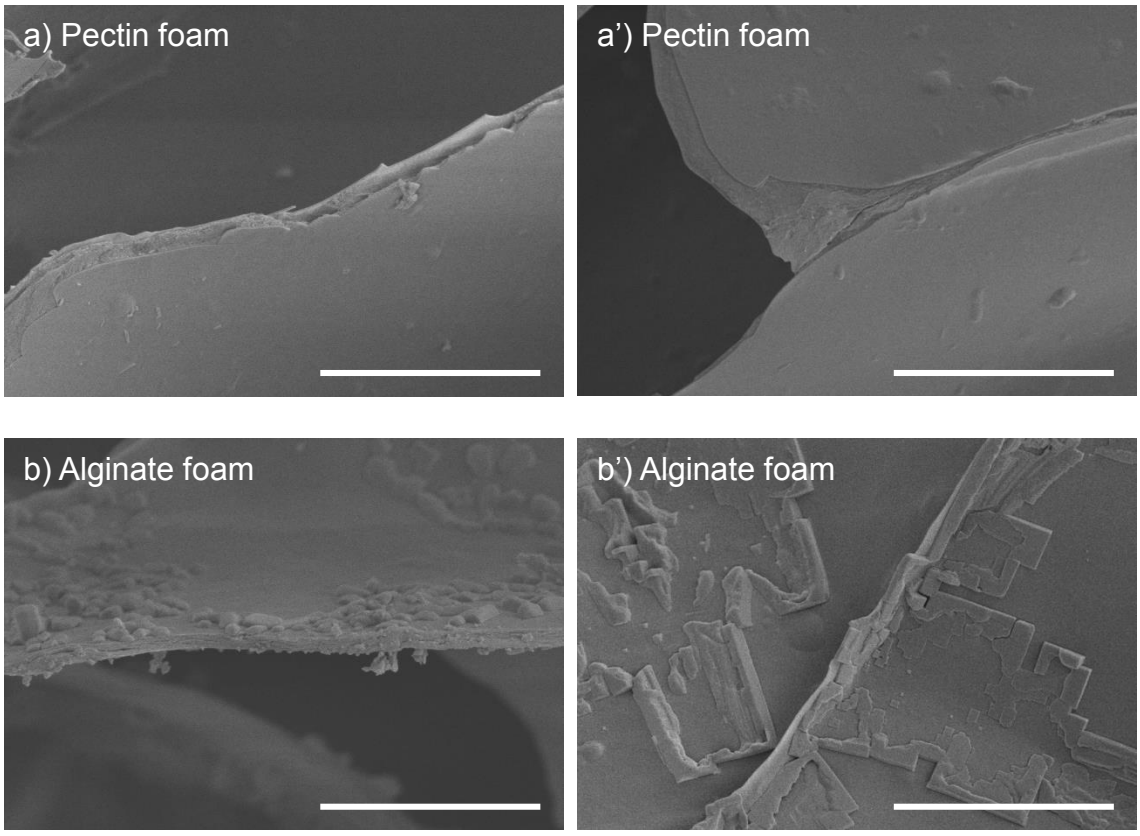

Figure V.13: After treatment by vapors of silica precursor (TEOS) in an acidic atmosphere (HCl), pectin samples are coated by a smooth layer of silica (a and a'). Alginate samples (b and b') present square-like structures on top of the pore wall surface. Scale bars: 10 µm.

The constitutive monomers of pectin and alginate have similar pKa values (3.5 for galacturonic acid[491], 3.4 for mannuronic acid and 3.7 for guluronic acid[491]). pH values of both aqueous polymer solutions are different (about 3 for pectin and 7 for alginate), which may result in higher negative charge in alginate. Assuming the ionization state does not significantly change after drying, ionic interactions with the negatively charged silica and the polymer surfaces may therefore be different between pectin and alginate. The presence of sodium cations in alginate might be expected to have a screening effect on the negative charges of alginate, but as was mentioned previously at least part of this sodium is associated to chlorine in surface crystals of sodium chloride. Repulsive electrostatic interactions may explain the slower deposition rate of silica on the surface of alginate. Longer exposure time would therefore be required for the formation of a percolating silica layer on the alginate scaffolds.

Amounts of viable encapsulated *P. aeruginosa* tend to sharply decrease during long storage, especially in non-desiccated atmospheres. The addition of hydrochloric acid to the atmosphere may present further challenges, even though the fact that the cells are embedded within the polymer wall may provide some degree of protection. As a result, it seems that vapor phase silica deposition is not the best suited technique for coating of alginate based material. Other sol-gel silica approaches have therefore been explored.

V.2.a.ii Sodium silicates-based sol-gel chemistry

The main alternative to vapor phase sol-gel silica deposition is the use of a liquid phase sol-gel process. Two main routes are commonly used: the alkoxide route, where silica precursors such as TEOS are hydrolyzed and subsequently condensed and the silicate route, where basic solutions of commonly named waterglass are acidified to yield formation of a silica gel. Combination of LUDOX colloidal particles suspensions and sodium silicate solutions allows the formation of tailor-made gels, with various gelling times, mechanical and optical properties[492]. One drawback regarding liquid phase routes is the necessity to use water as a solvent to ensure non cytotoxicity. Immersion of the biopolymer foam in aqueous solutions results in rapid dissolution of the material. It is however possible to crosslink alginate by using divalent cations such as Ca^{2+} to yield the formation of "egg box" crosslinking point, resulting in the formation of a non-water soluble material. Use of a liquid silica deposition phase therefore requires a prior step of crosslinking. Silica formation from alkoxides precursors (such as TEOS) is easy to handle and presents tuning possibilities due to the wide variety of available functionalized precursors. The main drawback to the use of TEOS is the formation of ethanol during the hydrolysis of the precursor. The LUDOX/silicate route has previously be proven to be more efficient than the alkoxide route for the direct encapsulation of bacteria in silica gels[220]. It was therefore chosen for the addition of silica on alginate porous foams.

Material and methods

Alginate foams were prepared as previously described by freeze-casting at 10°C/min of a 40 g/L solution of alginate and subsequent vacuum drying. Dry foams were then immerged in a 0.5 M solution of $CaCl_2$ during 24h at 4°C. Foams were then rinsed with water and briefly deposited on absorbing paper to removed excess water from the pores. The samples were then immerged in a premixed solution of LUDOX and silicates. The LUDOX/silicate mixture was prepared as follows. A 0.2 M in Si solution of sodium silicates and a 7.8 M in Si solution of LUDOX were prepared separately. Sodium silicate at 27 wt% (waterglass) was obtained from Sigma-Aldrich. LUDOX TM-50 (50 wt% suspension colloidal suspension of silica particles in water) was purchased also from Sigma-Aldrich. A 50:50 mixture was prepared from these two solutions to yield a total Si concentration of 4M (0.1 M from silicates and 3.9 M from LUDOX). The mixture was then acidified to pH = 5 by addition of HCl 4M. The gelling time for this mixture was 1 h at room temperature.

Crosslinked alginate foams were added to the LUDOX/silicate solution and maintained 45 min under elliptic agitation. Foams were removed from the LUDOX/silicate solution before gelling and rinsed with deionized water. Samples were then left at ambient temperature and humidity for 45 min. Samples were then stored in water for further uses.

For SEM observation, samples were dried. Samples were immerged in successive bath of increasing ethanol content (20%, 40%, 60%, 80% and 100%). Samples were left at least 2 h

hours in each bath and 48 h in 100% ethanol. Samples were then left to dry at room temperature. Samples were then cut and sputtered with 20 nm of gold.
Samples were weighed before addition of silica and after complete drying in order to evaluate mass gain.

After the silica deposition process, samples gained between 35% and 55% of weight mass, which is comparable to the mass gain for vapor phase silica deposition on typical pectin samples.
With the view of encapsulating cells in these matrices, it seems preferable to remain in a hydrated environment after formation of the silica gel to prevent further cell damage from drying. However, in order to easily characterize the silica layer it necessary to dry the samples, which may result in significant changes at the macro scale (shrinkage) but also on the microscopic scale (modification of the silica condensation state). Figure V.14 illustrate the shrinking of foams alginate crosslinked foams (with and without silica) after dehydration in ethanol and drying.

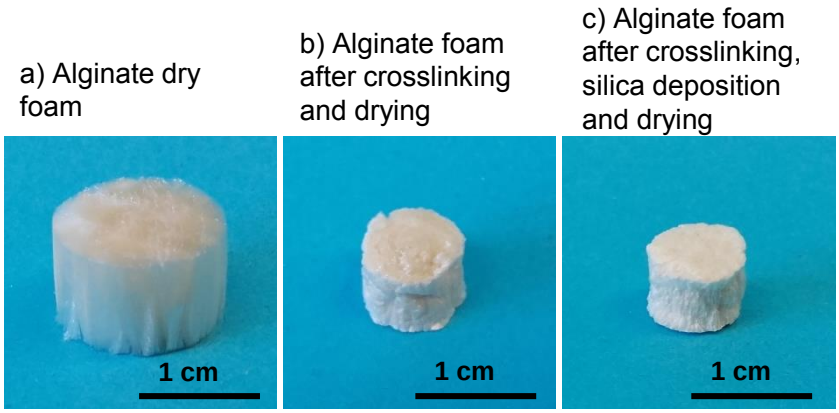

Figure V.14: Freeze-casted alginate foams and crosslinked alginate foams (b) shrink significantly after drying compared to alginate foams directly after lyophilization (a). Foams of crosslinked alginate coated with silica undergo similar shrinkage.

This contraction has a direct influence on the pore morphology as can be seen in Figure V.15 (a and b). The general structure of freeze-casted alginate foams can still be seen with the presence of oriented pores. The shape of the pores is however altered since the pore walls themselves are distorted due to capillary forces involved during drying (see Figure V.15 a' and b').
The main advantage of the liquid phase silica deposition is its capability to introduce large amounts of silica in a short time. This is however accompanied by a major drawback, since it becomes much more difficult to control the repartition and homogeneity of the silica layer. It can be seen at the macroscopic scale since the LUDOX/silica mixture only penetrates in the foam to a limited depth. The center of the foam is not fully impregnated, which results in an inhomogeneous repartition of the silica throughout the foam. This inhomogeneity also results in the partial obstruction of the porosity (see Figure V.15 b).

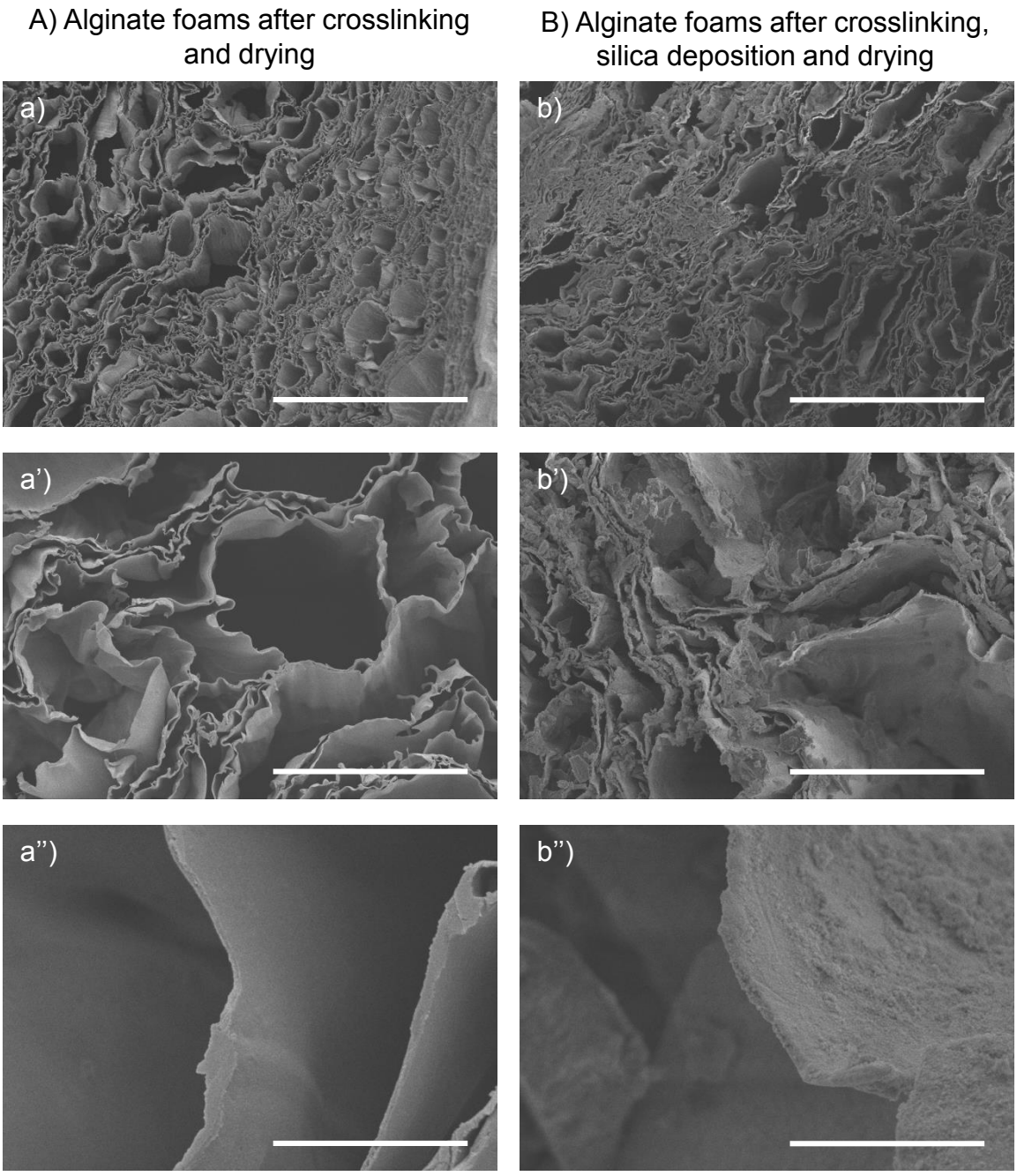

Figure V.15: Significant foam shrinkage can be observed due to the drying step necessary for SEM observation. Both crosslinked and dried alginate foams (a, a' and a'') and alginate foams crosslinked and coated with silica (b, b' and b'') before drying present very similar aspects. Oriented pores can still be observed, but significant distortion of the pore walls results irregularities in the shape of the pore themselves (a' and b'). Upon closer observation a granulose-looking surface can be seen on the silica-coated samples (b'') which is not visible on samples simply crosslinked (a''). This layer is however very inhomogeneous in thickness. Scale bars: 500 µm.

The silica layer itself appears not very homogeneous in the alginate pore walls (see Figure V.15 b''). The granular aspect can be explained by the chosen synthetic route since it is mainly composed of silica particles from the LUDOX suspensions, aggregated by the use of sodium silicates. The deposited silica does not appear to form a full percolated layer, but rather small aggregates on the surface of the polymer, which may result in inefficient protection against degradation in soils.

V.2.a.iii Assessment of the behavior of the hybrid foams in soil

The behavior of several alginate-based macroporous foams was assessed in real soil samples over two months.

Material and methods

Different alginate foams were prepared as previously described for assessment of the behavior in soil. Alginate foams simply freeze-dried were used as controls (no crosslinking). Samples of alginate foams crosslinked by $CaCl_2$ and samples crosslinked and coated with silica by impregnation in LUDOX and silicates were compared. Samples were introduced in the soil (see Annex p 204) either in hydrated state or after dehydration by successive bathes of increasing content of ethanol. Each sample was placed in 110 g of soil rehydrated by 18 mL of deionized water (see Annex p 211).

The vials were sealed with Parafilm™ and maintained at 20°C. The aspect of the foams was regularly visually assessed. Samples were removed after 21 days and dehydrated in successive bathes of increasing ethanol content (20%, 40%, 60%, 80% and 100%), cut and sputtered with 20 nm of gold for SEM observation.

In-soil assays were performed at the Laboratoire de Geologie de l'ENS, in collaboration with Pierre Barre. Compared to pectin, alginate foams (directly after freeze-drying, no crosslinking or silica deposition) seem less prone to immediate degradation in soil. Pectin samples were immediately rehydrated by the moisture content in the soil (see Chapter III p 112), resulting in the disappearance of the sample after one week in soil. In case of alginate however, even though significant contraction may be observed, the samples are still recognizable after 3 weeks (see Figure V.16 a). Shrinkage may be attributed to impregnation by water from the surrounding soil, resulting in a filling of the pores and the presence of capillary forces likely to shrink the material. Furthermore, hydration of the pore walls may significantly modify their mechanical properties and even rheological behavior.

The crosslinked samples (with or without silica) show no clear change at the macroscopic scale. Samples that were introduced in the hydrated state in the soil (see Figure V.16 d and e) tend to slightly shrink due to probable partial dehydration. On the other hand, samples that were introduced in a dry state (Figure V.16 b and c) do not appear to undergo any change in aspect even after almost two month.

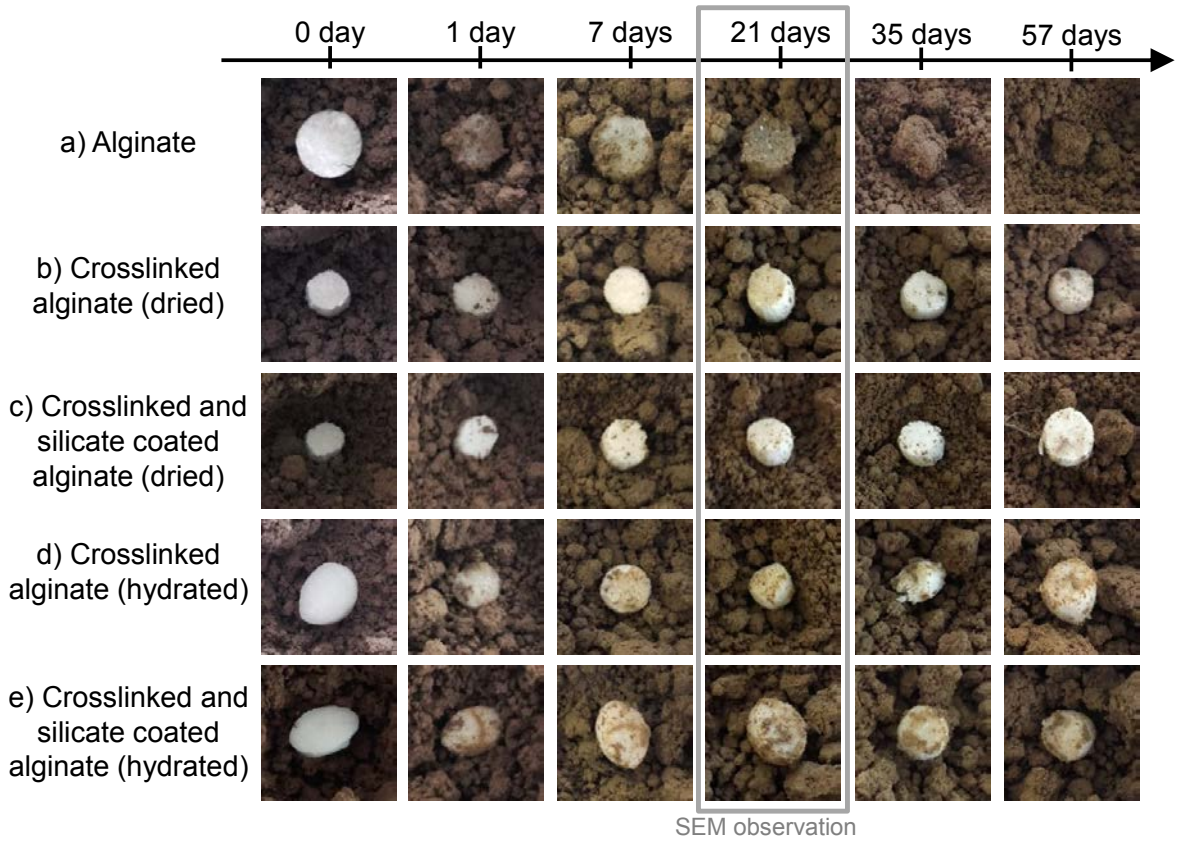

Figure V.16: Foams obtained by simple freeze-casting of alginate (a) undergo significant aspect modifications. After one day the foam appears to have shrunk and after one week there seem to be a degradation of the material. Alginate foams which were crosslinked and dried (b) or crosslinked, silica coated and dried (c) do no change in aspect, even after two months in soil. Similar samples introduced in a hydrated state (only crosslinked (d) or crosslinked and silica-coated (e)), seem to shrink slightly after one day, but remain stable afterward.

Upon SEM observation, it can clearly be seen that the pore morphology of non-crosslinked foam has been completely altered (see Figure V.17 b) compared to the initial foam structure (Figure V.17 a). This might once again be attributed to the rehydration of the alginate pore walls, resulting in partial aggregation and remodeling of the pore walls. It must however be highlighted that samples are dried before SEM observation, which may be responsible for slight morphology modifications, especially further contraction of the pore walls due to capillary forces.

SEM observation of the foams retrieved after 3 weeks in soil (see Figure V.18) show no significant modification in the pore morphology. Contractions due to drying can be observed, but except for this, the oriented pores can still clearly be observed. The silica layers do not seem to be significantly modified by the 3-week stay in the soil (see Figure V.18 b'' and d'').

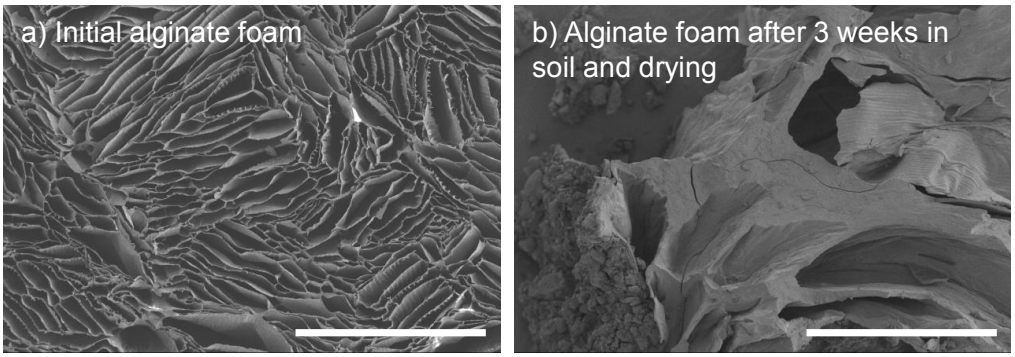

Figure V.17: The oriented and organized porosity of freeze-casted alginate foams (a) is completely lost after a 3-week stay in a hydrated soil and subsequent drying for SEM observation (b). Scale bars: 500 µm.

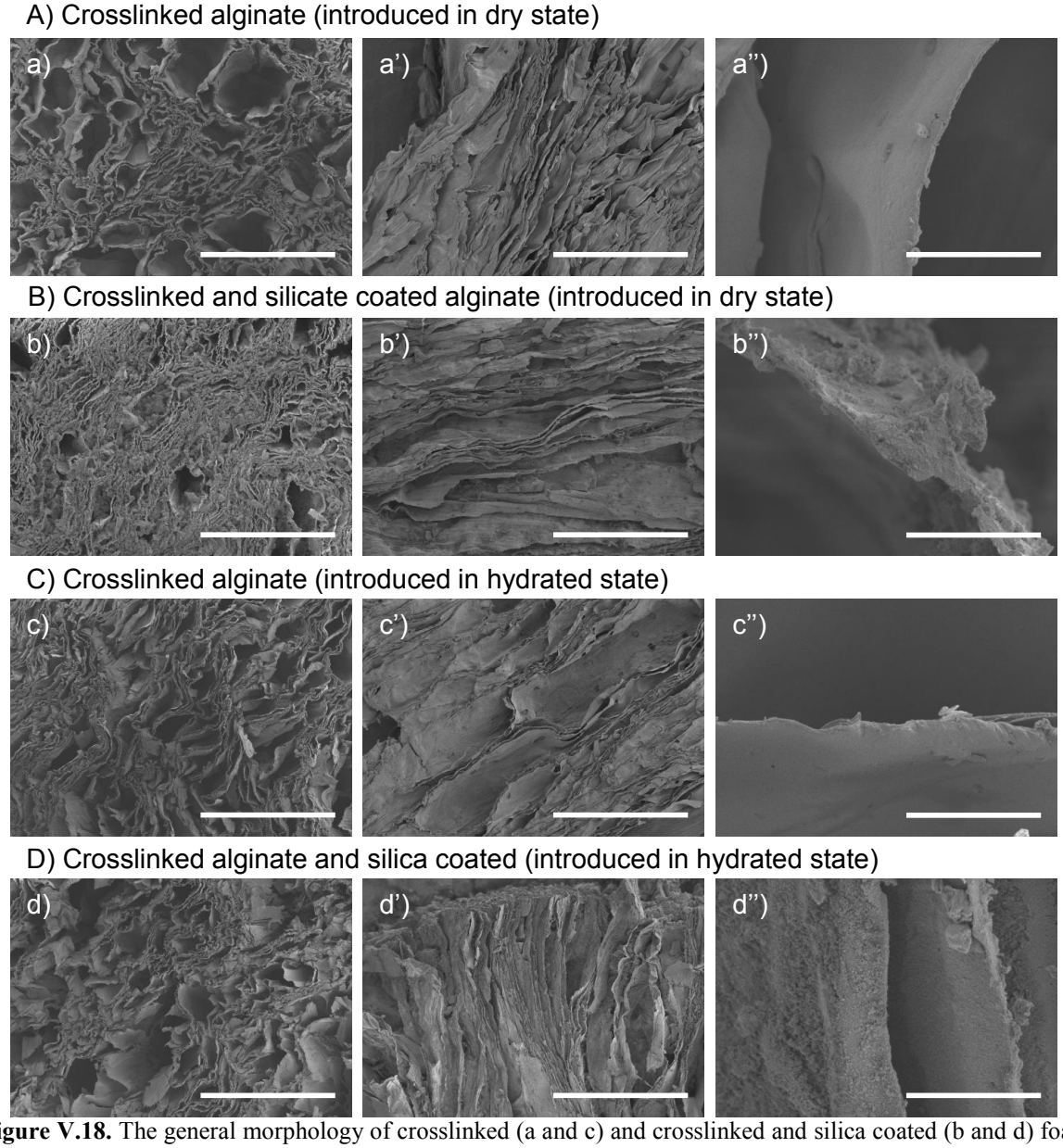

Figure V.18. The general morphology of crosslinked (a and c) and crosslinked and silica coated (b and d) foams is not altered by a 3-week stay in hydrated soil. Oriented channel-like pore can still be observed after a stay in soil and subsequent drying for SEM observation (a',b',c' and d'). Initial dry (a and b) or hydrated state (c and) of the samples does not seem to have a significance on the ageing behavior. At higher magnification (a'',b'',c'',d'') the silica layers do not see to be significantly modified. Scale bars: 500 µm for a,a',b,b',c,c',d, and d', 10 µm for a'',b'',c'' and d''.

From a structural point of view, silica does not seem to enhance to durability of the material after 2 month in soil. Simple crosslinking seems efficient in preventing the degradation of the material. Both hydrated and dried materials have similar behavior. This might be explained by rapid water exchanges between the soil and the foam, as suggested by the shrinking of the hydrated foams. The conservation of the aligned and oriented porosity is expected to favor water mass exchanges through capillarity. From the application point of view, these exchanges should to be advantageous, since they are essential to the efficient diffusion of pollutants toward the encapsulated metabolically active species.

V.2.b Cell survival in silica coated foams

P. aeruginosa cells have successfully been encapsulated in alginate freeze-casted matrix. Survival rates were satisfactory (2.10^8 CFU/mL) after freezing and vacuum drying and even after 3 days of storage foams still contained about 5.10^6 CFU/mL. Silica deposition by contact with vapors of TEOS did however not prove very efficient from a processing point of view.

V.2.b.i Silica coating by aqueous sol-gel chemistry

Silica coating was therefore performed by sol-gel chemistry of LUDOX and silicates. This proved efficient in quickly adding high amounts of inorganic moiety to the polymer foams. The final goals was however not simply to design a hybrid alginate/silica foam, but to create a matrix destined to host bacteria. It must therefore be verified that the process used to add the inorganic moiety to the cell-loaded polymer foam is compatible with cell survival.

Material and methods

P. aeruginosa was encapsulated in alginate foams as previously described by freeze-casting at 5°C/min of a stationary phase cell suspension in alginate and PIPES buffer and subsequent vacuum drying. Samples were then immerged in a 0.5 M solution of $CaCl_2$ (filtered at 0.2 µm) and kept 24h at 4°C to ensure homogeneous crosslinking of the sample. The foams were then rinsed in sterile water and the excess water in the pores was removed by briefly putting the samples in contact with absorbing paper. The samples were then plunged in a mixture of 50 vol% of LUDOX ([Si]=7.8 M) and 50 vol% of sodium silicates ([Si]=0.2 M) acidified to pH=5 by HCl 4M. Total concentration in Si was therefore 4M. Samples were soaked 45 min in this mixture and removed before gelation. Samples were briefly rinsed with sterile water and left 30 min at room temperature and ambient humidity. Samples were then typically kept in sterile water at 4°C.

Samples were included in epoxy embedding medium (see Annex p 200) and 50 nm to 80 nm slices were cut for TEM observation.

For confocal microscopy, samples were cut to thin slices (less than 1 mm) and place on glass slide before addition of Live/Dead® dye (Propidium Iodide at a 0.3 mM concentration and

Syto 9 at a 0.05 mM concentration). The foams were then washed thrice with water to remove excess dye and embedded in Dako fluorescence mounting medium for confocal microscopy observation.
Confocal microscopy (see Annex p201) acquisitions were performed on about 40 µm of thickness with a 0.3 µm step. A z projection of all images was made for cell counting.

P aeruginosa cells were embedded in alginate foams. SEM microscopy allowed for observation of the cells, either under a polymer layer, or directly when pore walls were cut appropriately (see Figure V.19).

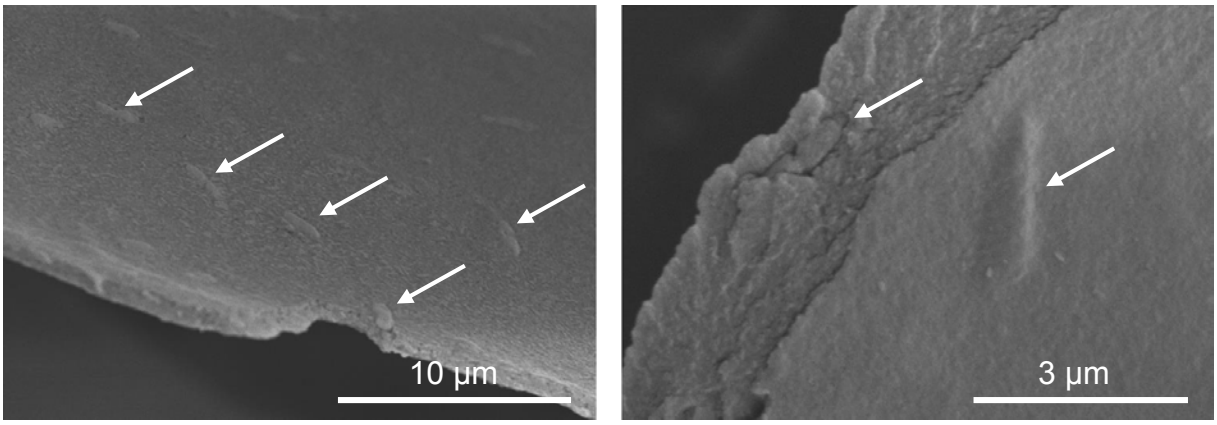

Figure V.19: *P. aeruginosa* cells could be observed within the alginate pore walls.

The polymer foams were then crosslinked and coated with silica. TEM observations (Figure V.20 a and a') showed the presence of cells directly within the polymer walls. Cells themselves are surrounded by lighter areas which seem to indicate that the cells are actually in cavities slightly larger than them. This is possibly due to shrinkage of the cells during the fixation and drying treatments necessary to TEM observation, but it can however not be excluded that initial freeze-drying may be responsible for the cell shrinkage. The presence of silica after the coating process (Figure V.20 b and b') is noticeable as aggregates of monodisperse spherical particles (about Ø = 30 nm) from the LUDOX colloidal suspension. TEM observations confirm that silica does not form a homogeneous layer on the polymer wall, on the contrary silica scattered particles aggregates are only present in small amounts. Cells encapsulated in silica-coated alginate have a similar aspect compared to *P. aeruginosa* embedded in simply crosslinked matrices.
Cell themselves appear more or less rounded, even if *P. aeruginosa* is a bacillus. This is due to the various angles at which the bacteria were cut. Since *P. aeruginosa* is elongated, transversal cut yield apparent rounded bacteria, while longitudinal cuts yield elongated shapes. Statistically however due to the aspect ratio of the cell shapes, it is more likely to observed bacteria cut in a transversal fashion.

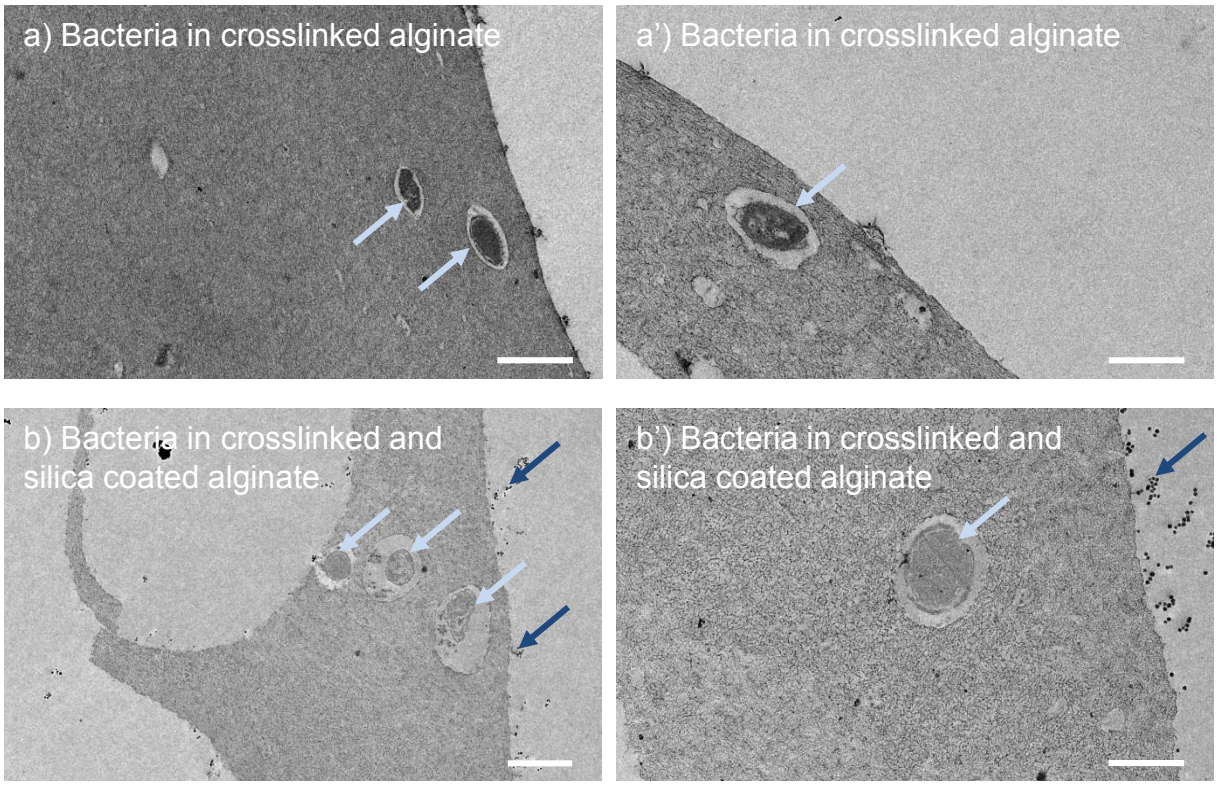

Figure V.20: Bacteria (light blue arrows) can be observed within the walls of crosslinked alginate foams (a and a') and crosslinked and silica coated alginate foams (b and b'). Cells are entrapped in small cavities within the polymer matrix. Silica can be seen as small particle aggregates (dark blue arrows) but does not form a continuous or homogeneous layer. Scale bars: 1 µm for a and b, 500 nm for a' and b'.

To combine structural and functional analysis of the encapsulated cells, foams were stained with LIVE/DEAD® viability kits. The kit is composed of Syto 9® dye capable of staining in fluorescent green both living and dead cells. The second component, Propidium Iodide can only permeate through the membrane of dead cells, resulting in red staining and diminution of the green fluorescence if Syto 9® is also present[493]. Depending on the experimental conditions, it has however been reported that stained *P. aeruginosa* dead cell may still exhibit green fluorescence resulting in green staining of living cells and yellow staining of dead cells[494]. The samples were included in fluorescence mounting medium for observation in confocal microscopy to prevent bleaching of the dyes.

At low magnification stained cells underline the structure of the foams. The advantage here is that the material is mounted directly in the hydrated state. This means that the pore wall distortion and pore contraction observed in SEM due to the drying step are mainly avoided. Thin slices of soft, hydrated matrix must however be cut for observation in confocal microscopy, which may result in slight morphology deformations due to the blade, especially in bending of the structure. Samples coated with silica appear less distorted (see Figure V.21 b) compared to samples simply crosslinked (Figure V.21 a), which might be due to modification of the mechanical properties in presence of silica gels.

At higher magnification individual cells may be observed (see Figure V.21 a and b). A large majority of them appear stained in red, which means that cells are structurally damaged.

A few cells are however stained in green, which means that cells are intact and therefore considered as viable. This low viability rate is due to a number of factors. The encapsulation process itself, as it was previously mentioned, is not innocuous. Both freezing and drying of *P. aeruginosa* may be responsible for cell death. The silica deposition process (both crosslinking and immersion in LUDOX and silicates) may also induce cell death. 16% of living cells can be observed on the confocal microscopy images. This value must however be considered with precaution, since it was only measure on a single image (on 400 cells). Possible heterogeneities of the samples are therefore no taken in account. In addition counting was performed on projections in the z axis of 40 µm of sample resulting in possible cell superposition.

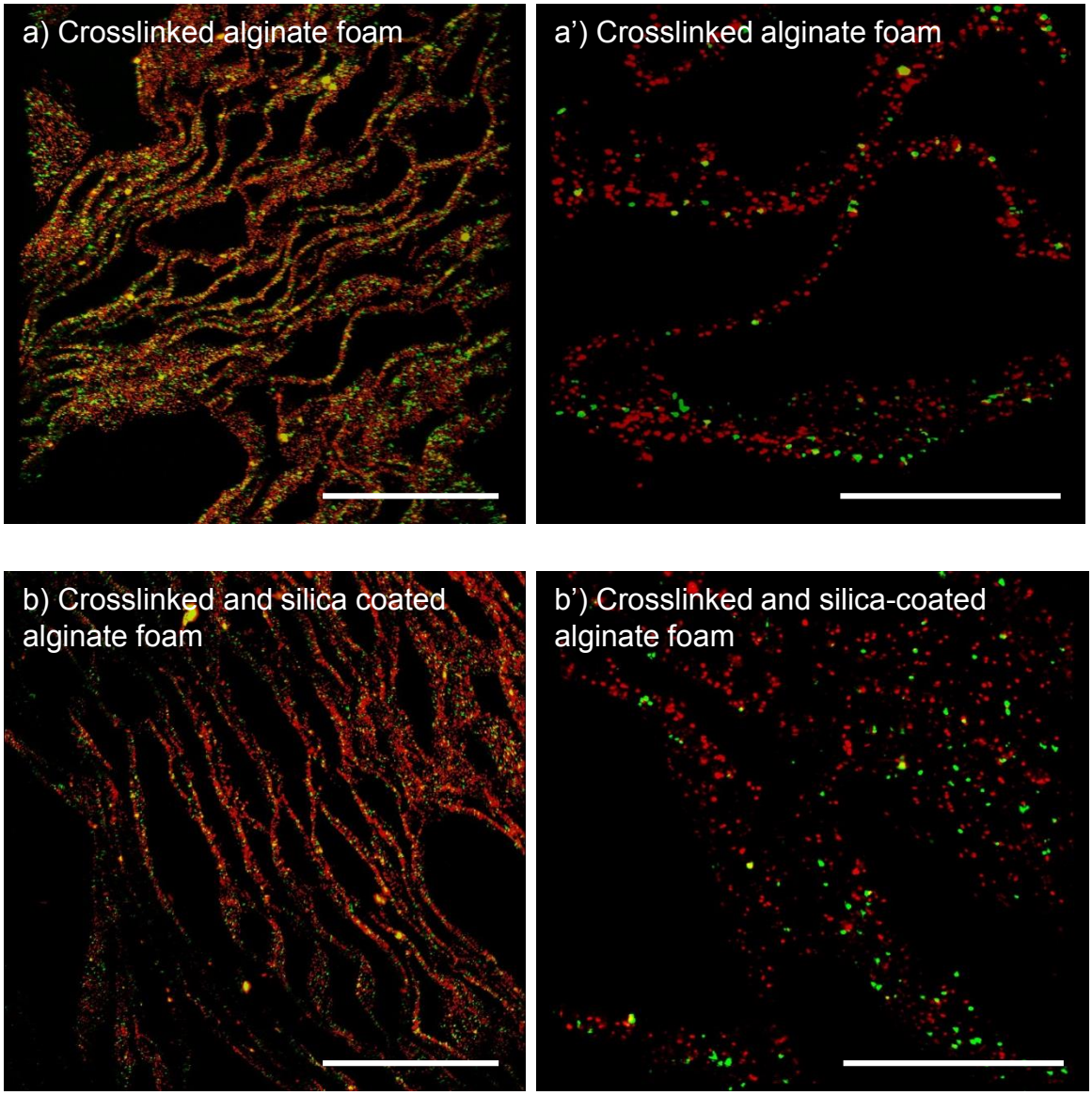

Figure V.21: Living encapsulated cells are stained in green by Syto 9® dye and dead cells are stained in red by propidium iodide. The high concentration of cells within the pore walls allows the observation of the porous morphology of the foam at low magnification. Crosslinked and silica coated samples (b) seem to undergo less deformation during sample preparation than simply crosslinked foams (a). At higher magnification, no significant difference in cell repartition or live and dead ratio is noticeable between crosslinked materials (a') and crosslinked and silica-coated material (b'). Scale bars: 200 µm for a and b, 50 µm for a' and b'.

No significant difference in cell repartition and green/red ratio can be observed between crosslinked samples and crosslinked and silica-coated samples, which may indicate that most viability loss occurs during freezing and drying and possibly during rehydration in the crosslinking media.

V.2.b.ii Cell viability at various encapsulation stages

Cell survival to the freezing and drying steps has been previously assessed, resulting in about 2.10^8 CFU/mL in dry foams. Silica deposition was then performed through aqueous sol-gel synthesis to provide enhanced matrix stability. Even if sol-gel synthesis under mild conditions, cell is may happened during these supplementary processing step. Plate counting was performed to monitor cell viability along the encapsulation process.

Material and methods

Estimation of the cell viability was performed by plate counting. Part of the samples was dispersed in water immediately after vacuum drying as a control. Part of the samples was dispersed in water after 24h at 4°C in the crosslinking medium. Samples were cut into pieces of about 1 mm and vigorously shaken in water. Part of the samples were coated with silica and dispersed in water right after silica gelation (similarly, samples were cut down to 1 mm pieces and vigorously shaken in water). Silica coated samples were placed in water or LB at 30°C under static conditions for 3 days, rinsed in water, cut and dispersed in water.

Cell suspensions obtained from samples dispersion at different stages were diluted and plates on LB-Agar gels, and subsequently incubated 24h at 37°C before counting the number of colonies formed. Samples were prepared in triplicate and each dilution was plated in triplicate.

In order to dissociate the influence of the various encapsulation steps, several plate countings were performed (see Figure V.22). Plate counting presents no difficulty in the case of simple freeze-dried matrices, since alginate alone is soluble in water. However after the crosslinking step, the materials do not dissolve in water anymore (which is the goal from a structural point of view in the final application, but a problem for characterization of the encapsulated cells). As a result, the best way to performed plate counting was to shred the foams in pieces about 1 mm and to suspend them in water. This suspension was then vigorously shaken in order to disperse the encapsulated cells in the supernatant. This method however includes several aspects which may not be very reproducible, especially regarding the cell extraction process. The results of the plate counting can therefore only give an idea about the general variation of the viable population, but this value may be underestimated due to the fact that part of the encapsulated cells may not be efficiently extracted from the matrix. Another possibility would be to modify the nature of the supernatant in order to reverse the crosslinking of the alginate network. It is for instance possible to use non-gelling ions (Na^+) or chelating agents

(EDTA)[179,495] to disrupt the "eggbox" reticulation points and solubilize the alginate gel. This would however introduce a number of supplementary parameters and steps, each of which may modify the survival rate of the cells. As a result it would be difficult to dissociate the effects of the crosslinking itself from the effects the reversion of the crosslinking. These limitations must be kept in mind when comparing plate counting from alginate foams alone which dissolve completely, and crosslinked materials (or crosslinked and silica coated materials).

As can be seen in Figure V.22 a small drop in the apparent number of CFU/mL can be observed after 24h of crosslinking. Besides the fact that this value may be underestimated due to the dispersion method, a portion of the encapsulated cells may actually be lost during this processing step. The crosslinking medium is a 0.5 M of $CaCl_2$, which may be responsible for osmotic damages. It must however be remembered that the cells are not in suspension, but immobilized within the alginate pore walls. As a result effects of a possible osmotic shock are difficult to predict.

This crosslinking step must also be seen as a rehydration step. As was mentioned in Chapter IV, control of humidity conditions for storage of dry, cell-loaded polysaccharide foams is a key feature in survival rates. Good survival rates were obtained in desiccated atmospheres, however ambient humidity results in very low or zero survival rates. Complete rehydration was obtained when foams were immerged in water for plate counting, resulting however in the dissolution of the polysaccharide foam. Although influence of the rehydration medium on survival of freeze-dried bacteria has previously been investigated [365,496], use of water yielded satisfactory survival rate. Immersion in the aqueous crosslinking medium may be considered as complete rehydration of the cells, assuming a rapid diffusion of water molecules through the polysaccharide walls. Influence of the crosslinking step is therefore expected to have a limited impact on cell viability, which seems confirmed by plate counting.

Crosslinked foams were then coated with silica, by gelation of a LUDOX/silicate solution. Various cells have previously been encapsulated in silica gels, either by the use of alkoxide precursors[209,497] or LUDOX and silicates as precursors[113,203]. The chosen silicification method may therefore be expected to be compatible with cell survival, all the more since cells are protected by a layer of crosslinked alginate. A slight diminution of viability can be observed in silica coated foams compared to simply crosslinked foams (see Figure V.22 d and c respectively), but this variation may be due to previously mentioned incertitude regarding the dispersion method which are difficult to precisely quantify.

In order to evaluate the capability of the cells to recover from the various encapsulation steps, silica-coated foams were placed at 30°C under static conditions for three days, both in sterile water and liquid broth. Samples were washed three times with sterile water and subsequently cut down before dispersion in water for plate counting. For material stored in water about 3.10^7 CFU/mL were counted and 1.10^8 CFU/mL were monitored in foams maintained in LB medium (see Figure V.22 e and f). This seem to indicate that cells are capable of efficiently recover from encapsulation in appropriate culture conditions. These results must however

once again be considered with caution. In addition to the difficulties regarding complete extraction of the encapsulated cells prior to plate counting, which could lead to an underestimation of the number of viable cells, possible cell leaching must be considered. When foams are stored in a liquid medium, a small fraction of the immobilized cells may leach from the matrix, even if the matrix is crosslinked and coated with silica. Even very small amounts of cells in the initial storage solution may however result in large cells concentrations in the supernatant after three days at 30°C especially in the case of LB medium. Even if the samples were thoroughly washed before plate counting, it is possible that some non-encapsulated from the supernatant remained on the surface of the pore walls, resulting in an overestimation of the number of CFU/mL encapsulated in the material.

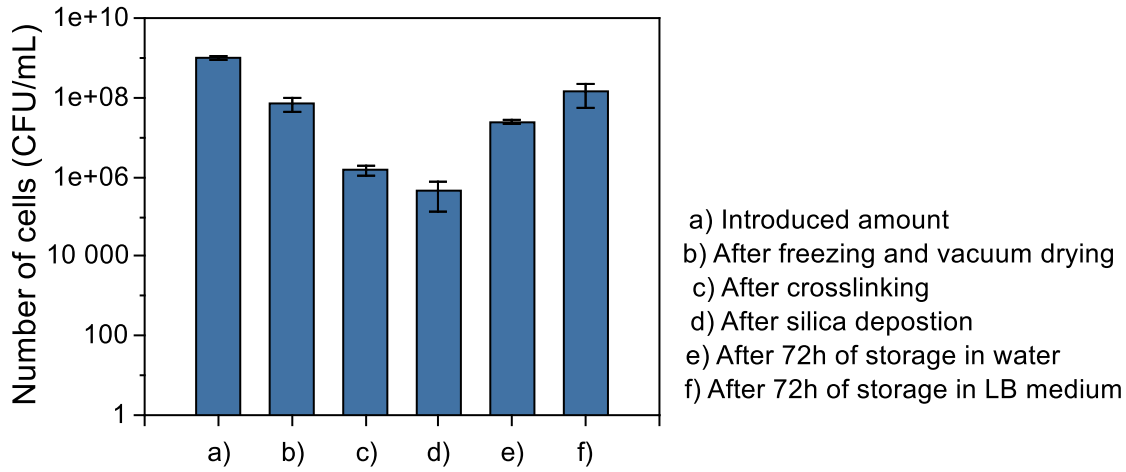

Figure V.22: Freeze-casting at 5°C/min of suspension of *P.aeruginosa* (a) at a concentration of 10^9 CFU/mL in alginate and PIPES buffer and subsequent vacuum drying (b) resulted in the encapsulation of 7.10^7 CFU/mL. After crosslinking of the alginate matrix (c), 1.10^6 CFU/mL were monitored and the viability rate was of 3.10^5 CFU/mL immediately after silica deposition (d). When cell-loaded foam were stored at 30°C in water (e) or LB medium (f), cell counting revealed the presence of 2.10^7 CFU/mL and 1.10^8 CFU/mL respectively. All values are significantly different (at $p < 0.05$).

The cell leaching issue is crucial when considering the targeted application. Introduction of an exogenous microorganism in a polluted soil can be necessary for efficient remediation, but leaching of the encapsulated bacteria may result in disturbance of the ecosystem's balance, which should be prevented.

V.2.b.iii Assessment of cell leaching

Assessment of leaching directly in soil represents a major challenge due to the presence of numerous endogenous microorganisms. It would therefore be difficult to distinguish by simple means such as plate counting the endogenous microorganisms from the soil and the microorganisms introduced by the foam. Leaching in liquid medium may be easier to assess but may not be representative of the behavior of the device in soil. As a compromise, leaching was assessed at the surface of LB-agar gels.

Material and methods

P. aeruginosa was encapsulated as previously described in alginate/silica hybrid foams. After culture in LB medium, cells were collected and dispersed in alginate and PIPES buffer. The suspension was freeze-casted at 5°C/min and vacuum-dried. The resulting dry alginate foam was crosslinked in a 0.5 M $CaCl_2$ solution and coated with silica (gelation of a LUDOX/silicate solution).

The resulting foams were place on LB agar plates and left at room temperature for several days.

In order to compare the leaching possibilities in a matrix simply crosslinked and in a matrix crosslinked and coated with silica, samples were placed on LB-agar gels (Figure V.23).

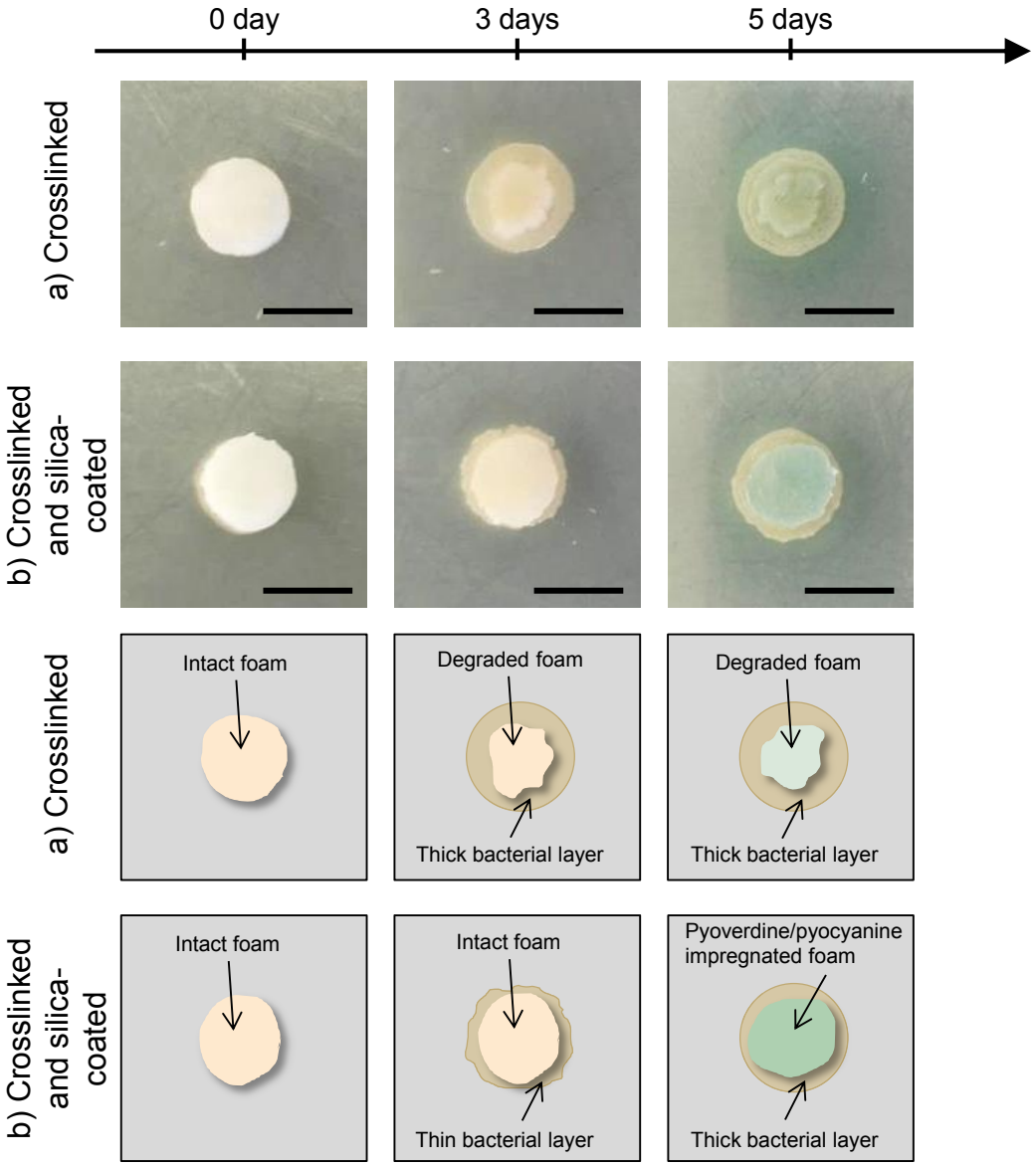

Figure V.23: When alginate samples are simply crosslinked (a) a larger halo of bacteria can be observed compared to samples that were both crosslinked and coated with silica (b). Samples with no silica appear to shrink slightly. After 5 days at room temperature, a greenish coloration can be observed due to the production of pyoverdine and pyocyanine by encapsulated *P. aeruginosa*. Scale bars: 1 cm.

After three days, a halo of bacteria could be observed around both samples with or without silica (see Figure V.23). The halo of bacteria however appears more dense and regular around foams that were not coated with silica, which could indicate that the silica layer prevents cells leaching. Interestingly, the bacterial colonies do not seem to expend further after 5 days. The non-silica coated foams also appear to shrink slightly, while the silica coated ones remain identical. Shrinking might partially be explained by partial drying of the foams, which would result in high capillary solicitation on the pore walls. The presence of silica may provide enhance mechanical resistance against such contraction. The foams are however also likely to be degraded by bacterial activity. Degradation of the polymer matrix could result in enhanced leaching. If wall have polymer-silica core-shell structure, leaching could be prevented even if the polymer core is degraded and the general structure can be retained. After 5 days, foams are colored in green (the color is more intense in the silica coated sample). This is likely due to the secretion of pyoverdine and pyocyanine by *P. aeruginosa,* which is indicative of metabolic activity.

As mentioned earlier the silica coating process from a mixture of LUDOX and silicates has both advantages and drawbacks from a structural point of view. The method allows for rapid deposition of large amounts of silica. The counterpart to this efficiency is the low level of control over the thickness, the morphology and the homogeneity of the silica layer itself, as well as the necessity to crosslink the polymer structure prior to silica deposition. The fact that foams with or without silica seem to age in similar way in soil (when no cells are encapsulated) may lead to question the necessity of addition of a silica layer. It seems however that this silica layer, even if it is not homogenous across the alginate pore walls, allows for a limitation of cell leaching, which is a considerable advantage from the application standpoint.

V.3 Bioremediation assays

P. aeruginosa was encapsulated in hybrid macroporous foams and survival rates were monitored at various stages of the encapsulation process. After freezing, drying, crosslinking and silica deposition, apparent number viable of encapsulated cells was still around 3.10^5 CFU/mL. Presence of living encapsulated cells was confirmed by confocal microscopy. These evaluations of cell viability (either plate counting or staining) were based on the capability of the cells to replicate or on physical integrity of the cells, but the crucial information from the application standpoint is the metabolic activity of the cells. In order to assess the efficiency of the bionanocomposite, the degradation capabilities towards several pollutants were investigated.

V.3.a Choice of a target pollutant

As mentioned in Chapter IV, *P. aeruginosa* has been used in a wide range of bioremediation processes. It must however be underlined that in most cases, the strains used are directly collected and cultivated from polluted sites. It was therefore essential to identify a pollutant that could be degraded by free cells of the specific available strain, before assessing the efficiency of the encapsulated bacteria.

A first group of targeted pollutant was polyaromatic hydrocarbons (PAH) which have been documented as potentially degraded by *P. aeruginosa*[447–449]. PAH are of major concern as soil pollutants due the wide range of possible sources and potentially high levels of toxicity[25,28]. These compounds presented the additional interest of being detectable by fluorescence spectroscopy at low concentrations. They have however low solubility in aqueous media. Unfortunately, degradation assays for anthracene and pyrene in water were not conclusive.

Azo dyes were then chosen as potential models of pollutant[251,458]. These compounds are less ubiquitous than PAH since they are mainly localized in industrial effluents from the textile industry[31]. The large volume of contaminated waste however represent a serious concern[30]. Concentrations of Reactive Black 5[498] and Methyl Orange were measured by UV-vis spectroscopy with or without suspensions of *P. aeruginosa*, but no significant difference could be observed.

In order to illustrate bioremediation capabilities of the device, a different approach was then selected. Reactive Black 5 was set as the model pollutant and a bacterial strain capable of degrading this particular contaminant was then chosen.

V.3.b Decolorization of Reactive Black 5 by *Shewanella Oneidensis*

Shewanella oneidensis, has been reported to have degrading abilities towards dyes[499,500]. Degradation proved very efficient in mineral medium, both for Methyl Orange and Reactive Black 5. Reactive Black 5 (hereafter noted RB5) (see Figure V.24) was used for further assays due to its higher solubility in water.

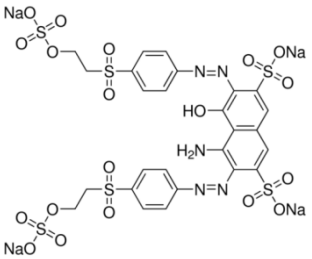

Figure V.24: Chemical structure of Reactive Black 5.

Shewanella Oneidensis is, like *Pseudomonas aeruginosa*, a gram-negative bacteria found in a wide range of habitats. Similarities between the two species are not anecdotic, since the first isolated *Shewanella* species were initially classified as *Pseudomonas*, before being renamed a few years later[501]. *S. Oneidensis* is capable of both aerobic and anaerobic metabolisms and is well-known for its capability to reduce heavy metals[502,503] in anaerobic conditions. These properties of oxydo-reduction have also been used in the design of microbial fuel cells[504]. The versatility of *S. Oneidensis* allows for growth in various conditions. Optimal growth is monitored at 30°C, but *S.Oneidensis* is capable of growing at much lower temperatures (3°C)[505]. In terms of growth medium, *S. Oneidensis* can be grown in LB and plated on LB-agar gels[506]. More specific growth medium with different carbon and nitrogen sources can be designed, resulting in various metabolic activities[500].

Efficiency of *S. Oneidensis* for remediation of Remazol Black 5 was first assessed in "ideal" conditions in order to validate the microorganism/pollutant model. Discoloration was monitored in a MR1 medium adapted to *S. Oneidensis* to confirm the bioactivity of this strain, prior to the addition of parameters such as the presence of the encapsulating matrix or the use of soil as a medium.

Material and methods

MR1 strain of Shewanella Oneidensis was stored in 30 vol% glycerol aliquots at -80°C. About 10 µL of aliquot was dispersed in 10 mL of LB medium in a glass tube and pre-cultivated for 24h at 30°C and 150 rpm up to a 0.9 OD. The pre-culture was then diluted by a factor 50 in the culture medium (see Annex p 204 for composition) (typically 0.8 mL were diluted in 39.2 mL of medium) and placed at 30°C and 150 rpm. After 20h of culture part of the culture suspension was autoclaved. Reactive Black 5 degradation assays were then performed in the same medium at 37°C in static conditions over 24h. Three concentrations of Reactive Black 5 (0 mg/L, 10 mg/L and 100 mg/L) were investigated. Samples were prepared with no bacteria and autoclaved bacteria for control and with bacteria directly transferred from the culture medium. Each degradation assay was performed in triplicate.

For determination of dye concentrations, 1.5 mL of suspension was centrifuged 10 min at 5000 rpm. The supernatant was mixed with 1.5 mL of PBS 2X before acquisition of the absorbance spectra. If needed, samples were diluted in order for the concentration to be within the linearity range determined by the calibration curve (see Annex p 207). Absorbance maximum for Reactive Black 5 was found to be 598 nm.

Plate counting was performed on samples containing fresh bacteria in the initial suspensions and after 24h. Successive dilutions of the cells suspensions were plated in triplicate and incubated 24h at 37°C.

Figure V.25 present the visual aspect of the various degradation assays after 24h. Efficiency of *S. Oneidensis* for decolorization of Reactive Black 5 was visually confirmed, both at a concentration of 10 mg/L (Figure V.25 a) and at 100 mg/L (see Figure V.25 b). These concentrations are not representative of actual pollutant concentrations on contaminated sites, but they work as efficient models for a proof of concept, within the limitations of easy and efficient detection in laboratory conditions.

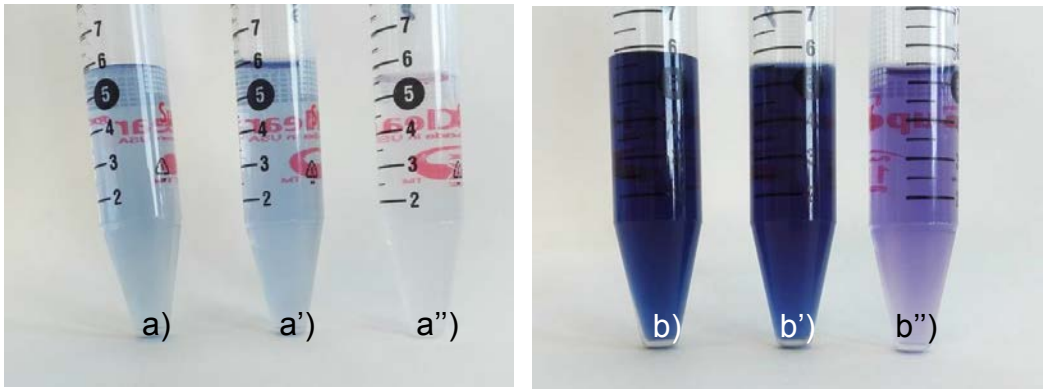

a) [RB5] = 10 mg/L – No bacteria
a') [RB5] = 10 mg/L – Autoclaved bacteria
a'') [RB5] = 10 mg/L – Fresh bacteria

b) [RB5] = 100 mg/L – No bacteria
b') [RB5] = 100 mg/L – Autoclaved bacteria
b'') [RB5] = 100 mg/L – Fresh bacteria

Figure V.25: Control samples of RB5 solutions at 10 mg/L (a) and 100 mg/L (b) after 24h of incubation at 37°C and samples containing about 10^7 U/mL of autoclaved *S. Oneidensis* (a' and b') appear identical. Samples inoculated with 10^7 CFU/mL of fresh *S. Oneidensis* appear either discolored when the initial dye concentration was 100 mg/L (b'') or completely colorless when the initial dye concentration was 10 mg/L (a'').

For quantification of the discoloration efficiency, samples were centrifuged to remove the spectroscopic contribution due to diffusion by suspended cells, and absorbance was measured at 598 nm. Samples containing 0 mg/L of RB5 but same cell contents were used as baselines. As can be seen from Figure V.26 no significant difference can be seen between samples containing no cells and autoclaved cells, either at 10 mg/L RB5 or 100 mg/L in RB5. After 24h about 10% of discoloration can be observed in the case of 10 mg/L solutions and 3% of discoloration in the case of 100 mg/L solutions, in absence of viable cells. This may reflect the instability of the compound in the considered incubation conditions (mineral medium at 37°C).

When the medium was inoculated with 10^7 CFU/mL of *S. Oneidensis* significant discoloration could be observed both in 10 mg/L and 100 mg/L solutions (see Figure V.26 a and b). A slight shift and deformation in the absorbance maxima (see Figure V.26 a' and b') could be observed (to 594 nm and 588 nm for [RB5] = 10 mg/L and [RB5] = 100 mg/L respectively).

Results presented are for absorbance measured at 598 nm. One possible explanation could be the formation of intermediary degradation products, such as aromatic compounds.

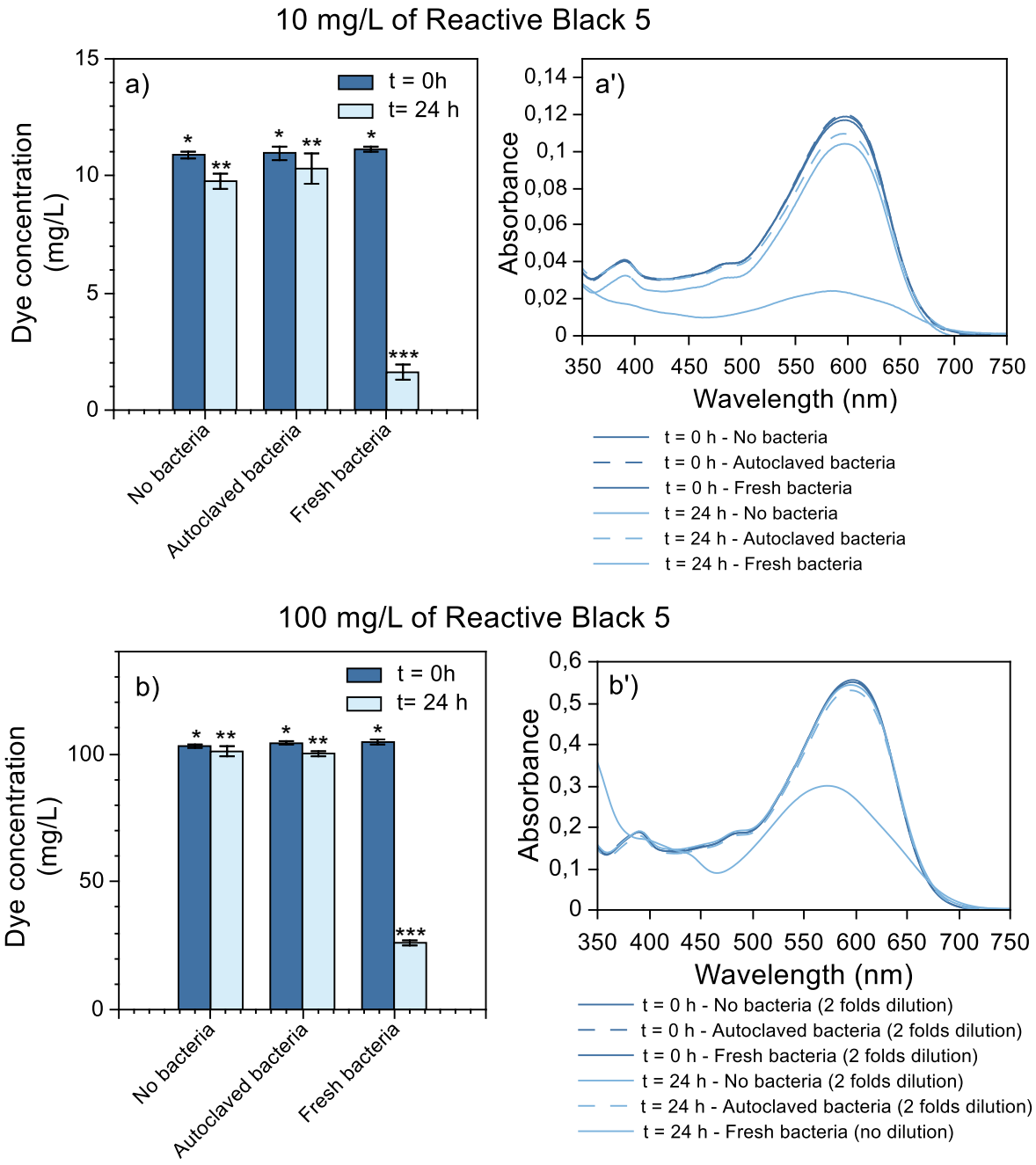

Figure V.26: Addition of fresh *S. Oneidensis* cells results in significant drop in RB5 concentration either from an initial concentration of 10 mg/L (a) or 100 mg/L (b). UV-vis spectra display a slight shift in maxima after discoloration (a' and b'). Values marked by the same number of stars are not statistically different (at $p < 0.05$).

Discoloration rate was higher for an initial RB5 concentration of 10 mg/L (86%) compared to initial concentration of 100 mg/L (75%). Higher dye content may be responsible for toxicity toward cells as has been observed in other decolorization processes[251].

Suspensions inoculated with the same amount of cells but with different dye contents were plated after 24h of incubation at 37°C, in static conditions. Cell growth was observed in

absence of RB5 and with both 10 mg/L and 100 mg/L of dye. Final cell concentrations were not significantly different, which seems to indicate that there is no significant toxicity.
S. Oneidensis proved to be an efficient model for decolorization of Remazol Black 5, in suspension in an adapted medium. This is however only a pre-requisite toward the actual proof of concept, since the degradation process of interest is not in solution but in soil, with cells encapsulated in the previously described macroporous hybrid foam.

V.3.c Soil depollution

Moving from a model of biodegradation of cells in suspension in a liquid media to a model of encapsulated cells for depollution of soil is likely to induce several changes in the assessment of degradation efficiency. The presence of soil as a medium makes the monitoring of dye content more difficult. In addition the presence of soil introduces the issue of adsorption of the dye on soil particles and of diffusion inside the soil itself, as well as endogenous bioremediation phenomena. Encapsulation of the functional units in a matrix is likely to significantly change remediation kinetics due limitations in terms of substrate diffusion inside the material itself.

Material and methods

S. Oneidensis was encapsulated according to the protocol previously described for encapsulation of P.aeruginosa. S. Oneidensis was pre-cultivated in LB medium for 24 h (up to 0.9 OD). This pre-culture was then diluted by a factor 50 in fresh LB medium and cultivated 7 h at 30°C and 150 rpm (up to 2.2 OD). The medium was centrifuged and the pellets were dispersed in alginate and PIPES buffer to yield the following concentrations: 10^9 CFU/mL of S. Oneidensis, 40 g/L of alginate, 100 mM of PIPES buffer. The suspension was then freeze-casted at 5 °C/min and vacuum dried. Blank samples were prepared in the same manner but without introduction of cells. Foams were then crosslinked 6 h in $CaCl_2$ (0.5 M) and subsequently impregnated with LUDOX/silicate at pH=5 ($[Si]_{LUDOX}$ = 3.9 M and $[Si]_{silicates}$ = 0.1 M). Foams were rinsed and left at room temperature until formation of silica gel before being introduced in soil for remediation assays. Samples were prepared in triplicate.
Efficiency the encapsulation was controlled by dissolution of part of the cell loaded foams directly after vacuum drying in water and plate counting.
In typical remediation assays, 10 g of soil (silt loam Luvisol sampled at the Versilles INRA station) was soaked with 7 mL of simplified mineral medium (see composition in Annex p 204) containing 0.5 g/L in RB5. After 42h under static conditions at 37 °C, 7 mL of PBS 2X was added and the mixture was vigorously shaken for. 2 mL of supernatant was centrifuged 10 min at 5000 rpm and the UV-vis absorbance spectrum was measured (samples were diluted by an appropriate factor to fit in the linearity range of the calibration if needed). Assays were made in triplicate with cell-loaded foams and blank foams. Control were performed in triplicate with soil in contact with the [RB5] = 0.5 g/L solution, soil in contact with the mineral medium only ([RB5] = 0 g/L) and soil in contact with [RB5] = 0.5 g/L inoculated

with 3.5.10^7 CFU/mL of free S. Oneidensis. 7 mL of the [RB5] = 0.5 g/L in simplified mineral medium solution was also incubated 42h at 37°C with no soil or bacteria to assess the stability of the dye in the considered medium.

Bioremediation efficiency was assessed at small scale in upper horizon silt loam Luvisol kindly provided by the Laboratoire de Géologie de l'ENS as a typical soil sample from the Parisian region. Concentrations of pollutant in leaching water were monitored in presence or in absence of encapsulated *S. Oneidensis.* Cell-loaded foams were left in contact with a soil soaked by a solution of RB5, which may be seen as a model of industrial spill. Samples were incubated at 37°C to ensure rapid diffusion and degradation kinetics, but such temperature is mostly not representative of actual polluted sites. The soil samples were then briefly washed to simulate water infiltrations, and dye concentration in this supernatant was monitored.
Visual observation (see Figure V.27) shows that RB5 concentration appears to be much lower than the initial 0.5 g/L in all rinsing solutions. This is to be expected from dye adsorption on soil particles. The discoloration may also be due to the presence of endogenous microbial species capable of degrading RB5. To further characterize the dye concentrations in rinsing solutions, UV-vis spectra were measured.

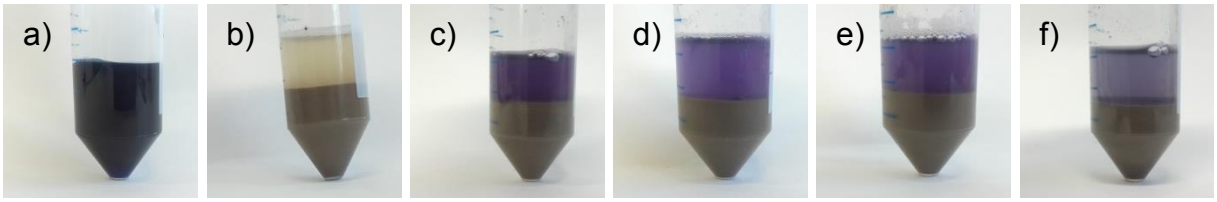

a) RB5 in mineral medium
b) Mineral medium + soil
c) RB5 in mineral medium + soil
d) RB5 in mineral medium + soil + blank foam
e) RB5 in mineral medium + soil + cell-loaded foam
f) RB5 in mineral medium + soil + free bacteria (at 3.5.10^7 CFU/mL)

Figure V.27: Soil soaked in [RB5] = 0.5 g/L solutions in simplified mineral medium were incubated 42h at 37°C.

As was mentioned earlier, slight maxima shifts could be observed in discolored solutions (see Figure V.28 B). Once again absorbance was measured at 598 nm, even though slight peak deformation and shifts could be noticed. A yellowish coloration of the simplified mineral medium alone could be observed (see Figure V.27 b). This contribution was subtracted from the values measured in presence of RB5.

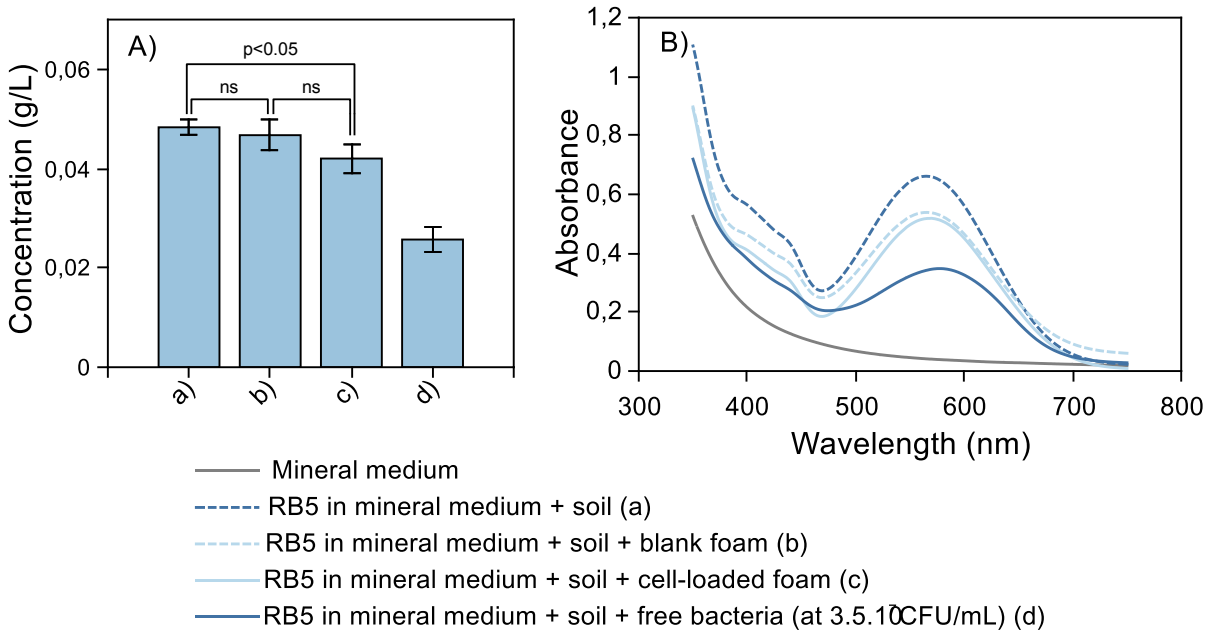

Figure V.28: No significant difference in discoloration can be observed between soil alone (a) and soil containing blank foams (b). Discoloration is slightly enhanced with cell-loaded foams(c) compared to soil alone (a). Discoloration is much more efficient when concentrated suspensions of free cells was added to the soil (d). ns: non statistically significant difference (at $p<0.05$).

A slight discoloration (4.5%) of discoloration was observed on the control solution of RB5 in the simplified mineral medium after 42h at 37°C, which is consistent with stability observations reported in paragraph V.3.b .

Contact with the soil alone resulted in significant reduction of the dye concentration in the rising water, since final measured concentration was 0.048 g/L (see Figure V.28 a), which corresponds to a 90.4% decolorization rate. This discoloration is likely due to a combination of adsorption and endogenous microbial degradation, since the soil used is not sterile. Adsorption for an initial dye concentration of 0.1 g/L in water at 25°C was found to be 0.038 mg_{dye}/g_{soil} after 24h (see Chapter III, p118). Such a dye loading could account for a drop of concentration to 0.47 g/L. Even considering the changes in adsorption kinetics due to the higher temperature (37°C *vs* 25°C), the longer exposure time (42 h *vs* 24 h) and the change in medium (mineral medium *vs* water), it is unlikely that the observed discoloration is solely due to adsorption. Since the soil used is a field example of soil which has not been sterilized, the system should contain various endogenous microbial species. The use of mineral medium and incubation temperature are likely to have stimulated the biodegradation phenomena in the soil, resulting in the high discoloration rate observed. The final concentration in the system containing only soil was therefore used as a control value.

Introduction of blank foams does not induce a statistical difference in the final RB5 concentration of the washing medium (see Figure V.28 b). The main contribution of such foam would be dye adsorption on the foam itself. Such effect may however be difficult to observe due to the low mass/mass ratio between the foam and the soil.

Rinsing water from the soil sample treated with the hybrid cell loaded foam proved to have a final RB5 concentration significantly compared to the control with soil alone (see Figure V.28 a and c). Final RB5 concentrations were 0.042 g/L and 0.048 g/L respectively, which represents a 12.5% discoloration for the cell loaded foam compared to the control. This difference is not very big, though statistically significant ($n_{samples}$=3, $p<0.05$). The difference in concentration between assays in presence of blank foams and cell-loaded foams were however not statistically different (see Figure V.28 b and c). This means that the observed efficiency of the cell loaded foam may be attributed to a combination of dye adsorption on the foam and biological activity.

As may be expected, dye concentration in rinsing water for soil directly inoculated with free bacteria is much lower (0.026 g/L or 46.8% of discoloration compared to the soil control) compared to the other assays. Free cells are indeed less likely to be subjected to diffusion limitations, which may help their efficiency compared to encapsulated cell. In this case however the main reason for the difference observed and the relatively low efficiency of the depollution device may be explained by a simple parameter that was not yet discussed in this paragraph: the amount of viable encapsulated cells. The encapsulation process has been developed and optimized using *P. aeruginosa* strain as a model. *S. Oneidensis* was however chosen for its superior dye degradation capabilities. The same process and conditions were used for the encapsulation of this second bacteria strain. Unfortunately, under these conditions only 300 CFU/mL were counted in freeze-dried foams, and this number is likely to be even lower after silica deposition. As a result it is difficult to compare efficiency of free and entrapped cells due to the very large difference in the number of introduced cells (less than 900 encapsulated CFU *vs* $2.5.10^8$ free CFU).

The bionanocomposite device composed metabolically active bacteria encapsulated in an alginate/silica porous matrix proved to be efficient in the discoloration of rinsing solution from a RB5 polluted soil. The effect was however very limited due to the fact that a very small amount of CFU *S. Oneidensis* was immobilized in the hybrid foam. A large number of cells was initially introduced in the material, and it cannot be excluded that part of the non-replicating cell may still have a metabolic activity toward RB5. It seems however that the remediation process could greatly benefit from the optimization of the encapsulation conditions. The immobilization process was initially optimized for *P.aeruginosa*, which allowed identification of several key parameters in the encapsulation efficiency, including formulation of the matrix (type of polymer, addition of buffer or cryoprotective agents), growth phase of the bacteria or freezing-rate. These parameters would have to be adapted to *S. Oneidensis* MR1 to ensure optimal encapsulation efficiency. Use of a different bacterial species may even uncover other relevant encapsulation parameters, to which *P. aeruginosa* is not especially sensitive.

Conclusion

P. aeruginosa was successfully encapsulated in alginate freeze-casted foams. Alginate proved efficient in maintaining cell viability for several days in desiccated conditions, which could be of use for vapor phase deposition of silica.

In the case of alginate-based materials however, these silica depositions conditions resulted in the formation of large amounts of sodium chloride rather than a smooth silica layer. The silica deposition process was therefore modified. Use of a liquid phase silica deposition required crosslinking of the alginate foams, but presented the advantage of rapid deposition and immediate rehydration of the encapsulated cells. Cell survival was monitored throughout the encapsulation and silica deposition processes. Despite a small viability drop during encapsulation, cells were still capable of growth. The drawback to this deposition technique in liquid phase was the relative lack of control regarding the amount of deposited silica and the uniformity of the silica layer, compared to the vapor phase deposition. The hybrid materials however proved to be very stable in soil. (see Figure V.29).

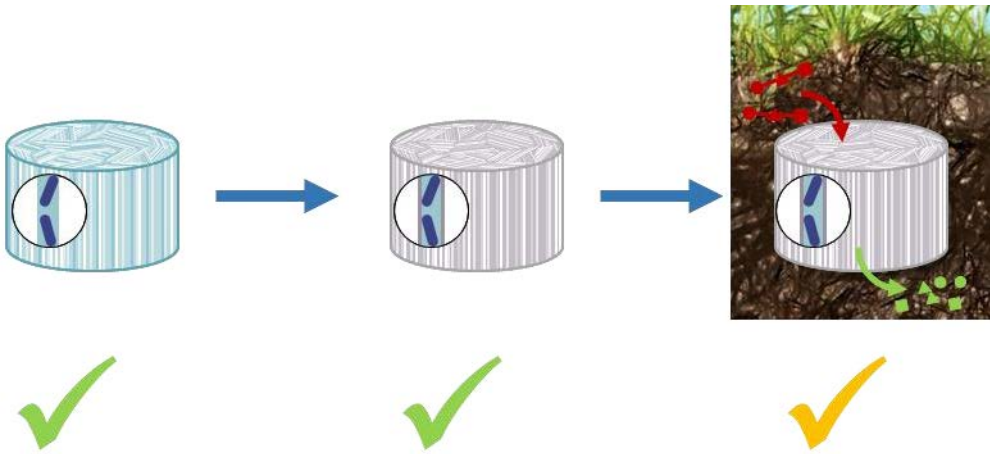

Figure V.29: Efficient encapsulation of *P. aeruginosa* was achieved and viability was maintained throughout the silica deposition process. *S. Oneidensis* was encapsulated and efficiency regarding remediation of Reactive Black 5 was assessed.

Despite efficient encapsulation, the *P. aeruginosa* strain used proved inefficient for remediation of the tested pollutants (mainly PAHs and dyes). On the other hand *S. Oneidensis* was very efficient in degrading Reactive Black 5. The latter bacteria was therefore chosen for remediation assays in soil. Lower dye concentrations were monitored in rinsing water when the cellularized hybrid foam was introduced in the soil. The differences observed were however very small, which may be attributed to the limited amount of viable *S. Oneidensis* cells encapsulated in the macroporous hybrid foam. These low survival rates can be explained by the fact that the encapsulation protocol was optimized for *P. aeruginosa*. Despite the similarities between the two bacteria species, behavior regarding freezing and drying may be significantly different. Key parameters such as culture medium, freezing temperature, presence of additives or composition of the rehydration medium should allow for the optimization encapsulation and increase of the viable cell content, which should in turn allow for better characterization of the bioremediation potential of the device.

General conclusions and perspectives

The goal of this work was the design of a new type of cellularized materials for soil bioremediation. Several key requirements were identified both in terms of structure and functionality to maximize the efficiency for the targeted application. Since encapsulated microorganisms (more specifically bacteria) were used as the biofunctional units of the device, it was essential to preserve their metabolic activity. The depollution efficiency not only depends on the activity of the encapsulated cells but also on the accessibility of the targeted substrates (in this case, soil contaminants). One limitation was however the need to prevent dissemination of the chosen metabolically active exogenous organisms within the soil, in order to avoid possible disturbance of the endogenous ecosystem. The matrix had therefore to be designed keeping these constraints in mind. Two main pathways were explored to design and control the encapsulating matrix. First the composition of the matrix was chosen to ensure maximal compatibility with the functional units while providing sufficient structural integrity and stability to withstand prolonged use in soils. In addition the shaping process needed to be carefully engineered to provide both an oriented porosity to favor substrate diffusion and encapsulation conditions compatible with maximal bacterial survival rates. These two aspects could however not be considered separately since the nature of the matrix components and the possibilities in terms of processing are mutually dependent.

Regarding the composition of the matrix, biopolymers were selected for their intrinsic biocompatibility as well as their versatility in terms of shaping possibilities. In particular, biopolymer solutions could be processed by freeze-casting. Such a method allowed simultaneous encapsulation of the functional unit and shaping of the matrix into a porous foam. The main limit to the use of cellularized freeze-casted biopolymer foams as soil remediation devices was however the instability of biopolymer-based materials. To prevent rapid degradation of the matrix and subsequent leaching of the encapsulated bacteria, an inorganic moiety was associated to the biopolymer structure. Sol-gel silica appeared as especially relevant thanks to the mild synthetic conditions required.

Design of cellularized macroporous hybrid materials by freeze-casting required the development of a multi-step encapsulation process, taking into account the structural and functional requirements of the targeted application. The general strategy of this work was not to fully engineer each aspect of the process individually but rather to identify the key parameters at each stage of the encapsulation, their interdependence and their influence on the other steps of the process.

The possibilities in terms of general structure and morphologies were first evaluated by ice-templating of beet-root pectin aqueous solutions. Various freezing setups were investigated (freezing in conventional freezers at -20°C and -80°C, use of a liquid nitrogen bath, use of a freeze-casting setup) and revealed the crucial importance of the presence and orientation of a temperature gradient to obtained well controlled and aligned porosity. Freeze-casting offers a wide range of possibilities in terms of morphological control. Parameters regarding the formulation of the initial solution (type of solvent, type of polymer, presence of additives etc…) or the freezing setup (number of cold fingers, geometry of the cooling element,

patterning of the cold surface etc…) might be explored to gain further control over the pore structure and yield original morphologies.

The pectin-based macroporous foams were then modified by addition of a silica layer on the pore-wall surface. The silica was deposited through exposure to tetraethoxysilane vapors in presence of an acid aqueous atmosphere to promote hydrolysis and condensation at the surface of the pectin pore walls while preventing their dissolution. The method proved efficient for the deposition of a fully percolated and homogeneous silica layer, without any pore obstruction. The deposition kinetics allowed for fine tuning of the final silica thickness, which in turn granted control of the mechanical properties of the foam. The final structure could be described as a macroporous hybrid material composed of pectin-silica core-shell walls. The presence of the silica layer proved efficient in preventing dissolution of the foam in aqueous medium. Ageing of the foams was also monitored in silt loam Luvisol soil and hybrid materials were stable over 5 weeks. These hybrid materials were also used for adsorption of a model contaminant (Reactive Black 5 (RB5), which is a common dye, mainly used in the textile industry) in liquid medium. Interestingly, the device was also efficient when placed with a real soil sample impregnated with a dye solution. This could be an indication of good substrate diffusion from the soil to the material. Such materials could be of interest in themselves. From a material scientists' perspective the original hybrid structure could be tuned to yield a wide variety of morphologies and properties. This could be used for various applications including biomedical scaffolds or vehicles for controlled drug delivery, but also in environment science for materials combining adsorption properties, oriented porosity and mechanical stability.

In this case however the structure was used as a matrix for the encapsulation of metabolically active microorganisms. The components and processing techniques were chosen keeping in mind the constraints imposed by the presence of microorganisms (use of water as a solvent, no exposure to high temperature, use of biopolymers). Efficiency of freeze-casting for direct encapsulation in the previously described matrix however still needed to be confirmed. *S. cerevisiae* was used as a first model for encapsulation. The density of living cells, viscosity of the pectin suspension and considered ice-front velocities were compatible with entrapment of the cells within the pectin walls. The cell metabolic activity was preserved after freezing and drying. Yeast cells are a good laboratory model but are not especially relevant from the bioremediation perspective. A second model organism, *P. aeruginosa*, was therefore investigated. Freeze-casting also proved compatible with survival of this bacterial species, despite the biological stress generated by freezing and drying. Although freezing and drying protocols have been developed to prevent cell damages for cell cryopreservation, they usually require introduction of cryoprotective compounds such as glycerol or lyoprotective compounds such as trehalose. In the freeze-casting encapsulation process, no common cryopreservative is added. The presence of a biopolymer such as pectin may however provide some degree of protection against deleterious effects of freezing and mechanical solicitations. In addition to the presence of cryoprotectant, another crucial parameter in conventional

cryopreservation is the control of the cooling rate. The freeze-casting technique confers a good control over this parameter which allowed for further optimization of the encapsulated cell survival rate. This encapsulation matrix however proved limited regarding long term survival of the entrapped bacteria. This was problematic regarding the silica coating step, which requires several days to several weeks to yield a silica layer thick enough to provide long term structural stability.

The composition of the matrix had therefore to be modified and encapsulation was performed in a different polysaccharide. Bacteria encapsulated in alginate displayed higher survival rates compared to cells in pectin matrices, especially after 24 h of storage. The sol-gel vapor phase deposition was however far less efficient in the case of alginate foams. Sol-gel deposition was therefore performed in liquid phase through the aqueous route (mixture of sodium silicates and commercial colloidal particles), by taking advantage of the crosslinking properties of alginate in presence of divalent cations (in this case $Ca^{2+)}$. The silica deposition method proved to be an efficient and quick alternative to vapor phase silica deposition. The hybrid materials obtained by this method showed good stability in the reference soil previously mentioned over 2 months. From a functional perspective, viable cells were observed within the hybrid macroporous foam at the different steps of the encapsulation process and cell growth could be obtained after freezing, drying, crosslinking and silica coating. The silica layer obtained by the liquid aqueous sol-gel route seemed to have a beneficial influence to prevent cell leaching. The assessment of this effect was however only performed on agar gels as a model of solid environment. Evaluation of leaching within the actual reference soil could be of great interest but would require extensive analytical resources (for instance using 16S rRNA sequencing). Control of the silica layer porosity (either obtained by vapor phase deposition or through the liquid aqueous sol-gel route) could provide control over the material's diffusion properties. Such a controlled membrane could be of great interest in various applications such as drug or cell delivery. Tuning of the barrier properties of the silica layer may also be decisive for soil depollution, since the contaminant must diffuse into the polymer layer. To assess the efficiency of cellularized macroporous hybrid materials as depollution devices, various model pollutants were investigated.

The specific *P. aeruginosa* strain used for the development of the encapsulation protocol was unfortunately inefficient for the degradation of the tested contaminants. As a result a different approach was pursued. A contaminant model was set (RB5) and a bacterial species with bioremediation capabilities regarding this specific contaminant was then selected. *Shewanella oneidensis* displayed high RB5 discoloration capabilities and was therefore further used as the functional unit of the cellularized alginate-silica porous material. The efficiency of the material was evaluated in the reference soil previously mentioned. The soil was oversaturated with a concentrated RB5 solution and dye concentration of rinsing water was monitored after incubation. The addition of the cellularized hybrid porous material in the soil resulted in a slight but statistically significant drop in the contaminant concentration. This system therefore proved to be an efficient proof of concept. Several pathways can be considered in order to

confirm these results and enhance the efficiency of the depolluting material. The main limitation of the specific *S. oneidensis*-alginate-silica structure was the very low viable cell loading. This can be explained by the fact that the various encapsulation parameters were optimized for maximal survival of *P. aeruginosa*. As a result several conditions may be optimized to increase the concentration of viable *S. Oneidensis* in the porous matrix. One of the most efficient ways to increase the survival rate may be by tuning the cooling rate during freeze-casting as it was demonstrated that an optimum freezing-rate, which is cell dependent, can be found. Other parameters such as the growth phase, growth medium or initial cell concentration may also be modified to adjust the cell survival rate. The depollution model in itself may also be improved in order to be closer to field conditions. In this proof of concept, the soil was oversaturated with a mineral medium containing high dye concentrations and incubated at 37°C to maximize substrate diffusion and bacterial metabolic activity. These conditions were however likely to be responsible for biostimulation of the endogenous microbial population since the used soil was a non-sterilized field sample. Efficiency of the cell-loaded material may therefore be monitored with different soil hydration levels, various contaminants and nutrient contents as well as different incubation temperature in order to fully dissociate the effect of the endogenous biostimulation from the bioaugmentation.

This proof of concept nonetheless appears has as a very encouraging step towards the elaboration of efficient materials for *in situ* soil depollution. Thanks to its adaptability, the described encapsulation process may be used for the entrapment of a wide variety of microorganisms (bacteria but also fungi or algae for instance). Through the choice of the appropriate microorganisms (or consortia) and tuning of the encapsulating matrix properties (in terms of diffusivity, mechanical behavior, stability etc...), tailor-made depollution materials may be designed for specific contaminated soils.

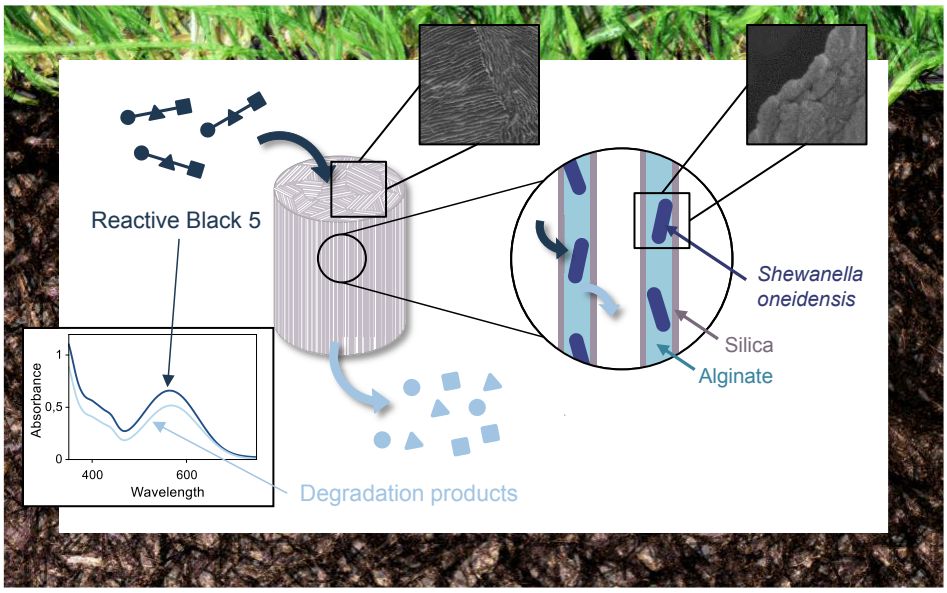

Visual summary: Bacteria were encapsulated in biopolymer-silica macroporous foams. Entrapment of the cells and unidirectional porosity were obtained by freeze-casting and silica coating was performed by sol-gel chemistry. The *Shewanella oneidensis*-loaded alginate-silica porous material proved efficient in the discoloration of a soil containing Reactive Black 5.

Annexes

Publications

- *Journal articles*

- Christoph, S.; Barré, P.; Haye, B.; Coradin, T.; Fernandes, F. M., Ice-templated hybrid biofoams: bacterial encapsulation, viability and biodegradation activity in soil, *Submitted **2017***
- Christoph, S.; Hamraouia, A.; Bonnin, E.; Garnier, C.; Coradin, T., Fernandes, F. M., Ice-templating pectin: towards texture, mechanics and capillary properties control in fully biodegradable foams, *In preparation **2017***
- Christoph, S., Kwiatoszynski, J., Coradin, T. and Fernandes, F. M. Cellularized Cellular Solids via Freeze-Casting, *Macromol. Biosci.,* **2016,** *16* (2), 182–187
- Christoph, S.; Fernandes, F. M.; Coradin, T., Immobilization of Proteins in Biopolymer-Silica Hybrid Materials: Functional Properties and Applications, *Curr. Org. Chem.,* **2015**, *19* (17), 1669–1676

- *Book section*

- *Bionanocomposites: Integrating Biological Processes for Bio-inspired Nanotechnologies*
  Chapitre 5.4 : Bionanocomposite materials for biocatalytic applications
  Editors : Carole Aime, Thibaud Coradin
  Wiley, **2017**

Communications

- *Poster presentation*

- HINT Training School : Bottom-up Approaches of Hybrid Materials: Preparation and Design, Ljubljana, Slovenia; **2015**
- International Symposium on Macroporous Materials: From Novel Preparation Techniques to Advanced Applications, Paris, France; **2016**

- *Oral presentations*

- EMRS 2016, Lille, France; **2016**
- CellMAT 2016, Dresden, Germany; **2016**

Characterizations

- Microscopy

- *SEM/EDX*

Scanning Electron Microscopy was performed on Hitachi S-3400N microscope. An Oxford Instruments - X-max module could be equipped for Energy Dispersive X-Ray spectroscopy.
For SEM observation were samples were usually cut with a scalpel into slices thinner than 1 mm and coated with 20 nm of gold by metal sputtering. Observations were typically conducted under 3 to 4 kV acceleration and 30 µA probe current. If required, the samples were previously dehydrated by successive bathes of increasing ethanol content. The samples were plunged at least 30 mins (up to several hours depending on the sample size) in ethanol solutions at 20, 40, 60, 80 and 100%. The ethanol impregnated samples were then left to dry at room temperature.
For EDX analysis, the samples were cut in the same way and coated with 20 nm of carbon. Analysis was typically performed under 10 kV acceleration and 30 µA probe current. Titanium was used as reference.

- *SEM-FEG*

SEM observations were also performed using a Hitachi SU-70 equipped with a Field Emission Gun.
The samples were cut as previously described and coated with 5 nm of platinum by metal sputtering. The acceleration voltage was typically 1 kV and the emission current was 44 µA.

- *TEM*

Transmission Electron Microscopy was performed on a Cryomicroscope Tecnai spirit G2 equipped with a Gatan Orius camera.
Prior to observation, samples were embedded in epoxy resin.
The samples were stabilized 24h in a 8% paraformaldehyde solution and fixated in in a glutaraldehyde solution (8% glutaraldehyde in a 0.05M cacodylate buffer). After rising with a 0.1M cacodylate buffer and 0.6 M saccharose solution, the samples were fixated by osmium tetraoxyde. After rinsing with 50% overnight, the samples were dehydrated with successive bathes of ethanol (50, 70, 95 and 100%) and a bath of propylene oxide. The samples were then embedded in epoxy resin (mixture of Araldite, E812, dodecenylsuccinic anhydride (DDSA), N,N-dimethylbenzylamine (BDMA) and N-methylacetamide (NMA)).
After drying of the embedding resin (3 days at 60°C), slices (between 50 nm and 80 nm) were cut on a Leica EM UC7 microtome. Samples were contrasted with uranyle acetate one day before TEM observation.

- *Confocal microscopy*

Confocal microscopy was performed at the Center for Interdisciplinary Research in Biology (CIRB) at College de France. Observations were performed on Leica DMI6000 inverted microscope. Acquisitions were performed on about 40 µm along the z axis with 0.3 µm steps. Samples were incubated 30 min with Live/Dead® dye (Propidium Iodide at a 0.3 mM concentration and Syto 9 at a 0.05 mM concentration) and rinsed with sterile water before observations. Images were analyzed with Fiji software, using the "3D projection" function.

• Spectroscopy

- *IR*

Infra Red Spectroscopy was performed on a Perkin Elmer Spectrum 400 FT-IR/FT-NIR Spectrometer equipped with Universal ATR sampling accessory. Samples were crushed or shredded into less than 1 mm large fragments. A few milligrams of sample were placed on the diamond detector.

- *UV-vis*

UV-visible spectroscopy was performed on CARY 5000 from Agilent Technologies. Typically, water was used as reference and baseline was adjusted on the dispersing medium (for instance phosphate buffer saline). Wavelength range was adapted to the considered species to detect. Scan rate was typically 600 nm/min, data interval was 1 nm, average time was 0.1 s and spectral band width was 2 nm.
Calibration curves for the different components observed are provide in the Experimental section, p207.

• TGA

Thermogravimetric analysis was performed on Netzsche STA 409 PC Luxx thermal analyzer. Samples were crushed or shredded into less than 1 mm large fragments. Between 10 and 20 mg of sample were place in the crucible. Thermal analysis was performed under air between 25 °C and 1200 °C, at 5 °C/min.

• Rheology

Rheology measurements were performed on a MCR 302 Anton Paar rheometer under plane-cone geometry. The cone diameter was 24.969 mm with a 1.0110° angle and a 50 µm truncation. Aqueous pectin solutions at various concentrations were prepared by magnetic stirring overnight at room temperature. Measurements were performed with shear rates between 1 and 100 s^{-1}.

- Mechanical compression

Stress/strain curves were acquired on an Instron 5965 universal testing machine equipped with a 100 N load cell. Samples were cut into 1 cm^3 cubic and compressed up to 50% strain at constant displacement rate of 1mm/min. The stress/strain curves were typically acquired for 5 replicates per type of sample.

- Data treatment

- *Directional analysis*

SEM images were analyzed using the Fiji software and the Orientation J plugin (OrientationJ, java plugin for Fiji/ImageJ, written by Daniel Sage at the Biomedical Image Group, EPFL, Switzerland[401]). Color orientation maps were obtained using orientation as hue value, constant saturation and original image for brightness. Cubic spline gradient was used with a 8 px Gaussian window.

- *Statistical analysis*

Data presented are typically the mean value on triplicate samples (mechanical compression of performed on 5 replicates, plate counting were usually performed on triplicate sample, and each sample was plate in triplicate). The error bars are standard deviation values.
For pore size analysis 150 measurements were typically performed on SEM images (100 measurements on a x50 magnification image and 50 measurements on a x100 magnification image). Data were presented in box-and-whisker plots, presenting median, value, mean value as well as 25th-75th and 5th-95th percentiles (see Figure A.1).

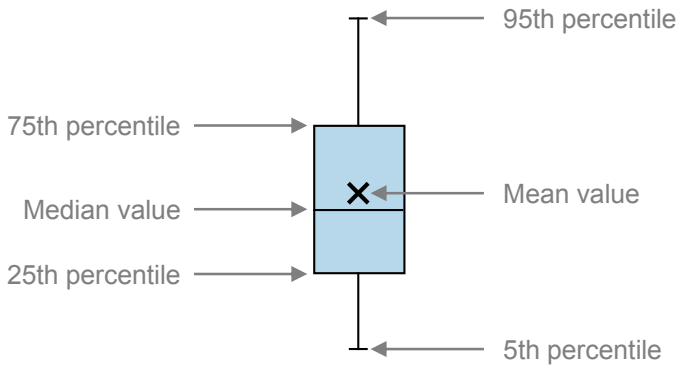

Figure A.1: Box-and-whiskers plots display the mean and median values as well as the 25^{th}-75^{th} and 5^{th}-95^{th} percentiles.

Statistical significance was tested using a Student test at two samples, using a level at the level of significance $p < 0.05$.

Experimental section

- Material

Commercials chemicals were usually purchased from Sigma-Aldrich and use as received. Solvents at reagent grade (ethanol, N,N-dimethylformamide) were purchased from VWR.
Beet root pectin was kindly provided by Estelle Bonnin and Catherine Garnier at the Biopolymères Interaction Assemblages laboratory at INRA Nantes
The reference soil was kindly provided by Pierre Barré at the Laboratoire de Géologie de l'ENS. The soil is upper horizon (0-30 cm) of silt loam Luvisol[507], developed on loess deposits. The texture of the samples was characterized by 18 % clay (particles < 2 µm), 57 % silt (2 µm < particles < 50 µm) and 25 % sand (particles > 50 µm). The cation exchange capacity (11 $cmol_{(+)}/kg$) is saturated mainly by calcium. The pH is 6.1 and the total organic carbon content of the upper horizon is 13 g_{carbon}/kg_{soil}. The soil was typically rehydrated with 0.16 mL_{water}/g_{soil} (18 mL of water for 110 g of soil).
Water use was typically deionized water (9.2 MΩ.cm). For microbiology, water was filtered at 0.2 µm.

- Microbiology

- *Culture media*

LB medium (lysogen broth, also known as Luria-Bertani medium) was prepared from deionized water and 20 g/L of commercial LB powder (Sigma-Aldrich Lennox broth, 10 g/L tryptone, 5 g/L yeast extract, 5 g/L NaCl). The solutions were autoclaved 2h at 100°C.
YPD (Yeast Peptone Dextrose) medium was purchased from Gibco.
Mineral media were prepared with the compositions presented in Table A.1 to Table A.6. The medium was sterilized by ultrafiltration at 0.2 µm. Simplified mineral medium was used for assessment of soil depollution (V.3.c) and MR1 medium was used for decolorization assays in liquid phase (V.3.b).

Table A.1: Simplified mineral medium composition (After Yang *et al.*[500]).

Compound	Concentration (g/L)
KH_2PO_4	1.5
Yeast Extract	1
NaCl	0.5
NH_4Cl	0.1
Lactate	2

Table A.2: MR1 medium composition.

Compound	Concentration (mM)	Concentration (mL/L)

NH_4Cl	8.5	/
K_2HPO_4	1.3	/
$MgSO_4.7H_2O$	0.23	/
KH_2PO_4	1.6	/
$(NH_4)_2SO_4$	1.7	/
Trace mix	/	1
Selenite mix	/	1
Vitamin mix	/	1
Amino acids	/	1
Lactate	30	/

Table A.3: Trace element mix composition.

Compound	Concentration (µM)
Na_2-EDTA	8.1
$FeSO_4.7H_2O$	4
$CoCl_2.6H_2O$	0.8
$ZnCl_2$	0.31
$NiCl_2.6H_2O$	0.1
$Na_2MoO_4.4H_2O$	0.087
H_3BO_4	4.8
$CuCl_2.2\ H_2O$	0.01
$MnCl_2.4H_2O$	0.25

Table A.4: Selenite mix composition.

Compound	Concentration (µM)
NaOH	12.5
$Na_2SeO_3.5H_2O$	11.4
$Na_2WO_4.2H_2O$	12.1

Table A.5: Vitamin mix composition.

Compound	Concentration (µM)
4-aminobenzoic acid	0.29
D-(+) biotin	0.041
nicotinic acid	0.81
Ca-(+) pantothenate	0.21
pyridoxamine dihydrochloride	0.41
thiaminium dichloride	0.29
Riboflavin	1.32

Table A.6: Amino acid mix composition.

Compound	Concentration (mM)
L-glutamic acid	13.6
L-arginine	11.5
DL-serine	19.6

- *Preparation of agar plates*

LB-Agar gels for plate counting were prepared from commercial LB-Agar powder (Sigma-Aldrich) dissolved at 35 g/L in deionized water and autoclaved 2h at 100 °C. Plates were prepared either with 20 mL of solution for Petri dishes (Ø=90 mm), or with 2 mL of solution per well in 12 well plates (Ø = 22 mm).

- *Bacteria storage*

Pseudomonas aeruginosa (ATCC® 27853™ strain) was stored at -80°C in 30% glycerol aliquots. About 10 µL of aliquot was added to 10 mL of LB medium in 30 mL glass tubes. The cell suspension was incubated 24h at 30°C and 150 rpm.

The optical density (OD) after this pre-culture was comprised between 0.8 and 0.9. This cell suspension was then diluted to 10^{-7} and 100 µL of this dilution was spread on a LB-agar plate in Ø=90 mm petri dish. This plate was incubated 24h at 37°C, resulting in the formation of 10

to 20 colonies on average (which corresponds to 1.10^9 to 2.10^9 CFU/mL). This plate was stored at 4°C up to 3 weeks and individual colonies were used to prepare fresh cultures before each experiment.

- *Bacteria culture*

Preparation of fresh cultures was always preceded by a pre-culture step. One colony of the previously mentioned storage plate was introduced in 10 mL of fresh LB medium in 30 mL glass tube and incubated 24h at 30°C and 150 rpm. The OD reached values around 0.8 on average. The culture itself was then made in 75 cm² culture flasks with 1.2 mL of the 0.8 OD pre-culture and 58.8 mL of fresh LB medium (dilution of the pre-culture by a 50 factor). Cultures were incubated at 30°C and 150 rpm for various times until the desired OD was obtained.

- *Bacteria encapsulation*

Bacteria were cultivated as previously mentioned, typically 5h up to 0.5 OD (viability was also investigated after 24h of culture). The culture was centrifuged 10 min at 5000 rpm and pellets were dispersed in water (typically 3 mL of water for 60 mL of culture). This suspension was the mixed with a solution at 50 g/L in pectin and 125 mM in PIPES (typically 1 mL of bacteria suspension for 4 mL of PIPES/pectin solution). The final concentrations were 40 g/L in pectin, 100 mM in PIPES and about 10^9 CFU/mL.

- *Plate counting*

Plate counting was generally performed in 12 well plates (see Figure A.2). Bacteria suspensions were obtained directly from culture or from dissolution of cellularized biopolymer foams in sterile water. In the case of cellularized hybrid foam, the matrix was previously shredded into less than 1 mm fragments and suspended in water before vigorous agitation.
The bacteria suspensions were diluted in water (logarithmic successive dilutions) and four dilutions were plated in triplicate for each sample. Plates were incubated 24 h at 37°C before counting. The number of CFU/mL was estimated using the dilutions yielding between 5 and 50 colonies.

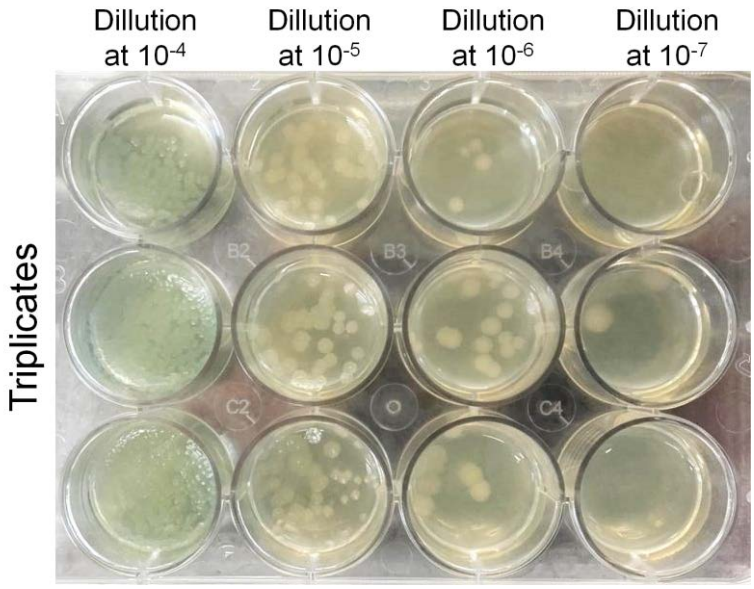

Figure A.2: For plate counting, 50 µL of 4 successive dilutions were spread in triplicate, in 12 well-plates filled with LB-agar gel.

- Titration

- *Reactive Black 5*

Reactive Black 5 (RB5) concentration were measured by UV-vis spectrometry at 598 nm. Typically, the samples were centrifuged 10 min at 5000 rpm and diluted by a factor 2 in 2X PBS to ensure constant pH in all measurements. The calibration curve used for concentration calculations is shown in Figure A.3.

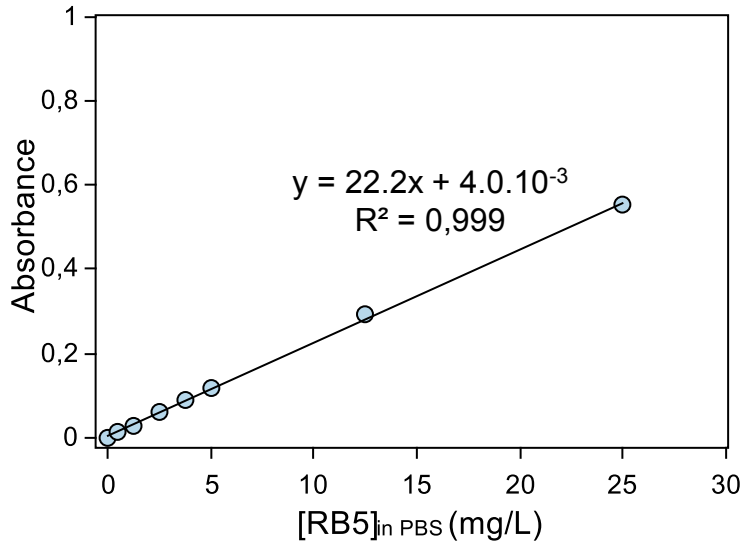

Figure A.3: Calibration curve for RB5 solutions at 598 nm.

- *RITC grafted pectin*

Beet root pectin was grafted with rhodamine isothiocyanate (RITC). A 10 g/L pectin solution in carbonate buffer (pH = 9.3) was prepared. 10 mL of 1 g/L solution of RITC in N,N-Dimethylformamide was added and the solution was left under magnetic agitation at room temperature overnight. The solution was dialysed using a MWCO 3500 membrane and freeze-dryed.
Samples (foams and calibration solutions) were typically prepared using 10 wt% of RITC-grafted pectin and 90 wt% of non-grafted pectin.
Uv-vis absorbance was measured at 558 nm and pectin concentration was calculated using the calibration curve presented in Figure A.4.

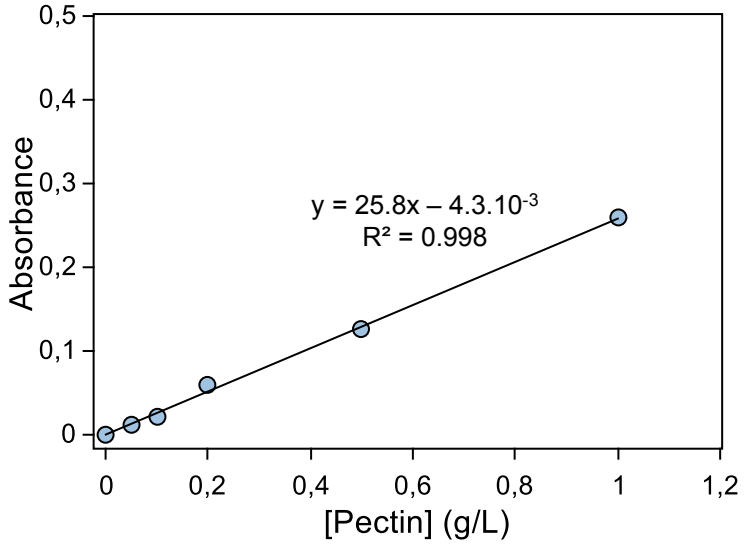

Figure A.4: Calibration curve for RITC-grafted pectin at 558 nm.

- *Silica*

Silica concentration was measured using the blue silicomolybdic titration method[427]. Typically 75µL of solution A (20 g/L ammonium molybdate tetrahydrate, 60 mL/L hydrochloric acid) was added to 800 µL of appropriately diluted samples (samples were left 24h under agitation at room temperature after dilution) to yield the formation of silicomolybdic acid. After 30 min at room temperature, 375 µL of solution B (20 g/L oxalic acid, 6.67 g/L 4-methylaminophenol sulphate, 4 g/L anhydrous sodium sulfite, 100 mL/L sulphuric acid) was added and the solution was left 2h at room temperature before the absorbance at 810 nm was measured.

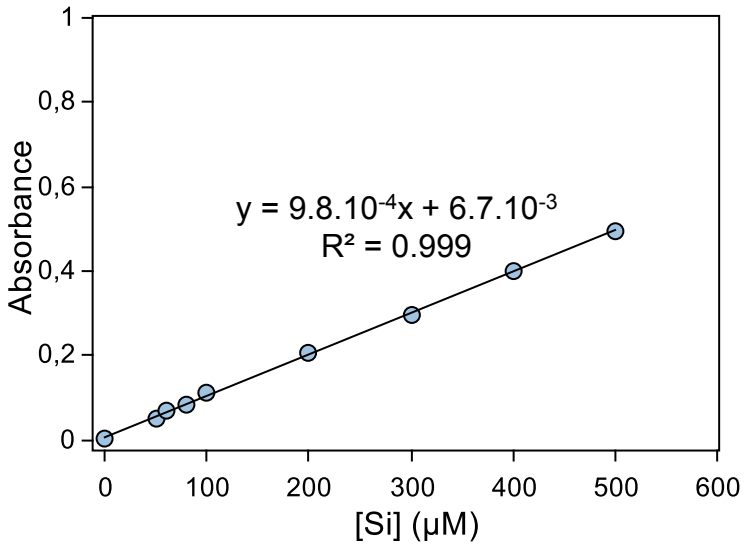

Figure A.5: Calibration curve for silicon content (blue silicomolybdic titration method) at 810 nm.

- Ice-templating

- *Freeze-casting*

Freeze-casting was performed using the setup presented in Figure A.6. The setup was composed of a copper rod (Ø = 15 mm) plunging into a liquid nitrogen tank. A heating resistance and a thermocouple were adjusted on the cold finger and linked to a PID controller to control the temperature at the top of the copper finger. Polypropylene (PP) molds could be adapted on top of the copper rod to put samples in contact with the cold finger.
In typical experiments 3 mL of suspension (pectin or alginate solution, with or without cells) were placed in the PP mold and equilibrated 3 min at 20°C. a chosen temperature ramp (between 1°C/min and 10 °C/min) was then applied down to -60°C.

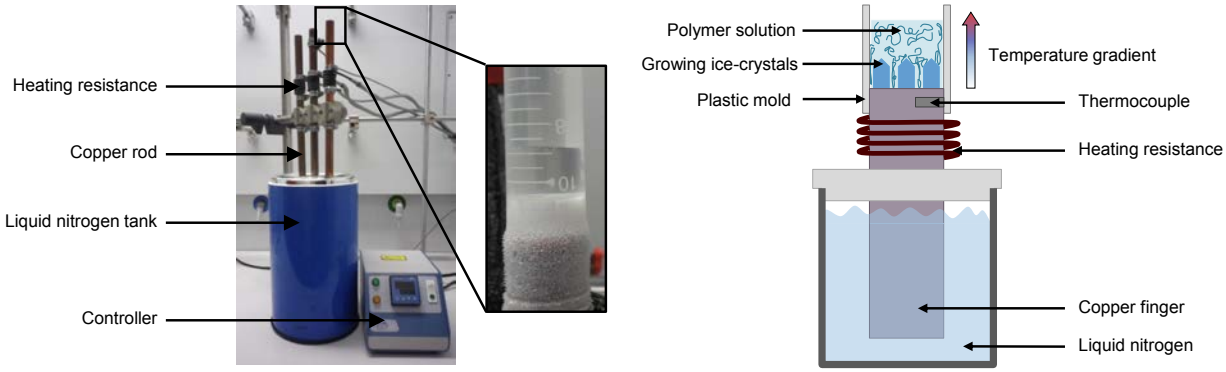

Figure A.6: Freeze-casting setup.

- *Alternative freezing methods*

Samples were frozen in different conditions for comparison with the freeze-casting technique. Conventional freezers at -20°C and -80°C as well as a liquid nitrogen bath were used.

Typically 4 mL of solution was poured in a Ø = 19 mm polyethylene mold or 1.8 mL was poured in a 2 mL cryotube. The sample was then placed overnight into the freezer or 5 min in a liquid nitrogen bath.

- *Drying*

Frozen samples were lyophilized in a Christ Alpha 2-4 LD freeze-dryer under a 0.05 mbar vacuum. Samples were dried at 24 h, either directly in the freeze-dryer chamber or in side vials.

- Sol-gel chemistry

- *Vapor phase deposition*

Biopolymer foams were kept at least 24 h in a desiccated atmosphere and weighed before the beginning of the silica deposition. Cylindrical samples were cut down to the desired thickness and place in the deposition chamber presented in Figure A.7. The chamber diameter approximate volume was 1 L. The setup was composed of a saturated NaCl acid aqueous solution (typically 17 mL of 37 % HCl, 133 mL of water and 60 g of NaCl) and of 4 vials (Ø = 29 mm) containing 10 mL of tetraethyl orthosilicate (TEOS). The deposition chamber was sealed a kept at 30°C typically between 1 and 14 days. The samples were then kept 24 h at 30°C in an open container and 24 h at room temperature in a desiccated atmosphere before final weighing.

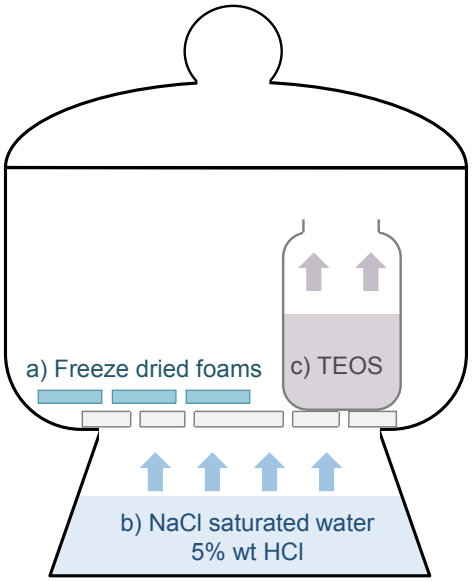

Figure A.7: Freeze-dried macroporous pectin foams (a) were place in a closed vessel in presence of an acidic atmosphere (b) and vapors of TEOS (c). The deposition chamber was maintained at 30°C throughout the deposition process.

- *Liquid aqueous route*

Freeze-casted alginate foams were crosslinked 24 h at 4°C in a 0.5 M $CaCl_2$ solution. After rinsing the sample were plunged in a solution containing typically 2 mL of LUDOX TM-50 ($[Si]_{LUDOX}$ = 7.8 M) and 2 mL of sodium silicates ($[Si]_{silicates}$ = 0.2 M) and acidified to pH = 5 with HCl 4 M (total [Si].= 4 M). After 45 min (before gelling) the samples were removed and rinsed with water. After 45 min at room temperature samples were stored in sterile water at 4°C.

- In-soil assays

- *Ageing in soil*

The fate of hybrid macroporous foams in a reference soil (upper horizon silt loam Luvisol) was assessed over a least one month. Samples (typically 40 mg) were buried in 110 g of soil previously rehydrated with 18 mL of deionized water. The vials were sealed with Parafilm® and kept at 20°C. The state of the foams was regularly assessed visually for macroscopic aspects and with SEM for microscopic structure.

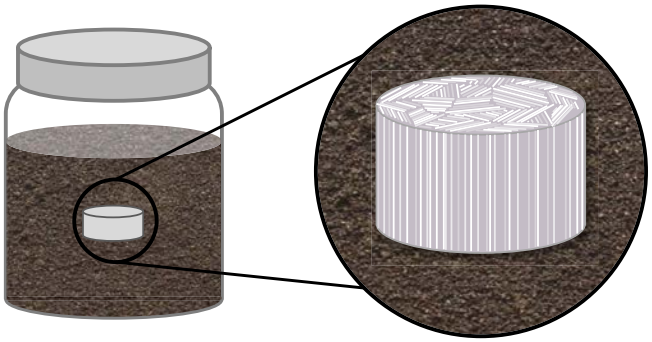

Figure A.8: Ageing behavior of macroporous hybrid foams was assessed in a upper horizon silt loam Luvisol.

- *Behavior in simulated polluted soils*

Influence of macroporous hybrid foams (with or without encapsulated bacteria) on polluted soil was assessed using Reactive Black 5 (RB5) as a model contaminant.
10 g of soil was saturated with 7 mL of RB5 solution (typically 100 mg/L in water or 500 mg/L in mineral medium). The soil was incubated (either 24 h at 25 °C or 42 h at 37 °C) and washed with 7 mL of PBS 2X. The supernatant was then centrifuged 10 min at 5000 rpm and absorbance at 598 nm was measured to calculate the residual RB5 concentration (see calibration curve p 207).

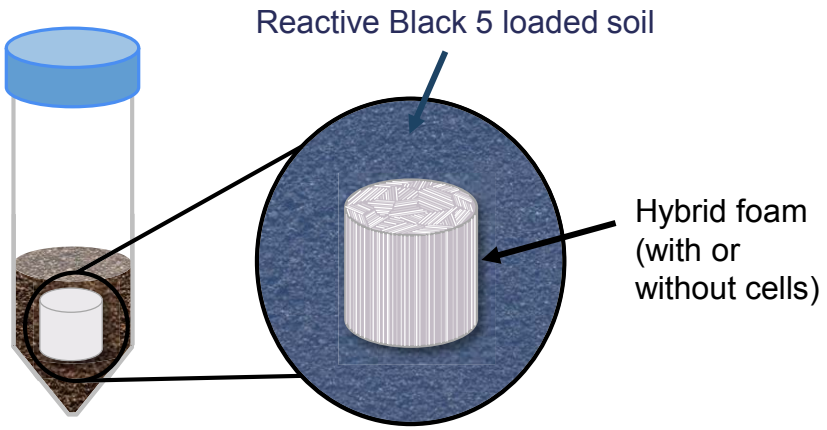

Figure A.9: Influence of macroporous hybrid foams on simulated polluted soils was assessed using RB5 as a model contaminant.

Complementary results

- Foam wetting behavior

Material and methods

Pectin foam were prepared by freeze-casting as previously described. Foams were prepared from 20 g/L, 30 g/L, 40 g/L and 50 g/L aqueous pectin solutions at 10 °C/min and from 40 g/L pectin solution at 1°C/min, 5 °C/min and 10°C/min. Samples were vacuum dried 48 h at 0.05 mbar and cut to about 0.8 cm height. Samples were put in contact with the surface of a solution of Disperse Red 1 (0.2 g/L) in ethanol. The wetting was recorded and the wetting profile was extracted from the videos using the Fiji software.

Only a limited number of points were recorder for each wetting profile due to the rapid foams impregnation. All samples (regardless of the initial polymer concentration or freezing rate) had similar impregnation profiles, despite variations in the size and shape of the pore (see II.4).

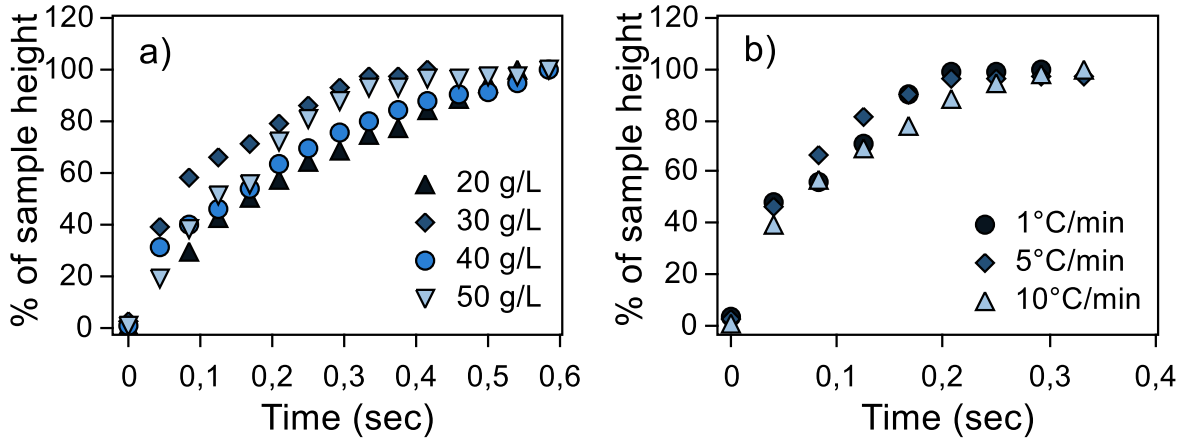

Figure A.10: Pore size variations induced by different initial pectin concentration or freezing rates have no significant effect on the wetting profiles of the foams.

- Assessment of the reproducibility and robustness of the vapor phase silica deposition process

Material and method

Pectin samples were prepared as previously mentioned by plunging 1.8 mL of 40 g/L pectin solution in liquid nitrogen and subsequently freeze-drying the samples.
Samples were placed in the silica deposition chamber with either 5 wt% or 20 wt% HCl solution, with or without NaCl (400 g/L). Either 4 vials with either 10 mL or 20 mL of TEOS were introduced in the chamber.
Reproducibility of the method was also assessed by adding silica to a large number of samples at the same time (18 samples, half were removed after 7 days of exposition and the rest was left 14 days in the chamber). HCl concentration was 5 wt% and 400 g/L of NaCl were added to the acidic aqueous solution. 4 vials with 10 mL of TEOS were introduced in chamber.

Figure A.11 a presents silica contents variations depending on the deposition time for a wide range of conditions (different initial TEOS amounts, HCl concentrations and presence of NaCl). No clear influence of the tested parameters can be observed. The general deposition kinetics appears to be independent of the three tested parameters. Each set of conditions was however only tested on a limited number of samples, so that these assays do not take in account possible variations in a series of sample exposed to the same conditions.
To assess distribution of the added silica content on samples place simultaneously in the deposition chamber 18 samples were exposed to TEOS vapors. Two deposition times were investigated (7 days for 9 samples and 14 days for 9 samples).
When a large number of samples are silicified at the same time, a wide distribution of silica content can be observed. The histogram of the silica contents is presented in Figure A.11 b. Mean values are 35 ± 13 $\%_{SiO2}$ and 50 ± 7 $\%_{SiO2}$ for samples left 7 days and 14 days respectively. After only 7 days of silica depositions silica content range from 16 $\%_{SiO2}$ to 53$\%_{SiO2.}$ After 14 days, the mean silica content increases, but most interestingly the values distribution is much smaller. This may be explained by the fact that TEOS content may not be homogeneously distributed throughout the sealed vessel, as was demonstrated in the case of TMOS vapors[415]. Samples closer to TEOS vials may have higher silica contents. The diminution of the distribution width at long deposition times may be explained by the saturation phenomenon previously described. Samples closer to the precursor source may be coated faster, but final silica content are similar.

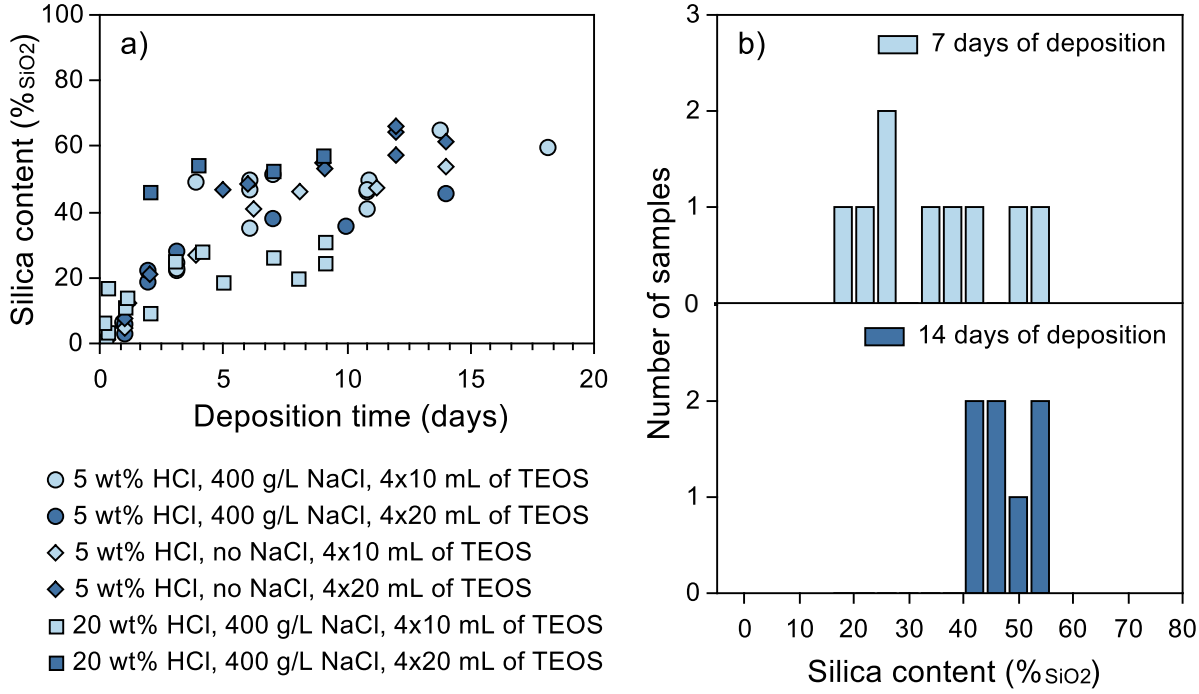

Figure A.11: Silica content evolution does not seem to depend strongly on the HCl and NaCl content or on the introduced volume of TEOS (a). A wide distribution of silica content may be observed when a large number of samples are coated simultaneously, however this distribution is narrower after longer deposition times (b).

- Encapsulation of yeasts in pectin-silica hybrid foams

Material and methods

Pectin foams containing encapsulated S. cerevisiae cells were prepared as previously described. The foams were then immerged for 10h in pre-hydrolyzed TEOS at room temperature. The sample were then rinsed with a 50/50 water/ethanol mixture and dried at room temperature. The cell loaded hybrid materials were observed in SEM microscopy, after sputtering with 20 nm of gold.

The dry hybrid foams were immerged in a methylene blue solution and kept under static conditions at room temperature until complete discoloration of the dye. Non-encapsulated yeast cells and foam with no encapsulated cells were used as controls.

The silica deposition protocol results in strong contraction and deformation of the foams (Figure A.12 a, b and c). This is mainly due to the rinsing and drying step, where the material is subjected to high capillary forced. The use of several successive bath of increasing ethanol content may diminish the contraction of the foams. This may represent an advantage from the structural point of view, but contact with absolute ethanol is cytotoxic for most cells. *S. cerevisiae* are however use in brewery and have a certain degree of tolerance towards the presence of ethanol. Furthermore, the cells are embedded in a pectin layer which may provide additional protection against deleterious effects of ethanol. As a result a 50/50 water/ethanol mixture seemed to be an acceptable compromise between the structural properties and the viability of the encapsulated species.

After silica deposition, the cells can still be seen within the pectin pore walls. On top of the pectin layer, a smooth looking layer of silica can be observed (Figure A.12 a', b' and c').

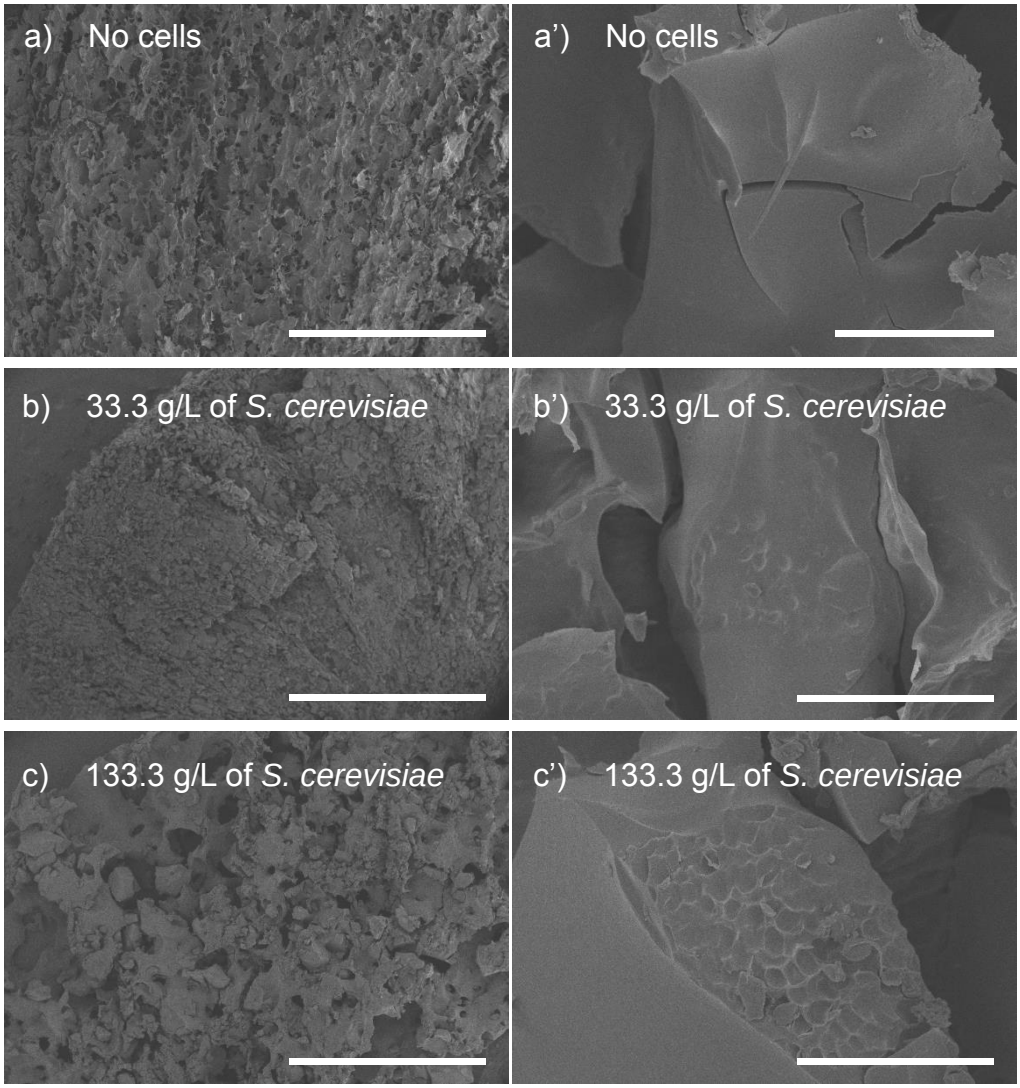

Figure A.12: SEM observation of *S. cerevisiae* cells in pectin foams. Foams containing 0 g/L (a and a'), 33.3 g/L (b and b') and 133 g/L (c and c') of yeast cells are slightly contracted by the rinsing and drying treatment. Cells can still be seen within the silica coated pectin wall. Scale bars: 1 mm in a, b and c, 20 µm in a', b' and c'.

Discoloration efficiency towards methylene blue of the encapsulated yeast was assessed in an aqueous solution of methylene blue dye at room temperature.

The foams containing no yeast were able to adsorb the methylene blue, but this resulted in the coloration of the foams themselves (Figure A.13 b). On the contrary, the samples containing yeast remained colorless, which means that the dyes was adsorbed but also efficiently reduced into its colorless form. It is however to be noticed that the discoloration occurs significantly slower compared to a suspension of free yeast cells. This might be attributed to a loss of viable cells during the various steps of encapsulation since freezing, drying under vacuum, silica deposition and rinsing with a 50% ethanol solution may all be deleterious to the survival and metabolic activity of *S. cerevisiae.* In addition diffusion issues must also be taken in account since the substrates must go through both the silica and pectin layers, resulting in significantly slower kinetics.

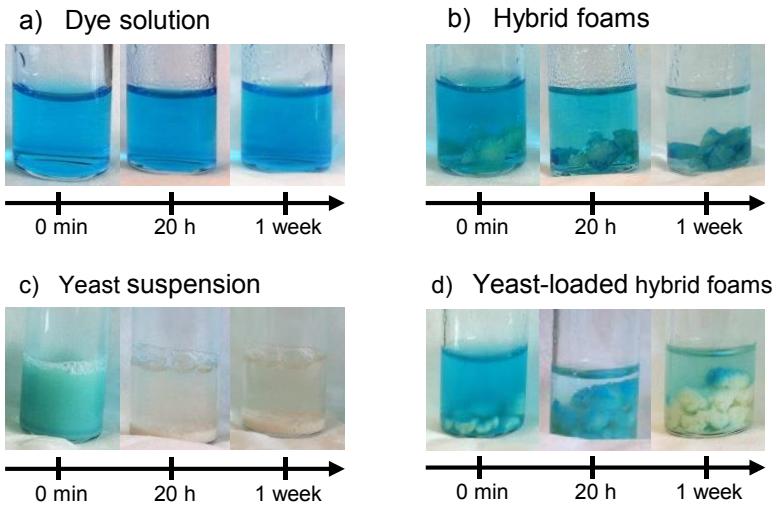

Figure A.13: Foams containing encapsulated yeasts (d) were able to efficiently discolor a methylene blue solution (a). Non-encapsulated yeast (c) were able to discolor the dye solution quicker, but control foams with no encapsulated yeast (b) were only able to adsorb the model of pollutant.

The *S. cerevisiae* / methylene blue system has been used as a model to show the feasibility of a depolluting device based on microorganisms entrapped in a pectin-silica hybrid matrix. This model is however limited since methylene blue is only reduced to a colorless state. In addition *S. cerevisiae,* though being a common and useful model in microbiology, has no significant uses in bioremediation.

This encapsulation assay with a simple and sturdy microorganism however works as a good proof of concept toward the encapsulation of more relevant, but also more sensitive organisms such as bacteria.

- EDX analysis of alginate and pectin foam after vapor phase silica deposition process

Material and methods

Polymer foams were obtained by freeze-casting of 40 g/L solutions of polymers (either beet root pectin or sodium alginate) at 10 °C/min and vacuum dried during 24 h.. Dry foams were cut to 1 mm thick discs and maintained 24h in a desiccated atmosphere before weighting of the initial mass. The samples were then placed in a vapor phase silica deposition chamber in presence of a 5 wt% HCl in water mixture saturated by NaCl and four vials containing 10 mL of TEOS. The samples were removed after 4 or 10 days. The samples were left 24h at 30°C and ambient humidity and 24h at room temperature in a desiccated atmosphere before final weighing. For energy-dispersive X-Ray spectroscopy (EDX) samples were sputtered with 20 nm of carbon.

Atomic analysis of the pectin-based samples revealed the presence of high amounts of silicon and oxygen (see Figure A.14 a). The theoretical oxygen: silicon ratio in silica is 2 : 1. However in silica obtained through sol-gel at ambient temperature defects are to be expected. In this case however, the polymer itself contains non-negligible amounts of oxygen which limits the quantitative aspect of this analysis. It must also be pointed out that the EDX technique usually requires the use of plane and smooth surfaces for quantitative analysis, which is not the case here. This analysis however remains a good source of qualitative information regarding the nature of the observed layer. Mapping of the identified elements (see Figure A.14 a') confirms that the silicon and oxygen are homogeneously distributed on the pectin pore wall. EDX analysis on alginate-based foam highlights the presence of high amount of chlorine and sodium, and lower amounts of silicon and oxygen (see Figure A.14 b). The presence of silicon may indicate the partial deposition of silica on the alginate surface. Once again, the presence of oxygen can largely be attributed to the polymer itself, but part of it may be due to the presence of small silica contents. The high chlorine and sodium amounts can easily be traced to the nature of the polymer and the conditions used for silica deposition. In this case the polymer used is alginate, or more precisely alginic acid sodium salt. This means that non-negligible amounts of sodium are introduced in the initial solution and remain in the solid foam after drying. The silica deposition chamber is saturated by a HCl/water atmosphere. As a result it is not surprising to detect traces of chlorine on the samples. Part of the chlorine may be deposited on the pore wall and in presence of the sodium form crystals of sodium chloride, which can be observed as geometric structure on the polymer surface. This theory is supported by the element mapping (see Figure A.14 b'), which shows that oxygen and small amounts of silicon are homogeneously distributed on the pore wall, while chlorine and sodium are concentrated on the square-shaped structures observed in SEM.

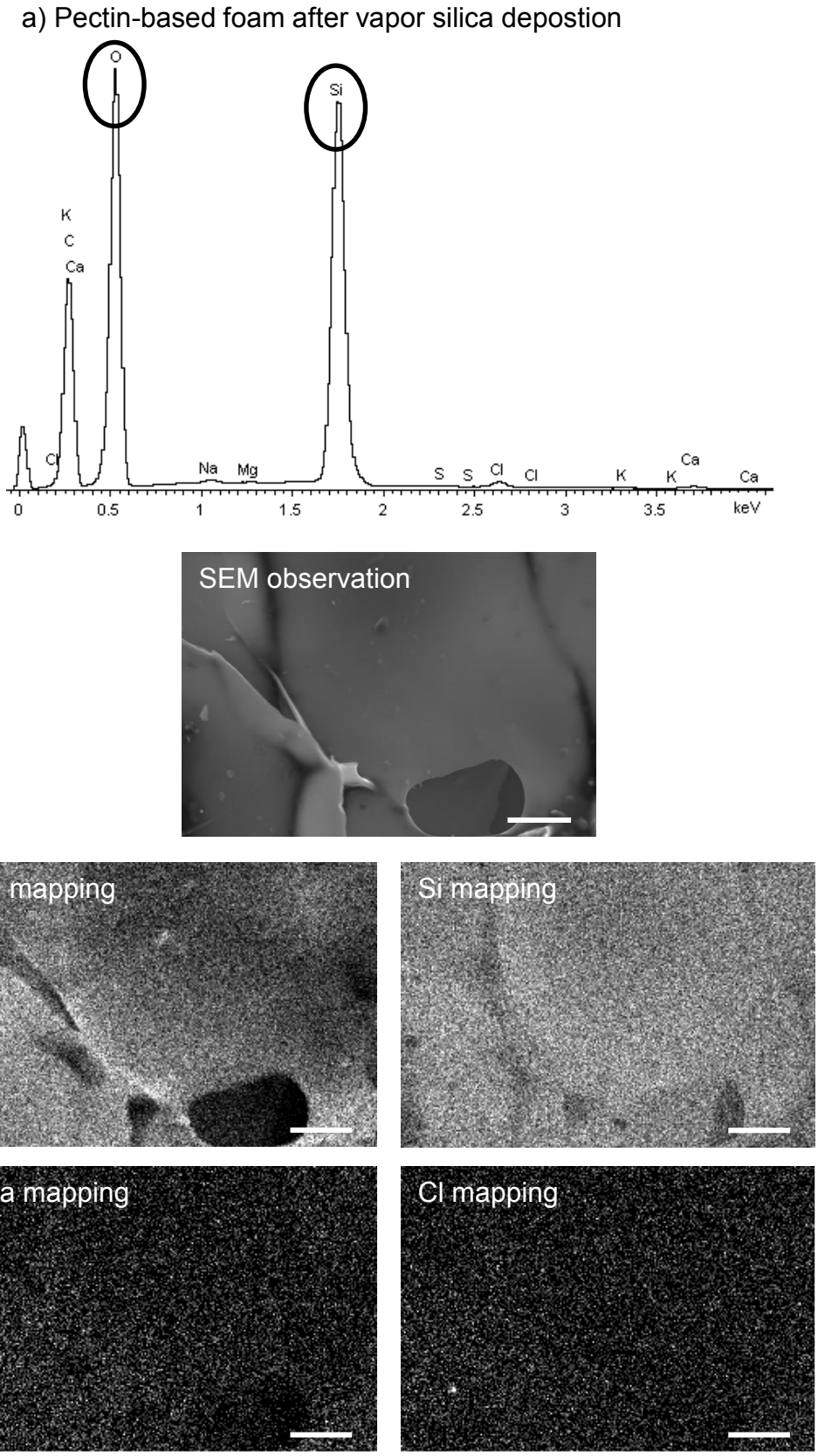

Figure A.14: Pectin-based foams present high contents of oxygen and silicon (a) which may be assumed to be part of a silica layer. These two elements are homogeneously distributed on the whole pore wall surface (a'). In alginate-based material, the two main detected elements are sodium and chloride (b). They are mainly concentrated in the square-like structures observed on the surface of the pore wall (b') which are likely to be NaCl crystals. Scale bars: 10 μm.

b) Alginate-based foam after vapor silica depostion

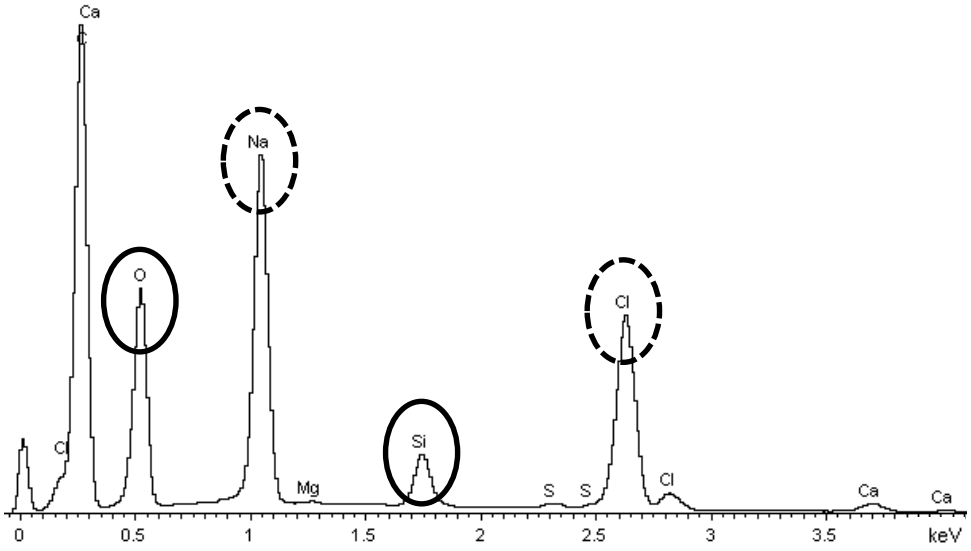

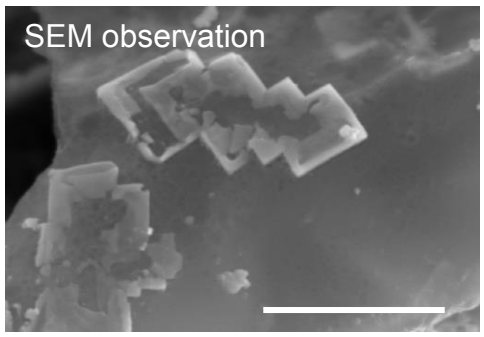

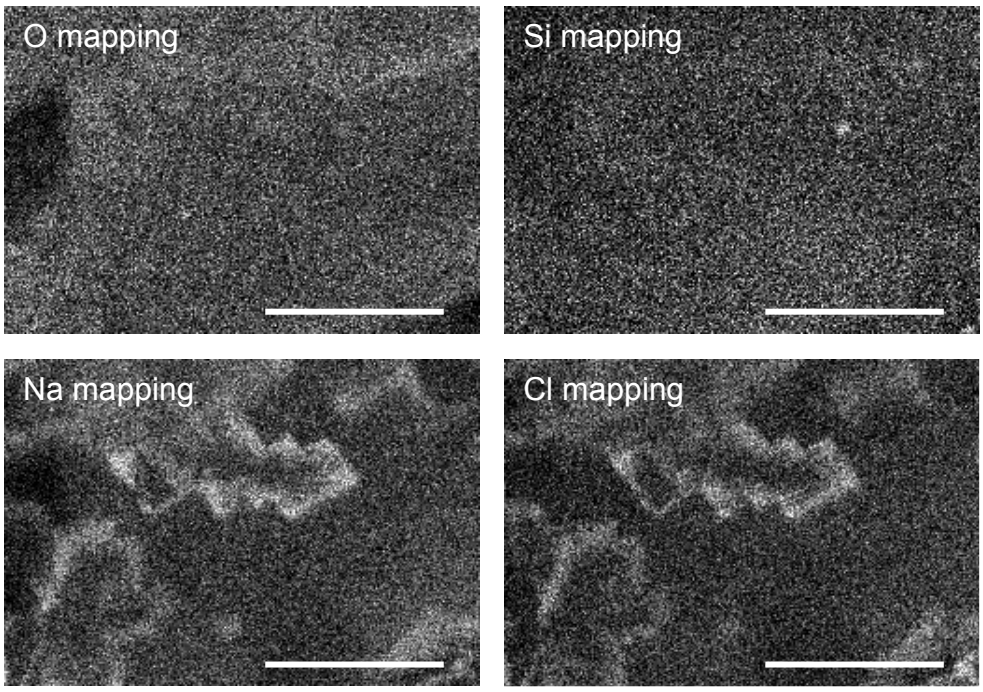

Figure A.14(continued): Pectin-based foams present high contents of oxygen and silicon (a) which may be assumed to be part of a silica layer. These two elements are homogeneously distributed on the whole pore wall surface (a'). In alginate-based material, the two main detected elements are sodium and chloride (b). They are mainly concentrated in the square-like structures observed on the surface of the pore wall (b') which are likely to be NaCl crystals. Scale bars: 10 µm.

Abbreviations

AU	Arbitrary Unit
CFU	Colony Forming Units
CNRS	Centre National de la Recherche Scientifique
DM	Degree of methylation
EDX	Energy Dispersive X-Ray
ENS	Ecole Normale Supérieure
EPT	Equilibrium Partition Theory
FC	Freeze-casting
GalA	Galacturonic acid
HG	Homogalacturonan
HM	High methoxy
INRA	Institut National de la Recherche Agronomique
IR	Infra Red
K_{ow}	Octanol-water partition coefficient
LB	Lysogen broth (also known as Luria-Bertani medium)
LM	Low methoxy
NMR	Nuclear Magnetic Resonance
OD	Optical density
PBS	Phosphate Buffer Saline
PIPES	Piperazine-N,N′-bis(2-ethanesulfonic acid)
PVA	Poly(vinyl alcohol)
RB5	Reactive Black 5
RG-I	Rhamnogalacturonan I
RG-II	Rhamnogalacturonan II
Rha	Rhamnose
RITC	Rhodamine isothiocyanate
SEM	Scanning Electron Microscopy
TEM	Transmission Electron Microscopy
TEOS	Tetraethoxy silane (also known as tetraethyl orthosilicate)
TGA	Thermogravimetric Analysis
TMOS	Tetramethyl orthosilicate
UV-Vis	Ultraviolet-visible

Résumé en Français

Au cours des dernières années, l'importance de l'impact environnemental humain sur les différents écosystèmes de la planète s'est imposée comme un enjeu majeur dans la conscience collective. Cette prise de conscience a engendré de nombreuses initiatives pour la surveillance, la prévention ou la remédiation des sites pollués, tant au niveau individuel qu'à l'échelle internationale. La pollution des sols représente un problème d'autant plus sérieux puisque la contamination ce type d'écosystème est susceptible d'avoir des répercussions sur un grand nombre d'organismes vivants par le biais de dispersion et bioaccumulation (lixiviation des sols, accumulations dans les plantes et microorganismes etc…). De plus, les sont particulièrement difficiles à traiter, en comparaison avec des eaux usées par exemple. Les approches *ex situ* impliquent des contraintes logistiques non négligeables et sont susceptibles de perturber fortement les écosystèmes considérés. Les approches *in situ* sont, elles, soumises aux limitations intrinsèques d'un milieu solide complexe et dynamique.

La bioremédiation est la réponse de la Nature à la contamination d'un écosystème donné. Elle consiste en l'accumulation ou la dégradation de polluants par des organismes vivants, notamment des plantes, mais aussi des animaux (comme des insectes ou vers de terre par exemple) ou encore des microorganismes (soit eucaryotes, *i.e.* des champignons, soit procaryotes, *i.e.* des bactéries). Les capacités de récupération des écosystèmes (bioatténuation) ne sont cependant pas toujours suffisantes pour engendrer un retour total ou suffisamment rapide du sol à son état initial. Dans ce cas-là, deux approches principales peuvent être envisagées pour compléter la récupération naturelle du sol. La biostimulation consiste en l'ajout de différents nutriments dans le sol pour accroitre l'activité métabolique des populations microbiennes endogènes. La principale limite à cette approche est cependant la composition des populations microbiennes qui ne sont pas nécessairement adaptées aux contaminants considérés. La bioaugmentation consiste, elle, en l'introduction d'organismes exogènes pour afin de mettre en place une communauté microbienne capable de dégrader les polluants ciblés. Cette approche est cependant soumise à certaines restrictions puisqu'elle implique l'ajout dans le sol de microorganismes susceptibles de causer des déséquilibres notables dans l'écosystème considéré. L'usage d'organismes vivants, peu importe le type de bioremédiation envisagé, est limité par leur sensibilité vis-à-vis de leur environnement direct. Les propriétés physico-chimiques du sol (par exemple la concentration en contaminants ou co-contaminants, le pH, la salinité, la température etc…) peuvent être préjudiciables à la viabilité ou l'activité métabolique des microorganismes impliqués dans les mécanismes de bioremédiation.

Une approche pour limiter l'impact de l'environnement des microorganismes est l'immobilisation des cellules dans une matrice permettant de les accueillir et de les protéger de condition physico-chimiques nuisibles. De plus, ce type d'encapsulation peut permettre de minimiser la dissémination des microorganismes exogènes dans l'écosystème considéré afin de prévenir de possibles déséquilibres. L'élaboration d'une matrice idéale pour l'encapsulation d'organismes vivants présente cependant un défi à de nombreux niveaux.

Les deux objectifs principaux des approches de bioremédiation basées sur des organismes encapsulés sont l'efficacité du procédé de dépollution et le confinement des organismes exogènes. Ces deux objectifs sont cependant soumis à l'influence d'un grand nombre de paramètres (voir Figure A.15). Certains de ces paramètres dépendent directement des caractéristiques du site pollué (type de sol, température, propriétés physico-chimiques du sol mais également nature du contaminant) mais d'autres sont plutôt liées au matériau cellularisé lui-même. Le matériau peut être considéré comme l'association d'une unité fonctionnelle (les microorganismes encapsulés) et d'une unité structurale (la matrice d'encapsulation). L'efficacité du procédé de dépollution dépend principalement de l'activité métabolique des organismes encapsulés, mais la structure de la matrice est également susceptible d'avoir une influence significative puisqu'elle modifie les phénomènes de diffusion des substrats et donc la cinétique de dépollution. Les aspects fonctionnels et structuraux doivent donc être considérés pour l'élaboration d'un matériau efficace pour la dépollution des sols.

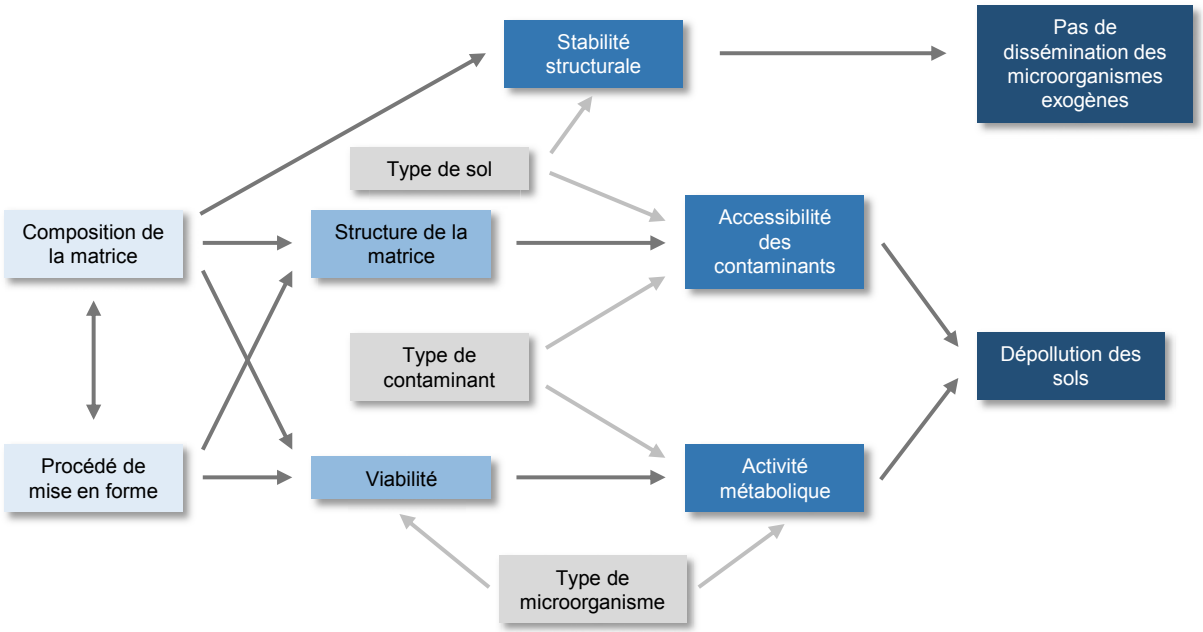

Figure A.15: Les procédés de bioremédiation reposant sur l'utilisation de microorganismes encapsulés comme unités fonctionnelles sont influencés par une large gamme de paramètres interdépendants.

Le contrôle de ces aspects peut être modulé par deux voies interdépendantes. La composition de la matrice d'encapsulation doit être sélectionnée de façon à assurer la non-toxicité vis-à-vis des organismes encapsulés, mais également vis-vis de l'ensemble de l'écosystème considéré. Le choix des composants de la matrice doit aussi tenir compte des exigences en matière de stabilité dans les sols, afin de minimiser la dissémination des organismes exogènes immobilisés. Le choix de la composition ne peut cependant pas être fait indépendamment des considération d'ingénierie des matériaux et plus particulièrement des aspects de mise en forme des matériaux qui doivent être compatibles avec la survie des microorganismes immobilisés.

Concernant la composition de la matrice, la littérature met en lumière l'intérêt des biopolymères comme matrices d'encapsulation. Ces polymères peuvent être trouvés dans les organismes vivants notamment dans les matrices extracellulaires ou les parois cellulaires des plantes. En conséquence la majorité de ces biopolymères présentent une bonne cytocompatibilité, ce qui est essentiel pour l'encapsulation de cellules. Cette cytocompatibilité va cependant souvent de pair avec une biodegradabilité, ce qui peut être un avantage important pour des applications biomédicales, mais peut se révéler problématique du point de vue de la stabilité de la matrice. Une approche permettant la modulation des propriétés de la matrice, tout en conservant une partie de la composition chimique du matériau, consiste en l'utilisation de structures hybrides ou composites. De fait l'utilisation d'une structure hybride biopolymère-inorganique et plus particulièrement l'utilisation de matériaux hybride biopolymères-silice pourrait s'avérer utile dans l'élaboration de matériaux pour la bioremédiation des sols.

Du point de vue structural, les matrices d'encapsulation peuvent adopter de nombreuses formes. Concernant l'application ciblée, l'utilisation d'un matériau macroporeux pourrait être un avantage notable du point de vue de de la diffusion des substrats. La méthode du freeze-casting peut être utilisée pour mettre en forme de nombreux matériaux (des céramiques aux polymères) de façon à obtenir une large gamme de matériaux à porosité contrôlée et notamment des matériaux à porosité orientée. Ce type de porosité pourrait représenter un avantage décisif pour faciliter la mobilité des substrats ciblés par transport capillaire.

Ces travaux portent donc sur l'élaboration de matériaux hybrides contenant des microorganismes encapsulés *via* un procédé de freeze-casting. L'approche pour la préparation de ces matériaux est basée sur un procédé en deux étapes :

1. encapsulation des microorganismes choisis dans une matrice poreuse de biopolymère par freeze-casting

2. dépôt d'une couche de silice par chimie du sol-gel

Chacune de ces étapes doit être adaptée à la nature des composés utilisés et contrôlée pour garantir la morphologie souhaitée et la compatibilité avec la survie cellulaire. La stratégie adoptée pour identifier les paramètres d'intérêt pour le contrôle structural et fonctionnel des matériaux a été de commencer par l'élaboration séquentielle du matériau hybride en l'absence de microorganismes (obtention d'une structure de biopolymère à porosité orientée et dépôt de silice par. Le procédé ainsi mis au point a ensuite été utilisé pour l'obtention du matériau cellularisé, les différentes étapes étant modulées pour garantir une survie optimale des microorganismes (voir Figure A.16).

Les possibilités en terme de structure et de morphologie ont dans un premier temps été évaluées par congélation de pectine de betterave en solution aqueuse. Plusieurs dispositifs de congélation ont été étudiés (congélation dans des congélateurs conventionnels à -20°C et -80°C, utilisation d'un bain d'azote liquide et utilisation d'un montage de freeze-casting). Ces essais ont permis de mettre en évidence le rôle de la présence d'un gradient de température dans l'obtention de de matériaux avec une porosité orientée.

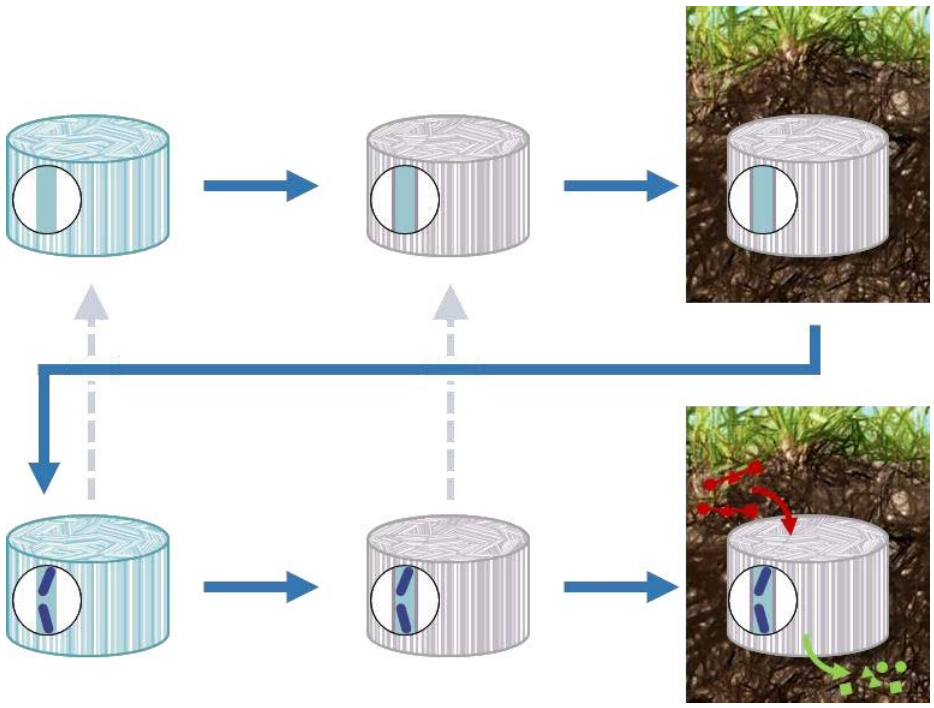

Figure A.16: Le procédé de mise en forme a d'abord été mis au point en l'absence de microorganismes de façon à identifier les paramètres pertinents du point de vue structural. Le procédé a ensuite été adapté pour l'encapsulation de microorganismes. L'efficacité du matériau pour des applications de dépollution a enfin été évaluée dans un sol de référence contenant un polluant modèle.

Les mousses macroporeuses de pectine ainsi obtenues ont ensuite été modifiées par l'addition d'une couche de silice à la surface des parois des pores. La silice a été déposée par exposition des mousses de pectine à des vapeurs de tétraéthyl orthosilicate en présence d'une atmosphère acide à humidité contrôlée afin de permettre l'hydrolyse et la condensation à la surface des parois des pores, tout en limitant leur dissolution. Cette méthode a permis l'obtention d'une couche de silice entièrement percolée et homogène, sans obstruction des pores. La cinétique de dépôt a pu être contrôlée pour maîtriser l'épaisseur de la couche déposée de façon à influencer les propriétés mécaniques du matériau. La structure hybride peut ainsi être décrite comme un matériau hybride macroporeux avec des parois présentant une structure de type cœur-coquille. La présence de silice a permis de limiter la dissolution des mousses dans des conditions hydratées. Le vieillissement des mousses a notamment été observé dans un sol de type Luvisol, où les matériaux ont présenté une bonne stabilité durant 5 semaines. Ces matériaux hybrides ont également été utilisés pour l'adsorption en milieu liquide d'un polluant modèle (Reactive Black 5, un colorant fréquemment utilisé dans l'industrie textile). Les matériaux ont également été testés dans un sol imprégné par une solution du même colorant. La diminution de la concentration apparente en colorant dans le sol pourrait être une indication de la capacité des substrats à diffuser du sol vers le matériau.

La structure ainsi mise au point a ensuite été utilisée comme matrice d'encapsulation pour des organismes avec des capacités de bioremédiation. Les composants et les méthodes de mise en forme ont été choisis initialement en tenant compte des contraintes imposées par la présence finale des microorganismes (utilisation d'eau comme solvant, températures modérées, utilisation de biopolymères). L'utilisation du freeze-casting comme méthode d'encapsulation a d'abord été confirmée sur la levure *Saccharomyces cerevisiae* comme organisme modèle. La densité de cellules viables, la viscosité de la solution de polymère utilisée ainsi que la vitesse de front de glace employés ont notamment permis d'assurer l'immobilisation des cellules à l'intérieur des parois des pores du matériau. L'activité métabolique des cellules après congélation et séchage a pu être partiellement conservée. Les levures sont de on modèles de laboratoire mais n'ont pas d'intérêt spécifique en matière de bioremédiation. Un deuxième modèle, la bactérie *Pseudomonas aeruginosa*, a donc été étudié. La méthode du freeze-casting s'est également avérée compatible avec la survie des bactéries, en dépit du stress biologique induit par la congélation et la lyophilisation. Les procédés de cryoprotection et lyoprotection conventionnels nécessitent généralement l'utilisation d'additifs comme le glycérol ou le tréhalose. Dans le cas de l'encapsulation par le biais du freeze-casting aucun cryoprotecteur n'a été utilisé. La présence de biopolymère semble cependant fournir un

certain degré de protection vis-à-vis des dommages causés par les contraintes osmotiques et mécaniques lors de la congélation. La vitesse de congélation est également un paramètre crucial dans les protocoles conventionnels de cryoprotection. La technique du freeze-casting a l'avantage de coférer un bon contrôle sur les vitesses de refroidissement, ce qui a permis l'optimisation des taux de survie cellulaire lors de l'encapsulation. L'encapsulation dans une matrice de pectine de betterave s'est cependant avérée limitée du point de vue de la survie à long terme. Cette limitation est problématique compte-tenu des durées importantes (plusieurs jours à plusieurs semaines) nécessaires à l'obtention d'une couche de silice d'épaisseur suffisante par la méthode du dépôt en phase vapeur.

La composition de la matrice a donc été modifiée par l'usage de différents polysaccharides. Un meilleur taux de survie des bactéries encapsulées a été observé dans les matrices d'alginate comparées aux matrices de pectine, en particulier après 24h de stockage. Le dépôt de silice en phase vapeur était cependant fortement ralenti dans le cas de l'alginate. Le dépôt de silice a donc été effectué par le biais de chimie-sol gel en phase aqueuse (utilisation d'un mélange de silicates de sodium et d'un mélange commercial de particules de silice colloïdale), en utilisant des possibilités de réticulation de l'alginate en présence d'ions divalents (ici Ca^{2+}). Les matériaux hybrides obtenus par ce procédé sont stable jusqu'à 2 mois dans le sol de référence utilisé pour des essais de vieillissement. Du point de vue fonctionnel, des bactéries viables ont pu être observées aux différents stades du procédé d'encapsulation et après dépôt de silice. La couche de silice déposée semble également permettre la limitation des phénomènes de dissémination des bactéries encapsulée.

L'efficacité de la matrice cellularisée en tant que matériau pour la dépollution a ensuite été évaluée en présence de différents polluants modèles. La souche de *Pseudomonas aeruginosa* utilisée pour l'optimisation du procédé d'encapsulation n'a malheureusement pas présenté d'activité significative pour la dégradation des contaminants modèles étudiés. Una pproche différente a donc été adoptée, en fixant un contaminant cible (le Reactive Black 5) et une souche bactérienne capable de dégrader ce polluant an ensuite été sélectionnée. La bactérie *Shewanella oneidensis* a donc été utilisée en tant qu'unité fonctionnelle du matériau alginate-silice. L'efficacité du matériau cellularisé a été étudiée dans le sol de référence mentionnée précédemment. Le sol a été saturé par une solution concentrée de RB5 et la concentration en colorant dans le surnageant a été mesurée après incubation. L'ajout des matériaux dans le sol a permis une faible diminution de la concentration apparente en colorant. L'effet n'est cependant que peu marqué, du faible nombre de bactéries *Shewanella oneidensis* viable encapsulées, ce qui s'explique par le fait que le procédé d'encapsulation a été optimisé pour

un autre type de bactéries. Plusieurs options sont envisageables pour confirmer ces observations et améliorer l'efficacité du matériau dépolluant. La principale voie d'amélioration consisterait à optimiser les paramètres d'encapsulation de *Shewanella oneidensis*, par exemple en ajustant la vitesse de refroidissement lors du freeze-casting, en ajustant la composition de la matrice (présence d'additifs par exemple) ou encore en modifiant les conditions de culture (milieu de culture, phase de croissance). Le modèle pour les essais de dépollution pourrait également être amélioré pour se rapprocher des conditions de terrain (en termes de température ou de taux d'hydratation par exemple).

Ce matériau reste néanmoins une preuve de concept encourageante en vue de l'élaboration de matériaux pour la dépollution des sols *in situ*. Grace à son adaptabilité, le procédé d'encapsulation décrit pourrait être utilisé pour l'immobilisation d'une large gamme de microorganismes (bactéries, champignons, algues etc…). Ainsi, par le choix de microorganismes appropriés (ou de consortia) et la modulation des caractéristiques de la matrice (en termes de propriétés de diffusion, mécaniques, stabilité etc…), des matériaux sur mesure pourraient être créés pour la dépollution de sites contaminés spécifiques.

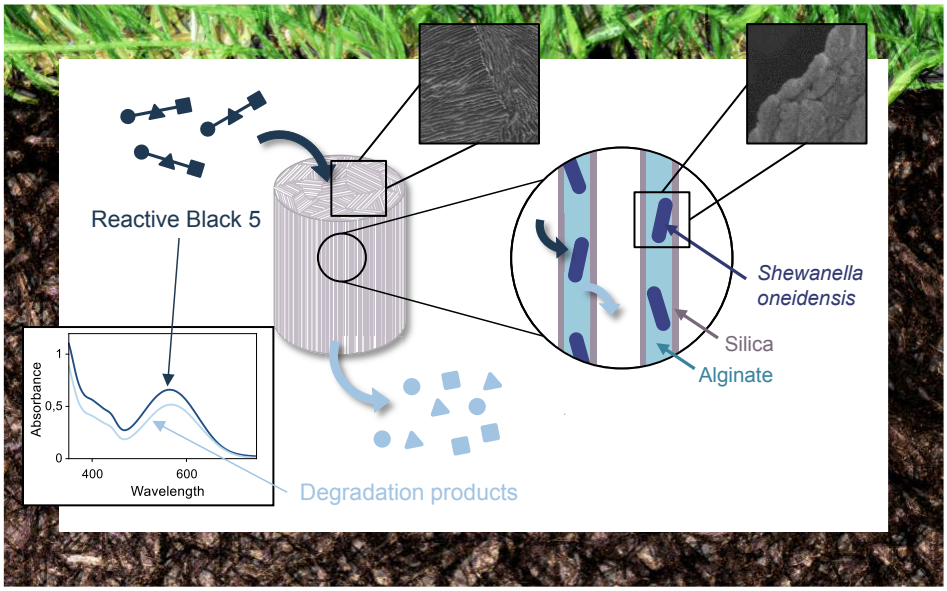

Figure A.17: Des bactéries bioactives ont été encapsulées dans un matériau hybride poreux. La technique du freeze-casting a été utilisée comme un moyen d'obtenir à la fois une encapsulation efficace des cellules et une morphologie contrôlée. La chimie du sol-gel a permis d'obtenir une couche de silice sur les parois des pores. Les matériaux poreux hybrides à base d'alginate et silice contenant la bactérie *Shewanella oneidensis* ont ainsi pu être utilisés pour la dégradation du Reactive Black 5 dans un sol de référence.

Bibliography

1. Adams, G. O., Fufeyin, P. T., Okoro, S. E. & Ehinomen, I. Bioremediation, Biostimulation and Bioaugmention: A Review. *Int. J. Environ. Bioremediation Biodegrad.* **3,** 28–39 (2015).
2. Juwarkar, A. A., Singh, S. K. & Mudhoo, A. A comprehensive overview of elements in bioremediation. *Rev. Environ. Sci. Bio/Technology* **9,** 215–288 (2010).
3. Cassidy, M. B., Lee, H. & Trevors, J. T. Environmental applications of immobilized microbial cells: A review. *J. Ind. Microbiol.* **16,** 79–101 (1996).
4. Lim, F. & Sun, A. M. Microencapsulated Islets as Bioartificial Endocrine Pancreas. *Science (80-.).* **210,** 908–910 (1980).
5. Gasperini, L., Mano, J. F. & Reis, R. L. Natural polymers for the microencapsulation of cells. *J. R. Soc. Interface* **11,** 20140817–20140817 (2014).
6. Coradin, T., Nassif, N. & Livage, J. Silica-alginate composites for microencapsulation. *Appl. Microbiol. Biotechnol.* **61,** 429–34 (2003).
7. Léonard, A. *et al.* Whole-cell based hybrid materials for green energy production, environmental remediation and smart cell-therapy. *Chem. Soc. Rev.* **40,** 860–885 (2011).
8. Chen, J. P. & Lin, Y. S. Decolorization of azo dye by immobilized *Pseudomonas luteola* entrapped in alginate-silicate sol-gel beads. *Process Biochem.* **42,** 934–942 (2007).
9. Soltmann, U. & Böttcher, H. Utilization of sol-gel ceramics for the immobilization of living microorganisms. *J. Sol-Gel Sci. Technol.* **48,** 66–72 (2008).
10. Gutiérrez, M. C. *et al.* Hydrogel scaffolds with immobilized bacteria for 3D cultures. *Chem. Mater.* **19,** 1968–1973 (2007).
11. Gros, R. Fonctionnement et qualité des sols soumis à des perturbations physiques et chimiques d'origine anthropique : réponses du sol , de la flore et de la microflore bactérienne tellurique . (Université de Savoie, 2002).
12. Shayler, H., McBride, M. & Harrison, E. *Sources and Impacts of Contaminants in Soils*. *Cornell Waste Management Institute* (2009).
13. Finlay, S. E., Moffat, A., Gazzard, R., Baker, D. & Murray, V. Health impacts of wildfires. *PLoS Curr.* 1–21 (2012).
14. Arias-Estévez, M. *et al.* The mobility and degradation of pesticides in soils and the pollution of groundwater resources. *Agric. Ecosyst. Environ.* **123,** 247–260 (2008).
15. Gevao, B., Semple, K. T. & Jones, K. C. Bound pesticide residues in soils: A review. *Environ. Pollut.* **108,** 3–14 (2000).
16. Anjum, R., Rahman, M., Masood, F. & Malik, A. in *Environmental Protection Strategies for Sustainability* (eds. Malik, A. & Grohmann, E.) 295–328 (Springer Netherlands, 2012).
17. Odukkathil, G. & Vasudevan, N. Toxicity and bioremediation of pesticides in agricultural soil. *Rev. Environ. Sci. Bio/Technology* **12,** 421–444 (2013).
18. Aktar, W., Sengupta, D. & Chowdhury, A. Impact of pesticides use in agriculture: their benefits and hazards. *Interdiscip. Toxicol.* **2,** 1–12 (2009).
19. Pimentel, D. Amounts of pesticides reaching target pests: Environmental impacts and ethics. *J. Agric. Environ. Ethics* **8,** 17–29 (1995).
20. Pimentel, D. & Levitan, L. Pesticides: Amounts Applied and Amounts Reaching Pests. *Bioscience* **36,** 86–91 (1986).
21. Migliore, L., Fiori, M., Spadoni, A. & Galli, E. Biodegradation of oxytetracycline by Pleurotus ostreatus mycelium: A mycoremediation technique. *J. Hazard. Mater.* **215–216,** 227–232 (2012).
22. Cerniglia, C. E. Biodegradation of polycyclic aromatic hydrocarbons. *Curr. Opin. Biotechnol.* **4,** 331–338 (1993).
23. Freeman, D. J. & Cattell, F. C. R. Woodburning as a source of atmospheric polycyclic aromatic hydrocarbons. *Environ. Sci. Technol.* **24,** 1581–1585 (1990).
24. Dubowsky, S. D., Wallace, L. A. & Buckley, T. J. The contribution of traffic to indoor concentrations of polycyclic aromatic hydrocarbons. *J. Expo. Anal. Environ. Epidemiol.* **9,** 312–321 (1999).
25. Johnsen, A. R., Wick, L. Y. & Harms, H. Principles of microbial PAH-degradation in soil. *Environ. Pollut.* **133,** 71–84 (2005).
26. Yu, K. S. H., Wong, A. H. Y., Yau, K. W. Y., Wong, Y. S. & Tam, N. F. Y. Natural attenuation, biostimulation and bioaugmentation on biodegradation of polycyclic aromatic

hydrocarbons (PAHs) in mangrove sediments. *Mar. Pollut. Bull.* **51,** 1071–1077 (2010).
27. Wilson, S. C. & Jones, K. C. Bioremediation of soil contaminated with polynuclear aromatic hydrocarbons (PAHs) : a review. *Environ. Pollut.* **81,** 229–249 (1993).
28. Haritash, A. K. & Kaushik, C. P. Biodegradation aspects of polycyclic aromatic hydrocarbons (PAHs): a review. *J. Hazard. Mater.* **169,** 1–15 (2009).
29. Bolden, A. L., Kwiatkowski, C. F. & Colborn, T. New look at BTEX: Are ambient levels a problem? *Environ. Sci. Technol.* **49,** 5697–5703 (2015).
30. Carmen, Z. & Daniela, S. Textile Organic Dyes – Characteristics , Polluting Effects and Separation / Elimination Procedures from Industrial Effluents – A Critical Overview. in *Organic Pollutants ten years after the stockholm convention - Environmental and analytical update* 55–86 (2010).
31. Pereira, L. & Alves, M. in *Environmental Protection Strategies for Sustainability* (eds. Malik, A. & Grohmann, E.) 111–162 (Springer Netherlands, 2012).
32. Puvaneswari, N., Muthukrishnan, J. & Gunasekaran, P. Toxicity assessment and microbial degradation of azo dyes. *Indian J. Exp. Biol.* **44,** 618–626 (2006).
33. Robinson, T., McMullan, G., Marchant, R. & Nigam, P. Remediation of dyes in textile effluent: A critical review on current treatment technologies with a proposed alternative. *Bioresour. Technol.* **77,** 247–255 (2001).
34. Valls, M. & de Lorenzo, V. Exploiting the genetic and biochemical capacities of bacteria for the remediation of heavy metal pollution. *FEMS Microbiol. Rev.* **26,** 327–38 (2002).
35. Bryan, G. W. & Langston, W. J. Bioavailability, accumulation and effects of heavy metals in sediments with special reference to United Kingdom estuaries: a review. *Environ. Pollut.* **76,** 89–131 (1992).
36. McLachlan, M. S. Bioaccumulation of hydrophobic chemicals in agricultural food chains. *Environ. Sci. Technol.* **30,** 252–259. (1996).
37. Järup, L. Hazards of heavy metal contamination. *Br. Med. Bull.* **68,** 167–182 (2003).
38. Stokes, J. D., Paton, G. I. & Semple, K. T. Behaviour and assessment of bioavailability of organic contaminants in soil: relevance for risk assessment and remediation. *Soil Use Manag.* **21,** 475–486 (2005).
39. Sijm, D., Kraaij, R. & Belfroid, A. Bioavailability in soil or sediment: Exposure of different organisms and approaches to study it. *Environ. Pollut.* **108,** 113–119 (2000).
40. Chung, N. & Alexander, M. Effect of soil properties on bioavailability and extractability of phenanthrene and atrazine sequestered in soil. *Chemosphere* **48,** 109–115 (2002).
41. D. Sijm *et al.* in *Risk Assessment of Chemicals: An introduction* (eds. Leeuwen, C. J. & Vermeire, T. G.) 73–158 (Springer, 2007).
42. Vermeire, T. G. *et al.* in *Risk Assessment of Chemicals: An introduction* (eds. Van Leeuwen, C. J. & Vermeire, T. G.) 227–273 (Springer, 2007).
43. Shea, D. Developing national sediment quality criteria. *Environ. Sci. Technol.* **22,** 1256–1261 (1988).
44. Di Toro, D. M. *et al.* Technical basis for establishing sediment quality criteria for nonionic organic chemicals using equilibrium partitioning. *Environ. Toxicol. Chem.* **10,** 1541–1583 (1991).
45. Muncke, J. Estimating the Organic Carbon Partition Coefficient and Its Variability for Hydrophobic Chemicals. **33,** 2390–2394 (1999).
46. Noble, A. Partition coefficients (n-octanol-water) for pesticides. *J. Chromatogr. A* **642,** 3–14 (1993).
47. Pignatello, J. J. & Xing, B. Mechanisms of Slow Sorption of Organic Chemicals to Natural Particles. *Environ. Sci. Technol.* **30,** 1–11 (1996).
48. Alexander, M. Aging, bioavaiability, and overestimation of risk from environmental pollutants. *Environ. Sci. Technol.* **34,** 4259–4265 (2000).
49. Jones, K. C. & de Voogt, P. Persistent organic pollutants (POPs): state of the science. *Environ. Pollut.* **100,** 209–221 (1999).
50. Ehlers, L. J. & Luthy, R. G. Contaminant bioavailability in soil and sediment. *Environ. Sci. Technol.* **37,** 295–302 (2003).
51. Arnold, S. F. *et al.* Synergistic Activation of Estrogen Receptor with Combinations of

Environmental Chemicals. *Science (80-.).* **272,** 1489–1492 (1996).
52. Megharaj, M., Ramakrishnan, B., Venkateswarlu, K., Sethunathan, N. & Naidu, R. Bioremediation approaches for organic pollutants: a critical perspective. *Environ. Int.* **37,** 1362–75 (2011).
53. Han, D. *et al.* Study on the Hydrolysis Kinetics of Dimethyl Disulfide. *Water, Air, Soil Pollut.* **228,** 234 (2017).
54. Venkatesan, S., Sudhahar, V., Senthurpandian, V. K. & Murugesan, S. Urea hydrolysis of tea soils as influenced by incubation period, soil pH, and nitrification inhibitor. *Commun. Soil Sci. Plant Anal.* **38,** 2295–2307 (2007).
55. Sturini, M. *et al.* Environmental photochemistry of fluoroquinolones in soil and in aqueous soil suspensions under solar light. *Environ. Sci. Pollut. Res.* **21,** 13215–13221 (2014).
56. EPA Series: A Citizen's Guide to Cleanup Technologies. *CLU-IN* (2012). Available at: https://clu-in.org/products/citguide/. (Accessed: 11th July 2017)
57. Tajudin, S., Azmi, M. & Nabila, A. Stabilization/Solidification Remediation Method for Contaminated Soil: A Review. *IOP Conf. Ser. Mater. Sci. Eng.* **136,** 12043 (2016).
58. Simon, F. G. & Müller, W. W. Standard and alternative landfill capping design in Germany. *Environ. Sci. Policy* **7,** 277–290 (2004).
59. Falciglia, P. P., Giustra, M. G. & Vagliasindi, F. G. A. Low-temperature thermal desorption of diesel polluted soil: Influence of temperature and soil texture on contaminant removal kinetics. *J. Hazard. Mater.* **185,** 392–400 (2011).
60. Dermont, G., Bergeron, M., Mercier, G. & Richer-Laflèche, M. Soil washing for metal removal: A review of physical/chemical technologies and field applications. *J. Hazard. Mater.* **152,** 1–31 (2008).
61. Mulligan, C. N., Yong, R. N. & Gibbs, B. F. Surfactant-enhanced remediation of contaminated soil: A review. *Eng. Geol.* **60,** 371–380 (2001).
62. Piña, J., Merino, J., Errazu, A. F. & Bucalá, V. Thermal treatment of soils contaminated with gas oil: Influence of soil composition and treatment temperature. *J. Hazard. Mater.* **94,** 273–290 (2002).
63. Tsitonaki, A. *et al.* In Situ Chemical Oxidation of Contaminated Soil and Groundwater Using Persulfate: A Review. *Crit. Rev. Environ. Sci. Technol.* **40,** 55–91 (2010).
64. Ludwig, R. D. *et al.* In situ chemical reduction of Cr(VI) in groundwater using a combination of ferrous sulfate and sodium dithionite: A field investigation. *Environ. Sci. Technol.* **41,** 5299–5305 (2007).
65. Hamer, G. Bioremediation: A response to gross environmental abuse. *Trends Biotechnol.* **11,** 317–319 (1993).
66. Iwamoto, T. & Nasu, M. Current bioremediation practice and perspective. *J. Biosci. Bioeng.* **92,** 1–8 (2001).
67. Kulcu, R. & Yaldiz, O. Determination of aeration rate and kinetics of composting some agricultural wastes. *Bioresour. Technol.* **93,** 49–57 (2004).
68. Fogarty, A. M. & Tuovinen, O. H. Microbiological degradation of pesticides in yard waste composting. *Microbiol. Rev.* **55,** 225–233 (1991).
69. Shannon, M. A. *et al.* Science and technology for water purification in the coming decades. *Nature* **452,** 301–310 (2008).
70. Khan, M. Z., Mondal, P. K. & Sabir, S. Aerobic granulation for wastewater bioremediation: A review. *Can. J. Chem. Eng.* **91,** 1045–1058 (2013).
71. Hatzinger, P. B., Whittier, M. C., Arkins, M. D., Bryan, C. W. & Guarini, W. J. In-Situ and Ex-Situ Bioremediation Options for Treating Perchlorate in Groundwater. *Remediat. J.* **12,** 69–86 (2002).
72. Azubuike, C. C., Chikere, C. B. & Okpokwasili, G. C. Bioremediation techniques-classification based on site of application: principles, advantages, limitations and prospects. *World J. Microbiol. Biotechnol.* **32,** 1–18 (2016).
73. Yao, Z., Li, J., Xie, H. & Yu, C. Review on Remediation Technologies of Soil Contaminated by Heavy Metals. *Procedia Environ. Sci.* **16,** 722–729 (2012).
74. Salt, D. E. *et al.* Phytoremediation: a novel strategy for the removal of toxic metals from the environment using plants. *Bio/technology* **13,** 468–474 (1995).

75. Samanta, S. K., Singh, O. V. & Jain, R. K. Polycyclic aromatic hydrocarbons: Environmental pollution and bioremediation. *Trends Biotechnol.* **20,** 243–248 (2002).
76. Bamforth, S. M. & Singleton, I. Bioremediation of polycyclic aromatic hydrocarbons: current knowledge and future directions. *J. Chem. Technol. Biotechnol.* **80,** 723–736 (2005).
77. Ron, E. Z. & Rosenberg, E. Biosurfactants and oil bioremediation. *Curr. Opin. Biotechnol.* **13,** 249–252 (2002).
78. Mazzeo, D. E. C., Levy, C. E., de Angelis, D. de F. & Marin-Morales, M. A. BTEX biodegradation by bacteria from effluents of petroleum refinery. *Sci. Total Environ.* **408,** 4334–4340 (2010).
79. Kaushik, P. & Malik, A. Fungal dye decolourization: Recent advances and future potential. *Environ. Int.* **35,** 127–141 (2009).
80. Khan, R., Bhawana, P. & Fulekar, M. H. Microbial decolorization and degradation of synthetic dyes: a review. *Rev. Environ. Sci. Bio/Technology* **12,** 75–97 (2012).
81. Saratale, R. G., Saratale, G. D., Chang, J. S. & Govindwar, S. P. Bacterial decolorization and degradation of azo dyes: A review. *J. Taiwan Inst. Chem. Eng.* **42,** 138–157 (2011).
82. Singh, S., Kang, S. H., Mulchandani, A. & Chen, W. Bioremediation: environmental clean-up through pathway engineering. *Curr. Opin. Biotechnol.* **19,** 437–444 (2008).
83. Ali, H., Khan, E. & Sajad, M. A. Phytoremediation of heavy metals-Concepts and applications. *Chemosphere* **91,** 869–881 (2013).
84. Paz-Ferreiro, J., Lu, H., Fu, S., Méndez, A. & Gascó, G. Use of phytoremediation and biochar to remediate heavy metal polluted soils: A review. *Solid Earth* **5,** 65–75 (2014).
85. Meagher, R. B. Phytoremediation of toxic elemental and organic pollutants. *Curr. Opin. Plant Biol.* **3,** 153–162 (2000).
86. Cunningham, S. D., Berti, W. R. & Huang, J. W. Phytoremediation of contaminated soils. *Trends Biotechnol.* **13,** 393–397 (1995).
87. Hickman, Z. A. & Reid, B. J. Earthworm assisted bioremediation of organic contaminants. *Environ. Int.* **34,** 1072–1081 (2008).
88. Iranzo, M., Sainz-Pardo, I., Boluda, R., Sanchez, J. & Mormeneo, S. The use of microorganisms in environmental remediation. *Ann. Microbiol.* **51,** 135–143 (2001).
89. Watanabe, K. Microorganisms relevant to bioremediation. *Curr. Opin. Biotechnol.* **12,** 237–241 (2001).
90. Lim, S. L., Chu, W. L. & Phang, S. M. Use of Chlorella vulgaris for bioremediation of textile wastewater. *Bioresour. Technol.* **101,** 7314–7322 (2010).
91. Perales-Vela, H. V., Peña-Castro, J. M. & Cañizares-Villanueva, R. O. Heavy metal detoxification in eukaryotic microalgae. *Chemosphere* **64,** 1–10 (2006).
92. Wang, J. & Chen, C. Biosorption of heavy metals by *Saccharomyces cerevisiae*: A review. *Biotechnol. Adv.* **24,** 427–451 (2006).
93. Lu, X.-Y., Zhang, T. & Fang, H. H.-P. Bacteria-mediated PAH degradation in soil and sediment. *Appl. Microbiol. Biotechnol.* **89,** 1357–71 (2011).
94. Brim, H. *et al.* Engineering Deinococcus radiodurans for metal remediation in radioactive mixed waste environments. *Nat. Biotechnol.* **18,** 85–90 (2000).
95. Hao, R., Lu, A. & Wang, G. Crude-oil-degrading thermophilic bacterium isolated from an oil field. *Can. J. Microbiol.* **50,** 175–182 (2004).
96. Dojka, M. A., Hugenholtz, P., Haack, S. K. & Pace, N. R. Microbial Diversity in a Hydrocarbon- and Chlorinated-Solvent-Contaminated Aquifer Undergoing Intrinsic Bioremediation. *Appl. Environ. Microbiol.* (1998).
97. Silva, Í. S. *et al.* Bioremediation of a polyaromatic hydrocarbon contaminated soil by native soil microbiota and bioaugmentation with isolated microbial consortia. *Bioresour. Technol.* **100,** 4669–4675 (2009).
98. Fu, P. & Secundo, F. Algae and Their Bacterial Consortia for Soil Bioremediation. *Chem. Eng. Trans.* **49,** 427–432 (2016).
99. Glick, B. R. Phytoremediation: Synergistic use of plants and bacteria to clean up the environment. *Biotechnol. Adv.* **21,** 383–393 (2003).
100. Kinnersley, A. M. The role of phytochelates in plant growth and productivity. *Plant Growth Regul.* **12,** 207–218 (1993).

101. Mulligan, C. N. Environmental applications for biosurfactants. *Environ. Pollut.* **133,** 183–198 (2005).
102. National Research Council. in *In Situ Bioremediation : When Does it Work ?* 16–46 (The National Academic Press, 1993).
103. Park, J. H. *et al.* Role of organic amendments on enhanced bioremediation of heavy metal(loid) contaminated soils. *J. Hazard. Mater.* **185,** 549–74 (2011).
104. Suttinun, O., Luepromchai, E. & Müller, R. Cometabolism of trichloroethylene: concepts, limitations and available strategies for sustained biodegradation. *Rev. Environ. Sci. Bio/Technology* **12,** 99–114 (2012).
105. Vassil, A. D., Kapulnik, Y., Raskin, I. & Salt, D. E. The Role of EDTA in Lead Transport and Accumulation by Indian Mustard1. *Plant Physiol.* **117,** 447–453 (1998).
106. Timmis, K. N., Steffan, R. J. & Unterman, R. Designing microorganisms for the treatment of toxic wastes. *Annu. Rev. Microbiol.* **48,** 525–557 (1994).
107. Timmis, K. N. & Pieper, D. H. Bacteria designed for bioremediation. *Trends Biotechnol.* **17,** 201–204 (1999).
108. Alvarenga, N., Birolli, W. G., Seleghim, M. H. R. & Porto, A. L. M. Biodegradation of methyl parathion by whole cells of marine-derived fungi Aspergillus sydowii and Penicillium decaturense. *Chemosphere* **117,** 47–52 (2014).
109. Trevors, J., Elsas, J. Van, Lee, H. & Wolters, A. Survival of alginate-encapsulated Pseudomonas fluorescens cells in soil. *Appl. Microbiol. Biotechnol.* 637–643 (1993).
110. Park, J. H., Hong, D., Lee, J. & Choi, I. S. Cell-in-Shell Hybrids: Chemical Nanoencapsulation of Individual Cells. *Acc. Chem. Res.* **49,** 792–800 (2016).
111. Carturan, G., Campostrini, R., Dire, S., Scardi, V. & Alteriis, E. Inorganic gels for immobilization of biocatalysts: inclusion of invertase-active whole cells of yeast (*Saccharomyces cerevisiae*) into thin layers of SiO2 gel deposited on glass sheets. *J. Mol. Catal.* **57,** L13-16 (1989).
112. Townsend-Nicholson, A. & Jayasinghe, S. N. Cell electrospinning: A unique biotechnique for encapsulating living organisms for generating active biological microthreads/scaffolds. *Biomacromolecules* **7,** 3364–3369 (2006).
113. Nassif, N. *et al.* Living bacteria in silica gels. *Nat. Mater.* **1,** 42–44 (2002).
114. Sheldon, R. A. Enzyme Immobilization: The Quest for Optimum Performance. *Adv. Synth. Catal.* **349,** 1289–1307 (2007).
115. Archelas, A. *et al. Biocatalysis - From Discovery to Application*. (1999).
116. Wandrey, C. in *Immobilized Cells: Basics and Applications* (eds. Buitelaar, R. M., Bucke, C., Trampe, J. & Wijffels, R. H.) 3–16 (Elsevier Science, 1996). doi:10.1016/S0921-0423(96)80003-7
117. Wang, G. H. & Zhang, L. M. A biofriendly silica gel for in situ protein entrapment: Biopolymer-assisted formation and its kinetic mechanism. *J. Phys. Chem. B* **113,** 2688–2694 (2009).
118. Schuleit, M. & Luisi, P. L. Enzyme immobilization in silica-hardened organogels. *Biotechnol. Bioeng.* **72,** 249–53 (2001).
119. Zhang, Y. *et al.* Protamine-Templated Biomimetic Hybrid Capsules: Efficient and Stable Carrier for Enzyme Encapsulation. *Chem. Mater.* **20,** 1041–1048 (2008).
120. Konsoula, Z. & Liakopoulou-Kyriakides, M. Starch hydrolysis by the action of an entrapped in alginate capsules α-amylase from Bacillus subtilis. *Process Biochem.* **41,** 343–349 (2006).
121. Hsu, A. F., Foglia, T. A. & Piazza, G. J. Immobilization of lipoxygenase in an alginate-silicate solgel matrix : formation of fatty acid hydroperoxides. *Biotechnol. Lett.* **19,** 71–74 (1997).
122. Brady, D. & Jordaan, J. Advances in enzyme immobilisation. *Biotechnol. Lett.* **31,** 1639–1650 (2009).
123. Perullini, M., Rivero, M. M., Jobbágy, M., Mentaberry, A. & Bilmes, S. a. Plant cell proliferation inside an inorganic host. *J. Biotechnol.* **127,** 542–548 (2007).
124. Kumari, A., Yadav, S. K. & Yadav, S. C. Biodegradable polymeric nanoparticles based drug delivery systems. *Colloids Surfaces B Biointerfaces* **75,** 1–18 (2010).
125. Gombotz, W. R. & Wee, S. Protein release from alginate matrixes. *Adv. Drug Deliv. Rev.* **31,** 267–285 (1998).

126. Censi, R., Di Martino, P., Vermonden, T. & Hennink, W. E. Hydrogels for protein delivery in tissue engineering. *J. Control. Release* **161,** 680–692 (2012).
127. Kim, T. H. *et al.* Therapeutic foam scaffolds incorporating biopolymer-shelled mesoporous nanospheres with growth factors. *Acta Biomater.* **10,** 2612–2621 (2014).
128. Orive, G. *et al.* Cell encapsulation: promise and progress. *Nat. Med.* **9,** 104–107 (2003).
129. Orive, G. *et al.* History, challenges and perspectives of cell microencapsulation. *Trends Biotechnol.* **22,** 87–92 (2004).
130. Sakai, S., Ono, T., Ijima, H. & Kawakami, K. Aminopropyl-silicate membrane for microcapsule-shaped bioartificial organs: Control of molecular permeability. *J. Memb. Sci.* **202,** 73–80 (2002).
131. Coradin, T., Mercey, E., Lisnard, L. & Livage, J. Design of silica-coated microcapsules for bioencapsulation. *Chem. Commun.* 2496–2497 (2001).
132. Lim, S. Y., Kim, K.-O., Kim, D.-M. & Park, C. B. Silica-coated alginate beads for in vitro protein synthesis via transcription/translation machinery encapsulation. *J. Biotechnol.* **143,** 183–9 (2009).
133. Liu, Z., Liu, B., Zhang, M., Kong, J. & Deng, J. Al2O3 sol-gel derived amperometric biosensor for glucose. *Anal. Chim. Acta* **392,** 135–141 (1999).
134. Lloyd, C. R. & Eyring, E. M. Protecting heme enzyme peroxidase activity from H2O2 inactivation by sol-gel encapsulation. *Langmuir* **16,** 9092–9094 (2000).
135. Miao, Y. & Tan, S. N. Amperometric hydrogen peroxide biosensor with silica sol – gel / chitosan film as immobilization matrix. *Anal. Chim. Acta* **437,** 87–93 (2001).
136. Chen, X., Cheng, G. & Dong, S. Amperometric tyrosinase biosensor based on a sol–gel-derived titanium oxide–copolymer composite matrix for detection of phenolic compounds. *Analyst* **126,** 1728–1732 (2001).
137. Shitanda, I., Takamatsu, S., Watanabe, K. & Itagaki, M. Amperometric screen-printed algal biosensor with flow injection analysis system for detection of environmental toxic compounds. *Electrochim. Acta* **54,** 4933–4936 (2009).
138. Cooney, M. J., Svoboda, V., Lau, C., Martin, G. & Minteer, S. D. Enzyme catalysed biofuel cells. *Energy Environ. Sci.* **1,** 320 (2008).
139. Rooke, J. C., Meunier, C., Léonard, A. & Su, B.-L. Energy from photobioreactors: Bioencapsulation of photosynthetically active molecules, organelles, and whole cells within biologically inert matrices. *Pure Appl. Chem.* **80,** 2345–2376 (2008).
140. Velasquez-Orta, S. B., Curtis, T. P. & Logan, B. E. Energy from algae using microbial fuel cells. *Biotechnol. Bioeng.* **103,** 1068–1076 (2009).
141. Rabaey, K. & Verstraete, W. Microbial fuel cells: Novel biotechnology for energy generation. *Trends Biotechnol.* **23,** 291–298 (2005).
142. Baronian, K. H. R. The use of yeast and moulds as sensing elements in biosensors. *Biosens. Bioelectron.* **19,** 953–962 (2004).
143. Shitanda, I., Takada, K., Sakai, Y. & Tatsuma, T. Compact amperometric algal biosensors for the evaluation of water toxicity. *Anal. Chim. Acta* **530,** 191–197 (2005).
144. Belkin, S. Microbial whole-cell sensing systems of environmental pollutants. *Curr. Opin. Microbiol.* **6,** 206–212 (2003).
145. Su, L., Jia, W., Hou, C. & Lei, Y. Microbial biosensors: A review. *Biosens. Bioelectron.* **26,** 1788–1799 (2011).
146. Husain, Q. & Ulber, R. Immobilized Peroxidase as a Valuable Tool in the Remediation of Aromatic Pollutants and Xenobiotic Compounds: A Review. *Crit. Rev. Environ. Sci. Technol.* **41,** 770–804 (2011).
147. Klein, S. *et al.* Encapsulation of *Pseudomonas sp.* ADP cells in electrospun microtubes for atrazine bioremediation. *J. Ind. Microbiol. Biotechnol.* **39,** 1605–1613 (2012).
148. Halma, M. *et al.* Bacteria encapsulated in layered double hydroxides: Towards an efficient bionanohybrid for pollutant degradation. *Colloids Surfaces B Biointerfaces* **126,** 344–350 (2015).
149. Perullini, M., Jobbágy, M., Mouso, N., Forchiassin, F. & Bilmes, S. a. Silica-alginate-fungi biocomposites for remediation of polluted water. *J. Mater. Chem.* **20,** 6479 (2010).
150. Mallick, N. Biotechnological potential of immobilised algae for wastewater N, P and metal

removal: a review. *BioMetals* **15,** 377–390 (2002).
151. Shoulders, M. D. & Raines, R. T. Collagen Structure and Stability. *Annu. Rev. Biochem.* **78,** 929–958 (2010).
152. Klemm, D., Heublein, B., Fink, H. P. & Bohn, A. Cellulose: Fascinating biopolymer and sustainable raw material. *Angew. Chemie - Int. Ed.* **44,** 3358–3393 (2005).
153. Rehm, B. H. A. Bacterial polymers: biosynthesis, modifications and applications. *Nature* **8,** 578–592 (2010).
154. Banerjee, Mr. Mahapatra & D Banerjee. Fungal Exopolysaccharide: Production, Composition and Applications. *Microbiol. Insights* 1 (2013). doi:10.4137/MBI.S10957
155. Draget, K. I., Moe, S. T., Skjak-Bræk, G. & Smidsrød, O. in *Food Polysaccharides and their Applications* (eds. Alistair, S. M., Glyn, P. O. & A.Peter, W.) 289–334 (CRC Press, 2006).
156. Augst, A. D., Kong, H. J. & Mooney, D. J. Alginate hydrogels as biomaterials. *Macromol. Biosci.* **6,** 623–33 (2006).
157. Stanley, N. F. in *Food Polysaccharides and their Applications* (eds. Alistair, S. M., Glyn, P. O. & A.Peter, W.) 217–238 (CRC Press, 2006).
158. Piculell, L. in *Food Polysaccharides and their Applications* (eds. Alistair, S. M., Glyn, P. O. & A.Peter, W.) 239–288 (CRC Press, 2006).
159. Silva, J. A. L. da & Rao, M. A. in *Food Polysaccharides and their Applications* (eds. Alistair, S. M., Glyn, P. O. & A.Peter, W.) 353–412 (CRC Press, 2006).
160. Willats, W. G. ., Knox, J. P. & Mikkelsen, J. D. Pectin: new insights into an old polymer are starting to gel. *Trends Food Sci. Technol.* **17,** 97–104 (2006).
161. García-Ochoa, F., Santos, V. E., Casas, J. A. & Gómez, E. Xanthan gum: Production, recovery, and properties. *Biotechnol. Adv.* **18,** 549–579 (2000).
162. Katzbauer, B. Properties and applications of xanthan gum. *Polym. Degrad. Stab.* **59,** 81–84 (1998).
163. Rinaudo, M. Chitin and chitosan: Properties and applications. *Prog. Polym. Sci.* **31,** 603–632 (2006).
164. Smidsrød, O. & Varum, K. M. in *Food Polysaccharides and their Applications* (eds. Alistair, S. M., Glyn, P. O. & A.Peter, W.) 497–520 (CRC Press, 2006).
165. Coffey, D. G., Bell, D. A. & Henderson, A. in *Food Polysaccharides and their Applications* (eds. Alistair, S. M., Glyn, P. O. & A.Peter, W.) 147–180 (CRC Press, 2006).
166. Zobel, H. F. & Stephen, A. M. in *Food Polysaccharides and their Applications* (eds. Alistair, S. M., Glyn, P. O. & A.Peter, W.) 25–86 (CRC Press, 2006).
167. Copeland, L., Blazek, J., Salman, H. & Tang, M. C. Form and functionality of starch. *Food Hydrocoll.* **23,** 1527–1534 (2009).
168. Lee, C. H., Singla, A. & Lee, Y. Biomedical applications of collagen. *Int. J. Pharm.* **221,** 1–22 (2001).
169. Altman, G. H. *et al.* Silk-based biomaterials. *Biomaterials* **24,** 401–416 (2003).
170. Shukla, R. & Cheryan, M. Zein: The industrial protein from corn. *Ind. Crops Prod.* **13,** 171–192 (2001).
171. Feldman, D., Lacasse, M. & Beznaczuk, L. M. Lignin-polymer systems and some applications. *Prog. Polym. Sci.* **12,** 271–299 (1986).
172. Boerjan, W., Ralph, J. & Baucher, M. Lignin Biosynthesis. *Annu. Rev. Plant Biol.* **54,** 519–546 (2003).
173. *Chemistry, Manufacture and Applications of Natural Rubber*. *Chemistry, Manufacture and Applications of Natural Rubber* (Woodhead Publishing, 2014).
174. Mohnen, D. Pectin structure and biosynthesis. *Curr. Opin. Plant Biol.* **11,** 266–77 (2008).
175. *Food Polysaccharides and Their Applications*. (CRC Press, 2006). doi:doi:10.1201/9781420015164.ch6\r10.1201/9781420015164.ch6
176. Rinaudo, M. Main properties and current applications of some polysaccharides as biomaterials. *Polym. Int.* **57,** 397–430 (2008).
177. Christoph, S. & Fernandes, F. M. in *Bionanocomposites: Integrating Biological Processes for Bioinspired Nanotechnologies* (eds. Aimé, C. & Coradin, T.) 254–298 (Wiley, 2017).
178. Jarvis, M. C. Structure and properties of pectin gels in plant-cell walls. *Plant Cell Environ.* **7,** 153–164 (1984).

179. Smidsrod, O. & Skjak-Braek, G. Alginate as immobilization matrix for cells. *Minerva Biotecnol.* **8,** 71–78 (1990).
180. Rowley, J. A., Madlambayan, G. & Mooney, D. J. Alginate hydrogels as synthetic extracellular matrix materials. *Biomaterials* **20,** 45–53 (1999).
181. Goh, C. H., Heng, P. W. S. & Chan, L. W. Alginates as a useful natural polymer for microencapsulation and therapeutic applications. *Carbohydr. Polym.* **88,** 1–12 (2012).
182. Lee, K. Y. & Mooney, D. J. Alginate: Properties and biomedical applications. *Prog. Polym. Sci.* **37,** 106–126 (2012).
183. Grant, G. T., Morris, E. R., Rees, D. A., Smith, P. J. C. & Thom, D. Biological interactions between polysaccharides and divalent cations: The egg-box model. *FEBS Lett.* **32,** 195–198 (1973).
184. Tønnesen, H. H. & Karlsen, J. Alginate in drug delivery systems. *Drug Dev. Ind. Pharm.* **28,** 621–630 (2002).
185. Das, B., Roy, A. P., Bhattacharjee, S., Chakraborty, S. & Bhattacharjee, C. Lactose hydrolysis by beta-galactosidase enzyme: Optimization using response surface methodology. *Ecotoxicol. Environ. Saf.* **121,** 244–252 (2015).
186. Wang, N., Adams, G., Buttery, L., Falcone, F. H. & Stolnik, S. Alginate encapsulation technology supports embryonic stem cells differentiation into insulin-producing cells. *J. Biotechnol.* **144,** 304–312 (2009).
187. Christoph, S., Kwiatoszynski, J., Coradin, T. & Fernandes, F. M. Cellularized Cellular Solids via Freeze-Casting. *Macromol. Biosci.* **16,** 182–187 (2016).
188. Bozeman, J., Koopman, B. & Bitton, G. Toxicity testing using immobilized algae. *Aquat. Toxicol.* **14,** 345–352 (1989).
189. Agnihotri, S. A., Mallikarjuna, N. N. & Aminabhavi, T. M. Recent advances on chitosan-based micro- and nanoparticles in drug delivery. *J. Control. Release* **100,** 5–28 (2004).
190. Gan, Q. & Wang, T. Chitosan nanoparticle as protein delivery carrier-Systematic examination of fabrication conditions for efficient loading and release. *Colloids Surfaces B Biointerfaces* **59,** 24–34 (2007).
191. Gemeiner, P. *et al.* in *Immobilized Cells: Basics and Applications* (eds. Buitelaar, R. M., Bucke, C., Trampe, J. & Wijffels, R. H.) **11,** 76–83 (Elsevier Science, 1996).
192. Jawaheer, S., White, S. F., Rughooputh, S. D. D. V. & Cullen, D. C. Enzyme Stabilization Using Pectin As a Novel Entrapment Matrix in Biosensors. *Anal. Lett.* **35,** 2077–2091 (2002).
193. Nicodemus, G. D. & Bryant, S. J. Cell Encapsulation in Biodegradable Hydrogels for Tissue Engineering Applications. *Tissue Eng. Part B. Rev.* **14,** 149–165 (2008).
194. Brinques, G. B. & Ayub, M. A. Z. Effect of microencapsulation on survival of Lactobacillus plantarum in simulated gastrointestinal conditions, refrigeration, and yogurt. *J. Food Eng.* **103,** 123–128 (2011).
195. Liu, B., Cao, Y., Chen, D., Kong, J. & Deng, J. Amperometric biosensor based on a nanoporous ZrO2 matrix. *Anal. Chim. Acta* **478,** 59–66 (2003).
196. Fakhrullin, R. F. & Minullina, R. T. Hybrid cellular-inorganic core-shell microparticles: Encapsulation of individual living cells in calcium carbonate microshells. *Langmuir* **25,** 6617–6621 (2009).
197. Choy, J.-H., Park, J.-S., Kwak, S.-Y., Jeong, Y.-J. & Han, Y.-S. Layered Double Hydroxide as Gene Reservoir. *Mol. Cryst. Liq. Cryst. Sci. Technol. Sect. A. Mol. Cryst. Liq. Cryst.* **341,** 425–429 (2000).
198. Samindra, K. M. S. & Kottegoda, N. Encapsulation of curcumin into layered double hydroxides. *Nanotechnol. Rev.* **3,** 579–589 (2014).
199. Livage, J. in *Sol-Gel Technologies for Glass Producers and Users* (eds. Aegerter, M. A. & Mennig, M.) 3–14 (Springer US, 2004).
200. Brinker, J. C. & Scherer, G. W. *Sol-Gel Science - The Physics and Chemistry of Sol-Gel Processing*. (Academic Press, Inc., 1990).
201. Sakka, S. in *Handbook of Sol-Gel Science and Technology* (eds. Klein, L., Aparicio, M. & Jitianu, A.) 1–27 (Springer International Publishing, 2016).
202. Owens, G. J. *et al.* Sol-gel based materials for biomedical applications. *Prog. Mater. Sci.* **77,** 1–79 (2016).

203. Wang, X. *et al.* Sol-gel Encapsulation of Biomolecules and Cells for Medicinal Applications. *Curr. Top. Med. Chem.* **15,** 223–244 (2015).
204. Dickey, F. H. Specific adsorption. *J. Phys. Chem.* **58,** 695–707 (1955).
205. Johnson, P. & Whateley, T. L. On the use of polymerizing silica gel systems for the immobilization of trypsin. *J. Colloid Interface Sci.* **37,** 557–563 (1971).
206. Braun, S., Rappoport, S., Zusman, R., Avnir, D. & Ottolenghi, M. Biochemically active sol-gel glasses: The trapping of enzymes. *Mater. Lett.* **10,** 1–5 (1990).
207. Coradin, T. & Livage, J. Aqueous silicates in biological sol – gel applications: new perspectives for old precursors. *Acc Chem Res* **40,** 819–26 (2007).
208. Meunier, C. F., Rooke, J. C., Léonard, A., Van Cutsem, P. & Su, B.-L. Design of photochemical materials for carbohydrate production via the immobilisation of whole plant cells into a porous silica matrix. *J. Mater. Chem.* **20,** 929–936 (2010).
209. Darder, M. *et al.* Algae–silica systems as functional hybrid materials. *J. Mater. Chem.* **20,** 9362–9369 (2010).
210. Carturan, G., Dal Toso, R., Boninsegna, S. & Dal Monte, R. Encapsulation of functional cells by sol-gel silica: actual progress and perspectives for cell therapy. *J. Mater. Chem.* **14,** 2087–2098 (2004).
211. Gupta, R. & Chaudhury, N. K. Entrapment of biomolecules in sol-gel matrix for applications in biosensors: problems and future prospects. *Biosens. Bioelectron.* **22,** 2387–99 (2007).
212. Meunier, C. F., Dandoy, P. & Su, B. L. Encapsulation of cells within silica matrixes: Towards a new advance in the conception of living hybrid materials. *J. Colloid Interface Sci.* **342,** 211–224 (2010).
213. Guan, C. *et al.* Bioencapsulation of living yeast (Pichia pastoris) with silica after transformation with lysozyme gene. *J. Sol-Gel Sci. Technol.* **48,** 369–377 (2008).
214. Ferrer, M. L., Yuste, L., Rojo, F. & Del Monte, F. Biocompatible sol-gel route for encapsulation of living bacteria in organically modified silica matrixes. *Chem. Mater.* **15,** 3614–3618 (2003).
215. Brasack, I., Böttcher, H. & Hempel, U. Biocompatibility of modified silica-protein composite layers. *J. Sol-Gel Sci. Technol.* **19,** 479–482 (2000).
216. Harper, J. C. *et al.* Encapsulation of S. cerevisiae in poly(glycerol) silicate derived matrices: Effect of matrix additives and cell metabolic phase on long-term viability and rate of gene expression. *Chem. Mater.* **23,** 2555–2564 (2011).
217. Gill, I. & Ballesteros, A. Encapsulation of biologicals within silicate, siloxane, and hybrid sol-gel polymers: An efficient and generic approach. *J. Am. Chem. Soc.* **120,** 8587–8598 (1998).
218. Shchipunov, Y. A., Karpenko, T. Y., Bakunina, I. Y., Burtseva, Y. V. & Zvyagintseva, T. N. A new precursor for the immobilization of enzymes inside sol-gel-derived hybrid silica nanocomposites containing polysaccharides. *J. Biochem. Biophys. Methods* **58,** 25–38 (2004).
219. Bhatia, R. B., Brinker, C. J., Gupta, A. K. & Singh, A. K. Aqueous sol-gel process for protein encapsulation. *Chem. Mater.* **12,** 2434–2441 (2000).
220. Coiffier, A., Coradin, T., Roux, C., Bouvet, O. M. M. & Livage, J. Sol–gel encapsulation of bacteria: a comparison between alkoxide and aqueous routes. *J. Mater. Chem.* **11,** 2039–2044 (2001).
221. Avnir, D., Braun, S., Lev, O. & Ottolenghi, M. Enzymes and Other Proteins Entrapped in Sol-Gel Materials. *Chem. Mater.* **6,** 1605–1614 (1994).
222. Drisko, G. L. & Sanchez, C. Hybridization in materials science - Evolution, current state, and future aspirations. *Eur. J. Inorg. Chem.* 5097–5105 (2012). doi:10.1002/ejic.201201216
223. C. Sanchez, B. Julian, P. Belleville & Popall, M. Applications of hybrid organic-inorganic nanocomposites. *J. Mater. Chem.* **15,** 3559–3592 (2005).
224. Darder, M., Aranda, P. & Ruiz-Hitzky, E. Bionanocomposites: A New Concept of Ecological, Bioinspired, and Functional Hybrid Materials. *Adv. Mater.* **19,** 1309–1319 (2007).
225. Aimé, C. & Coradin, T. Nanocomposites from biopolymer hydrogels: Blueprints for white biotechnology and green materials chemistry. *J. Polym. Sci. Part B Polym. Phys.* **50,** 669–680 (2012).
226. Boury, B. & Plumejeau, S. Metal oxides and polysaccharides: an efficient hybrid association for materials chemistry. *Green Chem.* **17,** 72–88 (2014).

227. Christoph, S., Fernandes, F. M. & Coradin, T. Immobilization of proteins in biopolymer-silica hybrid materials. 1669–1676 (2015).
228. Coradin, T. in *Nanocomposites with Biodegradable Polymers: Synthesis, Properties, and Future Perspectives* (ed. Mittal, V.) 166–188 (Oxford University Press, 2011).
229. Coradin, T. & Livage, J. Synthesis and Characterization of Alginate / Silica Biocomposites. *J. Sol-Gel Sci. ans Technol.* **26,** 1165–1168 (2003).
230. Agoudjil, N. *et al.* Design and properties of biopolymer–silica hybrid materials: The example of pectin-based biodegradable hydrogels. *Pure Appl. Chem.* **84,** 2521–2529 (2012).
231. Lee, E. J. *et al.* Membrane of hybrid chitosan-silica xerogel for guided bone regeneration. *Biomaterials* **30,** 743–750 (2009).
232. Mahony, O. *et al.* Silica-gelatin hybrids with tailorable degradation and mechanical properties for tissue regeneration. *Adv. Funct. Mater.* **20,** 3835–3845 (2010).
233. Coradin, T., Allouche, J., Boissière, M. & Livage, J. Sol-Gel Biopolymer / Silica Nanocomposites in Biotechnology. *Curr. Nanosci.* **2,** (2006).
234. Wang, D. *et al.* Highly flexible silica/chitosan hybrid scaffolds with oriented pores for tissue regeneration. *J. Mater. Chem. B* **3,** 7560–7576 (2015).
235. Palchesko, R. N., Lathrop, K. L., Funderburgh, J. L. & Feinberg, A. W. In vitro expansion of corneal endothelial cells on biomimetic substrates. *Sci. Rep.* **5,** 7955 (2015).
236. Budnyak, T. M., Pylypchuk, I. V, Tertykh, V. a, Yanovska, E. S. & Kolodynska, D. Synthesis and adsorption properties of chitosan-silica nanocomposite prepared by sol-gel method. *Nanoscale Res. Lett.* **10,** 87 (2015).
237. Heichal-Segal, O., Rappoport, S. & Braun, S. Immobilization in Alginate-Silicate Sol-Gel Matrix Protects β-Glucosidase Against Thermal and Chemical Denaturation. *Bio/Technology* **13,** 798–800 (1995).
238. Perullini, M. *et al.* Improving bacteria viability in metal oxide hosts via an alginate-based hybrid approach. *J. Mater. Chem.* **21,** 8026 (2011).
239. Sakai, S., Ono, T., Ijima, H. & Kawakami, K. In vitro and in vivo evaluation of alginate/sol-gel synthesized aminopropyl-silicate/alginate membrane for bioartificial pancreas. *Biomaterials* **23,** 4177–4183 (2002).
240. Desmet, J. *et al.* Highly efficient, long life, reusable and robust photosynthetic hybrid core–shell beads for the sustainable production of high value compounds. *J. Colloid Interface Sci.* **448,** 79–87 (2015).
241. Desimone, M. F. *et al.* Fibroblast encapsulation in hybrid silica–collagen hydrogels. *J. Mater. Chem.* **20,** 666–668 (2010).
242. Shchipunov, Y. a., Burtseva, Y. V., Karpenko, T. Y., Shevchenko, N. M. & Zvyagintseva, T. N. Highly efficient immobilization of endo-1,3-beta-D-glucanases (laminarinases) from marine mollusks in novel hybrid polysaccharide-silica nanocomposites with regulated composition. *J. Mol. Catal. B Enzym.* **40,** 16–23 (2006).
243. Assifaoui, A., Bouyer, F., Chambin, O. & Cayot, P. Silica-coated calcium pectinate beads for colonic drug delivery. *Acta Biomater.* **9,** 6218–6225 (2013).
244. Deng, L., Shang, L., Wen, D., Zhai, J. & Dong, S. A membraneless biofuel cell powered by ethanol and alcoholic beverage. *Biosens. Bioelectron.* **26,** 70–73 (2010).
245. Li, F., Chen, W., Tang, C. & Zhang, S. Development of hydrogen peroxide biosensor based on in situ covalent immobilization of horseradish peroxidase by one-pot polysaccharide-incorporated sol-gel process. *Talanta* **77,** 1304–1308 (2009).
246. Ramachandran, S., Coradin, T., Jain, P. K. & Verma, S. K. *Nostoc calcicola* immobilized in silica-coated calcium alginate and silica gel for applications in heavy metal biosorption. *Silicon* **1,** 215–223 (2010).
247. Vemmer, M. & Patel, A. V. Review of encapsulation methods suitable for microbial biological control agents. *Biol. Control* **67,** 380–389 (2013).
248. Moslemy, P., Neufeld, R. J. & Guiot, S. R. Biodegradation of gasoline by gellan gum-encapsulated bacterial cells. *Biotechnol. Bioeng.* **80,** 175–184 (2002).
249. Sarioglu, O. F., Keskin, N. O. S., Celebioglu, A., Tekinay, T. & Uyar, T. Bacteria encapsulated electrospun nanofibrous webs for remediation of methylene blue dye in water. *Colloids Surfaces B Biointerfaces* **152,** 245–251 (2017).

250. Sakkos, J. K., Kieffer, D. P., Mutlu, B. R., Wackett, L. P. & Aksan, A. Engineering of a silica encapsulation platform for hydrocarbon degradation using *Pseudomonas sp.* NCIB 9816-4. *Biotechnol. Bioeng.* **113,** 513–521 (2016).
251. Tuttolomondo, M. V., Alvarez, G. S., Desimone, M. F. & Diaz, L. E. Removal of azo dyes from water by sol-gel immobilized *Pseudomonas sp. J. Environ. Chem. Eng.* **2,** 131–136 (2014).
252. Lake, R. A. & Lewis, E. L. Salt Rejection by Sea Ice during Growth. *J. Geophys. Res.* **75,** 583 (1970).
253. Deville, S. in *Freezing Colloids: Observations, Principles, Control, and Use* 1–43 (Springer International Publishing, 2017).
254. Deville, S. Ice-templating, freeze casting: Beyond materials processing. *J. Mater. Res.* **28,** 2202–2219 (2013).
255. Maxwell, W., Gurnick, R. S. & Francisco, C. Preliminary investigation of the freeze- casting method for forming refractory powders. *Natl. Advis. Commitee Aeronaut.* (1954).
256. Deville, S. Freeze-casting of porous ceramics: A review of current achievements and issues. *Adv. Eng. Mater.* **10,** 155–169 (2008).
257. Wegst, U. G. K., Schecter, M., Donius, A. E. & Hunger, P. M. Biomaterials by freeze casting. *Philos. Trans. A. Math. Phys. Eng. Sci.* **368,** 2099–121 (2010).
258. Waschkies, T., Oberacker, R. & Hoffmann, M. J. Control of lamellae spacing during freeze casting of ceramics using double-side cooling as a novel processing route. *J. Am. Ceram. Soc.* **92,** 79–84 (2009).
259. Deville, S., Saiz, E., Nalla, R. K. & Tomsia, A. P. Freezing as a path to build complex composites. *Science* **311,** 515–8 (2006).
260. Deville, S., Saiz, E. & Tomsia, A. P. Ice-templated porous alumina structures. *Acta Mater.* **55,** 1965–1974 (2007).
261. Tong, H. ming, Noda, I. & Gryte, C. C. Formation of anisotropic ice-agar composites by directional freezing. *Colloid Polym. Sci.* **262,** 589–595 (1984).
262. Chino, Y. & Dunand, D. C. Directionally freeze-cast titanium foam with aligned, elongated pores. *Acta Mater.* **56,** 105–113 (2008).
263. Mahler, W. & Bechtold, M. F. Freeze-formed silica fibres. *Nature* **285,** 27–28 (1980).
264. Launey, M. E. *et al.* Designing highly toughened hybrid composites through nature-inspired hierarchical complexity. *Acta Mater.* **57,** 2919–2932 (2009).
265. Deville, S. in *Freezing Colloids: Observations, Principles, Control, and Use* 171–252 (Springer International Publishing, 2017).
266. Deville, S. *et al.* Influence of particle size on ice nucleation and growth during the ice-templating process. *J. Am. Ceram. Soc.* **93,** 2507–2510 (2010).
267. Deville, S. in *Freezing Colloids: Observations, Principles, Control, and Use* 91–170 (Springer International Publishing, 2017).
268. Arabi, N. & Zamanian, A. Effect of cooling rate and gelatin concentration on the microstructural and mechanical properties of ice template gelatin scaffolds. *Biotechnol. Appl. Biochem.* **60,** 573–579 (2013).
269. Lichtner, A., Roussel, D., Jauffrès, D., Martin, C. L. & Bordia, R. K. Effect of Macropore Anisotropy on the Mechanical Response of Hierarchically Porous Ceramics. *J. Am. Ceram. Soc.* **99,** 979–987 (2016).
270. Gutiérrez, M. C., Ferrer, M. L. & del Monte, F. Ice-Templated Materials : Sophisticated Structures Exhibiting Enhanced Functionalities Obtained after Unidirectional Freezing. *Chem. Mater.* **20,** 634–648 (2008).
271. Mukai, S. R., Nishihara, H. & Tamon, H. Formation of monolithic silica gel microhoneycombs (SMHs) using pseudosteady state growth of microstructural ice crystals. *Chem. Commun. (Camb).* 874–5 (2004).
272. Deville, S. in *Freezing Colloids: Observations, Principles, Control, and Use* 351–438 (Springer International Publishing, 2017).
273. Munch, E., Saiz, E., Tomsia, A. P. & Deville, S. Architectural control of freeze-cast ceramics through additives and templating. *J. Am. Ceram. Soc.* **92,** 1534–1539 (2009).
274. Zhang, Y., Hu, L., Han, J. & Jiang, Z. Freeze casting of aqueous alumina slurries with glycerol

for porous ceramics. *Ceram. Int.* **36,** 617–621 (2010).
275. Zhang, Y., Zuo, K. & Zeng, Y. P. Effects of gelatin addition on the microstructure of freeze-cast porous hydroxyapatite ceramics. *Ceram. Int.* **35,** 2151–2154 (2009).
276. Zuo, K. H., Zeng, Y. P. & Jiang, D. Effect of polyvinyl alcohol additive on the pore structure and morphology of the freeze-cast hydroxyapatite ceramics. *Mater. Sci. Eng. C* **30,** 283–287 (2010).
277. Deville, S. Freeze-casting of porous biomaterials: Structure, properties and opportunities. *Materials (Basel).* **3,** 1913–1927 (2010).
278. Yoon, B. H., Lee, E. J., Kim, H. E. & Koh, Y. H. Highly aligned porous silicon carbide ceramics by freezing polycarbosilane/camphene solution. *J. Am. Ceram. Soc.* **90,** 1753–1759 (2007).
279. Araki, K. & Halloran, J. W. Room-temperature freeze casting for ceramics with nonaqueous sublimable vehicles in the naphthalene–camphor eutectic system. *J. Am. Ceram. Soc.* **87,** 2014–2019 (2004).
280. Zhang, H., Long, J. & Cooper, A. I. Aligned porous materials by directional freezing of solutions in liquid CO2. *J. Am. Chem. Soc.* **127,** 13482–13483 (2005).
281. Bai, H., Chen, Y., Delattre, B., Tomsia, A. P. & Ritchie, R. O. Bioinspired large-scale aligned porous materials assembled with dual temperature gradients. *Sci. Adv.* **1,** e1500849 (2015).
282. Deville, S. in *Freezing Colloids: Observations, Principles, Control, and Use* 549–592 (Springer International Publishing, 2017).
283. Deville, S. in *Freezing Colloids: Observations, Principles, Control, and Use* 253–350 (Springer International Publishing, 2017).
284. Sofie, S. W. & Dogan, F. Freeze Casting of Aqueous Alumina Slurries with Glycerol. *J. Am. Ceram. Soc.* **84,** 1459–1464 (2004).
285. Yoon, B.-H., Choi, W.-Y., Kim, H.-E., Kim, J.-H. & Koh, Y.-H. Aligned porous alumina ceramics with high compressive strengths for bone tissue engineering. *Scr. Mater.* **58,** 537–540 (2008).
286. Nishihara, H., Mukai, S. R., Yamashita, D. & Tamon, H. Ordered macroporous silica by ice templating. *Chem. Mater.* **17,** 683–689 (2005).
287. Xing, Z. *et al.* A floating porous crystalline TiO2 ceramic with enhanced photocatalytic performance for wastewater decontamination. *Eur. J. Inorg. Chem.* 2411–2417 (2013). doi:10.1002/ejic.201201494
288. Romeo, H. E., Trabadelo, F., Jobbágy, M. & Parra, R. 2D-ice templated titanium oxide films as advanced conducting platforms for electrical stimulation. *J. Mater. Chem. C* **2,** 2806 (2014).
289. Hong, C., Zhang, X., Han, J., Du, J. & Han, W. Ultra-high-porosity zirconia ceramics fabricated by novel room-temperature freeze-casting. *Scr. Mater.* **60,** 563–566 (2009).
290. Fukushima, M. & Yoshizawa, Y. I. Fabrication of highly porous honeycomb-shaped mullite-zirconia insulators by gelation freezing. *Adv. Powder Technol.* **27,** 908–913 (2016).
291. Li, W., Lu, K. & Walz, J. Y. Formation, structure and properties of freeze-cast kaolinite-silica nanocomposites. *J. Am. Ceram. Soc.* **94,** 1256–1264 (2011).
292. Chen, H. B., Chiou, B. Sen, Wang, Y. Z. & Schiraldi, D. A. Biodegradable pectin/clay aerogels. *ACS Appl. Mater. Interfaces* **5,** 1715–1721 (2013).
293. Soon, Y. M., Shin, K. H., Koh, Y. H., Lee, J. H. & Kim, H. E. Compressive strength and processing of camphene-based freeze cast calcium phosphate scaffolds with aligned pores. *Mater. Lett.* **63,** 1548–1550 (2009).
294. Fu, Q., Rahaman, M. N., Dogan, F. & Bal, B. S. Freeze casting of porous hydroxyapatite scaffolds. I. Processing and general microstructure. *J. Biomed. Mater. Res. - Part B Appl. Biomater.* **86,** 125–135 (2008).
295. Lee, E. J., Koh, Y. H., Yoon, B. H., Kim, H. E. & Kim, H. W. Highly porous hydroxyapatite bioceramics with interconnected pore channels using camphene-based freeze casting. *Mater. Lett.* **61,** 2270–2273 (2007).
296. Deville, S., Saiz, E. & Tomsia, A. P. Freeze casting of hydroxyapatite scaffolds for bone tissue engineering. *Biomaterials* **27,** 5480–5489 (2006).
297. Zmora, S., Glicklis, R. & Cohen, S. Tailoring the pore architecture in 3-D alginate scaffolds by controlling the freezing regime during fabrication. *Biomaterials* **23,** 4087–4094 (2002).

298. Lee, J., Deng, Y., Lee & Deng. The morphology and mechanical properties of layer structured cellulose microfibril foams from ice-templating methods. *Soft Matter* **7,** 6034–6040 (2011).
299. Köhnke, T., Lin, A., Elder, T., Theliander, H. & Ragauskas, A. J. Nanoreinforced xylan–cellulose composite foams by freeze-casting. *Green Chem.* **14,** 1864 (2012).
300. Pourhaghgouy, M. & Zamanian, A. Physical and mechanical properties of the fully interconnected chitosan ice-templated scaffolds. *J. Appl. Polym. Sci.* **132,** 1–7 (2015).
301. Schoof, H., Apel, J., Heschel, I. & Rau, G. Control of pore structure and size in freeze-dried collagen sponges. *J. Biomed. Mater. Res.* **58,** 352–357 (2001).
302. Kang, H. W., Tabata, Y. & Ikada, Y. Fabrication of porous gelatin scaffolds for tissue engineering. *Biomaterials* **20,** 1339–1344 (1999).
303. Asuncion, M. C. T., Goh, J. C. H. & Toh, S. L. Anisotropic silk fibroin/gelatin scaffolds from unidirectional freezing. *Mater. Sci. Eng. C* **67,** 646–656 (2016).
304. Gutiérrez, M. C. *et al.* Poly(vinyl alcohol) scaffolds with tailored morphologies for drug delivery and controlled release. *Adv. Funct. Mater.* **17,** 3505–3513 (2007).
305. Zhou, X. H. *et al.* Development of poly(vinyl alcohol) porous scaffold with high strength and well ciprofloxacin release efficiency. *Mater. Sci. Eng. C* **67,** 326–335 (2016).
306. Kwon, S. M., Kim, H. S. & Jin, H. J. Multiwalled carbon nanotube cryogels with aligned and non-aligned porous structures. *Polymer (Guildf).* **50,** 2786–2792 (2009).
307. Gutierrez, M. C. *et al.* Biocompatible MWCNT scaffolds for immobilization and proliferation of E. coli. *J. Mater. Chem.* **17,** 2992–2995 (2007).
308. Vickery, J. L., Patil, A. J. & Mann, S. Fabrication of graphene-polymer nanocomposites with higher-order three-dimensional architectures. *Adv. Mater.* **21,** 2180–2184 (2009).
309. Sun, H., Xu, Z. & Gao, C. Multifunctional, ultra-flyweight, synergistically assembled carbon aerogels. *Adv. Mater.* **25,** 2554–2560 (2013).
310. Jung, H. Do, Yook, S. W., Kim, H. E. & Koh, Y. H. Fabrication of titanium scaffolds with porosity and pore size gradients by sequential freeze casting. *Mater. Lett.* **63,** 1545–1547 (2009).
311. Plunk, A. A. & Dunand, D. C. Iron foams created by directional freeze casting of iron oxide, reduction and sintering. *Mater. Lett.* **191,** 112–115 (2017).
312. Ramos, A. I. C. & Dunand, D. C. Preparation and Characterization of Directionally Freeze-cast Copper Foams. *Metals (Basel).* **2,** 265–273 (2012).
313. Shen, X. *et al.* Assembly of colloidal nanoparticles directed by the microstructures of polycrystalline ice. *ACS Nano* **5,** 8426–8433 (2011).
314. Gao, H. L. *et al.* Macroscopic free-standing hierarchical 3D architectures assembled from silver nanowires by ice templating. *Angew. Chemie - Int. Ed.* **53,** 4561–4566 (2014).
315. Driscoll, D., Weisenstein, A. J. & Sofie, S. W. Electrical and flexural anisotropy in freeze tape cast stainless steel porous substrates. *Mater. Lett.* **65,** 3433–3435 (2011).
316. Hunger, P. M., Donius, A. E. & Wegst, U. G. K. Structure-property-processing correlations in freeze-cast composite scaffolds. *Acta Biomater.* **9,** 6338–6348 (2013).
317. Launey, M. E. *et al.* A novel biomimetic approach to the design of high-performance ceramic − metal composites A novel biomimetic approach to the design of high-performance ceramic – metal composites. *J. R. Soc. Interface* **7,** 741–753 (2010).
318. Estevez, L., Kelarakis, A., Gong, Q., Daas, E. H. & Giannelis, E. P. Multifunctional graphene/platinum/nafion hybrids via ice templating. *J. Am. Chem. Soc.* **133,** 6122–6125 (2011).
319. Wicklein, B. *et al.* Thermally insulating and fire-retardant lightweight anisotropic foams based on nanocellulose and graphene oxide. *Nat. Nanotechnol.* **10,** 277–283 (2014).
320. Wu, X. *et al.* Preparation of aligned porous gelatin scaffolds by unidirectional freeze-drying method. *Acta Biomater.* **6,** 1167–1177 (2010).
321. Turco, G. *et al.* Alginate/hydroxyapatite biocomposite for bone ingrowth: A trabecular structure with high and isotropic connectivity. *Biomacromolecules* **10,** 1575–1583 (2009).
322. Francis, N. L. *et al.* An ice-templated, linearly aligned chitosan-alginate scaffold for neural tissue engineering. *J. Biomed. Mater. Res. - Part A* **101,** 3493–3503 (2013).
323. Ojuva, A., Akhtar, F., Tomsia, A. P. & Bergström, L. Laminated adsorbents with very rapid CO2 uptake by freeze-casting of zeolites. *ACS Appl. Mater. Interfaces* **5,** 2669–2676 (2013).

324. Bi, H. *et al.* Highly enhanced performance of spongy graphene as an oil sorbent. *J. Mater. Chem. A* **2,** 1652–1656 (2014).
325. Gawryla, M. D. & Schiraldi, D. A. Novel absorbent materials created via ice templatinga. *Macromol. Mater. Eng.* **294,** 570–574 (2009).
326. Mukai, S. R., Nishihara, H. & Tamon, H. Porous properties of silica gels with controlled morphology synthesized by unidirectional freeze-gelation. *Microporous Mesoporous Mater.* **63,** 43–51 (2003).
327. Szepes, A., Ulrich, J., Farkas, Z., Kovács, J. & Szabó-Révész, P. Freeze-casting technique in the development of solid drug delivery systems. *Chem. Eng. Process. Process Intensif.* **46,** 230–238 (2007).
328. Minaberry, Y., Chiappetta, D. A., Sosnik, A. & Jobbágy, M. Micro/nanostructured hyaluronic acid matrices with tuned swelling and drug release properties. *Biomacromolecules* **14,** 1–9 (2013).
329. Nakagawa, K., Tamura, A. & Chaiya, C. Preparation of proteolytic microreactors by freeze-drying immobilization. *Chem. Eng. Sci.* **119,** 22–29 (2014).
330. Gutiérrez, M. C., Jobbágy, M., Rapún, N., Ferrer, M. L. & Del Monte, F. A biocompatible bottom-up route for the preparation of hierarchical biohybrid materials. *Adv. Mater.* **18,** 1137–1140 (2006).
331. Ferrer, M. L., Esquembre, R., Ortega, I., Reyes Mateo, C. & Del Monte, F. Freezing of binary colloidal systems for the formation of hierarchy assemblies. *Chem. Mater.* **18,** 554–559 (2006).
332. Pannier, A., Mkandawire, M., Soltmann, U., Pompe, W. & Böttcher, H. Biological activity and mechanical stability of sol-gel-based biofilters using the freeze-gelation technique for immobilization of Rhodococcus ruber. *Appl. Microbiol. Biotechnol.* **93,** 1755–1767 (2012).
333. Park, M. S., Golovin, A. A. & Davis, S. H. The encapsulation of particles and bubbles by an advancing solidification front. *J. Fluid Mech.* **560,** 415 (2006).
334. Ishiguro, H. & Rubinsky, B. Mechanical interactions between ice crystals and red blood cells during directional solidification. *Cryobiology* **31,** 483–500 (1994).
335. *Cryopreservation and Freeze-Drying Protocols*. (Humana Press, 2015).
336. Rothschild, L. J. & Mancinelli, R. L. Life in extreme environments. *Nature* **409,** 1092–1101 (2001).
337. Storey, K. B. & Storey, J. M. Natural freezing survival in animals. *Annu. Rev. Ecol. Syst.* **27,** 365–386 (1996).
338. Clark, M. S. & Worland, M. R. How insects survive the cold: Molecular mechanisms - A review. *J. Comp. Physiol. B Biochem. Syst. Environ. Physiol.* **178,** 917–933 (2008).
339. Costanzo, J. P., Lee, R. E. & Lortz, P. H. Glucose Concentration Regulates Freeze Tolerance in the Wood Frog Rana Sylvatica. *J. exp. Biol* **181,** 245–255 (1993).
340. Storey, K. B. & Storey, J. M. Natural freeze tolerance in ectothermic vertebrates. *Annu. Rev. Physiol.* **54,** 619–637 (1992).
341. Fuller, B. J. Cryoprotectants: The essential antifreezes to protect life in the frozen state. *Cryo-Letters* **25,** 375–388 (2004).
342. Barbas, J. P. & Mascarenhas, R. D. Cryopreservation of domestic animal sperm cells. *Cell Tissue Bank.* **10,** 49–62 (2009).
343. Lagerberg, J. W. in *Cryopreservation and Freeeze-Drying Protocols* (eds. Wolkers, W. F. & Oldenhof, H.) 353–368 (Humana Press, 2015).
344. Engelmann, F. Use of biotechnologies for the conservation of plant biodiversity. *Vitr. Cell. Dev. Biol. - Plant* **47,** 5–16 (2011).
345. Schumacher, H. M., Westphal, M. & Heine-Dobbernack, E. in *Cryopreservation and Freeeze-Drying Protocols* (eds. Wolkers, W. F. & Oldenhof, H.) 423–430 (Humana Press, 2015).
346. Hubálek, Z. Protectants used in the cryopreservation of microorganisms. *Cryobiology* **46,** 205–229 (2003).
347. Heckly, R. J. Preservation of microorganisms. *Adv. Appl. Microbiol.* **24,** 1–53 (1978).
348. Pegg, D. E. in *Cryopreservation and Freeeze-Drying Protocols* (eds. Wolkers, W. F. & Oldenhof, H.) 3–20 (Humana Press, 2015).
349. Polge, C., Smith, A. U. & Parkes, A. S. Revival of spermatozoa after vitrification and dehydration at low temperatures. *Nature* **164,** 666 (1949).

350. Lovelock, J. E. The mechanism of the protective action of glycerol against haemolysis by freezing and thawing. *Biochim. Biophys. Acta* **11,** 28–36 (1953).
351. Mazur, P. Kinetics of Water Loss from Cells at Subzero Temperatures and the Likelihood of Intracellular Freezing. *J. Gen. Physiol.* **47,** 347–369 (1963).
352. Mazur, P. Freezing of living cells : mechanisms and implications. *Am. Physiol. Soc.* **16,** 125–142 (1984).
353. Kocherbitov, V. The nature of nonfreezing water in carbohydrate polymers. *Carbohydr. Polym.* **150,** 353–358 (2016).
354. Boutron, P. Comparison with the theory of the kinetics and extent of ice crystallization and of the glass-forming tendency in aqueous cryoprotective solutions. *Cryobiology* **23,** 88–102 (1986).
355. Fahy, G. M. & Wowk, B. in *Cryopreservation and Freeeze-Drying Protocols* (eds. Wolkers, W. F. & Oldenhof, H.) 21–82 (Humana Press, 2015).
356. Fahy, G. M., MacFarlane, D. R., Angell, C. A. & Meryman, H. T. Vitrification as an approach to cryopreservation. *Cryobiology* **21,** 407–426 (1984).
357. Manuchehrabadi, N. *et al.* Improved tissue cryopreservation using inductive heating of magnetic nanoparticles. *Sci. Transl. Med.* **9,** (2017).
358. Liu, B. & Zhou, X. in *Cryopreservation and Freeeze-Drying Protocols* (eds. Wolkers, W. F. & Oldenhof, H.) 459–476 (Humana Press, 2015).
359. Keskintepe, L. & Eroglu, A. in *Cryopreservation and Freeeze-Drying Protocols* (eds. Wolkers, W. F. & Oldenhof, H.) 489–498 (Humana Press, 2015).
360. Morgan, C. a., Herman, N., White, P. a. & Vesey, G. Preservation of micro-organisms by drying: A review. *J. Microbiol. Methods* **66,** 183–193 (2006).
361. Heckly, R. J. Preservation of Bacteria by Lyophilization. *Adv. Appl. Microbiol.* **3,** 1–76 (1961).
362. Adams, G. D. in *Vaccine Protocols* (eds. Robinson, A., Hudson, M. J. & Cranage, M. P.) 223–243 (Humana Press, 2003).
363. Fonseca, F., Cenard, S. & Passot, S. in *Cryopreservation and Freeeze-Drying Protocols* (eds. Wolkers, W. F. & Oldenhof, H.) 477–489 (Humana Press, 2015).
364. Adams, G. D. J., Cook, I. & Ward, K. R. in *Cryopreservation and Freeeze-Drying Protocols* (eds. Wolkers, W. F. & Oldenhof, H.) 121–146 (Humana Press, 2015).
365. Navarta, L. G., Calvo, J., Calvente, V., Benuzzi, D. & Sanz, M. I. Freezing and freeze-drying of the bacterium Rahnella aquatilis BNM 0523: Study of protecting agents, rehydration media and freezing temperatures. *Lett. Appl. Microbiol.* **53,** 565–571 (2011).
366. Sultana, K. *et al.* Encapsulation of probiotic bacteria with alginate-starch and evaluation of survival in simulated gastrointestinal conditions and in yoghurt. *Int. J. Food Microbiol.* **62,** 47–55 (2000).
367. Gupta, P. & Nayak, K. K. Characteristics of Protein-Based Biopolymer and Its Application. *Polym. Eng. Sci.* **55,** 485–498 (2015).
368. Simkovic, I. Unexplored possibilities of all-polysaccharide composites. *Carbohydr. Polym.* **95,** 697–715 (2013).
369. Ridley, B. L., O'Neill, M. A. & Mohnen, D. Pectins: structure, biosynthesis, and oligogalacturonide-related signaling. *Phytochemistry* **57,** 929–967 (2001).
370. Srivastava, P. & Malviya, R. Sources of pectin, extraction and its applications in pharmaceutical industry - an overview. *Indian J. Nat. Prod. Resour.* **2,** 10–18 (2011).
371. May, C. D. Industrial pectins: Sources, production and applications. *Carbohydr. Polym.* **12,** 79–99 (1990).
372. Bartley, I. M. & Knee, M. The chemistry of textural changes in fruit during storage. *Food Chem.* **9,** 47–58 (1982).
373. Guillemin, F. *et al.* Distribution of pectic epitopes in cell walls of the sugar beet root. *Planta* **222,** 355–371 (2005).
374. Lau, J. M., McNeil, M., Darvill, A. G. & Albersheim, P. Structure of the backbone of rhamnogalacturonan I, a pectic polysaccharide in the primary cell walls of plants. *Carbohydr. Res.* **137,** 111–125 (1985).
375. O'Neill, M., Ishii, T., Albersheim, P. & Darvill, A. G. Rhamnogalacturonan II : Structure and Function of a Borate Cross-Linked Cell. *Annu. Rev. Plant Biol.* **55,** 109–139 (2004).

376. Yapo, B. M., Lerouge, P., Thibault, J. F. & Ralet, M. C. Pectins from citrus peel cell walls contain homogalacturonans homogenous with respect to molar mass, rhamnogalacturonan I and rhamnogalacturonan II. *Carbohydr. Polym.* **69,** 426–435 (2007).
377. Schols, H. A. & Voragen, A. G. J. in *Progress in Biotechnology* (eds. Visser, J. & Voragen, A. G. J.) **14,** 3–19 (Elsevier Science B.V, 1996).
378. Ralet, M. C. & Thibault, J. F. Interchain heterogeneity of enzymatically deesterified lime pectins. *Biomacromolecules* **3,** 917–925 (2002).
379. Vincken, J.-P. *et al.* If Homogalacturonan Were a Side Chain of Rhamnogalacturonan I. Implications for Cell Wall Architecture. *Plant Physiol.* **132,** 1781–1789 (2003).
380. Valdés, A., Burgos, N., Jiménez, A. & Garrigós, M. C. Natural Pectin Polysaccharides as Edible Coatings. *Coatings* **5,** 865–886 (2015).
381. Liu, L., Fishman, M. L. & Hicks, K. B. Pectin in controlled drug delivery – a review. *Cellulose* **14,** 15–24 (2006).
382. Munarin, F. *et al.* Pectin-based injectable biomaterials for bone tissue engineering. *Biomacromolecules* **12,** 568–577 (2011).
383. Mata, Y. N., Blázquez, M. L., Ballester, a., González, F. & Muñoz, J. a. Sugar-beet pulp pectin gels as biosorbent for heavy metals: Preparation and determination of biosorption and desorption characteristics. *Chem. Eng. J.* **150,** 289–301 (2009).
384. Guilherme, M. R. *et al.* Pectin-Based Polymer Hydrogel as a Carrier for Release of Agricultural Nutrients and Removal of Heavy Metals from Wastewater. *J. App* **117,** 3146–3154 (2010).
385. Jung, J., Arnold, R. D. & Wicker, L. Pectin and charge modified pectin hydrogel beads as a colon-targeted drug delivery carrier. *Colloids Surf. B. Biointerfaces* **104,** 116–21 (2013).
386. Gaona-Sanchez, V. A. *et al.* Pectin-based films produced by electrospraying. *J. Appl. Polym. Sci.* **133,** 1–10 (2016).
387. Neves, S. C. *et al.* Biofunctionalized pectin hydrogels as 3D cellular microenvironments. *J. Mater. Chem. B* **3,** 2096–2108 (2015).
388. White, R. J., Budarin, V. L. & Clark, J. H. Pectin-derived porous materials. *Chem. - A Eur. J.* **16,** 1326–1335 (2010).
389. Morris, E. R., Gidley, M. J., Murray, E. J., Powell, D. a. & Rees, D. a. Characterization of pectin gelation under conditions of low water activity, by circular dichroism, competitive inhibition and mechanical properties. *Int. J. Biol. Macromol.* **2,** 327–330 (1980).
390. Morris, E. R., Powell, D. A., Gidley, M. J. & Rees, D. A. Conformations and interactions of pectins. I. Polymorphism between gel and solid states of calcium polygalacturonate. *J. Mol. Biol.* **155,** 507–516 (1982).
391. Yang, Y., Zhang, G., Hong, Y., Gu, Z. & Fang, F. Calcium cation triggers and accelerates the gelation of high methoxy pectin. *Food Hydrocoll.* **32,** 228–234
392. Löfgren, C., Guillotin, S., Evenbratt, H., Schols, H. & Hermansson, A. M. Effects of calcium, pH, and blockiness on kinetic rheological behavior and microstructure of HM pectin gels. *Biomacromolecules* **6,** 646–652 (2005).
393. Pippen, E. L., McCready, R. M. & Owens, H. S. Gelation properties of partially acetylated pectins. *J Am Chem Soc* **72,** 813–816 (1950).
394. Ralet, M.-C., Crépeau, M.-J., Buchholt, H.-C. & Thibault, J.-F. Polyelectrolyte behaviour and calcium binding properties of sugar beet pectins differing in their degrees of methylation and acetylation. *Biochem. Eng. J.* **16,** 191–201 (2003).
395. Fishman, M. L., Cooke, P. H. & Hotchkiss, A. T. in *Green Polymer Chemistry: Biocatalysis and Biomaterials* (eds. Cheng, H. N. & Gross, R. A.) 71–86 (American Chemical Society, 2010).
396. Morris, G., Ralet, M.-C., Bonnin, E., Thibault, J.-F. & Harding, S. E. Physical characterisation of the rhamnogalacturonan and homogalacturonan fractions of sugar beet (Beta vulgaris) pectin. *Carbohydr. Polym.* **82,** 1161–1167 (2010).
397. Levigne, S., Ralet, M.-C. & Thibault, J.-F. Characterisation of pectins extracted from fresh sugar beet under different conditions using an experimental design. *Carbohydr. Polym.* **49,** 145–153 (2002).
398. Oosterveld, A., Beldman, G., Searle-van Leeuwen, M. J. F. & Voragen, A. G. J. *Pectic*

substances from sugar beet pulp : structural features , enzymatic modification , and gel formation. (1997).
399. Ralet, M. C., Thibault, J. F., Faulds, C. B. & Williamson, G. Isolation and purification of feruloylated oligosaccharides from cell walls of sugar-beet pulp. *Carbohydr. Res.* **263,** 227–241 (1994).
400. Ralet, M.-C., André-Leroux, G., Quéméner, B. & Thibault, J.-F. Sugar beet (Beta vulgaris) pectins are covalently cross-linked through diferulic bridges in the cell wall. *Phytochemistry* **66,** 2800–14 (2005).
401. Rezakhaniha, R. *et al.* Experimental investigation of collagen waviness and orientation in the arterial adventitia using confocal laser scanning microscopy. *Biomech. Model. Mechanobiol.* **11,** 461–473 (2012).
402. Ashby, M. F. *Materials Selection in Mechanical Design*. (Elsevier, 2005).
403. Bai, H. *et al.* Biomimetic gradient scaffold from ice-templating for self-seeding of cells with capillary effect. *Acta Biomater.* **20,** 113–119 (2015).
404. Zhang, H. *et al.* Aligned two- and three-dimensional structures by directional freezing of polymers and nanoparticles. *Nat. Mater.* **4,** 787–93 (2005).
405. Zhou, Y. *et al.* Freeze-casting of cellulose nanowhisker foams prepared from a water-dimethylsulfoxide (DMSO) binary mixture at low DMSO concentrations. *RSC Adv.* **3,** 19272 (2013).
406. Chou, T. *et al.* Organic inorganic hybrid coatings for corrosion protection. *J. Non. Cryst. Solids* **290,** 153–162 (2001).
407. Nakajima, A., Abe, K., Hashimoto, K. & Watanabe, T. Preparation of hard super-hydrophobic films with visible light transmission. *Thin Solid Films* **376,** 140–143 (2000).
408. Inama, L., Diré, S., Carturan, G. & Cavazza, A. Entrapment of viable microorganisms by SiO2 sol-gel layers on glass surfaces: Trapping, catalytic performance and immobilization durability of *Saccharomyces cerevisiae*. *J. Biotechnol.* **30,** 197–210 (1993).
409. Lofgreen, J. E. & Ozin, G. A. Controlling morphology and porosity to improve performance of molecularly imprinted sol–gel silica. *Chem. Soc. Rev.* **43,** 911–933 (2014).
410. Barron, A. R. CVD of SiO2 and related materials: An overview. *Adv. Mater. Opt. Electron.* **6,** 101–114 (1996).
411. Yong Ha, H., Woo Nam, S., hong, S. A. & Kook Lee, W. Chemical vapor deposition of hydrogen-permselective silica films on porous glass supports from tetraethylorthosilicate. *J. Memb. Sci.* **85,** 279–290 (1993).
412. Kim, E. J. & Gill, W. N. Analytical model for chemical vapor deposition of Si02 films using tetraethoxysilane and ozone. **140,** 315–326 (1994).
413. Foggiato, J. in *Handbook of Thin-Film Deposition Processes and Technologies* (ed. Seshan, K.) 111–150 (2001).
414. Nishiyama, N., Tanaka, S., Egashira, Y., Oku, Y. & Ueyama, K. Vapor-phase synthesis of mesoporous silica thin films. *Chem. Mater.* **15,** 1006–1011 (2003).
415. Gupta, G. *et al.* CVD for the facile synthesis of hybrid nanobiomaterials integrating functional supramolecular assemblies. *Langmuir* **25,** 13322–13327 (2009).
416. Campostrini, R. *et al.* Immobilization of plant cells in hybrid sol-gel materials. *J. Sol-Gel Sci. Technol.* **7,** 87–97 (1996).
417. Carturan, G., Dellagiacoma, G., Rossi, M., Dal Monte, R. & Muraca, M. Encapsulation of viable animal cells for hybrid bioartificial organs by the Biosil method. *Processes* **3136,** 366–373 (1997).
418. Carturan, G. *et al.* Gas-phase silicon alkoxide reactivity vs. Na-alginate droplets for conjugation of alginate and sol-gel technologies. *J. Sol-Gel Sci. Technol.* **37,** 69–77 (2006).
419. Callone, E., Campostrini, R., Carturan, G., Cavazza, A. & Guzzon, R. Immobilization of yeast and bacteria cells in alginate microbeads coated with silica membranes: procedures, physico-chemical features and bioactivity. *J. Mater. Chem.* **18,** 4839 (2008).
420. Wexler, A. & Hasegawa, S. Relative humidity-temperature relationships of some saturated salt solutions in the temperature range 0 degree to 50 degrees C. *J. Res. Natl. Bur. Stand. (1934).* **53,** 19 (1954).
421. Synytsya, A. *et al.* Fourier transform Raman and infrared spectroscopy of pectins. *Carbohydr.*

Polym. **54,** 97–106 (2003).
422. Almeida, R. M. & Marques, A. C. in *Handbook of Sol-Gel Science and Technology - Processing Characterization and Applications - Vol II* 65–90
423. Almeida, R. M. & Pantano, C. G. Structural investigation of silica gel films by infrared spectroscopy. *J. Appl. Phys.* **68,** 4225–4232 (1990).
424. Matos, M. C., Ilharco, L. M. & Almeida, R. M. The Evolution of Teos To Silica-Gel and Glass By Vibrational Spectroscopy. *J. Non. Cryst. Solids* **147,** 232–237 (1992).
425. Meille, S., Lombardi, M., Chevalier, J. & Montanaro, L. Mechanical properties of porous ceramics in compression: On the transition between elastic, brittle, and cellular behavior. *J. Eur. Ceram. Soc.* **32,** 3959–3967 (2012).
426. Kim, H. S. On the rule of mixtures for the hardness of particle reinforced composites. *Mater. Sci. Eng. A* **289,** 30–33 (2000).
427. Coradin, T., Eglin, D. & Livage, J. The silicomolybdic acid spectrophotometric method and its application to silicate/biopolymer interaction studies. *Spectroscopy* **18,** 567–576 (2004).
428. Attallah, O. A., Al-Ghobashy, M. A., Nebsen, M. & Salem, M. Y. Removal of cationic and anionic dyes from aqueous solution with magnetite/pectin and magnetite/silica/pectin hybrid nanocomposites: kinetic, isotherm and mechanism analysis. *RSC Adv.* **6,** 11461–11480 (2016).
429. Nesic, A. R., Velickovic, S. J. & Antonovic, D. G. Novel composite films based on amidated pectin for cationic dye adsorption. *Colloids Surfaces B Biointerfaces* **116,** 620–626 (2014).
430. Krysztafkiewicz, A., Binkowski, S. & Jesionowski, T. Adsorption of dyes on a silica surface. *Appl. Surf. Sci.* **199,** 31–39 (2002).
431. Han, H. *et al.* Removal of cationic dyes from aqueous solution by adsorption onto hydrophobic/hydrophilic silica aerogel. *Colloids Surfaces A Physicochem. Eng. Asp.* **509,** 539–549 (2016).
432. Ip, A. W. M., Barford, J. P. & McKay, G. A comparative study on the kinetics and mechanisms of removal of Reactive Black 5 by adsorption onto activated carbons and bone char. *Chem. Eng. J.* **157,** 434–442 (2010).
433. Cardoso, N. F. *et al.* Removal of remazol black B textile dye from aqueous solution by adsorption. *Desalination* **269,** 92–103 (2011).
434. Bergman, L. W. in *Two-Hybrid Systems: methods and Protocols* (ed. MacDonald, P. N.) **177,** 9–39 (Humana Press Inc., 2001).
435. Treco, D. A. & Winston, F. in *Current Protocols in Molecular Biology* (Wiley, 2008).
436. Davey, H. M. Life, death, and in-between: Meanings and methods in microbiology. *Appl. Environ. Microbiol.* **77,** 5571–5576 (2011).
437. Mensour, N. A., Margaritis, A., Briens, C. L., Pilkington, H. & Russell, I. in *Immobilized Cells: Basics and Applications* (eds. Buitelaar, R. M., Bucke, C., Trampe, J. & Wijffels, R. H.) **11,** 661–671 (Elsevier Science, 1996).
438. Bapat, P., Nandy, S. K., Wangikar, P. & Venkatesh, K. V. Quantification of metabolically active biomass using Methylene Blue dye Reduction Test (MBRT): measurement of CFU in about 200 s. *J. Microbiol. Methods* **65,** 107–116 (2006).
439. Nandy, S. K. *et al.* A high-throughput method for quantifying metabolically active yeast cells. *Yeast* **32,** 461–468 (2015).
440. Millard, P. J., Roth, B. L., Thi, H. P. T., Yue, S. T. & Haugland, R. P. Development of the FUN-1 family of fluorescent probes for vacuole labeling and viability testing of yeasts. *Appl. Environ. Microbiol.* **63,** 2897–2905 (1997).
441. LaBauve, A. E. & Wargo, M. J. in *Current Protocols in Microbiology* (Wiley, 2012). doi:10.1016/j.biotechadv.2011.08.021.Secreted
442. Holden, P. A. *et al.* Assessing the Role of *Pseudomonas aeruginosa* Surface-Active Gene Expression in Hexadecane Biodegradation in Sand. *Appl. Environ. Microbiol.* **68,** 2509–2518 (2002).
443. Chayabutra, C. & Ju, L.-K. Degradation of n -Hexadecane and Its Metabolites by *Pseudomonas aeruginosa* under Microaerobic and Anaerobic Denitrifying Conditions. *Appl. Environ. Microbiol.* **66,** 493–498 (2000).
444. Toledo, F. L., Calvo, C., Rodelas, B. & González-López, J. Selection and identification of bacteria isolated from waste crude oil with polycyclic aromatic hydrocarbons removal

capacities. *Syst. Appl. Microbiol.* **29,** 244–52 (2006).
445. Das, K. & Mukherjee, A. K. Crude petroleum-oil biodegradation efficiency of Bacillus subtilis and *Pseudomonas aeruginosa* strains isolated from a petroleum-oil contaminated soil from North-East India. *Bioresour. Technol.* **98,** 1339–45 (2007).
446. Karamalidis, A. K. *et al.* Laboratory scale bioremediation of petroleum-contaminated soil by indigenous microorganisms and added *Pseudomonas aeruginosa* strain Spet. *Bioresour. Technol.* **101,** 6545–6552 (2010).
447. Jacques, R. J. S. *et al.* Anthracene biodegradation by *Pseudomonas sp.* isolated from a petrochemical sludge landfarming site. *Int. Biodeterior. Biodegradation* **56,** 143–150 (2005).
448. Ghosh, I., Jasmine, J. & Mukherji, S. Biodegradation of pyrene by a *Pseudomonas aeruginosa* strain RS1 isolated from refinery sludge. *Bioresour. Technol.* **166,** 548–558 (2014).
449. Hwang, S. & Cutright, T. J. Biodegradability of aged pyrene and phenanthrene in a natural soil. *Chemosphere* **47,** 891–899 (2002).
450. Romero, M. C., Cazau, M. C., Giorgieri, S. & Arambarri, A. M. Phenanthrene degradation by microorganisms isolated from a contaminated stream. *Environ. Pollut.* **101,** 355–359 (1998).
451. Lin, C. W., Cheng, Y. W. & Tsai, S. L. Multi-substrate biodegradation kinetics of MTBE and BTEX mixtures by *Pseudomonas aeruginosa*. *Process Biochem.* **42,** 1211–1217 (2007).
452. Mukherjee, A. K. & Bordoloi, N. K. Biodegradation of benzene, toluene, and xylene (BTX) in liquid culture and in soil by *Bacillus subtilis* and *Pseudomonas aeruginosa* strains and a formulated bacterial consortium. *Environ. Sci. Pollut. Res.* **19,** 3380–3388 (2012).
453. Kim, S.-B., Park, C.-H., Kim, D.-J. & Jury, W. a. Kinetics of benzene biodegradation by *Pseudomonas aeruginosa*: parameter estimation. *Environ. Toxicol. Chem.* **22,** 1038–1045 (2003).
454. Drakou, E. M., Koutinas, M., Pantelides, I., Tsolakidou, M. & Vyrides, I. Insights into the metabolic basis of the halotolerant *Pseudomonas aeruginosa* strain LVD-10 during toluene biodegradation. *Int. Biodeterior. Biodegrad.* **99,** 85–94 (2015).
455. Noguera, D. R. & Freedman, D. L. Reduction and Acetylation of 2 , 4-Dinitrotoluene by a *Pseudomonas aeruginosa* Strain. *Appl. Environ. Microbiol.* **62,** 2257–2263 (1996).
456. Mercimek, H. A. *et al.* Degradation of 2,4,6-trinitrotoluene by P. aeruginosa and characterization of some metabolites. *Brazilia, J. Microbiol.* **46,** 103–111 (2015).
457. Oh, B. T., Shea, P. J., Drijber, R. a., Vasilyeva, G. K. & Sarath, G. TNT biotransformation and detoxification by a *Pseudomonas aeruginosa* strain. *Biodegradation* **14,** 309–319 (2003).
458. Jadhav, J. P., Phugare, S. S., Dhanve, R. S. & Jadhav, S. B. Rapid biodegradation and decolorization of Direct Orange 39 (Orange TGLL) by an isolated bacterium *Pseudomonas aeruginosa* strain BCH. *Biodegradation* **21,** 453–63 (2010).
459. Afzal, M., Iqbal, S., Rauf, S. & Khalid, Z. M. Characteristics of phenol biodegradation in saline solutions by monocultures of *Pseudomonas aeruginosa* and *Pseudomonas pseudomallei*. *J. Hazard. Mater.* **149,** 60–66 (2007).
460. Mita, L. *et al.* Bisphenol A removal by a *Pseudomonas aeruginosa* immobilized on granular activated carbon and operating in a fluidized bed reactor. *J. Hazard. Mater.* **291,** 129–135 (2015).
461. Hickey, W. J., Searles, D. B. & Focht, D. D. Enhanced Mineralization of Polychlorinated Biphenyls in Soil Inoculated with Chlorobenzoate-Degrading Bacteria. *Appl. Environ. Microbiol.* **59,** 1194–1200 (1993).
462. Shirkot, C. K., Shirkot, P., Dhall, S. P. & Gupta, K. G. Effectiveness of *Pseudomonas aeruginosa* for detoxification of tetramethylthiuram disulfide (TMTD) from contaminated soil. *Bull. Environ. Contam. Toxicol.* **44,** 317–324 (1990).
463. Song, H., Zhou, Z., Liu, Y., Deng, S. & Xu, H. Kinetics and Mechanism of Fenpropathrin Biodegradation by a Newly Isolated *Pseudomonas aeruginosa* sp. Strain JQ-41. *Curr. Microbiol.* **71,** 326–332 (2015).
464. Peter, G. & Reichart, O. The effect of growth phase, cryoprotectants and freezing rates on the survival of selected micro-organisms during freezing and thawing. *Acta Aliment.* **30,** 89–97 (2001).
465. Linker, A. & Jones, R. S. A New Polysaccharide Resembling Alginic Acid Isolated from Pseudomonads. *J. Biol. Chem.* **241,** 3845–3851 (1966).

466. Watanabe, K. & Baker, P. W. Environmentally relevant microorganisms. *J. Biosci. Bioeng.* **89,** 1–11 (2000).
467. Tabak, H. H. & Govind, R. in *Journal of Industrial Microbiology and Biotechnology* (eds. Sheehan, D. & Walker, J. M.) **18,** 330–339 (1997).
468. Gacesa, P. Bacterial alginate biosynthesis--recent progress and future prospects. *Microbiology* **144,** 1133–1143 (1998).
469. Sabra, W., Zeng, A. P. & Deckwer, W. D. Bacterial alginate: Physiology, product quality and process aspects. *Appl. Microbiol. Biotechnol.* **56,** 315–325 (2001).
470. Brownlee, I. *et al.* in *Alginates: Biology and Applications* (ed. Rehm, B.) **13,** 211–228 (Springer, 2009).
471. Tanriseven, A. & Doan, E. Immobilization of invertase within calcium alginate gel capsules. *Process Biochem.* **36,** 1081–1083 (2001).
472. Blandino, A., Macías, M. & Cantero, D. Immobilization of glucose oxidase within calcium alginate gel capsules. *Process Biochem.* **36,** 601–606 (2001).
473. Barron, N. *et al.* in *Immobilized Cells: Basics and Applications* (eds. R.H. Wijffels, Buitelaar, R. M., Bucke, C. & Tramper, J.) 379–383 (Elsevier, 1996).
474. Kuo, C. K. & Ma, P. X. Ionically crosslinked alginate hydrogels as scaffolds for tissue engineering: Part 1. Structure, gelation rate and mechanical properties. *Biomaterials* **22,** 511–521 (2001).
475. Leick, S., Henning, S., Degen, P., Suter, D. & Rehage, H. Deformation of liquid-filled calcium alginate capsules in a spinning drop apparatus. *Phys. Chem. Chem. Phys.* **12,** 2950 (2010).
476. Rhim, J.-W. Physical and mechanical properties of water resistant sodium alginate films. *LWT - Food Sci. Technol.* **37,** 323–330 (2004).
477. Remunan-Lopez, C. & Bodmeier, R. Mechanical, water uptake and permeability properties of crosslinked chitosan glutamate and alginate films. *J. Control. Release* **44,** 215–225 (1997).
478. Yamagiwa, K., Shimizu, Y., Kozawa, T., Ohkawa, A. & Onodera, M. Formation of calcium-alginate gel coating on biocatalyst immobilization carrier. *Journal of Chemical Engineering of Japan* **25,** 723–728 (1992).
479. Shapiro, L. & Cohen, S. Novel alginate sponges for cell culture and transplantation. *Biomaterials* **18,** 583–590 (1997).
480. Bhattarai, N. & Zhang, M. Controlled synthesis and structural stability of alginate-based nanofibers. *Nanotechnology* **18,** 455601 (2007).
481. Ding, Y., Zhao, Y., Tao, X., Zheng, Y.-Z. & Chen, J.-F. Assembled alginate/chitosan micro-shells for removal of organic pollutants. *Polymer (Guildf).* **50,** 2841–2846 (2009).
482. Duan, B., Hockaday, L. A., Kang, K. H. & Butcher, J. T. 3D Bioprinting of heterogeneous aortic valve conduits with alginate/gelatin hydrogels. *J. Biomed. Mater. Res. - Part A* **101,** 1255–1264 (2013).
483. Yan, X. L., Khor, E. & Lim, L. Y. Chitosan-alginate films prepared with chitosans of different molecular weights. *J. Biomed. Mater. Res.* **58,** 358–365 (2001).
484. Choi, Y. S. *et al.* Study on gelatin-containing artificial skin: I. Preparation and characteristics of novel gelatin-alginate sponge. *Biomaterials* **20,** 409–417 (1999).
485. Eiselt, P., Lee, K. Y. & Mooney, D. J. Rigidity of two-component hydrogels prepared from alginate and poly(ethylene glycol)-diamines. *Macromolecules* **32,** 5561–5566 (1999).
486. Alcântara, A., Aranda, P., Darder, M. & Ruiz-Hitzky, E. Bionanocomposites based on alginate–zein/layered double hydroxide materials as drug delivery systems. *J. Mater. Chem.* **20,** 9495 (2010).
487. Shimao, M. Biodegradation of plastics. *Curr. Opin. Biotechnol.* **12,** 242–247 (2001).
488. Chiellini, E., Corti, A., D'Antone, S. & Solaro, R. *Biodegradation of poly (vinyl alcohol) based materials*. *Progress in Polymer Science* **28,** (2003).
489. Paradossi, G., Cavalieri, F., Chiessi, E., Spagnoli, C. & Cowman, M. K. Poly(vinyl alcohol) as versatile biomaterial for potential biomedical applications. *J. Mater. Sci. Mater. Med.* **14,** 687–691 (2003).
490. Nuttelman, C. R., Henry, S. M. & Anseth, K. S. Synthesis and characterization of photocrosslinkable, degradable poly (vinyl alcohol)-based tissue engineering scaffolds. *Biomaterials* **23,** 3617–3626 (2002).

491. Draget, K. I., Skjåk Bræk, G. & Smidsrød, O. Alginic acid gels: the effect of alginate chemical composition and molecular weight. *Carbohydr. Polym.* **25,** 31–38 (1994).
492. Ben Ahmed, N. Conception de Bio-indicateurs de polluant organique et de métaux lourds par encapsulation de micro-algues dans une matrice de silice synthétisée par le procédé sol gel. (2016).
493. Sigma-Aldrich. Glucose (HK) Assay Kit - Product Information. (2003).
494. Stiefel, P., Schmidt-Emrich, S., Maniura-Weber, K. & Ren, Q. Critical aspects of using bacterial cell viability assays with the fluorophores SYTO9 and propidium iodide. *BMC Microbiol.* **15,** (2015).
495. Vogelsang, C. & Østgaard, K. in *Immobilized Cells: Basics and Applications* (eds. Buitelaar, R. M., Bucke, C., Trampe, J. & Wijffels, R. H.) **11,** 213–220 (Elsevier, 1996).
496. Costa, E., Usall, J., Teixido, N., Garcia, N. & Vinas, I. Effect of protective agents rehydration media and initial cell concentration on viability of Pantoea agglomerans strain CPA-2 subjected to freeze-drying. *J. Appl. Microbiol.* **89,** 793–800 (2000).
497. Nieto, A., Areva, S., Wilson, T., Viitala, R. & Vallet-Regi, M. Cell viability in a wet silica gel. *Acta Biomater.* **5,** 3478–3487 (2009).
498. Cuervo Lumbaque, E., Gomes, M. F., Da Silva Carvalho, V., de Freitas, A. M. & Tiburtius, E. R. L. Degradation and ecotoxicity of dye Reactive Black 5 after reductive-oxidative process: Environmental Science and Pollution Research. *Environ. Sci. Pollut. Res.* **24,** 6126–6134 (2017).
499. Wu, J., Kim, K.-S., Sung, N.-C., Kim, C.-H. & Lee, Y.-C. Isolation and characterization of Shewanella oneidensis WL-7 capable of decolorizing azo dye Reactive Black 5. *J. Gen. Appl. Microbiol.* **55,** 51–55 (2009).
500. Yang, Y. Y., Du, L. N., Wang, G., Jia, X. M. & Zhao, Y. H. The decolorisation capacity and mechanism of Shewanella oneidensis MR-1 for Methyl Orange and Acid Yellow 199 under microaerophilic conditions. *Water Sci. Technol.* **63,** 956–963 (2011).
501. Hau, H. H. & Gralnick, J. A. Ecology and Biotechnology of the Genus *Shewanella*. *Annu. Rev. Microbiol.* **61,** 237–258 (2007).
502. Bretschger, O. *et al.* Current production and metal oxide reduction by Shewanella oneidensis MR-1 wild type and mutants. *Appl. Environ. Microbiol.* **73,** 7003–7012 (2007).
503. Nealson, K. H., Belz, A. & McKee, B. Breathing metals as a way of life: Geobiology in action. *Antonie van Leeuwenhoek, Int. J. Gen. Mol. Microbiol.* **81,** 215–222 (2002).
504. Ringeisen, B. R. *et al.* High power density from a miniature microbial fuel cell using Shewanella oneidensis DSP10. *Environ. Sci. Technol.* **40,** 2629–2634 (2006).
505. Abboud, R. *et al.* Low-temperature growth of *Shewanella oneidensis* MR-1. *Appl. Environ. Microbiol.* **71,** 811–816 (2005).
506. Venkateswaran, K. *et al.* Polyphasic taxonomy of the genus *Shewanella* and description of *Shewanella oneidensis* sp. nov. *Int. J. Syst. Bacteriol.* **49,** 705–724 (1999).
507. Food and Agriculture Organization. *World reference base for soil resources 2006*. *World Soil Resources Reports* **103,** (2006).